

ELECTRODE POTENTIALS
IN FUSED ALKALI METAL SALTS

A Thesis

Submitted to the Faculty of Graduate Studies
In Partial Fulfillment of the Requirements
for the Degree of

Doctor of Philosophy

in Chemistry

Division of Natural Sciences and Mathematics
University of Saskatchewan, Regina Campus

by

Larry George Boxall

Regina, Saskatchewan

March, 1970

© Copyright 1970. L.G. Boxall

UMI Number: DC52114

UMI[®]

UMI Microform DC52114
Copyright 2006 by ProQuest Information and Learning Company.
All rights reserved. This microform edition is protected against
unauthorized copying under Title 17, United States Code.

ProQuest Information and Learning Company
300 North Zeeb Road
P.O. Box 1346
Ann Arbor, MI 48106-1346

UNIVERSITY OF SASKATCHEWAN, REGINA CAMPUS

FACULTY OF GRADUATE STUDIES

CERTIFICATION OF THESIS WORK

We, the undersigned, certify that ... Larry George Boxall

.....
candidate for the Degree of .. Doctor of Philosophy in Chemistry

has presented his thesis on the subject .. Electrode Potentials

..... in Fused Alkali Metal Salts

.....
that the thesis is acceptable in form and content, and that the student

demonstrated a satisfactory knowledge of the field covered by his thesis

in an oral examination held on April 24, 1970

External Examiner S. N. Flengas*

Professor of Metallurgy and Materials Science,
University of Toronto

Internal Examiners *P. L. Eager*

..... *R. R. Siro*

..... *J. H. Wolfson*

..... *W. J. ...*

..... *M. Johnson*

..... *A. ...*

.....

.....

.....

* Approval by letter dated
April 22, 1970.

PERMISSION TO USE POSTGRADUATE THESES

Title of thesis .. Electrode Potentials in Fused Alkali ..
..... Metal Salts ..
.....
Name of Author ... Larry George Boxall ..
Division or College Chemistry, Division of Natural Sciences and
Mathematics
Degree Doctor of Philosophy in Chemistry ..

In presenting this thesis in partial fulfillment of the requirements for a postgraduate degree from the University of Saskatchewan, I agree that the Libraries of this University shall make it freely available for inspection. I further agree that permission for extensive copying of this thesis for scholarly purposes may be granted by the professor or professors who supervised my thesis work or, in their absence, by the Chairman of the Division, the Head of the Department or the Dean of the College in which my thesis work was done. It is understood that any copying or publication or use of this thesis or parts thereof for financial gain shall not be allowed without my written permission. It is also understood that due recognition shall be given to me and to the University of Saskatchewan, Regina Campus, in any scholarly use which may be made of any material in my thesis.

Signature .. *Larry G. Boxall* ..

Date .. *April 24, 1970* ..

27/9/66
100 c.

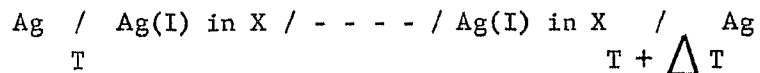
To Juli and Debbie

ABSTRACT

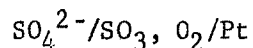
The published emf series in the alkali metal nitrite, nitrate, chloride, sulfate and carbonate melts are correlated to form a single (unified) emf series based on the standard aqueous hydrogen reference electrode at 25°C. Emf series in two different melts (X and Y) are correlated at a given temperature using the solvent junction cell:



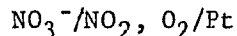
and two emf series in the same solvent, X, but at different temperatures, T and T + ΔT , are correlated using the thermoelectric cell:



The emf series in the ternary alkali metal sulfate eutectic at 550°C is extended by the development of a reversible gaseous sulfate electrode

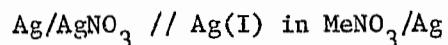


A redesigned gaseous nitrate electrode,



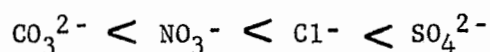
and gas control system are used to obtain values which substantiate the published potentials for the silver nitrate formation cell (250 to 400°C).

The activity coefficients, γ , for silver nitrate in six different alkali metal nitrate melts are determined as a function of temperature using the silver nitrate concentration cell:

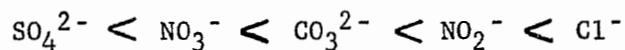


The effects of the liquid junction potential and the corrosion of the silver electrode by the nitrate melt in the concentration cell are included in the calculations. Equations interrelating the standard electrode potentials on the three concentration scales are developed using γ values to compensate for the non-ideality of the system.

The unified emf series show that at 550°C the order of stability with respect to oxidation for the anions in this study is as follows:



The silver(I) ion in the melts is only slightly stabilized by an increase in temperature or cation size, whereas a change in anion has a much greater effect; at 550°C the stability series is:



Reversible potentials ranging from 0.118 to 1.42 volts are calculated for oxyacid forming fuel cells at 550°C using the unified emf series. A lengthy review on the electrochemistry of nitrate melts and a series of density measurements on nitrate melts are also included in the investigation.

ACKNOWLEDGEMENTS

The author wishes to thank his supervisor, Dr. K.E. Johnson, for suggesting the research program and for his supervision during its completion and Professor W.B. McConnell for providing the research facilities of the University of Saskatchewan, Regina Campus.

A special vote of thanks is extended to the author's wife, Juli, for her patience, perseverance, technical assistance and typing of the thesis. The author's five-year-old daughter, Debbie, must receive a great deal of credit for her good nature and cooperation during the past year in spite of many a misplaced harsh word and being an orphan for much of the time. Without the cooperation and encouragement of the author's family, this work may have never been completed.

For their helpful discussions and encouragement, thanks is extended to the many friends in the university and in particular to Dr. K.W. Fung, Dr. J.R. Dickinson, Dr. R.W. Mise and Mr. M. Korchinski. Thanks also to Mrs. E. Murray for services above and beyond the call of duty in the running of an endless number of computer programs.

Thanks are extended to the Canadian Defence Research Board for a Grant (No. 5412-07) covering the period 1967-70, the University of Saskatchewan, Regina Campus, Chemistry Department, for a Summer Research Scholarship (1968) and the National Research Council of Canada for a Postgraduate Scholarship (1969-70) for providing financial assistance.

TABLE OF CONTENTS

Chapter		
1.	INTRODUCTION	1
	1.1 General Introduction	1
	1.2 Purpose of Investigation	2
	1.3 Experimental Approach	5
2.	PREVIOUS STUDIES ON THE PROPERTIES OF NITRITE MELTS	7
	2.1 Physical and Electrochemical Properties	7
	2.2 Electrodes and Electrode Potentials	15
	2.3 Gas Electrodes	16
3.	PREVIOUS STUDIES ON THE PROPERTIES OF NITRATE MELTS	18
	3.1 Physical Properties	18
	3.2 Chemical and Electrochemical Reactions in Nitrate Melts	23
	3.3 Electrodes and Electrode Potentials	40
	3.4 Activities and Thermodynamics of the Silver Ion in Alkali Nitrate Melts	44
	3.5 Thermoelectric Cells	56
	3.6 Gas Electrodes	67
	3.7 Aqueous// $(\text{Ag}, \text{Tl})\text{NO}_3$ Junction Potential	70
4.	PREVIOUS STUDIES ON THE PROPERTIES OF CHLORIDE MELTS	74
	4.1 Physical and Electrochemical Properties	74
	4.2 Electrodes and Electrode Potentials	79
	4.3 Activities and Thermodynamics of the Silver Ion in Alkali Chloride Melts	85
	4.4 Thermoelectric Cells	87
	4.5 Gas Electrodes	88
5.	PREVIOUS STUDIES ON THE PROPERTIES OF SULFATE MELTS	92
	5.1 Physical and Electrochemical Properties	92
	5.2 Electrodes and Electrode Potentials	96
	5.3 Gas Electrodes	96
6.	PREVIOUS STUDIES ON THE PROPERTIES OF CARBONATE MELTS	101
	6.1 Physical and Electrochemical Properties	101

6.2	Electrodes and Electrode Potentials	104
6.3	Gas Electrodes	105
6.4	Sulfate//Carbonate Solvent Junction Potentials	108
7.	RESULTS AND DISCUSSION: SILVER ACTIVITIES IN ALKALI NITRATE MELTS	111
7.1	Fundamental Equations and Definitions	111
7.2	Concentration Scales and Their Interrelationships	113
7.3	Calculation of Liquid Junction Potentials	120
7.4	Densities of Nitrate and Sulfate Melts	128
7.5	Silver Nitrate Activity Coefficients	142
7.6	Comparison of Results with Published Results	169
8.	RESULTS AND DISCUSSION: MIXED SOLVENT JUNCTION POTENTIALS	178
8.1	Nitrite//Nitrate Solvent Junction Potential	178
8.2	Nitrite-Nitrate//Nitrate Solvent Junction Potential	190
8.3	Chloride//Nitrate Solvent Junction Potential	192
8.4	Chloride//Sulfate Solvent Junction Potential	202
9.	RESULTS AND DISCUSSION: NITRATE THERMOCELLS	211
9.1	Seebeck Coefficient for Silver Nitrate	211
9.2	Dependence of Seebeck Coefficient on Concentra- tion and Temperature	214
9.3	Calculation of Thermoelectric Emfs in Nitrate and Chloride Melts	219
10.	RESULTS AND DISCUSSION: GAS ELECTRODES	223
10.1	The Emf of the Silver-Platinum Thermocouple in the Gas Electrode Systems	223
10.2	The $\text{NO}_2^-/\text{NO}_2/\text{Pt}$ Gas Electrode	226
10.3	The $\text{NO}_2^-/\text{NO}_2, \text{O}_2/\text{Pt}$ Gas Electrode	231
10.4	The $\text{SO}_4^{2-}/\text{SO}_3, \text{O}_2/\text{Pt}$ Gas Electrode	241
10.5	The $\text{H(I)}/\text{H}_2$ Gas Electrode	246
11.	CONCLUSIONS AND DISCUSSION	252
11.1	Summary of Results	252
11.2	Development of a Unified Emf Series	254
11.3	Practical Applications	267
12.	EXPERIMENTAL	271
12.1	Preparation and Purification of Melts	271

12.1.1	Nitrite melts	271
12.1.2	Nitrate melts	271
12.1.3	Chloride melts	274
12.1.4	Sulfate melts	278
12.1.5	Preparation of sodium pyrosulfate	279
12.2	Design of Isothermal Cells	283
12.3	Electrical Circuits and Measurements	290
12.4	General Operating Procedure	292
12.5	Analysis of Contents of Electrode Compartments	300
12.5.1	Nitrite analysis	302
12.5.2	Chloride analysis	302
12.5.3	Sulfate analysis	302
12.5.4	Lithium analysis	303
12.5.5	Sodium analysis	303
12.5.6	Potassium analysis	303
12.5.7	Silver analysis	307
12.6	Density Measurements	310
12.7	Nonisothermal Furnace	312
12.8	Gas Electrode Design	314
12.9	Gas Control System and Analysis	317
12.9.1	Gas purification	317
12.9.2	Gas control system	318
Appendix		
A.	COMPUTER PROGRAMS	329
B.	CALCULATION OF LIQUID JUNCTION POTENTIALS (E_J)	355
C.	CONVERSION FROM ONE CONCENTRATION SCALE TO ANOTHER FOR UNI-UNIVALENT FUSED SALT SOLUTIONS	363
REFERENCES		365

LIST OF TABLES

Table	Page
2.1 Values for the Parameters in the Conductance and Density Equations for Some Nitrite Melts	9
2.2 Values for the Parameters in Equation (2.11) for the Decomposition Potential of Some Nitrite Melts	10
3.1 Densities of Molten Nitrates	21
3.2 Activation Parameters for the Thermal Decomposition of Sodium Nitrate, Determined from the Rate Constant k , in Equation 3.11	23
3.3 Coefficients a (cal mole^{-1}) and α ($\text{cal mole}^{-1} \text{ } ^\circ\text{K}^{-1}$) for Binary Nitrate Mixtures at 350°C	55
3.4 Measured Potentials of the Electrochemical Cells 3.166 - 3.168	71
7.1 Conversion Between Concentration Scales	114
7.2 Calculated Liquid Junction Potentials, E_J , for the Cell: $\text{Ag}/\text{AgNO}_3//\text{Ag(I)}$ in MeNO_3/Ag	121
7.3 Volume of Silver Bob as Function of Temperature	129
7.4 Density of (0.54 Li, 0.46 Na) NO_3 Eutectic	131
7.5 Density of (0.41 Li, 0.59 K) NO_3 Eutectic	132
7.6 Density of (0.59 Li, 0.41 K) NO_3 Mixture	132
7.7 Density of (0.45 Na, 0.55 K) NO_3 Eutectic	133
7.8 Density of (0.78 Li, 0.085 Na, 0.135 K) $_2\text{SO}_4$ Eutectic	133
7.9 Density Parameters for the Equation: $D = a - b \times 10^{-4} T^\circ\text{C}$ (gms cm^{-3})	138
7.10 Densities of Nitrate and Sulfate Melts at Selected Temperatures	140

Table	Page
7.11 Computer Correction for Corrosion of Silver Electrode in (0.59 Li, 0.41 K)NO ₃ Mixture at 300°C	147
7.12 Corrosion of Silver in Nitrate Melts	148
7.13 Activity Coefficient, $\gamma_{N=0}$, of AgNO ₃ on Mole Fraction Scale at Infinite Dilution	168
7.14 Work Constant W (cal mole ⁻¹) and Coefficient α (cal mole ⁻¹ deg ⁻¹) for Binary Nitrate Mixtures at 350°C	172
8.1 Potentials for the Solvent Cell: Ag/Ag(I) in NaNO ₂ //Ag(I) in NaNO ₃ /Ag at 309 ± 2°C	182
8.2 Potentials at 309 ± 2°C for the Cell: Ag/Ag(I) in NaNO ₂ //Ag(I) in NaNO ₃ /Ag	185
8.3 Silver Concentration Cell with Different Cell Solvents at 309 ± 2°C	186
8.4 Standard Potentials at 309 ± 2°C for the Cell: Ag/Ag(I) in NaNO ₃ (100-X), NaNO ₂ (X)//Ag(I) (0.030 m) in NaNO ₃ /Ag	191
8.5 Potentials at 400 ± 2°C for the Solvent Cell: Ag/Ag(I) in (Li,K)Cl//Ag(I) in (Li,K)NO ₃ /Ag	196
8.6 Potentials at 400 ± 2°C for the Cell: Ag/Ag(I) in (Li,K)Cl//Ag(I) in (Li,K)NO ₃ /Ag	199
8.7 Temperature Dependence of the Potential of the Solvent Cell: Ag/Ag(I) in (Li,K)Cl//Ag(I) in (Li,K)NO ₃ /Ag	199
8.8 Potentials at 550 ± 2°C for the Solvent Cell: Ag/Ag(I) in (Li,K)Cl//Ag(I) in (Li,Na,K) ₂ SO ₄ /Ag	206
8.9 Potentials at 550 ± 2°C for the Cell: Ag/Ag(I) in (Li,K)Cl//Ag(I) in (Li,Na,K) ₂ SO ₄ /Ag	209
9.1 Seebeck Coefficient as a Function of Silver Nitrate Concentration at 350 ± 2°C	217

Table	Page
9.2 Values of ϵ_T^0 as a Function of Temperature	219
10.1 Polynomial Fit for the Emf of the Ag-Pt Thermo- couple as a Function of the Temperature	225
10.2 The Emf of the Ag-Pt Thermocouple with a Reference Junction at 0°C	225
10.3 The Potentials at $270 \pm 2^\circ\text{C}$ for the Cell: Ag/Ag(I) (0.030 m) in (Na,K)NO ₃ //(Na,K)NO ₃ /NO ₂ , O ₂ /Pt	232
10.4 Potentials at $270 \pm 2^\circ\text{C}$ for the Cell: Ag/Ag(I) (0.030 m) in (Na,K)NO ₃ //(Na,K)NO ₃ /NO ₂ , O ₂ /Pt	234
10.5 Standard Cell Potentials for the Cell Ag/Ag(I) in (Na,K)NO ₃ //(Na,K)NO ₃ /NO ₂ , O ₂ /Pt As a Function of Temperature	238
10.6 Potentials at $550 \pm 2^\circ\text{C}$ for the Cell Ag/Ag(I) (1.0 m) in (Li,Na,K) ₂ SO ₄ //(Li,Na,K) ₂ SO ₄ /SO ₃ , O ₂ /Pt	243
10.7 Standard Potentials at $550 \pm 2^\circ\text{C}$ for the Cell: Ag/Ag(I) in (Li,Na,K) ₂ SO ₄ //(Li,Na,K) ₂ SO ₄ /SO ₃ , O ₂ /Pt	244
10.8 Standard Cell Potentials for the Cell: H ₂ /H(I) in (Li,K)Cl//LiCl/Cl ₂ /C	249
10.10 Standard Cell Potentials for the Cell: Ag/Ag(I) in (Li,K)Cl//H(I) in (Li,K)Cl/H ₂ /Pt	250
10.11 Standard Cell Potentials at 450°C for the Cell: Ag/Ag(I) in (Li,K)Cl//LiCl/Cl ₂ /C	251
11.1 Electrochemical Cells Used to Develop Unified EMF Series	256
11.2 Unified EMF Series for Molten Salts	259
11.3 Corrected Standard Electrode Potentials in (Li,Na) ₂ CO ₃ from Reference (135)	260
11.4 Corrected Standard Electrode Potentials in (Li,Na) ₂ SO ₄ from Reference (136)	260

Table		Page
11.5	Standard Cell Potentials for the Cell: Ag/Ag(I) in (Na,K)NO ₃ //Ag(I) in MeNO ₃ /Ag	262
11.6	Standard Silver(I)/Silver Electrode Potentials in Nitrate Melts Versus a Standard Aqueous Hydrogen Reference Electrode at 25°C	263
11.7	Stability of Silver(I) in Several Fused Alkali Metal Salts at 550°C	266
11.8	Formation Potentials of Oxyacids	269
12.1	Fixed Points for Calibration of Thermocouple	290
12.2	Analytical Results for the Analysis of Various Melts for Alkali Metals	304
12.3	Analysis of Gas Mixture for SO ₃	328

LIST OF ILLUSTRATIONS

Figure		Page
7.1	Calculated Liquid Junction Potentials, E_J , for a Ag(I) in LiNO_3 Concentration Cell	122
7.2	Calculated Liquid Junction Potentials, E_J , for a Ag(I) in NaNO_3 Concentration Cell	123
7.3	Calculated Liquid Junction Potentials, E_J , for a Ag(I) in KNO_3 Concentration Cell	124
7.4	Calculated Liquid Junction Potentials, E_J , for a Ag(I) in (0.54 Li, 0.46 Na) NO_3 Concentration Cell	125
7.5	Calculated Liquid Junction Potentials, E_J , for a Ag(I) in (0.59 Li, 0.41 K) NO_3 Concentration Cell	126
7.6	Calculated Liquid Junction Potentials, E_J , (0.45 Na, 0.55 K) NO_3 Concentration Cell	127
7.7	Calibration of Silver Bob for Density Measurements	130
7.8	Density of (0.54 Li, 0.46 Na) NO_3 Eutectic Versus Temperature	134
7.9	Density of (0.41 Li, 0.59 K) NO_3 Eutectic Versus Temperature	135
7.10	Density of (0.59 Li, 0.41 K) NO_3 Mixture Versus Temperature	136
7.11	Density of (0.45 Na, 0.55K) NO_3 Eutectic Versus Temperature	137
7.12	Nernst Plot at 300°C for the Cell: $\text{Ag}/\text{AgNO}_3 // \text{Ag(I) in (Li,K)NO}_3/\text{Ag}$	144
7.13	Time Scale for Calculation of Silver Corrosion in Nitrate Melts	145

Figure		Page
7.14	Activity Coefficient, γ , for Ag(I) in LiNO ₃ at 300°C	150
7.15	Activity Coefficient, γ , for Ag(I) in LiNO ₃ at 350°C	151
7.16	Activity Coefficient, γ , for Ag(I) in LiNO ₃ at 400°C	152
7.17	Activity Coefficient, γ , for Ag(I) in NaNO ₃ at 300°C	153
7.18	Activity Coefficient, γ , for Ag(I) in NaNO ₃ at 350°C	154
7.19	Activity Coefficient, γ , for Ag(I) in NaNO ₃ at 400°C	155
7.20	Activity Coefficient, γ , for Ag(I) in KNO ₃ at 300°C	156
7.21	Activity Coefficient, γ , for Ag(I) in KNO ₃ at 350°C	157
7.22	Activity Coefficient, γ , for Ag(I) in KNO ₃ at 400°C	158
7.23	Activity Coefficient, γ , for Ag(I) in (Li,Na)NO ₃ at 300°C	159
7.24	Activity Coefficient, γ , for Ag(I) in (Li, Na)NO ₃ at 350°C	160
7.25	Activity Coefficient, γ , for Ag(I) in (Li,Na)NO ₃ at 400°C	161
7.26	Activity Coefficient, γ , for Ag(I) in (Li,K)NO ₃ at 300°C	162
7.27	Activity Coefficient, γ , for Ag(I) in (Li,K)NO ₃ at 350°C	163
7.28	Activity Coefficient, γ , for Ag(I) in (Li,K)NO ₃ at 400°C	164
7.29	Activity Coefficient, γ , for Ag(I) in (Na,K)NO ₃ at 300°C	165

Figure		Page
7.30	Activity Coefficient, γ , for Ag(I) in (Na,K)NO ₃ at 350°C	166
7.31	Activity Coefficient, γ , for Ag(I) in (Na,K)NO ₃ at 400°C	167
7.32	The Calculated Liquid Junction Potential, E _J , Versus (1-N) ² at 350°C	174
8.1	AgNO ₂ in NaNO ₂ Concentration Cell at 309 ± 2°C	179
8.2	AgNO ₃ in NaNO ₃ Concentration Cell at 309 ± 2°C	180
8.3	Nernst Plot at 309°C for the Solvent Cell	184
8.4	Standard Potential at 309°C for the Solvent Cell: Ag/Ag(I) in (N)NaNO ₂ + (100-N)NaNO ₃ //Ag(I) in NaNO ₃ /Ag	191
8.5	AgCl in (Li,K)Cl Concentration Cell at 400 ± 2°C	193
8.6	AgNO ₃ in (Li,K)NO ₃ Concentration Cell at 400 ± 2°C	194
8.7	Nernst Plot at 400°C for the Solvent Cell: Ag/Ag(I) in (Li,K)Cl//Ag(I) in (Li,K)NO ₃ /Ag	198
8.8	Temperature Dependence of the Potential for the Solvent Cell: Ag/Ag(I) in (Li,K)Cl//Ag(I) in (Li,K)NO ₃ /Ag	201
8.9	AgCl in (Li,K)Cl Concentration Cell at 550 ± 2°C	204
8.10	Ag ₂ SO ₄ in (Li,Na,K) ₂ SO ₄ Concentration Cell at 550 ± 2°C	205
8.11	Nernst Plot at 550°C for the Solvent Cell: Ag/Ag(I) in (Li,K)Cl//Ag(I) in (Li,Na,K) ₂ SO ₄ /Ag	208
9.1	EMF of Dilute Silver Nitrate Thermal Cell	216
9.2	Seebeck Coefficient at 350 ± 2°C Versus Silver(I) Concentration	218
10.1	EMF of Ag-Pt Thermocouple Versus Temperature	224

Figure		Page
10.2	EMF of Silver Nitrite Formation Cell at 270 ± 2°C Versus Log (P _{NO₂})	228
10.3	EMF of Silver Nitrite Formation Cell at 270 ± 2°C Versus Time	229
10.4	Silver Nitrate Formation Cell at 270 ± 2°C Versus Total Flow Rate of NO ₂ + O ₂	233
10.5	EMF of Silver Nitrate Formation Cell at 270 ± 2°C Versus Log $\left[\begin{matrix} P_{NO_2} & P_{O_2}^{1/2} \end{matrix} \right]$	236
10.6	Standard Potential of Silver Nitrate Formation Cell Versus Temperature	239
10.7	EMF of Silver Sulfate Formation Cell at 550 ± 2°C Versus Log $\left[\begin{matrix} P_{SO_3} & P_{O_2}^{1/2} \end{matrix} \right]$	245
12.1	Melt Preparation Tube Furnace	272
12.2	Chloride Eutectic Purification Apparatus	275
12.3	Vacuum Line for Chloride Purification	276
12.4	Polarogram of (Li,Na,K) ₂ SO ₄ Eutectic Melt at 550°C	280
12.5	Reaction Vessel to Prepare Na ₂ S ₂ O ₇	281
12.6	Isothermal Electrochemical Cell	284
12.7	Electrical Heating Circuit for Isothermal Furnace	286
12.8	Electrode Holder	289
12.9	Electrical Measuring and Generating Circuit for Isothermal Cell	293
12.10	System for Filling Electrode Compartments	294
12.11	Apparatus to Fill Electrode Compartments with Chloride Melt	298

Figure		Page
12.12	Polarogram of (Li,K)Cl Eutectic Melt at 450°C	301
12.13	Calibration Curve for Lithium Analysis by Atomic Absorption	305
12.14	Calibration Curve for Sodium Analysis by Flame Photometry	306
12.15	Calibration Curve for Potassium Analysis by Flame Photometry	308
12.16	Calibration Curve for Silver Analysis by Atomic Absorption	309
12.17	Density Apparatus	311
12.18	Cell for Thermoelectric Studies	313
12.19	Design of Gas Electrode	315
12.20	Nitrogen Dioxide Flow Meter	319
12.21	Calibration Curve for Nitrogen Flow Meter	320
12.22	Calibration Curve for Oxygen Flow Meter	321
12.23	Calibration Curve for Nitrogen Dioxide Flow Meter	323
12.24	Apparatus to Control P _{SO₃}	326

1. INTRODUCTION

1.1 General Introduction

Molten salts provide the chemist with a group of high-temperature solvents for systems operating at temperatures from a few degrees above room temperature up to 3000°C. The melts range from the simplest ionic liquids, such as the alkali metal halides, through the less simple oxy-anion melts such as the alkali metal nitrates, sulfates and carbonates to the often complex associated liquids such as molten phosphates, borates and silicates. In each case, the ionic character of the crystalline solid persists in the molten state, although local association reactions may take place. The wide variety in the structure and ionic nature of the many inorganic salts plus the almost complete miscibility for most of the melts provide the electrochemist with a group of solvents with conductivities ranging from zero to 500 times greater than the conventional aqueous electrolytes, and viscosities from 0.1 cp to 10^5 poise. Military and industrial establishments have used fused salts as moderators in nuclear reactors and as electrolytes in high temperature fuel cells and for the production of metals, particularly those which cannot be electrodeposited from aqueous and non-aqueous solutions at room temperature.

The growing interest in and use of molten salts, as testified to by the near exponential increase in literature on the subject since

the 1930s, has resulted in the publication of several books (1 - 3) and noteworthy reviews (4 - 7) devoted to the subject. Janz (8) and Blomgren (9) have recently reviewed the current status of the theories of fused salt solutions and their compatibility with experimental data. Many of the reviews have been devoted to specific aspects of the electrochemistry of melts, such as the emf of equilibrium cells (4, 10 - 14), the various types of electrodes (10, 14 - 16), electrode kinetics (17) and the electroanalytical techniques (5, 6). Much of the Russian literature for the years 1959 to 1965, which is normally unavailable, has been surveyed in a series of annual reviews (18). The modern uses of molten salts is exemplified by the survey by Cohn (19) in 1966 on the use of molten salt fuel cells in the past, present and future space program of the United States. He also included performance data on the various systems used in the Gemini and Apollo space programs.

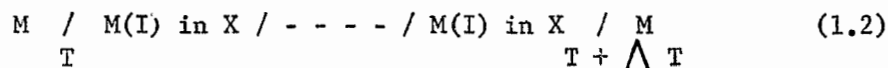
1.2 Purpose of Investigation

This study was initiated to examine the potential of an electrode in a fused salt system as a function of the nature of the solvent and the temperature of the electrochemical cell. From the data of this investigation it was possible to correlate the emf series which have been established for the various melts and in order to complete the data it was necessary to examine several gaseous electrodes which are reversible to the anion of the solvent and the non-ideality of the silver(I) ion in the alkali nitrate melts. The literature on the

electrochemistry of the alkali metal nitrite, nitrate, chloride, sulfate and carbonate melts, through December 1969, is reviewed in chapters two through six with an emphasis on the alkali metal nitrate melts in chapter three. (No general survey of the nitrate literature has previously been made.) This review shows that extensive emf series have been reported for many different melts at a variety of temperatures (20) depending upon the melting point of the solvent. One of the purposes of this investigation is to correlate the emf series in one solvent, X, with that in another solvent, Y, by the use of a solvent junction cell, at a given temperature, of the type:



If there is a temperature change as well, then an additional thermal cell in one of the solvents is required to connect the two temperatures, T and T + ΔT .



The use of these two types of cells makes it possible to relate all the electrode potentials in the different melts to one common reference electrode in a given solvent and at a given temperature (e.g., the standard aqueous hydrogen electrode at 25°C).

A second purpose of this investigation is to develop or improve gaseous electrodes which are reversible to the anion in the melt. The halogen, carbonate, nitrate and nitrite anion gas electrodes have been investigated and reported, although certain aspects of the latter two are questionable. No report could be found in the literature on a

reversible sulfate gas electrode involving the electrode reaction



In the measurement of formation potentials for many metal salts, reliable anion electrodes are essential. These electrodes are also the most favorable, thermodynamically, for emf measurements in the particular solvent.

The third purpose is to calculate the formation potentials of several oxyacids at elevated temperatures with the aid of the solvent junction cells, the hydrogen electrode potential in the lithium-potassium chloride eutectic and the oxyanion gas electrode potentials. The normal sequence that occurs in the direct measurement of the formation of nitric acid is



and the net thermodynamic values obtained are for the formation of water (equation 1.6). In the electrochemical cell, the nitric acid is never allowed to form and only the thermodynamics of reaction 1.4 are measured.

The practical application of this investigation is that it points out the feasibility of the development of gaseous fuel cell systems. The change from one solvent to another in one half of an electrochemical cell will increase the emf of a single solvent system by several hundred millivolts. The development of one uniformly based emf series

for all electrodes, temperatures and solvents will be a significant contribution to the entire field of electrochemistry in molten salts.

1.3 Experimental Approach

The investigation was limited to the alkali nitrite, nitrate, chloride and sulfate melts since either their pure melts or eutectics are molten below 560°C, the upper temperature limit of Pyrex glass. To work at higher temperatures more complex furnaces and Vycor glass-ware would have to be used throughout the system. The major part of the literature on molten salts deals with these low melting salts.

The silver(I)/silver electrode was used throughout this investigation because it is common to all the molten salt emf series compiled by Plambeck (20) as well as being the most common practical reference electrode. Also, the silver(I)/silver electrode is stable over a large range of temperatures and can be easily prepared by anodizing silver wire in the melt.

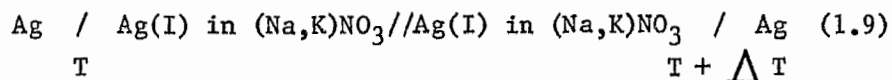
In order to make the required thermodynamic calculations, it was necessary to determine the activity coefficients for the silver ion in various melts (chapter seven) by studying the cell:



The results for the measurements on the silver solvent junction cells



and the silver thermal cells



are presented in chapters eight and nine respectively. A new type of platinum gas electrode and gas measuring and mixing system are reported in chapter ten along with data for the $\text{NO}_2^-/\text{NO}_2/\text{Pt}$, the $\text{NO}_3^-/\text{NO}_2$, O_2/Pt , the Cl^-/HCl , H_2/Pt and the $\text{SO}_4^{2-}/\text{SO}_3$, O_2/Pt gas electrodes. In chapter eleven the data from the previous chapters (seven through ten) and the literature review (chapters two through six) are used to develop a unified emf series for five melts and temperatures up to 550°C based on the standard hydrogen electrode at 25°C . The formation potentials for nitric, sulfuric and carbonic acids were calculated from the gaseous electrode potentials and reported in the final chapter.

2. PREVIOUS STUDIES ON THE PROPERTIES OF NITRITE MELTS

2.1 Physical and Electrochemical Properties

The published data on the physical and chemical properties of the molten alkali nitrites is much less than that for the nitrate systems. The absence of data on the nitrite systems is largely due to the experimental difficulties (e.g., the ease of oxidation to nitrate and the problems of drying the materials) in working with molten nitrites. Extensive binary and ternary phase diagrams involving alkali and alkaline earth nitrites have been published by Protesenko and co-workers (21 - 25). Their studies show that all the alkali nitrites except lithium nitrite are thermally stable up to temperatures about 100°C above their melting points (26). The presence of platinum acts as a catalyst for thermal decomposition and lowers the decomposition temperature.

Oza and Walawalkar (27) have studied the thermal decomposition of sodium and potassium nitrites and found that nitrites undergo decomposition in the initial stage as:



By studying the effects of nitric oxide, oxygen and nitrogen dioxide on the end products they concluded that the following secondary reactions must occur:





If reaction (2.3) proceeds at a moderate rate, then this chemical reaction will prevent the formation of a reversible $\text{NO}_2^-/\text{NO}_2$ gas electrode which is discussed later in this chapter (see section 2.3).

This proposed mechanism was challenged by Freeman's results (28) where the main product was found to be nitrogen with some oxygen and very little nitric oxide. Bond and Jacobs (29) pointed out that this discrepancy may be partly due to the different reaction vessels used by the investigators: Freeman used a platinum vessel whereas the other workers used an all-glass system. This suggests that the decomposition may be, in part, an heterogeneous reaction. Bond and Jacobs considered two possible reactions:



Since there is only a small amount of nitric oxide in the products, reaction (2.6) must be the major route.

The electrical conductance, k , (26) and density, D , (30) for all the pure alkali metal nitrites, as a function of the temperature, have been reported in the literature. The two properties are a linear function of the temperature and are given by the general formulas:

$$k = a + b \times 10^{-4} T \quad (2.7)$$

$$D = a' + b' \times 10^{-4} T \quad (2.8)$$

The constants for the five nitrite salts are summarized in Table 2.1.

TABLE 2.1

VALUES FOR THE PARAMETERS IN THE CONDUCTANCE
AND DENSITY EQUATIONS FOR SOME NITRITE MELTS

Parameter	LiNO ₂	NaNO ₂	KNO ₂	RbNO ₂	CsNO ₂
a (ohm ⁻¹ cm ⁻¹)	-0.685	-0.130	-0.280	-1.673	-0.282
b (ohm ⁻¹ cm ⁻¹ deg C ⁻¹)	60.0	51.6	34.8	57.7	24.3
a' (gm cm ⁻³)	1.739	1.976	1.993	2.696	3.258
b' (gm cm ⁻³ deg C ⁻¹)	-4.60	-6.18	-6.76	-8.25	-10.14

The equivalent conductance, Λ , for a molten electrolyte is given by

$$\Lambda = M k / D \quad (2.9)$$

where M is the equivalent weight of the salt. This equation follows from the classical definition

$$\Lambda = 1000 k / C \quad (2.10)$$

when it is applied to the upper limit of concentration for the electrolyte, i.e., the state of the single-salt melt as the electrolyte.

The transport numbers, t_+ , for the cations in sodium and potassium nitrite were measured by Duke and Victor (31) and found to be 0.75 ± 0.10 and 0.62 ± 0.06 , respectively. In both cases the t_+ was slightly larger than that for the corresponding nitrate salts. Unfortunately, the workers did not state the temperature at which the measurements were made or if the t_+ was a function of the temperature.

The electrochemical reduction of the pure nitrite melts has been discussed in several papers. Bartlett and Johnson (32) have reported

that the reduction process in the nitrite melt is as complex as that which occurs in the nitrate melts (chapter 3.2, page 23). The melt around the platinum cathode turned red at first and then green with the evolution of gas during the electrolysis of sodium nitrite (302°C) at a potential of -1.5 volts versus a silver(I)/silver reference electrode. The decomposition potential of the single-salt nitrite melts was found to be a function of the anode material by Protsenko and Protsenko (33). The decomposition potential for the alkali metal nitrite melts is given by the general equation

$$E_t = E_{t_0} + \frac{\Delta E}{\Delta t} (t - t_0) \times 10^{-3} \quad (2.11)$$

and the parameters for the five salts are summarized in Table 2.2.

TABLE 2.2

VALUES FOR THE PARAMETERS IN EQUATION (2.11) FOR THE DECOMPOSITION POTENTIAL OF SOME NITRITE MELTS

Salt	E_{t_0} (Volts)	t_0 (°C)	$\Delta E/\Delta T$	Anode Material
LiNO ₂	3.18	260	-2.17	Pt
	2.94	260	-3.58	C
NaNO ₂	1.70	360	-3.10	Pt
	1.50	360	-3.30	C
KNO ₂	1.44	460	-8.71	Ag
RbNO ₂	1.46	460	-4.79	Pt
CsNO ₂	1.59	460	-4.94	Pt

They proposed that the metal ion was reduced to the metal at the cathode



and that the nitrite ion was oxidized to form nitrate ion and nitric oxide at the anode:



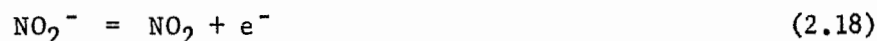
Two additional reactions which involve the active alkali metal produced at the cathode may occur to form various products:



The use of a carbon anode permits the possibility of two additional reactions which may explain the change in the decomposition potential:



The kinetics for the oxidation of the nitrite ion on both platinum (34) and graphite (35) have been reported in the literature. The overall anodic reaction on platinum is:

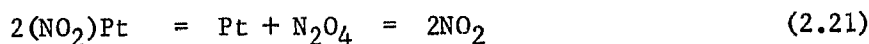


which, although at variance with the Russian workers (33), has been confirmed by several other investigators (36 - 38). The kinetic parameters were determined from current-voltage curves using pure nitrites and nitrites dissolved in a 1:1 sodium-potassium nitrate mixture. To interpret the electrode process which produces nitrogen dioxide from the oxidation of the nitrite ion on platinum, it was assumed that there was a single adsorbed intermediate. The proposed mechanism was

as follows:

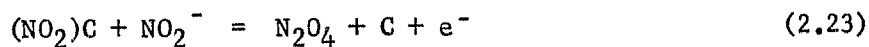


or

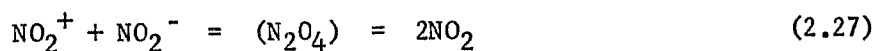


The adsorption of the intermediates was discussed in terms of both the Langmuir and the Temkin isotherms and similar conclusions were reached for each model. Although both reactions (2.20) and (2.21) are possible reaction paths, the type of reaction entities and the temperature involved in the system indicates that the former would be the most probable.

The analysis of the kinetics of the oxidation of nitrite ions on a graphite anode (35) produced two reaction schemes of which the first is closely related to that for the platinum anode (34). The two reaction schemes, in which either reaction (2.23) or (2.26) is the rate-determining step, assuming a low electrode surface coverage by reaction intermediates, are as follows:



and



The scatter of the results was interpreted as the consequence of the diffusion of nitrogen dioxide through the porous electrode material. The existence of the nitryl ion, NO_2^+ , in the reaction (2.26) has been the subject of much controversy and will be discussed in chapter 3.2 (page 23).

The electrochemical behavior of the nitrite ion and nitrogen dioxide in nitrate melts has been the subject of many recent papers. Swofford and McCormick (38) reported the oxidation of the nitrite ion in the sodium-potassium nitrate eutectic at 250°C occurring in the region of +0.2 to +1.0 volts versus a 0.07 M silver(I)/silver reference electrode. A plot of E vs $\log\left(\frac{i}{i_d - i}\right)$ yielded a value for the half wave potential ($E_{\frac{1}{2}}$) of +0.476 volts and verified that the oxidation was a one electron process. The height of the polarogram produced by the nitrite ion was shown to be directly proportional to the amount of sodium nitrite added or the amount of nitrate electrically reduced to nitrite (39).

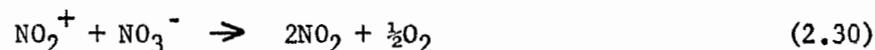
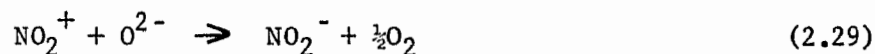
In a more recent paper McCormick and Swofford (37) used coulometric experiments to establish that the oxidation of nitrite to nitrogen dioxide was also a one electron process. It was thought that the low solubility of nitrogen dioxide $[5 \pm 3 \times 10^{-3} \text{ M at } 300^\circ\text{C} (40)]$ was responsible for the previous report of its inactivity (38). McCormick and Swofford (37) saturated the melt with nitrogen dioxide and left it for eighteen hours to equilibrate. They found that the nitrogen dioxide was active and it was the slow rate of dissolving in the melt that presented the erroneous interpretation of results. The oxidation of

the nitrite ion was shown (37) to be reversible by the wave analysis of current-voltage curves and chronopotentiograms. The low rate of solution for the gas interfered with the forward-to-reverse transition time ratio in the chronopotentiometric studies. The ratio varied from 6:1 at low current densities to 4:1 at high current densities while the expected ratio ($\approx 3:1$) was never realized.

As well as supporting the claim by Topol et al. (40) that the oxidation process is reversible, McCormick and Swofford (37) verified their proposed reaction between nitrogen dioxide and the nitrite ion.



Inman and Braunstein (41) found no evidence to support the existence of the nitryl ion, NO_2^+ , which might result from a further oxidation of nitrogen dioxide adsorbed on the electrode surface. They proposed that the nitryl ion would react rapidly with oxide (in the melt or on the platinum surface) or nitrate ion.



If the nitrogen dioxide had been adsorbed on the electrode, the chronopotentiometric forward-to-reverse time ratio should have approached unity instead of the 4:1 ratio. The second oxidation wave mentioned by Inman and Braunstein was completely absent in all of the studies performed by McCormick and Swofford (37). Topol et al. (40) have also claimed the existence of the nitryl ion in the acid-base dissociation of the nitrate ion.

2.2 Electrodes and Electrode Potentials

The use of metal electrodes in molten nitrites has been limited to platinum and silver. Calandra and Arvia (36) reported that the silver(I)/silver reference electrode in molten sodium nitrite was unstable due to chemical decomposition. The handbook (42) lists the decomposition temperature of silver nitrite as 140°C and most of the electrochemical cells were operated at about 300°C. Calandra and Arvia used a silver(I)/silver electrode in sodium nitrate-potassium nitrate melt which was connected to the nitrite melt by a Luggin Haber capillary. The diffusion of nitrite into the nitrate melt after a period of several hours caused chemical decomposition to occur (34). They found the best reproducible results were obtained by dipping a platinum wire into a nitrite melt saturated with nitrogen dioxide which was formed in situ by electrolysis.

Bartlett and Johnson (32) developed a silver(I)/silver electrode in sodium nitrite by anodizing the silver wire with a current efficiency of 100%. The silver electrode was found to be stable and the slope of the Nernst plot for a concentration cell experiment in sodium nitrite at 302°C was in agreement with the theoretical value. Bartlett (43) attempted to produce other metal ions in solution by anodic generation but it was found that oxidation of the melt preceded the anodic dissolution of the metal. A gas was evolved when cobalt, nickel and iron were anodically polarized in the melt. A white sludge was produced when magnesium was anodized. Platinum anodes became corroded after prolonged use and the color of the melt in the anode

compartments became green.

A reversible sodium(I)/sodium electrode in sodium nitrite has been reported by Calandra and Arvia (36, 44). The liquid sodium was formed in the cathode compartment by the electrolysis of the sodium nitrite melt using platinum electrodes at a current density ranging from 50 to 200 mA cm⁻². There is not enough thermodynamic data available to calculate ΔG° for the reaction:



However, the ΔG_{600}° was calculated to be -173.7 kcal mole⁻¹ (32) for the corresponding reaction in sodium nitrate.



This large negative value for ΔG_{600}° would suggest that the existence of the reversible sodium(I)/sodium electrode is questionable.

2.3 Gas Electrodes

Calandra and Arvia (36, 44) measured the potential of the sodium nitrite formation cell by electrolyzing the melt to produce a sodium electrode and a nitrite electrode. The Tafel slope taken from the current-voltage curves run on the nitrite electrode at 277°C was 109 ± 5 mV (≈ 2.303 RT/F) which indicates that the transfer coefficient, α , must be unity. The potential of the reversible nitrite electrode was also measured against a silver electrode in a 1:1 sodium-potassium nitrate mixture. The results of the different cells were as follows:

$$\text{Ag/Ag(I) in (Na,K)NO}_3//\text{NaNO}_2/\text{NO}_2/\text{Pt} \quad E_{306}^{\circ}\text{C} = -0.550\text{v} \quad (2.32)$$

$$\text{Na/NaNO}_2/\text{NO}_2/\text{Pt} \quad E_{306}^{\circ}\text{C} = 2.720\text{v} \quad (2.33)$$

Unfortunately, there is not enough thermodynamic data available to calculate the theoretical E^0 for sodium nitrite.

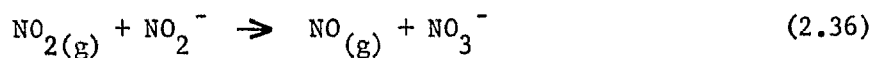
The nitrite electrode behaved ideally according to the Nernst equation when the nitrite and nitrogen dioxide concentrations were varied.



$$E = E^0 - \frac{RT}{F} \ln \frac{[\text{NO}_2^-]}{P_{\text{NO}_2}} \quad (2.35)$$

The nitrite concentration in a nitrate melt was varied by controlled reduction of the nitrate ion; oxide ion was also produced in the reduction of the nitrate ion but it is not known if it would interfere with the electrode reaction. The partial pressure of the nitrogen dioxide was lowered by sweeping the melt with nitrogen; however, poor results were obtained. A change of P_{NO_2} from 1 to 0.1 atm. reduced the potential by only 0.10 to 0.12 volts, whereas the theoretical reduction in potential is 0.111 volts.

If the nitrite electrode exists, there is a serious question whether it has any thermodynamic meaning. Several research teams have verified that nitrogen dioxide will enter into a direct chemical reaction with the nitrite ion (37, 43, 45).



The reaction would be greatly suppressed in dilute solutions of nitrite in nitrate; however, in pure nitrite melts the reaction would be present to a considerable degree. The existence of this side reaction would produce a mixed electrode reaction and make any thermodynamic analysis very difficult.

3. PREVIOUS STUDIES OF THE PROPERTIES OF NITRATE MELTS

3.1 Physical Properties

In molten salt studies the nitrate salts of the alkali metals have been used extensively as the solvent due to the ease of purification and handling and the low melting points of nitrate melts. The sodium and potassium salts have been the preferred solvents in past research due to the corrosive properties of lithium nitrate. The three pure nitrates melt between 270°C and 350°C, whereas their mixtures or eutectics have a much lower melting point. The 50:50 mole mixture of sodium-potassium nitrate melts at 220°C has been widely used in molten salt research. Janz (2) has tabulated the physical properties of most of the pure nitrate salts and Protsenko *et al.* (46) have reviewed the properties of nitrate mixtures. The purification technique and criterion for purity of nitrate melts has been discussed by several workers (39, 47). The general procedure is to oven-dry the salts, heat to melting, filter and purge with nitrogen for several hours. The criterion for purity as used by Swofford and Laitinen (39) was a residual current of less than 0.5 μ amp at an applied potential of -0.8 volts versus a 0.07 molal silver(I)/silver reference electrode using a platinum micro electrode (area = 10^{-3} cm²).

The structure of molten nitrates and the effective interionic distances discussed by James (48) was used by Kleppa and Hersh (49,

50) in their study on the heat of mixing in binary melts. They have reviewed the past literature on binary mixtures and developed the following general formula which relates the heat of mixing, ΔH^M , to the lattice energy, U , of the mixture and the interionic distance, d , in the two pure components.

$$\Delta H^M \approx -N(1 - N) U \left[\frac{d_1 - d_2}{d_1 + d_2} \right]^2 \quad (3.1)$$

From the equation in which N is the mole fraction of one of the components, it can be seen that ΔH^M increases as the difference between the ion sizes in the mixture increases and that ΔH^M reaches a maximum in a 50:50 mixture. The maximum value for ΔH^M in the lithium-sodium nitrate mixture is approximately 120 cal mole⁻¹ and in the lithium-potassium nitrate mixture it is approximately 480 cal mole⁻¹. Blander (1) has summarized the parameters for most binary mixtures of the nitrate salts of silver, thallium and the alkali metals. The heats of mixing silver nitrate with seven different binary alkali nitrate mixtures have been measured by Meschel and Kleppa (51). The viscosity of binary mixtures has also been related to the ion sizes by Murgulescu and Zuca (52). In a series of papers Isbell et al. (53) studied the cryoscopic behavior of solutes in molten alkali nitrates to determine the stability constants for complexes in nitrate melts. Their results were found to be in agreement with those obtained by spectrophotometric and electrical methods. The average value for the freezing point depression constant for lithium nitrate was 6.3 ± 0.1 degrees per mole of foreign ion.

The thallium nitrate-silver nitrate eutectic has the advantage of a very low melting point (82.2°C) (2) but the disadvantage of poisonous thallium vapors. The vapor pressure of pure thallium nitrate at 300°C is 5.6×10^{-3} mm Hg (54), whereas the vapor pressures of the alkali and silver nitrates are at least a factor of 100 below this value (55). Peleg (56) used a voltammetric method of analysis to determine the amount of water in the molten alkali nitrates as a function of its vapor pressure above the melt. He found that the water obeyed Henry's law with a constant, K_p , ranging from about 10^{-4} for lithium nitrate to a low of 10^{-6} mole water (mole solvent) $^{-1}$ (mm P) $^{-1}$ for potassium nitrate. An increase in temperature from 310°C to 370°C reduces the K_p value for lithium nitrate by a factor of over 2. By comparison the K_p value for nitrogen in sodium nitrate at 370°C is 1.31×10^{-7} moles nitrogen gas (mole melt) $^{-1}$ (mm P) $^{-1}$.

The densities of pure nitrate melts have been well tabulated (2) but, unfortunately, those of the binary mixtures are scattered throughout the literature and some systems have not been studied. The values for the parameters in the general density equation,

$$D = a - bT \quad (3.2)$$

are tabulated in Table 3.1 for the eutectics and mixtures which will be used in this current research. The density of the lithium-sodium nitrate eutectic (0.54:0.46) and mixture (0.59:0.41) have not been determined as of this date. The molar volumes were found to be additive to $\pm 1\%$ for most alkali nitrate and halide systems (57). The general formula used to calculate the molar volume, V , of a mixture

containing lithium, potassium, chloride and nitrate ions is as follows:

$$V = X_{K^+} X_{Cl^-} V_{KCl}^0 + X_{K^+} X_{NO_3^-} V_{KNO_3}^0 + X_{Li^+} X_{Cl^-} V_{LiCl}^0 + X_{Li^+} X_{NO_3^-} V_{LiNO_3}^0 \quad (3.3)$$

where X is the ion fraction and V^0 is the molar volume of the pure salt.

TABLE 3.1
DENSITIES OF MOLTEN NITRATES

Melt	a (gm cm ⁻³)	b (x 10 ⁴ gm cm ⁻³ °C ⁻¹)	Reference
0.5 LiNO ₃ 0.5 KNO ₃	2.033 ± 0.0007	6.83	57
0.625 LiNO ₃ 0.375 KNO ₃	2.010 ± 0.0006	6.57	57
0.5 NaNO ₃ 0.5 KNO ₃	2.134 ± 0.0009	7.73	58
0.41 LiNO ₃ 0.59 KNO ₃	2.111	7.80	59
0.45 NaNO ₃ 0.55 KNO ₃	2.290	13.3	59
0.6 LiNO ₃ 0.4 KNO ₃	2.043	6.9	60
0.6 LiNO ₃ 0.4 NaNO ₃	2.046	6.4	60

The thermal decomposition of sodium nitrate occurs in two steps

(29):



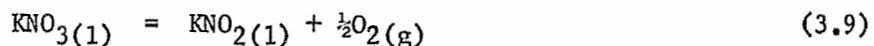


The decomposition of the nitrite was discussed in chapter 2.1 (pages 7-8). The initial decomposition of nitrate to nitrite has been well established for sodium nitrate (28, 29) and potassium nitrate (61).

The suggested mechanism is:



The initial reaction (3.4) is reversible (28) but the kinetic results show that oxygen has no effect on the rate of decomposition when the partial pressure of oxygen is approximately 0.2 atm (air). The equilibrium constants for the reaction,



was reported by Bartholomew (61) to be:

$$\log K = ((-27.6 \pm 1.2)/2.303 RT) + ((24.4 \pm 1.2)/2.303R) \quad (3.10)$$

for the temperatures from 550 to 750°C. The kinetics for both decomposition stages of sodium nitrate were well described by

$$\left[-\ln(1 - \alpha) \right]^{\frac{1}{3}} = kt \quad (3.11)$$

where α is the fraction decomposed at time t (29). The loss of weight corresponding to $\alpha = 1$ is equivalent to the decomposition from sodium nitrate to sodium oxide. The total decomposition of nitrate to nitrite occurs at 0.295. The activation parameters used to calculate k from the equation,

$$k = A \exp(-E/RT) \quad (3.12)$$

for the two stages are given in Table 3.2.

TABLE 3.2

ACTIVATION PARAMETERS FOR THE THERMAL DECOMPOSITION
OF SODIUM NITRATE, DETERMINED FROM THE RATE CONSTANT
 k , IN EQUATION 3.11

Reaction	E (Kcal mole ⁻¹)	log A (min ⁻¹)
$\text{NaNO}_3 = \text{NaNO}_2 + \dots$	40.3	7.33
$\text{NaNO}_2 = \text{Na}_2\text{O} + \dots$	42.8	7.67

These kinetic results agree fairly well with those of Freeman (28) who calculated the equilibrium constant for the initial decomposition stage at 600°C to be:

$$K_e = 5.88 = \frac{N_{\text{NaNO}_3}}{N_{\text{NaNO}_2}} \quad (3.13)$$

where N is the mole fraction of the salt in the system. The normal working range for the nitrate melts is from 200 to 400°C, depending upon their melting points.

3.2 Chemical and Electrochemical Reactions in Nitrate Melts

The theoretical and experimental aspects of electrical conductivity and ion mobilities in molten salts have been the subject of several recent and extensive reviews (62 - 64). The electrical conductivity of a large number of single salts as a function of temperature has been compiled by Janz (2) and Klemm (65). The specific conductance, k , is related to the internal mobilities, b_{ij} , by the equation,

$$k = \sum_i Z_i F C_i b_{ij} \quad (3.14)$$

where Z_i and C_i are the valence and concentration, respectively, of the i^{th} ion in the system. The internal mobility, b_{ij} , is the rate of migration of i with respect to j . The b_{+-} for a pure salt is simply given by

$$k = Z_+ F C_+ b_{+-} \quad (3.15)$$

The entire topic on ion mobilities in molten salts has been recently reviewed by Klemm (66). It has been shown that the internal mobilities are independent of the composition for the silver-sodium nitrate (67, 68), silver-potassium nitrate (69) and the sodium nitrate-nitrite (70) systems. Bloom et al. (70) concluded that the mobilities will be independent of composition, provided there are no intermediate phases in the solid state; these results contradict those of Honig and Ketelaar (71). Honig and Ketelaar used a paper electrophoresis technique with a glass fiber paper and radioactive tracers to study the sodium-potassium nitrate system. As the composition of the mixture was varied, the mobility of the nitrate ion remained constant; however, the sodium and potassium ions tended to have the same mobility which changed almost linearly from its value in pure sodium nitrate to that in pure potassium nitrate. It must be pointed out that their results differed from previous values by a range of 8% to 40%. King and Duke (72) found that the specific conductivity of binary nitrate mixtures showed only a slight negative deviation from linearity with the deviation increasing as the difference between the ion sizes

increased. The lithium-potassium nitrate system exhibited a maximum deviation of only about 4%; therefore, the mobilities in the nitrate systems are independent, to a first approximation, of composition.

The transference number of an ionic species, t_i , with respect to a reference point (i.e., a porous plug) is defined as the number of equivalents of the species passing the reference point per faraday of charge passed through the cell. The transport number, t_1 , is related to the valencies, Z_i , the concentrations, C_i , and the mobilities, b_i , of each ionic species, i , in the system by the equation:

$$t_1 = \frac{Z_1 F C_1 b_1}{\sum_i Z_i F C_i b_i} = \frac{Z_1 F C_1 b_1}{k} \quad (3.16)$$

In the case of a uni-univalent salt (+-) the transport number, t_+ , is equal to the ratio of b_+ to $(b_+ + b_-)$.

The electrolysis of the alkali nitrate melts has been the center of considerable controversy for the past several years; however, there is general agreement that at a platinum anode the end product is nitrogen dioxide and at a graphite anode the end product is carbon dioxide (73). The cathodic reaction is complicated by the reduction of either the nitrate ion by one of several routes or the metal ion to the metal. Bartlett and Johnson (32, 74) have calculated the standard theoretical potential for several possible electrolysis reactions in the nitrate melt (MeNO_3).

Anodic reaction:

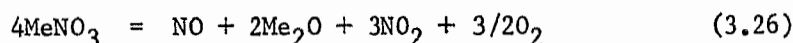
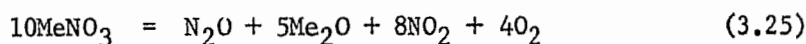
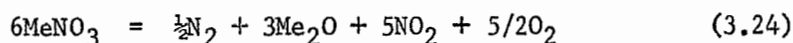
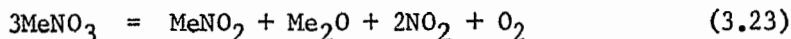


Cathodic reactions:





Overall reactions:



The calculated E° values for reactions 3.23 and 3.24 are almost identical and only slightly more positive than those for 3.25 and 3.26. The E° for reaction 3.27 is considerably more negative than any of the other values. For sodium nitrate at 227°C the E° values for the decomposition reactions 3.23 to 3.27 are -2.27, -2.22, -2.42, -2.66 and -3.74 volts, respectively. The ΔG° for the reaction:



can be calculated by combining reactions 3.24 and 3.27. The ΔG_{600}° for the reaction was found to be -173.7 kcal mole⁻¹ and this large negative value would suggest that the potential of the sodium electrode measured by Arvia *et al.* (75) is questionable. The large ΔG° would also explain the sparks observed at the cathode during electrolysis at high current densities.

The first workers to enquire closely into the cathodic reduction of nitrate melts were Hills and Johnson (76) and they found that the nitrate ion in sodium-potassium nitrate was reduced in two stages. Current-voltage curves, derived from a system using a platinum micro-electrode and a large platinum foil reference electrode, exhibited two cathodic peaks. At about -1.4 volts the current rose to a peak and then fell back to give a high residual current until the final peak was reached, which occurred at a potential of about -3.0 volts. The high residual current was temperature-dependent and had an activation energy of about 11 kcal mole⁻¹, which indicated that the process occurring was not diffusion controlled. Swofford and Laitinen (39) continued this work and obtained similarly shaped voltammetric curves in the sodium potassium nitrate eutectic at 250°C. There was a slight shift in the potentials due to the change of reference electrodes from a platinum foil to an 0.07 molar silver(I)/silver electrode. A small pre-peak at -0.9 volts was completely removed when the melt was purged with nitrogen. The peak was attributed to the presence of a contaminant such as water, which is appreciably soluble in nitrate melts (56, 77). The peak and after-peak currents were not substantially affected, thus the reduction process of the contaminant appears to be blocked by the onset of the peak process. The activation energy of 11 kcal mole⁻¹ was confirmed and is approximately three times that expected for any diffusion process. Since stirring of the melt also had little effect, it was concluded that reduction of the nitrate is a kinetic or surface-controlled process.

Oxide and nitrite were quantitatively identified as the products of the controlled potential reduction of nitrate. A precipitate, which formed on the platinum electrode during the electrolysis and dissolved in the melt on an open circuit, was shown to be sodium oxide since sodium and potassium nitrites are soluble in all proportions in the nitrate melt. The authors found it was possible to precipitate sodium oxide from pure potassium nitrate saturated with calcium oxide by adding a small amount of sodium nitrate. The absence of the first peak in pure potassium nitrate and its appearance when as little as 10% sodium nitrate by weight was added provides additional evidence for the sodium oxide film. From the current-voltage curves run on various solid micro-electrodes which had basically the same profile as that for the platinum electrode, Swofford and Laitinen concluded that the peak and after-peak current were dependent upon the properties of the bulk melt and were not due to the reduction of surface oxide films.

Swofford and Laitinen also carried out some chronopotentiometric studies on this eutectic. They found that the sodium oxide slowly dissolved into the melt and that the quantity of oxide which accumulated on the micro-electrode was directly dependent upon the current density.

These workers observed that when the cathode was maintained at -2.8 volts, a blue liquid was formed; this liquid then decomposed to give a colorless, odorless gas. On the basis of these observations they postulated that a meta-stable solution of alkali metal was formed

which subsequently reacted with the nitrate to form nitrogen and oxide.

Bartlett and Johnson (32) confirmed the previous work on the reduction of nitrate except they found that only 94% of the current passed through the system was accounted for by the amount of nitrite and oxide generated at the first peak voltage. This indicated that other processes must also have occurred at or before the peak potential. Some of the suggested products formed by these processes were nitrogen, nitrous oxide and nitric oxide. There was only a final decomposition wave in potassium nitrate at about -1.6 volts versus a 1.0 molal silver(I)/silver reference electrode which is approximately the same value as the peak potential in sodium nitrate. The melt in the cathode compartment turned green and small amount of gas was evolved. Neither red catholytes nor sparks were observed in the pure potassium nitrate melts although this phenomena was present in sodium nitrate melts. This was attributed to the absence of high concentrations of alkali metal oxide on the electrode since potassium oxide is soluble in the melt (39). Analysis of the cathode compartments in potassium nitrate showed that the efficiency of the electrical reduction process appeared to be 111% for platinum cathodes and 152% for silver cathodes. Since it is, of course, impossible to have an electro-reduction process with an efficiency greater than 100%, it was proposed that an electrochemical process in which the electrode metal is oxidized must have occurred simultaneously with the cathodic reaction. Bartlett and Johnson found that both silver and platinum were

oxidized during the electrolysis process, and therefore suggested that nitric oxide was formed during the reduction process which then reacted with the platinum to form the green platinum nitrosyl type complex which resembles those in the aqueous system.

In a polarographic study of alkali nitrate eutectics by Hills and Power (78), further support has been given to the postulation of the reduction of alkali nitrates by the process



The results of Arvia et al. (75) are in complete disagreement with all the results previously discussed. They maintain that the electrolysis of sodium nitrate produces liquid sodium at the cathode and gaseous nitrogen dioxide and oxygen at the anode. By means of a cell designed specifically to collect and make electrical contact with the sodium floating on top of the melt, Arvia claims to have developed reversible sodium(I)/sodium and $\text{NO}_3^-/\text{NO}_2$, O_2/Pt electrodes by electrolysis. The measured potential of the sodium nitrate formation cell agrees with those calculated from thermodynamic data; however, it must be pointed out that the sodium metal will reduce the melt at these experimental temperatures (cf. equation 3.28, page 26). The assumption that the $\text{NO}_3^-/\text{NO}_2$, O_2/Pt electrode is feasible and reversible has been substantiated by other workers and will be discussed more fully in chapter 3.6 (page 67).

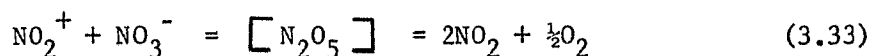
The kinetics of the oxidation of nitrate ions in silver nitrate and alkali nitrate has been investigated by Gupta and Sundheim (79) and Arvia and co-workers (73, 80, 81), respectively. Gupta and Sundheim measured the potential at 238.6°C as a function of the current

density of both a stationary and a rotating platinum electrode versus a silver electrode in purified silver nitrate. It was found that there are two distinct regions: the first occurs at low current densities ($\approx 10 \text{ mA/cm}^2$) with a potential below +0.5 volts and the second at high current densities ($\approx 100 \text{ mA/cm}^2$) with a potential near +0.95 volts. Rotation of the platinum electrode substantially decreased the over-voltage, η , at a constant current density for the first region but had very little effect upon the second; this indicated that the process in the first region was diffusion controlled, whereas that in the second was independent of transport. The slopes of Tafel plots indicated that the process in the first region was a two electron process and Gupta and Sundheim concluded that this was the discharge of oxide ions. However, the total products of electrolysis at both low and high current densities were nitrogen dioxide and oxygen in a 2:1 ratio. At the higher current densities these workers obtained a linear Tafel plot and suggested that the nitrate ion is oxidized to a short-lived intermediate species which rapidly and irreversibly decomposes. For the lower current density region it was postulated that the electrode reaction involves the preliminary dissociation of the nitrate ion to form the nitryl ion, NO_2^+ , and the oxide ion, O^{2-} ,

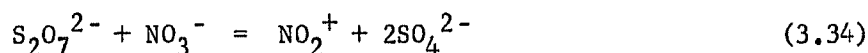


followed by the reactions:





If the last reaction (3.33) is not too rapid, depletion of the electroactive species, O^{2-} , from the vicinity of the electrode would produce a concentration polarization effect. The addition of pyrosulfate ion will reduce the oxide concentration by an acid-base reaction and increase the overpotential at a constant current density,



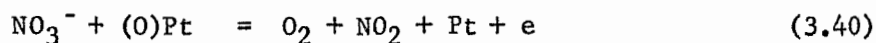
A substantial increase in the overpotential was observed for successive additions of sodium pyrosulfate.

Triaca and Arvia (80, 81) studied the influence of temperature on the anodic processes in silver nitrate and silver nitrate dissolved in 1:1 sodium-potassium nitrate mixture. They found that there were two distinctive temperature regions, the low temperature region from 220°C to 290°C and the high from 350°C to 470°C. The use of overvoltage versus log current density and the decay of overvoltage versus time curves showed that there were two distinct processes occurring in the low temperature region, one at low current densities and the other at high current densities. Triaca and Arvia claim that the low activity of the oxide ion in the low temperature region would prevent its discharge at the anode as suggested by Gupta and Sundheim. Their estimate for the oxide activity was obtained from Kust's and Duke's (82) equilibrium constant, K_{eq} , for the dissociation of the nitrate ion (reaction 3.30).

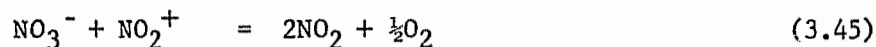
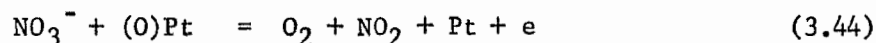
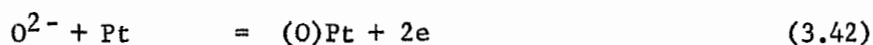
$$K_{\text{eq}} = [\text{NO}_2^+] [\text{O}^{2-}] \quad (3.36)$$

However, this determination was based on the reversibility of the $O^{2-}/O_2/Pt$ electrode which has been the subject of much controversy (cf. page 35). There is a factor of 10^{22} between the value of K_{eq} that Kust and Duke (82) obtained at $250^\circ C$ and that which Gupta and Sundheim obtained at $238^\circ C$.

Triaca and Arvia proposed the following mechanism, which involves adsorbed nitrate radicals and oxygen atoms, to account for all the facts:



At high temperatures the oxide activity increases so that the discharge of oxide becomes feasible and the proposed mechanism for the oxidation of nitrate ion changes to:



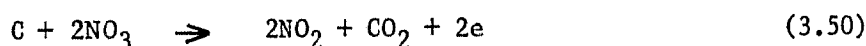
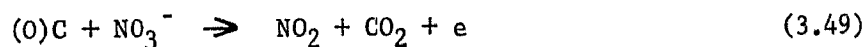
It should be pointed out that if the rate constant for equation 3.45 is small, the NO_2^+ concentration will build up, shift the equilibrium (3.41) to the left and prevent the supply of oxide for the cathodic reduction. The combining of equations 3.41 and 3.45 gives

the overall reaction



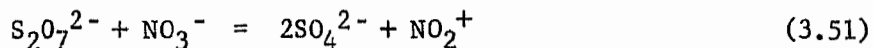
Since sodium oxide (39) and silver oxide (83) are insoluble or only slightly soluble in nitrate melts, this means that it would be impossible to obtain a pure sodium or silver nitrate melt; this is contrary to the facts. Gupta and Sundheim have shown that the anodic process occurring at low temperatures and low current densities is subject to transport control. As Triaca and Arvia's results were obtained with stationary electrodes, their interpretation is suspect. Polarographic studies (78) have confirmed that the overall oxidation products of nitrate are nitrogen dioxide and oxygen; however, there was no evidence for the presence of the nitryl ion.

Arvia and Triaca (73) have examined the kinetics of the oxidation of nitrates on graphite electrodes to help establish the dependence of the reaction mechanism on the electrode material. They studied only the low temperature region (230 to 320°C) of the reaction in silver nitrate and silver nitrate dissolved in a 1:1 sodium-potassium mixture. The experimental techniques used on the platinum anode (81) were utilized to obtain the following overall reaction and proposed mechanism:



The reaction involves the oxidation of the graphite electrode and consequently attention must be paid to the chemical oxidation of graphite by the nitrate ion. At high overvoltage a high degree of oxidation caused by the NO_3 intermediate is achieved, and the rate-determining step of the anodic reaction becomes equation 3.49. The analysis of the graphite kinetics was based on the past kinetics on platinum (81), which have been questioned, plus the correction for several additional side reactions.

The electrochemistry of oxide and nitryl ions has been the subject of a great deal of controversy in the literature. Kust and Duke (82) determined potentiometrically the dissociation constant (equation 3.36) for the dissociation of the nitrate ion (equation 3.30) in a 1:1 sodium-potassium nitrate solvent. The nitryl ion concentration was varied by adding the pyrosulfate ion to the nitrate solvent according to the reaction

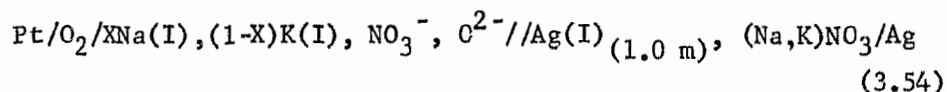


Oxide ion was introduced into the solvent by electrically reducing oxygen gas at a platinized platinum electrode. An oxygen electrode was set up by bubbling oxygen gas over a platinum flag and it was found to be reversible to the oxide concentration and the partial pressure of oxygen gas. With the aid of this electrode, they determined the value of the dissociation constant. The value of K_{eq} increased steadily with time; at 300°C it increased by a factor of five in 32 minutes. The values for K_{eq} were extrapolated back to zero time and the numerical values were

$$K_{\text{eq}}(250^\circ\text{C}) = (2.7 \pm 0.3) \times 10^{-26} \text{ M}^2 \quad (3.52)$$

$$K_{eq}(300^{\circ}\text{C}) = (5.7 \pm 0.1) \times 10^{-24} \text{ M}^2 \quad (3.53)$$

Gupta and Sundheim (79) reported a value of $1.4 \times 10^{-4} \text{ M}^2$ for the same dissociation equilibrium constant. Two factors may have contributed to this large discrepancy: first, Gupta and Sundheim assumed that all of the pyrosulfate in equation 3.51 reacted at once with the nitrate ions to produce NO_2^+ in equivalent proportions, whereas the other workers used an equilibrium constant for the reaction which had been previously measured by Duke and Yamamoto (84); secondly, Kust and Duke based their determination on an $\text{O}^{2-}/\text{O}_2/\text{Pt}$ electrode in an equimolar sodium-potassium nitrate melt while Gupta and Sundheim based their value on the change in overpotential at constant current density when pyrosulfate was added to the silver nitrate melt. In a later paper Kust (85) reported that the standard emf of the oxygen electrode was a function of the sodium-potassium ratio. He found that the potential of the cell



was given by

$$E^{\circ}(\text{T}, x_{\text{Na}}) = \left[0.6730 - 0.000130(\text{T} - 290^{\circ}\text{C}) \right] - \left[0.0830 + 0.000275(\text{T} - 290^{\circ}\text{C}) \right] x_{\text{Na}} \quad (3.55)$$

This represents a decrease of approximately 80 millivolts in E° when going from pure potassium nitrate to pure sodium nitrate at 290°C .

Kust concluded that the activity of the oxide ion was lower in the sodium nitrate than in the potassium nitrate due to solvation effects.

The activity coefficient for the oxide ion would have to change by about a factor of 5.2 to account for an 80 millivolt change, or the change may be due to the low solubility of oxide in sodium nitrate. The calculations in chapter 7.1 (page 111) show that the change in solvent from potassium nitrate to sodium nitrate at 300°C results in an increase of about 29 millivolts in the liquid junction potential; thus, the corrected $(E_{K(I)}^O - E_{Na(I)}^O)$ becomes approximately 110 millivolts.

The electrochemical behavior of the oxide ion in sodium nitrate-potassium nitrate eutectic melt at 250°C has been examined by Swofford and McCormick (38). They reviewed the previous methods for adding oxide to the melt and proposed oxalate as a desirable species for the production of oxide in the melt in a concentration range suitable for electrochemical study. A voltammetric wave was observed in the melt and was attributed to the oxidation of the oxide ion since the limiting current was linear with the amount of oxalate added or the number of coulombs used in the reduction of the nitrate ion. Wave analysis using a plot of E versus $\log \left[\frac{i}{(i_d - i)} \right]$ gave a slope of 0.12 which indicated a one electron reversible reaction instead of the expected two electron change. This phenomenon has been reported by several other workers (86, 87). The half wave potential was +0.024 volts versus a 0.01 molar silver(I)/silver reference electrode. These workers failed in their attempt to reduce oxygen electrically on a platinum electrode as reported by Kust and Duke (82). They found that the current due to the oxidation of oxide remained linear with the

constant current generation regardless of whether or not oxygen gas was bubbled over the electrode surface. They concluded that it is the melt itself and not the oxygen that was being reduced to produce oxide ion. This casts considerable doubt on the oxygen electrode due to the apparent electrochemical inactivity of the oxygen gas.

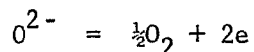
Voltammetric and chronopotentiometric measurements have been made on solutions of acids ($S_2O_2^{2-}$, HSO_4^- , NO_2) and bases (NO_2^- , NO , CO_3^{2-} , O^{2-} , OH^- , O_2^{2-}) in equimolar sodium-potassium nitrate melts at 275 to 350°C (40). These measurements failed to establish the presence of the nitryl ion in acidic nitrate melts but found a species chemically and electrochemically similar to dissolved nitrogen dioxide. This species was reduced in a one electron process to nitrite, but could not be oxidized. These electrochemical techniques had previously been successfully used in the study of NO^+ and NO_2^+ in concentrated sulfuric acid (88). Other independent studies on nitrate melts found no evidence to support the existence of the nitryl ion in nitrate melts (41, 78) which are at variance with the results of still other workers (89).

McCormick and Swofford (37) used chronopotentiometry and coulometric analysis to verify that the oxidation of oxide to oxygen is a one electron process (87, 90, 91) and not a two electron process (82, 92). They proposed that the anodic oxidation of oxide was to a peroxide which subsequently slowly decomposed chemically to give oxygen and oxide.



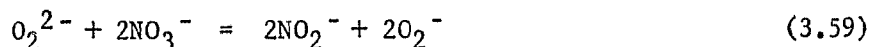


net reaction:



In reaction 3.56 there is a one electron change per mole of oxide. These equations explain the seeming "reversibility" of the "oxygen electrode," since the response to the oxide concentration is due to equation 3.56, and the response to the oxygen gas is due to equation 3.57. The evolution of gas from the anode in the electrolysis of oxide-containing melts begins some 20 to 30 seconds after the current starts to flow, indicating that chemical reaction 3.57 is slow and requires a build-up of peroxide before it can begin. Further support was provided when sodium peroxide was added to the nitrate melt; gas slowly evolved and analyses after the reaction was complete showed a stoichiometric increase in the amount of oxide in the melt.

The concept of peroxides has been used by Zambonin and Jordan (93) to explain the properties of the oxide ion in fused nitrates. They claim that the oxide does not exist in any appreciable concentration in molten nitrates due to its conversion to peroxide (O_2^{2-}) and superoxide (O_2^-).

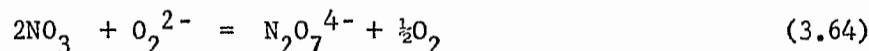


From voltammetric curves using a Levich rotated platinum disk electrode and a 0.07 molal silver(I)/silver reference electrode, they observed

the following reactions at the respective potentials:



The equilibrium constants for the reactions 3.58 through 3.60 at 229°C in an equimolar sodium-potassium nitrate solvent were evaluated to be approximately 3, $6.7 \pm 0.5 \times 10^{-11}$ and $3.5 \pm 1 \times 10^{-6}$, respectively. Zamboni and Jordan claim that the oxygen electrode is based on the $\text{O}_2\text{-O}_2^-$ redox couple and not the $\text{O}_2\text{-O}_2^{2-}$ redox couple as previously presumed, indicating that the electrochemistry of oxides in nitrate melts may require reevaluation. Part of the work by Shams El Din and Hosary (94) does not conform to equation 3.59 in that they claim pyronitrate is formed by the reaction



The reaction was found to be zero-order with respect to peroxide ion and has an activation energy of approximately 6.17 kcal mole⁻¹.

3.3 Electrodes and Electrode Potentials

The silver electrode, $\text{Ag(I)} + e = \text{Ag}$, has been used extensively in molten nitrates as a reference electrode. Many types of nitrate solvent have been used: silver nitrate (95, 96), alkali nitrates such as sodium nitrate (32, 97), eutectic nitrate mixtures such as sodium-potassium nitrate (38, 39), 50:50 mixtures, sodium-potassium nitrate (40) and ternary alkali nitrate eutectic (98). The silver(I)

ion was introduced into the melt by either adding silver nitrate directly (97, 99, 100) or by anodizing a silver electrode, a process which has been shown to be 100% current efficient (39, 99, 100). The emfs of silver nitrate concentration cells exhibit ideal Nernst behavior up to 0.5 mole percent in sodium-potassium nitrate eutectic (101, 102) and in sodium nitrate (99).

Glass frits (103), thin capillaries (104) and asbestos threads (101) have been used to separate the reference electrode nitrate melt from the nitrate melt under investigation. Hill and Blander (105) and Denning (106) reported difficulties in the construction and use of the asbestos thread junction. A stable reproducible electrode enclosed in Pyrex glass has been used successfully by several workers (107, 108). They claim that only the sodium ions are mobile in the glass membrane and the liquid junction potential across the membrane is negligible; thus the emf depends only on the difference of silver ion concentration on each side of the glass.

The solubility of silver oxide was determined by the use of potentiometric measurements by Shams El Din et al. (83). They found that the K_s in equimolar sodium-potassium nitrate was about 1000 times larger than the K_s in potassium nitrate ($K_s = 2.70 \times 10^{-16} \text{ mole}^3 \text{ kg}^{-3}$) at 350°C. They attributed the difference to the greater acidity of the sodium melt than the corresponding potassium melt. They did not consider the relative solubilities of the alkali oxides and they added oxide in the form of sodium peroxide. The corrosion of silver in various nitrate melts has been examined (98): its higher corrosion

rate in lithium nitrate at 325°C (21.5 mg cm⁻² day⁻¹) than in equimolar sodium-potassium nitrate (0.001 mg cm⁻² day⁻¹) was attributed to the higher acidic character of the lithium ion.

Hill, Hills, Young and Bockris (109) studied the silver(I)/silver couple in fused alkali nitrate and fused alkali chloride. Their experimental results were poor and the calculated values of exchange current, double layer capacities and diffusion coefficients are suspect. Hills and Johnson (76) used impedance measurements and concluded from the presence of a pseudo capacity peak for the silver(I)/silver couple that it was reversible in fused nitrates. Inman et al. (110) applied the single-pulse galvanostatic method to the silver-silver nitrate system in a fused sodium-potassium nitrate melt. They evaluated the exchange current density, i_0 , as 1.5 A cm⁻² at a current density of 3.23 mA cm⁻² and a temperature of 250°C. Observations of transients in the nanosecond range were made to evaluate cell resistance ($R = 2.96 \Omega$), double layer capacitance (approximately 120 μ F cm⁻²) and diffusion coefficients. As there are few direct measurements of double-layer capacitance in melts, the nature of the double layer is still relatively unknown. With the aid of a dropping mercury electrode, Randles and White (111) established double-layer capacitance curves in fused lithium-potassium nitrate and ternary alkali nitrate mixtures. The curves were relatively flat and the values ranged between 20 and 50 μ F cm⁻², which were remarkably close to those found in aqueous solutions. Several other workers (112 - 115) have reported values for the double layer capacitance on various electrode

materials.

The strong oxidizing power of molten nitrates severely limits the number of metal-metal ion electrode systems that can be used in this solvent. Narayan and Inman (116) found that cobalt is rapidly oxidized by the melt, whereas nickel is attacked much more slowly. These results and others (32) are consistent with thermodynamic calculations (74) which show that most of the common structural metals would be oxidized by the melt. The mercury oxide line on the Ellingham diagram lies above the nitrate redox lines and hence it was expected that mercury would not be oxidized by the nitrate melt. The use of a dropping mercury electrode in a fused nitrate solvent at 250°C (39) verifies this expectation. At higher temperatures the mercury is oxidized, but this may be due to the attack of oxygen evolved from the thermal decomposition of the melt.

Arvia and co-workers have published results based on the formation of a reversible alkali ion-alkali metal electrode during the electrolysis of the nitrate melt (75, 95, 117). They claimed that the cathodic and anodic reactions in the electrolysis of sodium nitrate are



and



respectively, and that the electrolysis products create a sodium nitrate formation cell:





Their experimental results for the first three alkali metal nitrates and silver nitrate (96) agree very well with the values calculated from thermodynamic data. Their reduction process to produce liquid sodium in the nitrate melt is in direct contradiction with the results of several other workers (chapter 3.2, page 23). They claimed that water impurities in the nitrate melts prevented other workers from duplicating their measurements.

The existence of gas electrodes in the nitrate melts has been reported by several workers. The oxygen electrode has already been discussed in chapter 3.2 (page 23) and the discussion of the nitrogen dioxide-oxygen electrode will be discussed in chapter 3.6 (page 67).

3.4 Activities and Thermodynamics of the Silver Ion in Alkali Nitrate Melts

It is well known that the change in Gibbs free energy, ΔG , for a chemical reaction, $aA + bB + \dots = lL + mM + \dots$, at a given temperature T is given by

$$\Delta G = \Delta G^\circ + RT \ln \frac{a_L^l \cdot a_M^m \cdot \dots}{a_A^a \cdot a_B^b \cdot \dots} \quad (3.69)$$

The ΔG° term represents the change in free energy if all the species are in a defined standard state and the logarithm term, containing the activity, a_i , of each ion in the system, compensates for the difference between the actual state and the defined standard state for the system.

If the reaction takes place in a reversible electrochemical cell with the passage of n faradays per mole of reaction, then

$$\Delta G = -nFE \quad (3.70)$$

and

$$E = E^{\circ} - \frac{RT}{nF} \ln \frac{a_L^1 \cdot a_M^n \cdot \dots}{a_A \cdot a_B \cdot \dots} \quad (3.71)$$

where E is the potential of the cell. The activity of the i^{th} species, a_i , is related to some physical concentration scale, C by

$$a_i = \gamma_i C_i \quad (3.72)$$

where γ_i is the activity coefficient. The values used for the standard electrode potential, E° , and the activity coefficient depend directly on the choice of standard states and concentration scales. The thermodynamic meaning and implications of each of these choices has been the subject of many papers and reviews (1, 11, 13, 14, 64, 118-120). Normally, the standard state chosen will be based upon either Raoult's law or Henry's law, depending upon the system. The pure liquid is the most convenient standard state to use when dealing with mixtures over a large composition range and the normal concentration unit associated with this choice is the mole or ion fraction (N or X). When working in dilute solutions it is normal to choose the hypothetical state with unit concentration ($C_i = 1$) and unit activity coefficient ($\gamma_i = 1$). Mathematically, the standard state is defined by $\gamma_i \rightarrow 1$ as $C_i \rightarrow 0$, the limiting dilution law. The molal, m , or the molar, M , concentration scales are usually used with

this definition of a standard state. The standard state for solids and gases is the normal state in which the gas at one atmosphere and the pure solid exist at the given temperature of the system. The standard states and concentration scales used in molten salts along with the application of Henry's and Raoult's laws in the derivation of thermodynamic relationships used in molten salts were only briefly discussed here since they are discussed at length in chapter 7.1 (page 111).

Several models have been chosen as a means of simplifying and predicting the thermodynamic properties of the system. The ideal solution is based on Raoult's law which assumes that there is complete random orientation in the solution. The heat of mixing is assumed to be zero. The thermodynamic values for the activity, a_i , the partial molar free energy, G_i , i.e., the chemical potential, and the entropy, S_i , for a species i in an ideal system in which its mole fraction is N_i are given by:

$$a_i = N_i \quad (3.73)$$

$$G_i = G_i^0 + RT \ln N_i \quad (3.74)$$

$$S_i = S_i^0 + R \ln N_i \quad (3.75)$$

A regular solution (121) is defined as a solution involving no entropy change when a small amount of one of its components is transferred to it from an ideal solution of the same composition, the total volume remaining unchanged. This implies that the species are still completely orientated; however, the restriction on the heat of mixing

and the relationship $a_i = N_i$ is nullified. The excess free energy, ΔG_i^E , which results from the transfer of one mole i from an ideal solution is given by

$$\Delta G_i^E = G_i^{\text{Reg.}} - G_i^{\text{Ideal}} = RT \ln \frac{a_i}{N_i} = RT \ln \gamma_i \quad (3.76)$$

$$\Delta S_i^E = 0 \quad (3.77)$$

Therefore,

$$\Delta \bar{H}_i^M = \Delta G_i^E = RT \ln \gamma_i \quad (3.78)$$

where $\Delta \bar{H}_i^M$ is the partial molar heat of mixing for component i in the given solution at a given temperature. The calorimetric experiments on heats of mixing by Kleppa et al. (122) gave molar heats of mixing for binary systems which could be fit semi-empirically by the equation

$$\Delta \bar{H}_1^M = \left[a + 2(b + c)N_1 - 3cN_1^2 \right] N_2^2 \quad (3.79)$$

where a , b and c are constants. For small values of N_1 the equation reduces to

$$\Delta \bar{H}_1^M = WN_2^2 = W(1 - N_1)^2 = RT \ln \gamma_1 \quad (3.80)$$

where W is called a work constant and is approximately equal to the value of " a ". The total heat of mixing, ΔH^M , is given by

$$\Delta H^M = (a + bN_1 + cN_1N_2)N_1N_2 \quad (3.81)$$

For binary alkali nitrate melts, Kleppa and co-workers (49, 50, 122)

found that the total heat of mixing could be represented to a good first approximation by the empirical equation

$$\Delta \bar{H}^M = -N_1 N_2 140 \delta^2 \text{ kcal mole}^{-1} \quad (3.82)$$

where

$$\delta = \frac{(d_1 - d_2)}{(d_1 + d_2)} \quad (3.83)$$

and d_1 and d_2 are the sums of the radii of the ions ($r_+ + r_-$) present in the two pure salts. The absence of a temperature term in equation 3.82 indicates that the parameters a , b and c and thus W are temperature independent to a first approximation. The values for Kleppa's parameters have been tabulated (49, 50, 122) for the binary nitrate melts and provide a check for the determination of W by other methods.

In a real system the excess entropy, S^E , will not be zero when a mole of a component is transferred from an ideal solution to the real solution as it was assumed to be for the regular solutions. Kleppa and co-workers (122) have suggested that the excess entropy is related to the concentrations by

$$S^E = \alpha N_1 N_2 \quad (3.84)$$

Ketelaar and Dammers-de Klerk (120) used this expression to develop an equation to calculate the activity coefficient of a salt in a binary system as a function of temperature and concentration. Values for α were obtained from the relationship

$$\frac{-S^E}{N_2} = \alpha N_2 = \frac{\Delta \bar{H}_1^M + nFE^E}{T} \quad (3.85)$$

where $\Delta \bar{H}_1^M$ was obtained from Kleppa's data and the excess emf, E^E ,

was determined from silver nitrate concentration cells. It should be noted that in equation 5 of their paper they state $nFE^E = G_1^E$, which is in error and should read $-nFE^E = G_1^E$. This error may have resulted from a misuse of sign conventions. The equations used in this text have been corrected for the omission of the minus sign. The final equation relating to temperature and concentration is as follows:

$$RT \ln \gamma_1 = \left[(a - \alpha T) + 2(b + c)N_1 - 3cN_1^2 \right] N_2^2 \quad (3.86)$$

The scatter of points in the plot of \bar{S}_1^E versus N_2^2 to obtain α was very large; however, the resulting α values indicated a negative excess entropy of the order of 0.1 to 0.2 cal mole⁻¹ °K⁻¹ for equimolar mixtures of fused nitrates. This indicates that W would slowly increase with temperature since

$$W = a - \alpha T \quad (3.87)$$

Scrosati et al. (123) have reviewed the first and second approximation equations to activity calculations in molten reciprocal salt systems. The reciprocal salt system contains two different cations and two different anions ($Me_1A_1 + Me_2A_2$). The Temkin activity coefficient (124) for the salt Me_1A_1 , $\gamma_{Me_1A_1}$, is given by

$$\gamma_{Me_1A_1} = \frac{a_{Me_1A_1}}{(X_{Me_1})(X_{A_1})} \quad (3.88)$$

where X is either the cation or anion fraction. The Temkin ideal solution has the same properties as the ideal solution previously discussed. Scrosati et al. compared the theoretical values for the

sodium fluoride-potassium iodide, sodium fluoride-potassium bromide and lithium fluoride-sodium chloride systems with the experimental results and found that it was necessary to correct for several systematic deviations. This introduces parameters, such as coordination number and band energies between the different ions in the melt (particular to each system) which must be evaluated and included in the equations; however, these parameters make the equations difficult to use and the equations are not accurate enough to warrant a detailed examination of this kind. A model based on the formation of "regular solutions" has been developed by Bloom and Welch (125). The theoretical values derived from their model for reciprocal molten salt solutions were shown to agree with the experimental values. However, in their calculations two parameters were evaluated from a known system and then the same constants were used to evaluate the activities in the remaining systems. Similar types of theoretical calculations of activity from models have been made by several workers (126 - 128) as well as ternary activities from binary activity data (129).

The activities of a binary system can be obtained from the combination of cryoscopic and calorimetric data (130). The activities along the liquid-solid curve in a phase diagram are determined from the expanded form of the van't Hoff equation:

$$\ln(a_{\text{solvent}}) = -\frac{\Delta H_0}{R} \left[\frac{1}{T_L} - \frac{1}{T_M} \right] + \frac{\Delta a}{R} \ln \frac{T_2}{T_M} \\ + \frac{\Delta b}{2R} [T_L - T_M] + \frac{\Delta c}{2R} \left[\frac{1}{T_L^2} - \frac{1}{T_M^2} \right] \quad (3.89)$$

where a_{solvent} is the activity of the solvent at the liquidous temperature, T_L , T_M is the melting point of the pure solvent and Δa , Δb and Δc are the differences in the heat capacity for the liquid and the solid. The integration constant ΔH_0^o is evaluated from the heat of fusion equation:

$$\Delta H_{f,T} = \Delta H_0^o + \Delta a T + \frac{\Delta b T^2}{2} - \frac{\Delta c}{T} \quad (3.90)$$

The partial molar heat of mixing, $\Delta \bar{H}^M$, is added to activity at T_L to obtain the activity at a temperature T in excess of T_L . If it is assumed that $\Delta \bar{H}^M$ is a linear function of temperature

$$\Delta \bar{H}^M = A + BT \quad (3.91)$$

then using the Gibbs-Helmholtz equation in the form

$$\frac{d \ln a}{dT} = \frac{-\Delta \bar{H}^M}{RT^2} \quad (3.92)$$

the activity of the solvent at any temperature T is given by the following:

$$\begin{aligned} \ln(a_{\text{solvent}, T}) &= \ln(a_{\text{solvent}, T_L}) + \frac{A}{R} \left[\frac{1}{T} - \frac{1}{T_L} \right] \\ &\quad - \frac{B}{R} \ln \frac{T}{T_L} \end{aligned} \quad (3.93)$$

The values for the constants (A and B) in equation 3.91 can be evaluated from calorimetric measurements of the heat of mixing and equations 3.79 and 3.81, developed by Kleppa and co-workers (122). At concentrations beyond the eutectic the solvent and solute exchange roles. The other activity in the system is obtained by graphical integration of the Gibbs-Duhem equation.

$$N_1 d \ln a_1 + N_2 d \ln a_2 = 0 \quad (3.94)$$

The authors estimated the uncertainty in this method to be less than 1% if graphical integration is not required; otherwise, the uncertainty is unknown.

Murgulescu and Sternberg (131) have reviewed four of the experimental methods for measuring activities in molten salts. The activity of a metal salt (MeX) in a mixture containing a common anion (MeX + Me'X) is related to the emf of the following formation cells by the equation:

$$E_1 = E^0 - \frac{RT}{nF} \ln a_{\text{MeX}} \quad (3.95)$$

$$\text{Me} / \text{MeX}_{(1)} / \text{C, X}_{2(g)} \quad \text{pure formation cell } E^0 \quad (3.96)$$

$a=1$

$$\text{Me/MeX}_{(1)} + \text{Me'X}_{(1)} / \text{C, X}_{(g)} \quad \text{dilute formation cell } E_1 \quad (3.97)$$

a_{MeX}

This method has the advantage of no liquid junction potential; however, the formation cells are difficult to set up. It is also assumed that the activity of the anion is independent of the cations present in the system. A concentration cell with transport is more practical to set up in the laboratory but a liquid junction potential (E_J) is introduced into the calculations.

$$\text{Me} / \text{MeX} // \text{MeX} + \text{Me'X} / \text{Me} \quad (3.98)$$

The activity for this cell is related to the measured emf (E_2) by the equation:

$$E_2 = \frac{RT}{nF} \ln a_{\text{MeX}} + E_J \quad (3.99)$$

The liquid junction potential can be calculated from the measured emfs

of an identical mixture in cells 3.96 to 3.98 by the equation

$$E_J = E_2 - (E^0 - E_1) \quad (3.100)$$

It should be noted that Murgulescu and Sternberg (131) have an error in sign in their equations (those which correspond to 3.99 and 3.100 above) which has been corrected in this text. They found that the liquid junction potential for many systems was less than one millivolt. Laity's results concur (97) but those of Ketelaar and Dammers-de Klerk do not (120). The decay of the emf of a formation cell, which has been set up by electrolysis, can be followed on an oscilloscope to determine the activity of the system. This method is valuable for systems in which it is difficult to set up formation cells (e.g., potassium bromide plus potassium chloride). The results obtained by the oscillographic method compare very well with the results from other measurements.

The cryoscopic method of determining activities is especially useful in the study of alkali halides having a common anion (e.g., lithium chloride plus potassium chloride) because the closely similar electrode potentials of the two cations preclude a determination by emf measurement. This method also allows the study of melts for which the formation cell (i.e., the gaseous anion electrode) is difficult to set up. The activity of a salt has also been determined from the measurement of its vapor-pressure over the molten system (132).

A considerable amount of work has been done on the measurement of the activity coefficient of silver nitrate in alkali nitrate mixtures utilizing a concentration cell. Most of the workers assumed the

liquid junction potential to be zero and fitted their results to the equation derived from the theory of regular solutions (3.80).

$$(1 - N_{\text{AgNO}_3})^2 W = RT \ln \gamma_{\text{AgNO}_3} \quad (3.101)$$

The work constant, W , was found by most workers to be a constant for mole fractions (N_{AgNO_3}) of silver nitrate below 0.5 and to be independent of the temperature. The value of W in the silver-lithium nitrate system (133 - 135) ranges from a low of 850 cal mole⁻¹ (136, 137) to a high value of 1245 cal mole⁻¹ (138). Most of the studies in the silver-sodium nitrate system (97, 133, 134, 136, 139, 140) agree on a value of 840 cal mole⁻¹ for W . A low of -300 cal mole⁻¹ (141) and a high of -40 cal mole⁻¹ (134) for W has been reported for the silver-potassium nitrate system (136, 137). The systems containing binary mixtures of alkali nitrates and silver nitrate have received relatively less attention. Typical values for W in the eutectic mixtures are: 950 for the lithium-sodium nitrate eutectic (127, 133, 136, 137, 142), 750 for the lithium-potassium nitrate eutectic (127, 136, 137, 142) and 420 for the sodium-potassium nitrate eutectic (136, 137, 143). The systems involving the cesium and rubidium nitrate salts have received very little attention (120, 137). In Guion's study (137) of the activities of silver nitrate in ternary nitrate melts, the mole fraction of silver nitrate was kept constant at 0.1 while the ratio of the other two alkali cations were varied. He derived equations to predict the excess free energy in a ternary system on the assumption that it behaved like a regular solution; however, the

equations proved to be very difficult to use. The work constant for silver nitrate in the lithium-sodium-potassium nitrate eutectic was found to be $780 \text{ cal mole}^{-1}$ (136).

With the aid of a reversible nitrate electrode (95) Ketelaar and Dammers-de Klerk (120) set up formation cells to study the activity of silver nitrate in each of the five pure alkali melts at 350°C ; this approach eliminated the liquid junction potential. By combining their results with the calorimetric data of Kleppa et al. (122) they demonstrated that the excess entropy in the nitrate system was not equal to zero, as had been previously assumed for regular solution behavior of the melts. The coefficient α was evaluated for each alkali salt and gave the temperature dependence of W at infinite dilution of silver nitrate from the equation:

$$W = a - \alpha T \quad (3.102)$$

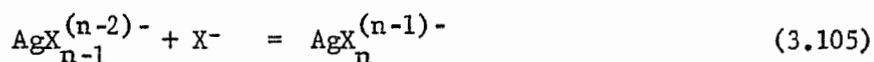
The parameter "a" is from Kleppa's et al. (122) equations for heats of mixing (equations 3.79 and 3.81) and the values of "a" and α are summarized in Table 3.3.

TABLE 3.3

COEFFICIENTS a (cal mole^{-1}) AND α ($\text{cal mole}^{-1} \text{ }^{\circ}\text{K}^{-1}$)
FOR BINARY NITRATE MIXTURES AT 350°C

Solvent	a	α	$W_{300^{\circ}\text{C}}$	$W_{350^{\circ}\text{C}}$	$W_{400^{\circ}\text{C}}$
(Ag,Li)NO ₃	+ 702	-0.37 ± 0.08	914 ± 46	933 ± 50	951 ± 54
(Ag,Na)NO ₃	+ 677	-0.64 ± 0.12	1044 ± 69	1076 ± 75	1108 ± 81
(Ag,K)NO ₃	- 303	-0.35 ± 0.15	$- 102 \pm 86$	$- 85 \pm 94$	$- 67 \pm 101$
(Ag,Rb)NO ₃	- 944	-0.80 ± 0.23	$- 485 \pm 132$	$- 445 \pm 143$	-405 ± 154
(Ag,Cs)NO ₃	(-1396)	-0.61 ± 0.22	-1046 ± 126	-1016 ± 137	-985 ± 148

The measurement of the activity of silver in a nitrate melt that contains some halide ion is complicated by the formation of a silver halide complex equilibrium



The entire field of silver complexes and other metal complexes in molten nitrates has been studied by many workers over the past years (99, 103, 118, 127, 142, 144-146). They have dealt with equilibrium constants, heats of reaction, deviations from various molten salt theories, ion size and charge effect, activity coefficients and other physical properties of the system. The topic of complexes in the nitrate melt may appear to be overworked; however, there are still some serious discrepancies in the results of many of the recent studies.

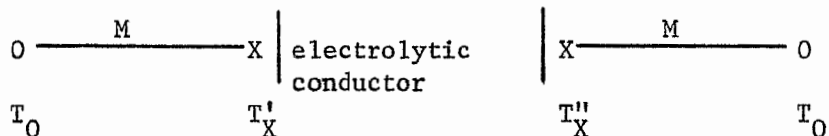
3.5 Thermoelectric Cells

The thermogalvanic cell or non-isothermal cell is defined as a galvanic cell in which the temperature is not uniform. A thermoelectric device consists entirely of electronic conductors whose state remains unchanged when a current is passed through it. The passage of a current through a thermogalvanic cell causes a change in the "chemical" state of the system at points where the fraction of the total current carried by one ion type varies with position and in

particular at the electrodes where the conduction changes from ionic to electronic.

Eastman (147) and Wagner (148) have presented a detailed theory of thermocells, and in recent years many workers have effectively used irreversible thermodynamics to explain the thermal emf of these cells (149 - 153). There are several excellent reviews on thermocells (154 - 157). Wartnerowicz, in a series of papers (158 - 160) has worked out the theoretical analysis of a molten salt thermocell as a thermoelectric generator and compared it with experimental data. He reports that the figure of merit, Z , for the fused salt system is lower than that for classical semiconductors; however, a great advantage of molten salts is that their physical parameters are relatively independent of the temperature and they can operate over a wide range of temperatures. The use of molten salts in thermoelectric cells appears to be promising; however, since available theoretical and experimental results are scarce, it is not possible to predict future practical applications.

Consider the typical cell:



where the electrodes X are chemically identical and equal. The sign convention used for thermal cells is the sign of the emf of the cell and the hot electrode are the same. The thermoelectric power, \mathcal{E} , is defined as:

$$\mathcal{E} = \left(\frac{\partial E}{\partial T''} \right)_{T'} \qquad T'' > T' \qquad (3.107)$$

The temperature gradient in the cell causes a concentration gradient to be slowly set up (Soret effect). If $T'' = T' + dT$, then the following relation holds:

$$dE = \left(\frac{\partial E}{\partial T} \right) dT + \left(\frac{\partial E}{\partial N_i} \right) dN_i \quad (3.108)$$

Initially $dN_i = 0$, thus the initial thermoelectric power, \mathcal{E}_{in} , is given by:

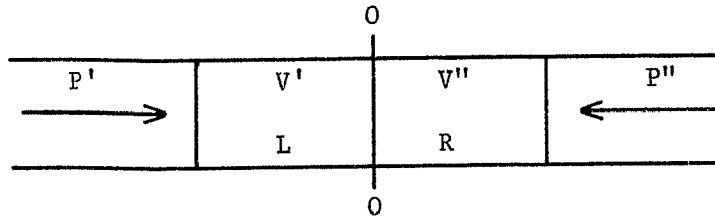
$$\mathcal{E}_{in} = \left(\frac{\partial E}{\partial T} \right) = \text{(Seebeck coefficient)} \quad (3.109)$$

By convention (161), the sign of the Seebeck coefficient is the same as that of the hot electrode. The static power, \mathcal{E}_{st} , is given by:

$$dN_i = f(dT) \quad (3.110)$$

$$\mathcal{E}_{st} = \frac{\partial E}{\partial T} + \left(\frac{\partial E}{\partial N_i} \right) \left(\frac{dN_i}{dT} \right) = \frac{dE}{dT} \quad (3.111)$$

To define the different entropies and heats involved, consider the following cell and conditions:



1. one mole of i crosses the 0-0 line from the left, L, to the right, R, by the mechanism responsible for diffusion or migration.
2. The net amount of other species crossing the 0-0 line is zero
3. $\Delta P = 0$
4. $\Delta T = 0$ at any point

5. The net heat exchange with the surroundings is zero;
however, there may be a flow of heat between R and L.

The ΔS in R equals $+s_i$ (the partial molar entropy of i). The transport of one mole of i by itself may not produce a change of s_i but rather some fraction, \bar{s}_i (transported entropy). To make up the difference the amount of heat flow is:

$$\hat{Q} = T(\bar{s}_i - s_i) \quad (3.113)$$

or the reduced heat of transport. The Eastman entropy of transfer, \hat{s}_i , is given by:

$$\hat{s}_i = \hat{Q}_i/T = \bar{s}_i - s_i \quad (3.114)$$

The Peltier effect was first observed in metallic conductors. When a current is passed through a junction between two different metals Y/Z there is another heating effect additional to the Joule heating. The Joule heating is proportional to the current squared, and thus can be distinguished from the Peltier effect (II_{YZ}) which represents the amount of heat flow required to keep the temperature constant with the passage of F coulombs of current. The change in the entropy at the Y/Z junction is given by:

$$dS = (C_p/T)dT + (\partial S / \partial P)dP \quad (3.115)$$

and at constant T and P, $dS = 0$.

The flow of 1 mole of electrons results in:

- a. The intake of the heat II_{YZ}
- b. The transport of entropy $\bar{s}_{e(Z)}$ by the electrons in Z entering the junction region and $\bar{s}_{e(Y)}$ leaving via Y

When a temperature gradient is applied to a homogeneous mixture of two or more components, there is a partial separation due to a migration process called thermal diffusion, thermal migration or the Soret effect. In a closed system with a constant temperature gradient, a steady state will be set up between the Soret effect and ordinary diffusion (Soret equilibrium). The Soret coefficient, σ , for a two component system is given as:

$$(\text{grad } \ln N)_{St} = - \sigma \text{ grad } T \quad (3.126)$$

where N = mole fraction, and St refers to the steady state. σ is usually positive for salts in water (i.e., the salts move to the colder end) having a value of approximately $3 \times 10^{-3} \text{ deg}^{-1}$ at 25°C .

From reversible thermodynamics the following equations can be derived for non-ionized solute, 1,

$$T\hat{S}_1 = \hat{Q}_1 = RT^2 \left[1 + \left(\frac{\partial \ln \gamma}{\partial \ln N} \right) \right] \quad (3.127)$$

where γ is the activity coefficient on the molality scale.

Slightly more complex equations are realized for an ionized solute, 12, ($12 \rightarrow \nu_1^1 + \nu_1^2$).

$$\begin{aligned} T(\nu_1^1 \hat{S}_1 + \nu_2^1 \hat{S}_2) &= \nu_1^1 \hat{Q}_1 + \nu_2^1 \hat{Q}_2 \\ &= (\nu_1^1 + \nu_2^1) RT^2 \left[1 + \left(\frac{\partial \ln \gamma_{\pm}}{\partial \ln N} \right) \right] \sigma \end{aligned} \quad (3.128)$$

$$\gamma_{\pm} = (\gamma_1^{\nu_1^1} \gamma_2^{\nu_2^1})^{-(\nu_1^1 + \nu_2^1)} \quad (3.129)$$

The emf of a cell in its initial state (uniform molality with a temperature gradient of dT/dX) is the sum of:

- a. The nonisothermal part of the metallic circuit

$$F \left(\frac{\partial E}{\partial X} \right) = \hat{S}_{e(M)} \left(\frac{dT}{dX} \right) \quad (3.130)$$

- b. Any metal/metal junctions
- c. The electrode/solution interface
- d. The nonisothermal solution

$$F \left(\frac{\partial E}{\partial X} \right)_{in} = - \left(\sum \frac{t_i}{Z_i} \hat{S}_i \right) \frac{\partial T}{\partial X} \quad (3.131)$$

The b and c potentials at the interfaces are identical except for a T factor and they can be expressed in terms of partial molar entropies of A^+ , A and the electrons, e, in the metals M and A.

$$F \frac{dE}{dT} = s_A - s_{A^+} - s_e \quad (3.132)$$

For a single component molten salt the total emf is given by:

$$F \left(\frac{dE}{dT} \right)_{in} = \left[t_2 (\hat{S}_1 + \hat{S}_2) - \bar{S}_1 - \hat{S}_{e(M)} + s_A \right] \quad (3.133)$$

$$F \mathcal{E}_{in} = \frac{II}{T} \quad (3.134)$$

To change to a non-uniform concentration cell only the emf of the appropriate cell with transport need be added. If the concentration changes from N to N + dN (Left to Right), the following equation holds:

$$FdE = 2RT t_2 \left[1 + \left(\frac{\partial \ln \gamma_{\pm}}{\partial \ln N} \right) \right]_T d \ln N + \left[t_2 (\hat{S}_1 + \hat{S}_2) - \bar{S}_1 - \bar{S}_{e(M)} + s_A \right] dT \quad (3.135)$$

and at the Soret equilibrium:

$$F \frac{dE_{st}}{dT} = - \left[\bar{S}_1 + \bar{S}_{e(M)} - s_A \right] = F \mathcal{E}_{st} \quad (3.136)$$

thus:

$$F(\mathcal{E}_{in} - \mathcal{E}_{st}) = t_2(\hat{S}_1 + \hat{S}_2) \quad (3.137)$$

The concentration dependences of the different quantities are given by:

$$s_i = s_i^o - R \ln N_i + s_i' \quad (3.138)$$

where s_i^o is the standard value on mole fraction scale and s_i' is the deviation from ideality (ionic interaction)

and similarly

$$\bar{S}_i = \bar{S}_i^o - R \ln N_i + \bar{S}_i' \quad (3.139)$$

$$\hat{S}_i = \hat{S}_i^o + \hat{S}_i' \quad (3.140)$$

$$\hat{Q}_i = \hat{Q}_i^o + \hat{Q}_i' \quad (3.141)$$

$$\mathcal{E}_{in} = \mathcal{E}_{in}^o + \frac{R}{F} \ln N_i + \mathcal{E}_{in}' \quad (3.142)$$

\hat{S} and \hat{Q} can not be determined for the individual ions but a reference scale can be set up. If the transported entropy of any ion i , \bar{S}_i , has been determined, a conventional standard Eastman entropy (147), $S_i^o = \bar{S}_i^o - s_i^{o \text{ conv.}}$, can be obtained. $s_i^{o \text{ conv.}}$ is the conventional standard entropy of i on the standard scale. Two different aqueous based scales have been used. ($s_{H^+}^o = 0$ and $s_{Cl^-}^o = 0$).

The \mathcal{E}_{in} is determined using a "U" cell with its two limbs at T_1 and T_2 . The potential of the isothermal cells at T_1 and T_2 may differ by up to $50 \mu V$; thus, Eastman used a temperature reversal

and average emf to eliminate this error. \mathcal{E}_{in} is linear in aqueous solutions over a 20°C change. The \mathcal{E}_{st} is more difficult than the \mathcal{E}_{in} to measure because convection must be avoided. A sandwich cell, consisting of a frit filled with the electrolyte between two temperature controlled electrodes, is used for the \mathcal{E}_{st} measurements.

The Peltier heat is measured in a divided calorimeter. An electrical heater is used to maintain a constant temperature. Different current densities were used and extrapolated to $I = 0$ to eliminate the Joule heating.

A derivation of an expression for the potential of a thermocell in the general case of an electrolytic solution has been given by Holtan et al. (162). In the special case of a one component molten salt (e.g., silver nitrate) in which the same forward and reverse reactions occur at the two electrodes, their equation reduces to

$$F\left(\frac{dE}{dT}\right)_{in} = -\bar{\bar{s}}_{AgNO_3} - \bar{\bar{s}}_e + s_{Ag} - (t_{NO_3^-})(s_{AgNO_3}) \quad (3.143)$$

upon the adoption of the definition

$$\bar{\bar{s}}_{AgNO_3} = (t_{Ag^+})(\bar{\bar{s}}_{Ag^+}) - (t_{NO_3^-})(\bar{\bar{s}}_{NO_3^-}) \quad (3.144)$$

Equation 3.143 is equivalent to the combination of equation 3.133 and 3.144 and a rearrangement of terms. The first two terms in 3.143 are entropies of transport and the last two are ordinary "thermodynamic" entropies. Sundheim and Rosenstreich (163) have measured $F\left(\frac{dE}{dT}\right)_{in}$ and calculated the values for the last three terms to evaluate $\bar{\bar{s}}_{AgNO_3}$ in equation 3.143 at 225°C, as follows:

$$F \left(\frac{dE}{dT} \right)_{in} = -7.93 \text{ eu} \quad (3.145)$$

$$s_{Ag} = 13.3 \text{ eu} \quad (3.146)$$

$$t_{NO_3^-} = 0.635 \quad (3.147)$$

$$s_{AgNO_3} = 49.14 \text{ eu} \quad (3.148)$$

$$\bar{s}_e = 0.03 \text{ eu} \quad (3.149)$$

$$\bar{s}_{AgNO_3} = -9.95 \text{ eu} \quad (3.150)$$

The Peltier heat calculated from the thermoelectric power $\frac{dE}{dT}$ is

$$II = -T \frac{dE}{dT} \quad (3.151)$$

$$II = 4.57 \text{ kcal equiv}^{-1} \text{ at } 305^\circ\text{C} \quad (3.152)$$

Sundheim and Resenstreich obtained an average value of $343 \mu\text{V deg}^{-1}$ for the Seebeck coefficient, $\left(\frac{dE}{dT} \right)_{in}$, of silver nitrate from 240°C to 310°C which agrees with the results of other workers (157, 164 - 167). Metz and Seifert (168) pointed out that there is no Soret effect in the single salt systems since there is only a single cation present. The addition of a second salt permits the Soret effect to operate in the system and it then becomes necessary to extrapolate back to time zero to obtain the Seebeck coefficient. The emf of the two-component cell changes slowly until it reaches a static value (at the Soret equilibrium), then the sum of the entropy of transfer for the two cations can be calculated using equation 3.137. The Seebeck coefficient, \mathcal{E}_{in} , of the mixture is related to the Seebeck coefficient, \mathcal{E}_{in}^o , of the pure electroactive salt by equation 3.142. The correction term, \mathcal{E}'_{in} , for the non-ideality is eliminated by the use of activities

instead of concentrations to give the equation

$$\mathcal{E}_{in}^{\circ} = \mathcal{E}_{in} - \frac{R}{F} \ln a_{Ag(I)} \quad (3.153)$$

when the electroactive salt is silver nitrate. Dupuy (166) developed the equation

$$\mathcal{E}_{in}^{\circ} = \mathcal{E}_{in} - \left[\frac{R}{F} \ln N_{Ag(I)} + \frac{R}{F} \ln \gamma_{Ag(I)} - \frac{\Delta \bar{H}_M}{FT} \right] \quad (3.154)$$

to relate the \mathcal{E}_{in} in the mixture to the \mathcal{E}_{in}° for the pure silver nitrate. The $\Delta \bar{H}_M$ is the partial heat of mixing and can be derived from calorimetric measurements. In an ideal solution equation 3.154 reduces to

$$\mathcal{E}_{in}^{\circ} = \mathcal{E}_{in} - \frac{R}{F} \ln N_{Ag(I)} \quad (3.155)$$

Typical values for the terms in equation 3.154 for the silver-lithium nitrate system at 265°C (164, 169) are

$$N = 0.2 \quad (3.156)$$

$$\Delta \bar{H}_M = 0.42 \mu V \quad (3.157)$$

$$\gamma = 1.656 \quad (3.158)$$

and

$$\mathcal{E}_{in} = -455 \mu V \text{ deg}^{-1} \quad (3.159)$$

to give

$$\mathcal{E}_{in}^{\circ} = -326 \mu V \text{ deg}^{-1} \quad (3.160)$$

The silver-sodium nitrate system has been studied by several workers (165, 170, 171) and the reported \mathcal{E}_{in}° is -319μ volts degree⁻¹ and the average values of 1.5 kcal mole⁻¹ for the heat of transport and -1.2 eu

for the entropy of transport is given for the silver(I) ion.

The Soret coefficient for silver nitrate in all of the alkali nitrates has been determined (171) and in each case it is found that the silver(I) migrates to the colder portion of the electrochemical cell.

3.6 Gas Electrodes

The work reported in the literature on gaseous electrodes in molten nitrates has been limited to mainly the "oxygen electrode" and the nitrate electrode. Kust (85) has recently published a review on the oxygen electrode. The oxygen-oxide couple was fully discussed previously in this chapter in connection with the electrochemistry of oxides in nitrate melts.

The main reasons for developing a gaseous electrode which is reversible to the anion of the melt is to permit the direct measurement of the formation potential of the pure salts and to eliminate liquid junction potentials. Arvia and co-workers have reported the existence of reversible formation cells for silver nitrate, lithium nitrate, sodium nitrate and potassium nitrate (75, 96, 117, 172). A specially designed U-shaped cell was used to trap the products of electrolysis at each electrode. A steady emf was rapidly established after the electrolysis had ceased. The potential was quickly reestablished after the two electrodes were momentarily shorted out. The bubbling of nitrogen through the melt at the anode was observed to cause faster decay in the emf than the bubbling of oxygen (96) which

was attributed to the slow removal of the nitrogen dioxide-oxygen mixture from around the platinum electrode. Even though their claims of an alkali ion-alkali metal electrode have been questioned (cf. chapter 3.3, page 40), their measured formation potentials for the nitrate salts were in close agreement over a wide temperature range with the theoretical values calculated from thermodynamic data. In a recent communication, Lunden (173) reviewed the use of gaseous electrodes in molten nitrates and nitrites and criticized much of the work done on these melts by Arvia et al. (75, 96, 117, 172).

Ketelaar and Dammers-de Klerk (174) have developed a reversible nitrate electrode consisting of a bristle of platinum wires through which a stream of nitrogen dioxide and oxygen is maintained. The brush consisted of about 100 platinum wires (0.3 mm x 100 mm) with an overall diameter of about 8 mm sealed in the end of a piece of glass tubing. The electrode was adjusted so that the brush just touched the melt and through capillary action the melt was drawn up into the brush. The gas was dispersed through the wires to make the required three-phase contact for the reaction



The study was carried out in pure silver nitrate with a silver reference electrode. The electrochemical cell is represented by



the overall chemical reaction by

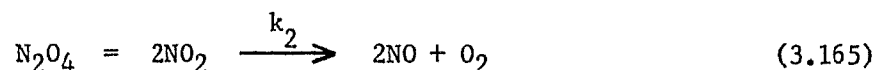


and the observed emf by

$$E = E^{\circ} + \frac{RT}{F} \ln \left[\frac{P}{P_{\text{NO}_2} P_{\text{O}_2}^{\frac{1}{2}}} \right] \quad (3.164)$$

The value of E° from this equation compared very well with the calculated value from thermodynamic data (95, 175-177) from 215°C to 360°C. They maintained a constant nitrogen dioxide-oxygen ratio throughout all the experiments, thus never really testing the logarithmic part of the Nernst equation. The micro-polarization technique was used to verify the reversibility of the nitrate electrode.

Some dissociation of the nitrogen dioxide into nitric oxide and oxygen takes place at the temperatures of the nitrate cell. From the thermodynamics (75, 175, 178) and the slow second order kinetics (179 - 181) for the reaction

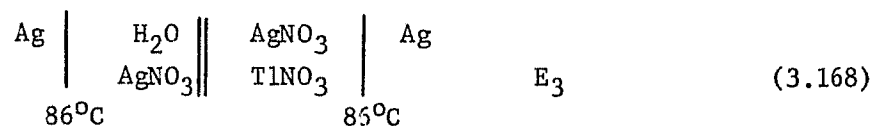


they concluded that the dissociation of the nitrogen dioxide could be neglected under the conditions (e.g., of residence time) in their experiment.

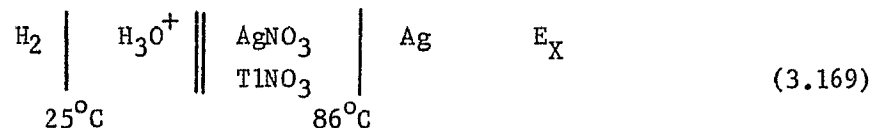
The nitrate electrode has been used in dilute solutions of silver nitrate in each of the alkali nitrate melts to determine the silver activity in each solvent (120). The nitrate electrode was used to eliminate the error introduced into the measurements by the assumption made by all previous workers that the liquid junction potential was zero in the silver nitrate concentration cells. The liquid junction potential has been shown to have a non-zero value for several systems (63, 182).

3.7 Aqueous // (Ag,Tl)NO₃ Junction Potential

Abraham (183) has shown that it is possible to establish a general electrochemical scale for both aqueous and fused salt solvents if a common reference electrode is selected. He chose the hydrogen electrode at 25°C as the common reference electrode. He used the following cells to determine the potential of the silver reference electrode in the silver-thallium nitrate eutectic at 86°C with respect to the hydrogen electrode:



The overall potential ($E_X = E_1 + E_2 + E_3$) for the cell



represents the difference between the electrode potentials based on the silver-silver, thallium nitrate eutectic reference electrode and the proposed general electrochemical scale.

The final electrochemical cell (3.169) was equivalent to a combination of three separate cells, a classical electrochemical cell

(3.166), a thermoelectric cell (3.167) and a solvent junction cell (3.168). The potential of each cell varied with the concentration of silver nitrate; however, the total emf remained constant as shown in Table 3.4.

TABLE 3.4

MEASURED POTENTIALS OF THE ELECTROCHEMICAL CELLS 3.166-3.168

Normality AgNO ₃	E ₁ (mV)	E ₂ (mV)	E ₃ (mV)	E _X (mV)
10 ⁻⁴	561	-71	346	836
10 ⁻³	620	-50	271	841
10 ⁻²	680	-39	196	837
10 ⁻¹	732	-20	121	833

The average potential, E_X, for the overall cell (3.169) was 837 mV.

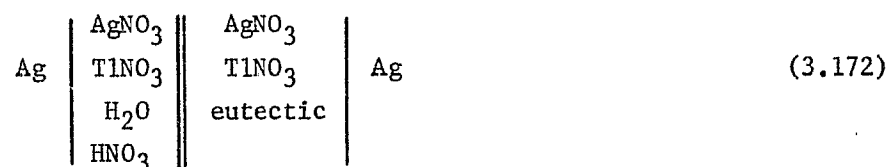
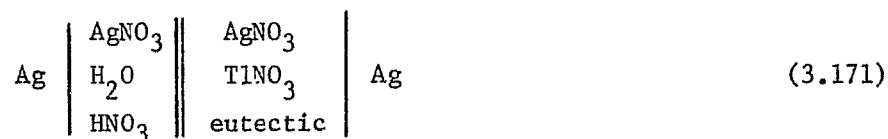
The mole fraction of silver nitrate in the nitrate eutectic was 0.533.

Assuming ideal behavior in the eutectic the standard electrode potential of a hypothetical silver-silver nitrate electrode at 86°C versus a Standard Hydrogen Electrode (S.H.E.) at 25°C is given by

$$\begin{aligned}
 E_X^{\circ} &= 0.837 - \frac{RT}{F} \ln(0.533) & (3.170) \\
 &= 0.837 - 0.0713 \log (0.533) \\
 &= 0.837 + 0.019 \\
 &= 0.856 \text{ volts}
 \end{aligned}$$

The final potentials E_X and E_X^o contain a contribution due to the liquid junction potential in cell 3.168.

Abraham and Hechler (184) continued the work on the aqueous-nitrate melt solvent junction to obtain definitive information on the liquid junction potential in the cell. They studied the following two cells at 91.5°C:



The acid content in the aqueous portion of each cell was adjusted to give a pH of 2.8 at 25°C. The acid increased the stability of the aqueous portion of the cells. The silver to thallium ratio in the second cell (3.172) was kept at the same value as it is in the eutectic. The silver concentration, C , in the aqueous half-cells was varied from 10^{-3} to 10^{-1} molar and the calculated activity coefficient, γ , for the silver ranged from 0.929 to 0.654. The observed emf for both cells was given by

$$E = E_{\text{melt}} - E_{\text{aq}}^{\circ} - \frac{RT}{F} \ln C \gamma + E_J \quad (3.173)$$

where E_{melt} = the electrode potential of silver in the eutectic

E_{aq}° = the standard aqueous silver electrode potential

E_J = liquid junction potential

The value of A as defined by

$$A = E + \frac{RT}{F} \ln C \gamma = E_{\text{melt}} - E_{\text{aq}}^{\circ} + E_J \quad (3.174)$$

was found to be 22.6 ± 0.5 mV for both cells (3.171 and 3.172). This indicates that E_J must be a constant value and, since there were large variations in the composition of the two aqueous half cells, they concluded that the liquid junction potential must be approximately zero for the aqueous-nitrate eutectic solvent junction. The measured values for the cells in this study were about 25 mV lower than those observed in their earlier work (183). This difference may be due in part to a temperature increase of 5.5°C and the addition of nitric acid to the later cells. Abraham and Hechler studied a similar system in which the melt was composed of the nitrate salts of silver, cesium, thallium and cadmium (185) and concluded that the liquid junction potential was zero for this system also. These results would seem to eliminate any objection to the bridging of aqueous solution and molten salt electrochemistries because of the presence of a liquid junction potential.

4. PREVIOUS STUDIES ON THE PROPERTIES OF CHLORIDE MELTS

4.1 Physical and Electrochemical Properties

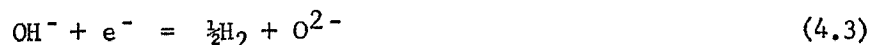
The lithium-potassium chloride eutectic (0.59:0.41) has received more attention than any of the other chloride melts due to its useful electrochemical range of about 3.6 volts (186) and its low melting point (352°C); the melting points of the pure alkali chlorides range from 610°C for lithium chloride to 801°C for sodium chloride. The conductivity, density, viscosity, vapor pressure and other physical properties of the pure metal chlorides and some mixtures of metal chlorides have recently been tabulated by Janz (2). Flengas and Ingraham (187) used the equimolar sodium-potassium chloride mixture (m.p. 658°C) as a solvent in the temperature range of 650°C to 900°C to evaluate the electrode potential and activity of fourteen different metals. The electrochemistry of individual metals in the various chloride melts has been included in many of the recent reviews (7, 10, 11, 14, 15, 18).

One of the main disadvantages of the lithium-potassium chloride eutectic is the hygroscopic nature of the lithium ion. There are two basic methods for the purification of the chloride eutectic: one utilizes hydrogen chloride gas (186, 188) and the other uses chlorine gas (189). If the moisture is not removed, hydrolysis occurs upon

fusion by the reactions:

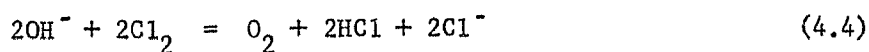


The hydrolysis products precipitate metal ions, a black glass and the hydroxide ion is more readily reduced than the alkali metals according to the equation:



In the hydrogen chloride method (186) the mixed salts are predried at 300°C under vacuum for several hours to eliminate most of the water before fusion occurs. Hydrogen chloride is then bubbled through the melt at 500°C to shift the hydrolysis reaction (4.1) far to the left; this step is then followed by further evacuation to volatilize the water. The last traces of hydrogen chloride are removed from the melt by a three-hour period under a high vacuum. In more recent work Laitinen et al. (188) have modified this method by the addition of magnesium metal to the final melt to displace any heavy metals, followed by filtration through a sintered glass frit to remove any metal precipitates or carbonaceous materials from the melt. The final melt was sealed in glass ampules and stored until needed.

The chlorine treatment (189) utilizes the same apparatus as the previous method, except that chlorine gas is used instead of hydrogen chloride gas. There is no need for predrying in this method and the hydroxide ions formed by hydrolysis are removed by the reaction



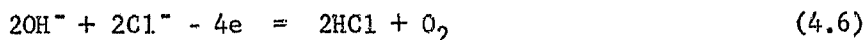
According to Maricle and Hume (189), the oxygen, hydrogen chloride and excess chlorine are completely removed by a forty-minute purge with argon gas.

The purity for both methods was checked by running a polarogram with a micro platinum or tungsten indicator electrode and a large platinum reference electrode. The wave produced by hydroxide occurs at approximately -1.6 volts versus the platinum reference electrode while those of hydrogen chloride and the alkali metal occur at approximately -0.5 to -1.5 and -2.6 volts, respectively (186). Recently, MacKenzie (190) has critically reviewed the chloride purification techniques and the various methods used to remove metal impurities.

Several French workers have used current voltage curves obtained from molten lithium-potassium chloride eutectic contaminated with hydroxide and oxide ions to evaluate the basic reactions involving oxide, hydroxide, water and the hydronium ion (191-195). Delarue (191) observed an oxidation wave at about ± 0.2 volts versus a platinum reference electrode and he attributed it to hydroxide or oxide ions.



OR



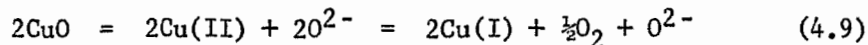
OR



He assumed that hydroxide ions do not exist in the melt, but are spontaneously converted to oxide ions.



From Delarue's investigations of solutions of metal oxides (lead oxide, nickel oxide, calcium oxide, magnesium oxide and cupric oxide) it can be inferred that these oxides are dissociated in the melt. The oxide ion may be oxidized either electrochemically or chemically:



Littlewood and Argent (86) have also studied the effect of aqueous contaminants on the redox potential of the equimolar sodium-potassium chloride melt at 700°C. They claim that a hydrogen electrode of the type $\text{HCl}_{(\text{g})}, \text{H}_{2(\text{g})}/\text{Pt}$ does not reach equilibrium in a chloride melt containing little or no aqueous impurities. This is contradicted by the later results obtained by Laitinen and Plambeck (196) in the lithium-potassium chloride eutectic.

Laitinen and Bhatia (197) have made an electrochemical study of metallic oxides in fused lithium-potassium chloride eutectic at 400 to 500°C. They reported that the oxygen electrode does not behave reversibly but several electrodes of the second kind (e.g., $\text{Cu}/\text{Cu}_2\text{O}$, O^{2-} ; Pt/PtO , O^{2-}) exhibited reversible behavior. Due to the rather high solubility of the metal oxides, the measuring capabilities of these electrodes are limited to oxide concentrations in excess of 10^{-3} molar or higher depending upon the system. The high solubility of the heavy metal oxides in the solvent was attributed to the complexing tendency of the chloride ion. The nature of these complex ions in a chloride melt has been studied by cryoscopic techniques (198) and vapor pressure measurements (199).

Modern instrumental methods have been employed recently to study electrode processes in molten salts. Laitinen and Osteryoung (200) applied the impedance method to solid platinum electrodes in fused lithium-potassium chloride eutectic at 450°C; however, residual currents due to impurities in the melt prevented quantitative interpretation of the data. They concluded that the platinum(II)/platinum electrode was reversible in the melt. Laitinen and Gaur (201) used the impedance method in a purer chloride eutectic to study the kinetics of the metal-metal ion couples for cobalt, zinc, lead, bismuth, nickel and cadmium. They found pseudocapacity peaks anodic to the equilibrium potentials for the system, suggesting predeposition of the metal due to some interaction with the solid platinum electrode. The analysis of the data was possible only after the data were corrected for adsorption of the metal ions on the electrode surface. The double pulse and the voltage step methods were used by Laitinen et al. (188) to determine the exchange current for the metals named above. The results for the cadmium couple were the same for both methods and agreed with the impedance method (201); however, the results for the zinc couple agreed with those from the two relaxation methods but not with the impedance measurement. The voltage-step method was found to be the easiest to use and the best suited for molten salt work. Hills and Johnson (113) using a faradaic impedance technique found that for the platinum couple the results were normal and they were able to evaluate the exchange current, but anomalous results were found for nickel. The capacity of the double layer in fused chloride melts has

been measured by several workers (113, 201, 202) and there is significant agreement between their results provided a very pure melt is used at all times.

4.2 Electrodes and Electrode Potentials

The first systematic measurement of equilibrium electrode potentials in lithium-potassium chloride eutectic was made by Senderoff and Brenner (203) using a silver chloride-silver reference system. Although the chlorine electrode had been used before (204), Laitinen and Pankey (205) were the first to thoroughly investigate and establish its attributes as a reference electrode and to measure its potential with respect to the platinum(II)/platinum reference electrode (206). Because the platinum(II)/platinum reference electrode is reliable and easily prepared, it has become the basis of a fairly comprehensive emf series which has been compiled into a noteworthy review by Plambeck (20). At temperatures in excess of 550°C the thermal instability of the platinum(II) becomes apparent and for this reason workers (207, 208, 310, 311) studying the temperature dependence of cell emfs have used the chlorine or silver(I)/silver reference electrode system. The potentials of both the platinum and silver electrode systems have been measured against the chlorine electrode as a function of temperature (205, 207, 208), thus making it possible to convert freely from one reference system to another. The chlorine electrode has the greatest thermodynamic value but is the most difficult of the three to use in the laboratory. The operation and characteristics of the chlorine

electrode will be discussed later in section 4.5 (page 88).

Hamer, Malmberg and Rubin calculated the theoretical emf of formation cells for 96 metal couples in pure solid or molten chloride (209) and later extended their calculations to fluoride, bromide and iodide systems (210) for temperatures from 25°C to 1500°C. Metz (211) used statistical mechanics to calculate the temperature dependence of the formation potential for lithium chloride but the calculation is long and complex, thus having very little practical application.

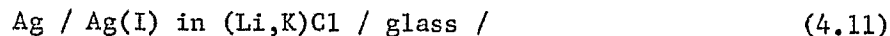
Due to the various methods of isolating the silver(I)/silver reference electrode from the rest of the system, its development has been the subject of many papers. Several workers (187, 203, 204, 212) have used an asbestos fiber sealed in silica glass to connect the silver reference electrode compartment with the rest of the melt at temperatures in excess of 600°C. Denning (106) replaced the asbestos fiber, which he found difficult to prepare, by a finely drawn out Luggin-Haber type capillary for work in molten potassium chloride at 800°C. Littlewood (213) objects to these types of reference electrodes since the asbestos plug or the capillary will let contamination from the working melt into the reference electrode. A reference electrode of the type



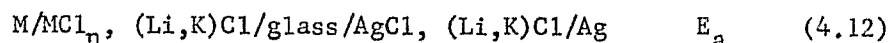
was found to be reproducible to ± 10 mV and to be unaffected by freezing followed by fusion. The Supremax glass sheath, approximately 1 mm thick, had a membrane resistance of 0.5 to 1 meg ohm and allowed no contamination in from the outside melt. Assuming that only the

cations were transported through the glass, Littlewood calculated the junction potential across the glass membrane to be 18.6 mV at 700°C. This compares fairly well with the estimated value of 21 mV from emf measurements. The potential of the silver(I)/silver reference electrode, 0.271 mole fraction silver chloride, in an equimolar sodium-potassium chloride melt at 700°C, versus a chlorine electrode, was 939 mV. Bockris et al. (108) claimed that only the solvent cations of the lithium-potassium chloride eutectic and not the silver ions could diffuse through a thin glass membrane reference electrode. The membrane was very fragile and had a resistance of about 2000 ohms. If a correction, based on the assumption that the glass was impermeable to the silver ion, was made for the membrane potential, the electrode obeyed the Nernst equation for silver concentrations from 7×10^{-3} to 5×10^{-2} silver chloride mole fraction in the temperature range from 350 to 550°C. It is difficult to understand how a thin glass membrane would not stop either ion.

Yang and Hudson (208) pointed out that although the chlorine electrode is the ideal reference electrode in chloride melts another reference electrode, such as



must be used due to the oxidizing properties of chlorine. They considered the following three cells in order to evaluate the junction potential across the glass membrane:



$$\text{Ag/AgCl, (Li,K)Cl/Cl}_2 \quad E_c \quad (4.14)$$

It can be shown that ΔE , defined as $\Delta E = E_a + E_c - E_b$, can be calculated from thermodynamics by

$$\Delta E = \frac{1}{nF} \left[\mu(\text{Cl}^- \text{ in } \text{MCl}_n, (\text{Li,K})\text{Cl}) - \mu(\text{Cl}^- \text{ in } \text{AgCl}, (\text{Li,K})\text{Cl}) \right] + E_m \quad (4.15)$$

The equation for ΔE is composed of two parts, the first is the difference in the chemical potential, μ , of the chloride ion on each side of the membrane and the second, E_m , is the membrane potential for the cell. In general the chemical potentials of the chloride ion are unknown; thus, only the total effect, ΔE , could be evaluated. They examined eight different metals over a range of temperatures, concentrations and membrane materials. The values for ΔE ranged from 1 to 50 mV depending upon the nature of the system. Some of the general trends which were observed are as follows:

1. ΔE is negligible when the metal chloride is silver chloride and tends to higher values as the tendency for metal to form complex ions increases;
2. ΔE decreases as the concentration of MCl_n decreases;
3. ΔE does not vary appreciably with temperature;
4. ΔE is not affected by the AgCl concentration until it exceeds 0.6 mole fraction, then ΔE becomes abnormally high;
5. ΔE is considerably higher for Vycor and quartz membranes than for Pyrex membranes.

They report that the reference electrode was reproducible to ± 2 mV and stable at 800°C for 40 hours with a potential change of less than a few millivolts.

The majority of workers in the lithium-potassium chloride eutectic use a medium or fine porosity sintered glass frit to separate the reference electrode from the rest of the system. When dealing with a short period of time, the diffusion through the frit, when it is used to separate dilute solutions of metal ions in the common solvent, can be neglected.

After platinum was established as a reference electrode (206), its anodic behavior in molten chloride was studied by several investigators. Laitinen *et al.* (188, 205) explained that the failure to oxidize iron(II) to iron(III) in the lithium-potassium chloride eutectic was due to the formation of platinum chloride on the platinum surface. Delarue (191) obtained a peak in the anodic portion of a voltammetric curve for a micro platinum electrode in the lithium-potassium chloride eutectic at 400°C. The peak began at -0.05 V and at approximately +0.1 V reached a maximum value of approximately 310 μ A mm⁻², after which the current dropped immediately to a small residual value. The final oxidation wave occurred at approximately +1.0 V versus a platinum(II)/platinum reference electrode. The cathodic portion exhibited a single decomposition wave at approximately -2.6 V provided the micro electrode had not been anodized. For a platinum electrode, maintained at +0.2 V for one minute, the cathodic polarization produced two cathodic waves, the first at approximately -1.0 V

and the second in excess of -2.0 V. The first wave was not reproducible and the current density varied from 100 to 400 μ A mm⁻². The anodic portion of these results have been verified and interpreted as the formation of a passive layer of platinum oxides (214) or potassium chloro-platinate (215). Asakwra and Mukaibo (216) studied the passivation of platinum in the lithium-potassium chloride eutectic by means of potential-sweep, galvanostatic, potentiostatic and potential-decay measurements. They explained their results on the basis of the following assumptions:

1. When the electrode potential reaches the passivation potential, E_0 , the electrode becomes covered with a non-conducting film;
2. The electrode process is controlled by the diffusion of platinum ions into the solution before passivation occurs.

The activity of the platinum ion, a_p , in the non-conducting film was related to the activity, a^0 , of the platinum ions in the solution by

$$a_p = a^0 \exp(nFE_0/RT) \quad (4.16)$$

The platinum ion is normally generated in the melts by coulometric oxidation; therefore, the question arises, will the potential of this electrode be equal to the potential of a platinum(II)/platinum electrode system in which the platinum(II) has been introduced by some other means, e.g., adding platinum chloride. If the anodic film remains on the platinum surface, it will undoubtedly affect the potential of the electrode to some degree and this would impair its usefulness

as a reference electrode.

4.3 Activities and Thermodynamics of the Silver Ion in Alkali Chloride Melts

The activity and activity coefficient for the silver ion or any other metal ion dissolved in an alkali metal chloride melt can be determined by studying the cell



where the measured potential, E, is given by:

$$E = E^{\circ} - \frac{RT}{F} \ln \frac{a_{\text{AgCl}}}{P_{\text{Cl}_2}^{1/2}} \quad (4.18)$$

and

$$\frac{a_{\text{AgCl}}}{N_{\text{AgCl}}} = \gamma_{\text{AgCl}} \quad (4.19)$$

The standard electrode potential of silver chloride as a function of temperature has been determined directly from the formation cell (168, 207, 217 - 223);



or from thermodynamic calculations (209). All of the determinations of E° agree within a few millivolts. In all the chloride melts that have been studied it was assumed that the chloride ion activity remains constant. The silver activity coefficient is greater than unity in solutions of lithium chloride (224, 225) and sodium chloride (217, 226, 227) but less than unity in potassium chloride (130, 204, 223, 228, 229) and cesium chloride (230). The partial molar excess free energy,

\bar{G}_i^E , varies almost linearly with the composition of a mixed solvent (A + B) from its value in pure A to that in pure B (230). \bar{G}_i^E is related to the activity coefficient, γ_i , of the i^{th} component by

$$\bar{G}_i^E = RT \ln \gamma_i \quad (4.21)$$

The activity coefficient for silver chloride in equimolar mixtures of sodium-potassium chloride (187, 230) and sodium-cesium chloride (230) is less than unity. The lithium-potassium chloride eutectic has been studied by several workers (203, 207, 225, 231) and the activity coefficient changed from 1.0 to about 2.0 with decreasing silver chloride concentrations. The coefficients exhibited a slight decrease in magnitude with an increase in temperature as would be predicted from the theory of regular solutions.

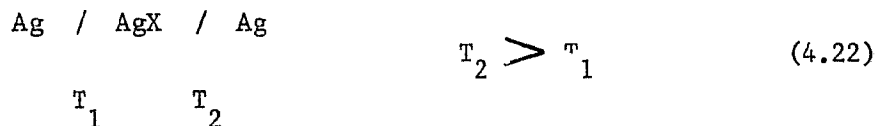
Flengas and Ingraham (187) have measured the activities of fourteen different metal chlorides in equimolar sodium-potassium chloride and Yang and Hudson (207) have studied twelve metal chlorides in the lithium-potassium eutectic. The γ values determined by the latter tend to be slightly larger in magnitude than those in the sodium-potassium chloride. This is partly due to different experimental conditions and the change in solvent. Yang and Hudson discussed the variation of γ with temperature, concentrations of the metal chloride, the size of the solute metal ion and the effect of these factors on the stability of the metal chloro complexes.

Lately, the excess free energies of mixtures with a common ion have been the subject of several papers (230, 232) and a review (11).

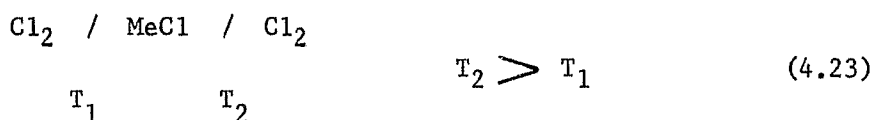
Lumsden (233) has calculated the heat of mixing for two molten alkali-metal halides with a common anion in terms of the interionic distances, the London constants for dispersion forces between the cations and the polarizability of the anion. The calculated values agreed well with published values and the treatment can be readily extended to multi-component systems. The thermodynamic properties of chloride systems have also been calculated from phase diagrams (1, 233, 234) and vapor pressure measurements (1, 233, 235).

4.4 Thermoelectric Cells

The work on thermocells in halide melts has been concentrated on cells of the type (149, 161, 168, 236-241)



or of the type (157, 161, 168, 239, 242, 243)



Sinistri and Pezzati (244) reported that the Seebeck coefficient, \mathcal{E} , for the silver chloride in a silver-potassium chloride mixture is related to that in pure silver chloride, \mathcal{E}^0 , by an equation similar to that for the nitrate systems (166). Metz and Seifert (168) examined the silver chloride thermal cell and determined the Seebeck coefficient for the cells 4.22, 4.23 and



They reported the Seebeck coefficient for cell 4.22 to be given by

$$\mathcal{E}_T^{\circ} = - 381 + 7.98 \times 10^{-3} T(^{\circ}\text{C}) \mu\text{V deg}^{-1} \quad (4.25)$$

and for cell 4.23 by

$$\mathcal{E}_T^{\circ} = - 725 + 0.24 \times 10^{-3} (T - 500^{\circ}\text{C}) \mu\text{V deg}^{-1} \quad (4.26)$$

Their results were compared with the previous results and were found to be in agreement with the majority of the published values.

Senderoff and Bretz (161) reported a Seebeck coefficient of $- 375 \mu\text{V deg}^{-1}$ for cell 4.22 and $- 644 \mu\text{V deg}^{-1}$ for cell 4.23. Both cells exhibited a linear relationship between the thermo emf and the temperature difference of the two electrodes for temperatures from 475 to 700°C. Meissner et al. (243) developed a thermal converter which used the cell 4.23 and a pump to circulate the chlorine produced at the hot electrode back to the cold electrode; the circulating gaseous electrode eliminated the problem of metal build-up on metal cathodes and the disappearance of metal anodes. They obtained a maximum efficiency of 4.5% in a silver chloride melt with a chlorine pressure of 0.4 atmospheres, one electrode being at 500°C and the other at 1300°C. The vaporization of the silver chloride limited the upper temperature or a higher efficiency would have been realized.

4.5 Gas Electrodes

The chlorine electrode consists of a graphite rod or tube over which chlorine gas is passed. The graphite requires special pretreatment to ensure rapid equilibrium between the chloride ion and the

chlorine gas. Several workers (11, 205, 223) have reviewed the various pretreatments and preparations of the electrode; these pretreatments and preparations include exposure to chlorine at elevated temperatures, exposure to fuming hydrochloric acid, electrolysis in molten silver chloride, and an exposure which alternated between chlorine gas and vacuum several times. The chlorine electrode in the lithium-potassium chloride eutectic was thoroughly examined at 450°C by Laitinen and Pankey (205); the standard electrode potentials on the molar, molal and mole fraction scale versus a standard platinum-(II)/platinum reference electrode was reported to be +0.323, +0.306 and +0.216 volts, respectively. They have also examined the bromide/bromine and iodide/iodine gas electrodes. The mechanism (245 - 247), kinetics (248) and reversibility (219, 223) of the chlorine electrode have been reported in the literature and they establish its reliability and thermodynamic value.

Inman (249) reported an oxygen electrode, $O_2^-/O_2/Au$, in the lithium-potassium chloride melt at 450°C that exhibited in a Nernst plot a slope of RT/F instead of the expected $RT/2F$ for the electrode reaction



Zambonin and Jordan (91) explained this observation using an oxide-superoxide system in which the electrode reaction is



Laitinen and Bhatia (197) found that the oxygen electrode was not reversible in a chloride melt; however, several metal oxide electrodes

of the second kind ($\text{Cu}/\text{Cu}_2\text{O}$, O^{2-} , Pt/PtO , O^{2-}) behaved reversibly in the chloride melt. A sulfur electrode was found to be reversible in the lithium-potassium chloride eutectic by Bodewig and Plambeck (250) and the electrode reaction was shown to be



An hydrogen-hydrogen chloride electrode suitable for use in the lithium-potassium chloride eutectic at 450°C has been prepared by Laitinen and Plambeck (196). It consisted of a mixture of hydrogen and hydrogen chloride gas bubbled over a platinized platinum flag immersed in the melt. The authors reviewed the previous work on hydrogen electrodes in melts containing aqueous contaminants. The reported E° for the electrode on the molar concentration scale versus a platinum reference electrode was -0.6935 ± 0.0047 volts which gives a value at 450°C of 1.0161 ± 0.0050 volts for the reaction



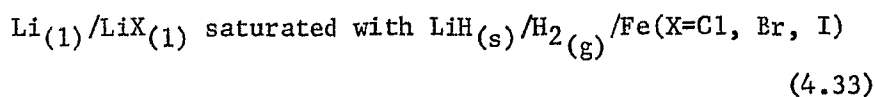
The experimental value for the formation of hydrogen chloride gas compared very well with N.B.S. and JANAF values. The standard state used in this work was one atmosphere pressure for the gases and the activity of the chloride ion as in the melt. The solubility (251, 252), electrical properties (253, 254) and the infrared spectra of hydrogen chloride dissolved in chloride melts have been reported by several Russian and Japanese workers. An electrode of a similar type has been reported for the hydrogen-hydrogen fluoride system (255) in the temperature range of 500 to 900°C in the formation cell:



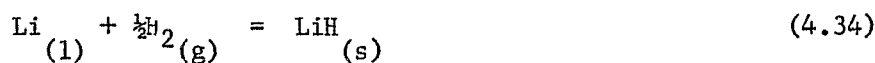
Johnson et al. (256) used a hydrogen-hydride ion electrode to study the thermodynamics of lithium hydride. The electrode reaction was



and the electrochemical cell that they used was



for which the cell reaction is:



The measured values for the formation of lithium hydride agreed with the literature value ($\Delta G_{298^\circ\text{K}}^\circ = -16.8 \text{ kcal mole}^{-1}$). Due to the possible use of the hydrogen-lithium hydride electrode in thermally regenerative fuel cells, Plambeck et al. (257) used voltammetric and chronopotentiometric techniques to investigate the electrochemistry of the electrode in the lithium-potassium chloride eutectic at 375°C. Due to the complexity of the system and the lack of general physical data related to the hydride-melt systems, it was difficult to quantitatively analyze their experimental data.

5. PREVIOUS STUDIES ON THE PROPERTIES OF SULFATE MELTS

5.1 Physical and Electrochemical Properties

The alkali metal sulfates are stable in air up to 800°C (258), whereas the thermal range of nitrate and carbonate melts exposed to air is much smaller. The general physical properties of the pure alkali metal sulfate melts and some mixtures have been tabulated by Janz (2). The two main eutectics used are a binary mixture of lithium sulfate and potassium sulfate (0.8:0.2, m.p. = 535°C)(259) and a ternary mixture of lithium sulfate, sodium sulfate and potassium sulfate (0.78:0.085:0.135, m.p. = 512°C)(260) and their respective densities at 550°C are 2.120 (58) and 2.13 (261) gm cc⁻¹. Kvist (262) has reported the conductivity of the lithium sulfate-potassium sulfate eutectic and pure lithium sulfate.

Stern and Weise (263) have reviewed and tabulated the data for the high temperature properties (such as phase changes) and the thermal decomposition of sixty inorganic sulfate salts. The thermal decomposition mainly results in the formation of the metal oxide plus sulfur trioxide, whereas the electrolytic reduction may result in products containing several different oxidation states of sulfur (74). Bartlett and Johnson (74) have shown that the thermodynamically favored anodic products from the electrolysis of solid or liquid sulfate are

formed at temperatures below 1200°K (927°C) according to



and at temperatures above 1200°K



They considered the possible cathodic reactions to be:



plus the side reaction involving the reduction of any sulfur trioxide formed by thermal decomposition followed by the decomposition of sulfite to sulfide and sulfate.



The reduction of the sulfur trioxide occurs about 2 to 3 volts before any of the other cathodic reactions; therefore, any appreciable amount of the sulfur trioxide in the melt will greatly reduce the useful working range of the sulfate melt. The thermodynamic calculations showed that the production of sulfide is favored up to a temperature of about 1700°K (1427°C) after which the deposition of the alkali metal is favored; hence, at temperatures below 1700°K reactive metals (iron or higher) will reduce the sulfate ion to produce the metal sulfide or oxide. In general, the thermodynamically favored reaction is

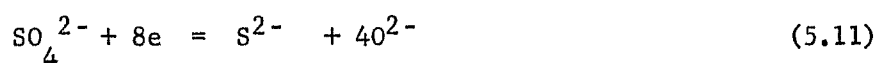


The cathodic products of the electrolysis of the lithium sodium potassium sulfate eutectic at temperatures between 550°C and 580°C were identified by Johnson and Laitinen (261) as sulfur, oxide and sulfite; whereas, Liu (264) reported the production of sulfite, oxide and sulfide from the lithium potassium sulfate eutectic at 625°C.

Liu reported that the limiting anodic process



occurred at +0.7 to +0.9 volts versus a one molal silver(I)/silver electrode while the limiting cathodic process was recorded at about -1.6 to -2.0 volts to give an overall working range of 2.3 to 2.9 volts in the sulfate melt. The predicted range from the thermodynamic calculations is 3.1 volts (74). The production of sulfite and sulfide accounted for 95% of the electricity according to the reactions



Johnson and Laitinen (261) found that the main products of the reduction of the lithium sodium potassium sulfate eutectic at 550°C were sulfur, oxide ion and a small amount of sulfite ion which decomposed to sulfur and sulfur dioxide in the melt. Any significant amount of sulfur gave a blue color at first, then rapidly changed to brown. Active metals (magnesium, iron, cadmium, nickel, zinc, thallium, lead) reduced the sulfate solvent to give sulfide, oxide and trace amounts of sulfur.

The limiting anodic current due to



occurred at about +0.6 volts versus a one molal silver(I)/silver reference electrode. The kinetics of this reaction have been studied by Flood and Forland (265).

The anodic electrolysis of the sulfate ion on a carbon anode at 700°C produces sulfur dioxide and carbon dioxide (266). The shape of the voltammetric reduction curve of the sulfate melt is similar to that for the nitrate reduction (39). The initial stage of the reduction is partially irreversible with a half-wave potential of -0.6 volts versus the silver(I)/silver reference electrode. The final reduction wave begins at about -2.3 volts. The initial reduction can be attributed to the reduction of sulfur trioxide formed by thermal decomposition and the difference in potential between the initial and final stage (1.7 volts) which agrees fairly well with the 2.1 volts predicted from thermodynamic calculations (74). The dissociation equilibrium which produces sulfur trioxide and causes the initial wave in the electroreduction process has been studied by Wrench and Inman (267) at 750°C. The equilibrium constant for the reaction



$$K = \frac{[\text{SO}_4^{2-}]}{[\text{SO}_3][\text{O}^{2-}]} \quad (5.14)$$

was found to be very high ($K > 100$) and the reaction is shifted far to the right.

The complexity of the system greatly increases with the addition of the chloride ion due to the formation of many complexes. Eighteen eutectics and 46 quaternary invariant points have been reported for the reciprocal quaternary system, Li,Na,K//SO₄²⁻,Cl (268) with the majority of the complexes occurring in the 0 to 30% chloride range.

5.2 Electrodes and Electrode Potentials

The reduction of the sulfate melt by active metals limits the number of metal electrodes that can exist in the melt; however, emf series of six redox couples in the ternary eutectic at 550°C (261) and of five metals in the binary eutectic at 625°C (264) have been reported. The reference electrode in both series is the silver(I)/silver electrode which has been firmly established (264) and verified (261) as a reliable and reversible reference electrode for the sulfate melts. The silver(I) ion has been added to the melt by coulometrically anodizing silver metal with 100% current efficiency or by adding silver sulfate.

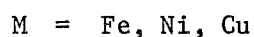
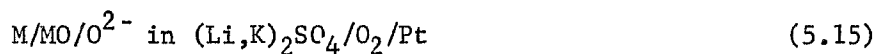
Kvist and Randsalu (269) have studied several thermoelectric cells in sulfate melts.

5.3 Gas Electrodes

Sulfate melts have been used to set up gas electrodes which were reversible to the oxide ions in the melt. In a series of papers Lux (270) reported the measurement of oxide activities with an oxygen electrode in the sodium potassium sulfate eutectic at 950°C. The

metal oxides were volatile and in order to interpret his results Lux found it necessary to extrapolate back to zero time.

Hill, Porter and Gillespie (271) set up a reversible oxygen electrode by surrounding a platinum wire immersed in a sulfate melt with oxygen.



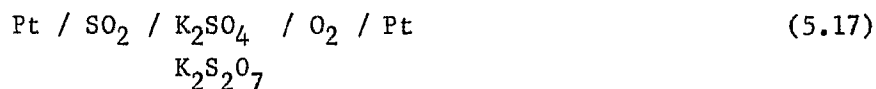
The cells took from 1 to 24 hours to stabilize and the emf remained after the oxygen gas was turned off; however, the experimental emfs agreed well with the values from other thermodynamic calculations.

Flood, Forland and Montzfeldt (272) used a sodium sulfate-sodium carbonate system to study the dependency of the emf on the oxide activity. They varied the oxide activity through the dissociation equilibrium of carbonate

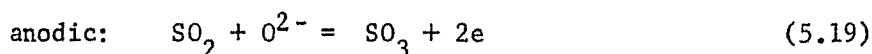


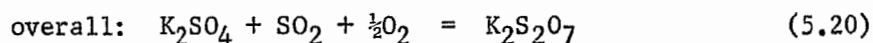
by changing the partial pressure of the carbon dioxide above the melt.

The oxygen electrode combined with a sulfur dioxide electrode has been used to measure the sulfur trioxide activities in potassium sulfate (273). The electrochemical cell used was the following:

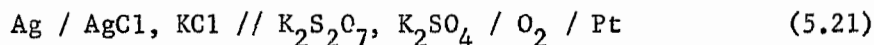


and the electrode reactions were:

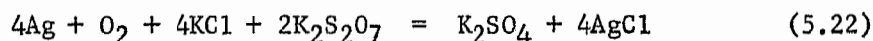




Bissell and Duke (274) reported a similar type of system for the following cell:



The standard potential for the overall reaction



was reported to be 1.02 volts at 450°C. The variation in the standard free energy change for the reaction was $\Delta G = -71680 - 29.5T$ cal mole⁻¹ and is in agreement with thermodynamic data from the literature.

Since potassium pyrosulfate is in equilibrium with sulfur trioxide in a sulfate melt (275),



the oxygen electrode in the sulfate-pyrosulfate mixture (274) may be considered as a type of sulfate gas electrode. Hauffe and Hoeffgen (276) have examined a $SO_4^{2-}/SO_3, O_2/Pt$ gas electrode in contact with solid, tempered pellets of silver sulfate at 600°C. The experimental emf for the cell



was 0.555 volts as compared to the calculated value of 0.508 volts. The gas mixture passed through the gas electrode contained sulfur trioxide, oxygen and nitrogen and the partial pressure of the oxygen was varied from 90 mm to about 760 mm. The sulfur trioxide is in equilibrium with oxygen and sulfur dioxide according to:



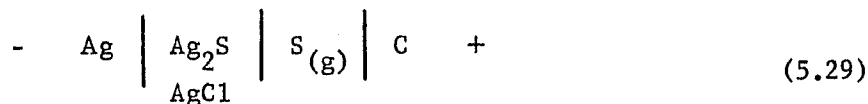
with an equilibrium constant, K, given by the equation (323):

$$K = \frac{[\text{SO}_3]}{[\text{SO}_2][\text{O}_2]^{\frac{1}{2}}} \quad (5.27)$$

$$\text{Log } K = 1.066 \times 10^4/T - 9.996 \quad (5.28)$$

The kinetics of the reaction are such that it requires three to five hours for equilibrium to be reached. The thermodynamic values for sulfur dioxide (263, 277-280), sulfur trioxide (263, 277-279, 281), and sulfuric acid (277) along with the phase diagrams of the systems containing sodium sulfate, potassium sulfate and sulfur trioxide (282) have been reported in the literature.

The $\text{S}^{2-}/\text{S}_{(\text{g})}$ gas electrode on carbon (283)

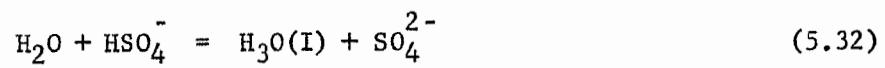


showed ideal Nernst behavior at temperatures from 490°C to 860°C for sulfur vapor pressures between 10^{-3} to 1 atmosphere provided the sulfide concentration was kept low. Arvia et al. (284) studied the kinetics of the hydrogen electrode in a sodium hydrogen sulfate melt (285) between the temperatures of 180°C and 345°C and found that its behavior resembled that of the standard hydrogen electrode in aqueous solutions at room temperatures. They explained their observations in terms of thermal decomposition



followed by the reaction of water with the melt





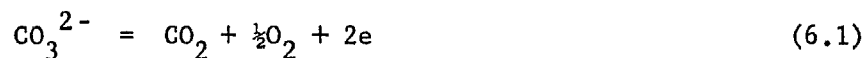
to form the hydronium ion which enters directly into the hydrogen electrode process as in the aqueous solutions.

6. PREVIOUS STUDIES ON THE PROPERTIES OF CARBONATE MELTS

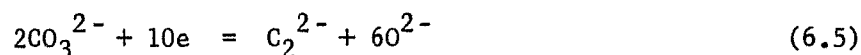
6.1 Physical and Electrochemical Properties

The physical, chemical and electrochemical properties of molten alkali carbonates have been recently reviewed by Janz (286) and Bartlett and Johnson (287). The ternary eutectic (0.435 Li_2CO_3 , 0.315 Na_2CO_3 , 0.25 K_2CO_3 ; m.p. = 397°C) and the lithium-sodium carbonate eutectic (0.53:0.47, m.p. = 500°C) have been used in the majority of the studies on the fused carbonate system. The densities and conductances have been measured for the single salt carbonate melts (2, 65, 286) and for several of the eutectic melts (288). The thermal decomposition of carbonate melts which is normally suppressed by an atmosphere of carbon dioxide (74) has been studied by some Russian workers (289) at 750°C for periods up to 400 hours with various atmospheres above the melt. They observed thermal decomposition of the ternary eutectic in air and argon but not in carbon dioxide.

The enthalpy and related thermodynamic properties of carbonate melts (290, 291) have been published in addition to the theoretical standard reversible decomposition voltages (74) calculated from thermal data. In the theoretical calculations Bartlett and Johnson (74) considered the anodic reaction in the electrolysis of solid or molten carbonate to be



whereas the cathodic reaction may be one or a combination of



In addition, the carbon dioxide atmosphere above the melt may be reduced to either carbon or carbon monoxide.



or



The calculations showed that the favored reaction at all temperatures in potassium carbonate (and above 600°C in sodium carbonate) was the deposition of the alkali metal. Below 600°C in sodium carbonate and at low temperatures in the other carbonates carbon is the favored product, but at higher temperatures carbon monoxide is the dominant one. Although the direct reduction of carbon dioxide would occur in all the melts, its activity in the melt is too low to make any significant contribution to the electrode reaction. Bartlett and Johnson presented their calculations in an Ellingham diagram, discussed the reduction of carbonates with metals and carbon, and compared their values with the experimental results.

The electrolysis of carbonate melts has been studied (287, 292, 293) and reviewed (286) by several workers. The products of the oxidation of carbonate melts are carbon dioxide and oxygen, but the

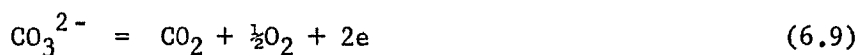
ratio of the two products is strongly dependent on the experimental conditions: at high current densities the $\text{CO}_2:\text{O}_2$ ratio is about 2:1 while at low current densities it is about 1:6. The excess of oxygen at the low current densities may be due to



The electrolytic reduction products at low temperatures ($< 600^\circ\text{C}$) are carbon and oxide while at temperatures above 700°C they are believed to be carbon monoxide and oxide ion. Current-voltage curves (287) obtained from the lithium-sodium carbonate eutectic at 550°C exhibited two waves in their cathodic portion and showed that the limiting oxidation process occurred at about +0.4 volts versus a silver(I)/silver reference electrode. The first, rather small and irreproducible cathodic wave at -1.2 volts was attributed to the reduction of carbon dioxide and the final limiting wave at -2.0 volts to the reduction of the carbonate ion. Janz (286) has summarized the decomposition potentials for the other carbonate melts.

Alumina has been proven to be one of the few materials that are not corroded by the carbonate melts and has been used extensively in the experimental work. If the redox potential of a metal exceeds that of the melt, it will corrode or oxidize in the melt and continue to do so until the two potentials are equal. The studies on the corrosion of silver, platinum, gold and several other metals (286, 287, 294, 295) have shown that the corrosion can be related to the partial pressures of oxygen and carbon dioxide over the melt. The redox potential, E , of the carbonate melt depends upon the partial pressures of the

oxygen and carbon dioxide in the gas phase.



$$E = E^{\circ} + \frac{RT}{2F} \ln \left[(P_{\text{CO}_2})(P_{\text{O}_2})^{\frac{1}{2}} \right] \quad (6.10)$$

The corrosion of a metal may be further complicated by the formation of an insoluble metal oxide and the possibility of passivation of the metal surface. The concentration of the oxide ion in the carbonate melt is controlled by the partial pressure of carbon dioxide and the carbonate dissociation equilibrium (92, 286, 295, 296)



The effect of water on the redox potential of the carbonate melt as well as the hydrolysis reactions that will occur in the melt have been investigated by Busson et al. (296). They proposed a new type of fuel cell in which the buffering effect of the acid-base pair ($\text{H}_2\text{O}/2\text{OH}^-$) suppresses the polarization due to proton transport to the electrodes. The operation of this new type of fuel cell was shown to be more economical than cells designed to use a combustive mixture of oxygen and carbon dioxide.

6.2 Electrodes and Electrode Potentials

The standard electrode potentials of the first three alkali metal electrodes, the CO_2/C electrode and the $\text{CO}_2, \text{CO}/\text{Au}$ electrode at 600°C and 750°C in the carbonate melt (292, 297) have been determined using a $\text{CO}_3^{2-}/\text{CO}_2, \text{O}_2/\text{Au}$ gas reference electrode. Bartlett and Johnson (287)

determined the standard electrode potentials of cobalt, nickel, the $\text{CO}_3^{2-}/\text{CO}_2$, O_2/Pt gas electrode and the silver electrode in a sulfate melt at 550°C for the lithium-sodium carbonate eutectic; for a reference electrode they used the silver(I)/silver electrode in carbonate which they found to be reversible and to show ideal Nernst behavior for concentrations between 4×10^{-3} and 4×10^{-2} molar. The silver was anodized at a current efficiency of nearly 100% and the stability of the carbonate melt was maintained under carbon dioxide at one atmosphere pressure. They reported that iron reduced the solvent but rhodium and platinum were noble. When copper was anodized, it became covered with oxide and turned the melt green. A theoretical emf series for molten carbonates has been calculated (298) and an experimental order of reactivity for several metals has been deduced from potentiostatic polarization curves (294, 299).

6.3 Gas Electrodes

The oxidation of carbonate



can be more accurately represented by two steps (300):



This indicates that the carbonate gas electrode in reality is an oxygen electrode run under a carbon dioxide atmosphere. The oxygen electrode has been verified for the ternary carbonate eutectic (300,

301), the sodium potassium carbonate eutectic (302), the lithium sodium carbonate eutectic (287) and a sodium sulfate-carbonate mixture (272) where the oxide concentration is controlled by the equilibrium equation

$$[O^{2-}] = \frac{K [CO_3^{2-}]}{P_{CO_2}} \quad (6.15)$$

Borucka and Sugiyama (301) showed that the platinum anodes used by the other workers were slowly corroded in the carbonate melt. They used a gold anode and a special gas control system to vary the flow of each gas independently in a detailed study at 800°C in the ternary eutectic. They found, among other things, that the gold anode gave slightly higher values than the platinum anode and this is in accord with the findings of Janz and Saegusa (303).

A reversible carbon dioxide - carbon monoxide gas electrode in molten carbonate at 700 to 800°C was used by Borucka (304) as a new reference electrode for the carbonate system. The electrode reaction for the electrode



was shown to obey the equation



The Boudouard equilibrium



$$\text{Log } K_B = \frac{8946}{T} - 9.2 \quad (6.19)$$

must be considered in this electrode system since carbon may be

deposited if

$$(P_{\text{CO}})^2 \geq \frac{P_{\text{CO}_2}}{K_B} \quad (6.20)$$

Borucka defined the zero potential of the gas electrode by the condition

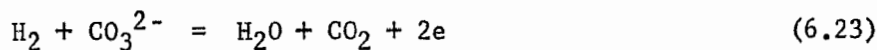
$$\frac{(P_{\text{CO}_2})^2}{P_{\text{CO}}} = 1 \text{ atmosphere} \quad (6.21)$$

and used this as a basis for a new potential scale for the carbonate melt.

In order to study the anodic behavior of smooth platinum electrodes in molten carbonates, Arkhyrov and Stepanov (305) examined a type of hydrogen electrode in carbonate melts. They set up the following cell by bubbling the appropriate gases over platinum flags immersed in the melt.



The electrode reactions are



with an overall reaction of



The three-phase contact required at each electrode was unsatisfactory and thus was offered as the explanation for the difference between the observed potentials and the theoretical values. The Russians did not take into account the side reactions which form methane (306) in this

type of carbonate fuel cell.

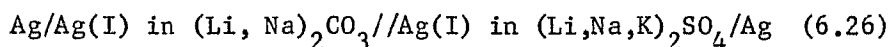
6.4 Sulfate//Carbonate Solvent Junction Potential

The silver carbonate/silver electrode and the gaseous carbonate electrode have been used as reference electrodes for studies in molten carbonates but these electrodes present many experimental difficulties. Several workers (292, 294, 307) have used, as a reference, the Danner-Rey electrode (308) which consists of a silver sulfate-silver electrode in a porcelain tube closed at the lower end and sealed around the emerging silver wire at the top. Electrical contact is made through the pores of the porcelain and often an additional porcelain sheath containing lithium-potassium sulfate eutectic is put around the Danner-Rey electrode to protect the silver sulfate from the gradual diffusion of carbonate through the porcelain. Busson et al. (307) reported the potential to be -0.57 volts between the reversible oxygen electrode in the ternary carbonate eutectic at 605°C and the Danner-Rey reference electrode. Unfortunately, these workers do not state the concentration of silver sulfate in the Danner-Rey electrode that was associated with this potential.

Borucka and Sugiyama (301) pointed out that the experimental conditions in the work by Busson et al. (307) made the presence of water inevitable. They claim that in spite of the increasing use of the Danner-Rey reference electrode in molten carbonate studies, it has never been properly evaluated either with respect to its stability, liquid junction or temperature coefficient. For these reasons they

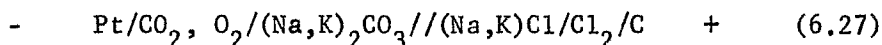
concluded that the potential of the $\text{CO}_3^{2-}/\text{O}_2$, CO_2/Au electrode relative to the Danner-Rey reference electrode measured by Busson et al. (307) can not be accepted as valid.

The use of a silver sulfate/silver reference electrode in molten carbonates has also been examined by Bartlett and Johnson (287). They set up the following concentration cell at 540°C :

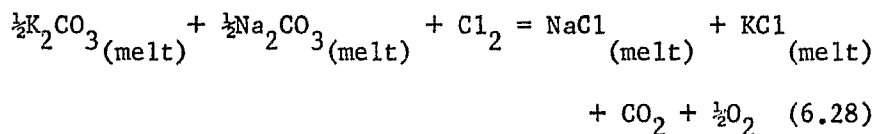


and found that it exhibited ideal Nernst behavior with a stability of ± 1 mV for each set of concentrations. They reported the potential of the $\text{CO}_3^{2-}/\text{CO}_2$, O_2/Pt electrode with respect to the silver sulfate reference electrode at 550°C on the molar, molal and mole fraction concentration scales were -0.523, -0.470 and -0.725 volts, respectively. The potential of the silver carbonate/silver electrode and the silver sulfate/silver reference electrode at 540°C and on the same three concentration scales were -0.253, -0.250 and -0.274 volts. No attempt was made to correct for the liquid junction potential or to use silver activities instead of silver concentrations in the system.

A chlorine electrode has also been used as a reference electrode in molten carbonates for temperatures from 770°C to 1000°C in the cell (309):



The calculated emf for the cell, based on the reaction,



at 800 and 900°C are 1.132 and 1.198 volts, respectively. Ozeryanaya et al. (309) obtained the following empirical equation for the temperature dependence of the experimental emf:

$$E = 0.446 + 6.40 \times 10^{-4} T^{\circ}\text{K (in volts)} \quad (6.29)$$

The experimental potentials at 800 and 900°C were 1.133 and 1.197 volts, respectively and agree with the calculated values.

7. RESULTS AND DISCUSSION

SILVER ACTIVITIES IN ALKALI NITRATE MELTS

7.1 Fundamental Equations and Definitions

The chemical potential, μ_i , of a component, i , in a mixture at equilibrium is given by:

$$\mu_i = \mu_i^0 + RT \ln a_i \quad (7.1)$$

at the temperature T , where a_i is the component's activity and μ_i^0 is its chemical potential in a standard state (312). The activity of a component in a Temkin Ideal solution (313, 314) for a uni-valent salt CA is given by

$$a_{CA} = X_C X_A \quad (7.2)$$

and for a general salt $B_r Y_s$ by

$$a_{B_r Y_s} = (X_B)^r (X_Y)^s$$

The ion fractions X_C and X_A are given by

$$X_C = \frac{n_C}{\sum n_{i^+}} \quad (7.3)$$

$$X_A = \frac{n_A}{\sum n_{i^-}} \quad (7.4)$$

where n_{i^+} and n_{i^-} represent the number of gram moles of the different cations and anions, respectively. In an ideal mixture of two

uni-univalent salts (CA + BA) which have one ion in common, the activities are related to the mole fractions N_{CA} and N_{BA} by

$$a_{CA} = N_{CA} \quad (7.5)$$

$$a_{BA} = N_{BA} = (1 - N_{CA}) \quad (7.6)$$

If the concentration of a solution is greater than the upper limit of the concentration range governed by Henry's Law, an activity coefficient, γ , must be introduced for each salt (118): for the uni-univalent salt this is given by

$$a_{CA} = X_C X_A \gamma_{CA} \quad (7.7)$$

and for the general salt $B_r Y_s$ by

$$a_{B_r Y_s} = (X_B)^r (X_Y)^s \gamma_{B_r Y_s} \quad (7.8)$$

The contribution of each component, i , to the total emf of a system is given by combining equations 7.1 and 7.8 with

$$\mu_i = -nFE_i \quad (7.9)$$

to give

$$E_{B_r Y_s} = E_{B_r Y_s}^0 - \frac{RT}{nF} \ln \left[(X_B)^r (X_Y)^s \gamma_{B_r Y_s} \right] \quad (7.10)$$

In this study only uni-univalent salts (simple salts) and mixtures with a single anion will be considered; therefore, since $X_A = 1$, X_C can be replaced by the mole fraction N_{CA} in equation 7.10 to give:

$$E_{CA} = E_{CA}^0 - \frac{RT}{F} \ln \left[N_{CA} \gamma_{CA} \right] \quad (7.11)$$

All of the electrode and cell potentials given in this work are

expressed according to the I.U.P.A.C. convention of 1953 (315).

7.2 Concentration Scales and Their Interrelationships

In molten salt studies three main concentration scales are used. The molality scale, m , is the simplest to use for dilute solutions but has no meaning for single salt systems. The molarity scale, M , is defined over the entire concentration range; however, it requires a knowledge of the density of the system as a function of both the temperature and the composition. The mole fraction scale, N , (assigning the value of unity to a pure salt) is almost directly proportional to the other two scales in dilute solutions; however, although the mole fraction activity coefficient approaches a constant value in dilute solutions, the constant does not equal unity as it does on the other two scales. The standard states for solids and gases at a given temperature are taken as the pure solid and the pure gas at a pressure of one atmosphere at the given temperature in all three scales. The pure salt in the molten state is used as the standard state for the mole fraction scale. The hypothetical concentration of unity is defined as the standard state for solutions on the molal and molar scales such that $\gamma \rightarrow 1$ as $C \rightarrow 0$. Only on the mole fraction scale can all the standard states be realized in an experimental system. On all the concentration scales the standard state for the ions of the solvent is the actual state of the ion in the solvent under one atmosphere pressure and the temperature of the measurement.

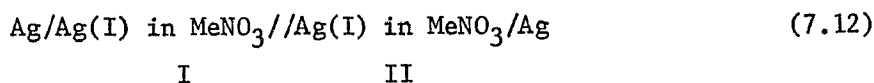
To utilize all of the material in the literature, free conversion between the concentrations, standard electrode potentials and activity coefficients on all three scales is necessary. The relationships required for the conversion from one concentration scale to another have been derived (see Appendix C, page 363) and are summarized in Table 7.1. The results are expressed in terms of two sets of equations; the first is valid for all concentrations and the second, which is simpler, is valid ($\pm 1\%$) only in dilute solutions ($N \leq 0.01$, $m \leq 0.1$, $M \leq 0.1$ for silver nitrate in most alkali nitrate systems).

TABLE 7.1
CONVERSION BETWEEN CONCENTRATION SCALES

From	M	m	N
To	All Solutions		
M =	M	$\frac{1000 m \cdot D}{1000 + m \cdot Mwt}$	$\frac{1000 N \cdot D}{Mwt' \cdot (1-N) + N \cdot Mwt}$
m =	$\frac{1000 M}{1000 D - M Mwt}$	m	$\frac{1000 N}{Mwt' (1 - N)}$
N =	$\frac{M \cdot Mwt'}{1000 D + M(Mwt' - Mwt)}$	$\frac{m \cdot Mwt'}{1000 + m \cdot Mwt'}$	N
Only Dilute Solutions			
M =	M	$m \cdot D'$	$\frac{1000 N \cdot D'}{Mwt'}$
m =	$\frac{M}{D'}$	m	$\frac{1000 N}{Mwt'}$
N =	$\frac{M \cdot Mwt'}{1000 D'}$	$\frac{m \cdot Mwt'}{1000}$	N

M - molarity m - molality N - mole fraction
D - density of solution D' - density of pure solvent
Mwt - molecular weight of solute Mwt' - molecular weight of solvent

It can be seen that the activity coefficients on the three concentration scales are interrelated by an examination of a silver concentration cell containing an alkali nitrate solvent (MeNO_3).



The emf of the cell after correction for the liquid junction potential, E_J , is given by the Nernst equation.

$$E = -\frac{RT}{F} \ln \left[\frac{C_I \gamma_I}{C_{II} \gamma_{II}} \right] \quad (7.13)$$

Changing from one concentration scale to another will not affect the emf of the cell; thus,

$$\frac{N_I \gamma_{N_I}}{N_{II} \gamma_{N_{II}}} = \frac{m_I \gamma_{m_I}}{m_{II} \gamma_{m_{II}}} = \frac{M_I \gamma_{M_I}}{M_{II} \gamma_{M_{II}}} \quad (7.14)$$

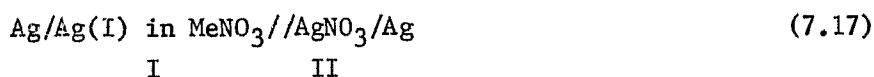
Using the formulas given in Table 7.1, the fractions in equation 7.14 containing m and M are rearranged to express all the concentrations in terms of N (the primes indicate the properties of the pure solvent rather than those of the solute).

$$\frac{\gamma_{N_I}}{\gamma_{N_{II}}} = \frac{\gamma_{m_I}^{(1-N_{II})}}{\gamma_{m_{II}}^{(1-N_I)}} = \frac{\gamma_{M_I}^{D_I((1-N_{II}) + N_{II}(Mwt/Mwt'))}}{\gamma_{M_{II}}^{D_{II}((1-N_I) + N_I(Mwt/Mwt'))}} \quad (7.15)$$

Further simplification can be achieved by setting $N_{II} = 0$ and, by definition, $\gamma_{m_{II}}$ and $\gamma_{M_{II}}$ must then be unity.

$$\frac{\gamma_{N_I}}{\gamma_{N=0}} = \frac{\gamma_{m_I}}{1 - N_I} = \frac{\gamma_{M_I}^{D_I}}{D_{II}((1-N_I) + N_I(Mwt/Mwt'))} \quad (7.16)$$

The ratio $\gamma_{N_I} / \gamma_{N=0}$ can be determined by direct measurements of the emf of a concentration cell. Cells which use the pure alkali nitrates or binary mixtures as the solvent have been studied at temperatures between 160°C and 500°C (depending on the melting point of the solvent and its range of stability) (1, 100, 316, 317). In one half of the cell the concentration was kept constant, as a reference electrode, and in the other half the concentration was varied from $N = 10^{-5}$ to 5×10^{-3} . Plots of E vs $\log N_{\text{AgNO}_3}$ gave straight lines with a slope of $\frac{2.303 RT}{F}$, within ± 0.5 mV (100). This indicated that the $\gamma_{N_I} / \gamma_{N_{II}}$ ratio must remain constant and that for concentrations up to about $N = 5 \times 10^{-3}$, $\gamma_{N_{\text{AgNO}_3}}$ must have the same value as $\gamma_{N=0}$; this value can be determined by examining a concentration cell containing pure silver nitrate in one half of the cell



The emf of the cell is given by

$$E = -\frac{RT}{F} \ln N_I \gamma_{N_I} + E_J \quad (7.18)$$

since $N_{II} = 1$ and $\gamma_{N_{II}} = 1$ by definition for pure AgNO_3 . Due to the high degree of sensitivity of γ to a small change in the emf, an estimate for the liquid junction potential, E_J , must be applied to all of the measurements. A one millivolt change produces a change

of about 0.035 in γ at 350°C for most of the systems.

In most cases, the standard cell potentials, E° , are initially evaluated on the molal concentration scale and then converted to the other scales if the required data is available for the cell. Since the molal activity coefficient for silver is unity in most of the dilute experimental cells, it is possible to calculate E_m° using only the Nernst equation, the molal concentrations and the observed emf of the cell after correction for the liquid junction potential. The relationships between E_m° and the corresponding values on the other two concentration scales (E_N° and E_M°) are dependent upon the physical properties of the solvent, the types of electrodes used and the type of experimental cell. The two basic types of cells used in this study were the solvent junction cell which has a common metal ion/metal electrode system in two different solvents and a cell which contains two different electrodes in a common solvent.

In the dilute solvent junction cells of the silver(I)/silver electrode system, the dilute solution interconcentration relationships given in Table 7.1 are valid and for the cell



the activity coefficients for the three concentration scales are:

$$\begin{aligned}\gamma_m &= 1 \\ \gamma_M &= 1 \\ \gamma_N &= \gamma_{N=0}\end{aligned}$$

The potential for the cell is given by

$$E = E^{\circ} - \frac{RT}{F} \ln \left[\frac{\gamma_{A}^{C}}{\gamma_{B}^{C}} \right]$$

and will not be affected by the concentration scale used for a given amount of silver(I) in each half cell. The relationship from Table 7.1

$$M = m D_{\text{solvent}} \quad (7.19)$$

and

$$E = E_m^{\circ} - \frac{RT}{F} \ln \left[\frac{m_A}{m_B} \right] = E_m^{\circ} - \frac{RT}{F} \ln \left[\frac{M_A}{M_B} \right] \quad (7.20)$$

are combined and simplified to give

$$E_M^{\circ} = E_m^{\circ} + \frac{RT}{F} \ln \left[\frac{D_A}{D_B} \right] \quad (7.21)$$

where D is the density of the pure solvent at the given temperature. The conversion from the molal to the mole fraction scale is derived by combining and simplifying the following two equations:

$$N = m \text{Mwt}_{\text{solvent}} \times 10^{-3} \quad (7.22)$$

$$E = E_m^{\circ} - \frac{RT}{F} \ln \left[\frac{m_A}{m_B} \right] = E_N^{\circ} - \frac{RT}{F} \ln \left[\frac{\gamma_{N(\text{in A})}^{N_A}}{\gamma_{N(\text{in B})}^{N_B}} \right] \quad (7.23)$$

to give

$$E_N^{\circ} = E_m^{\circ} + \frac{RT}{F} \ln \left[\frac{\gamma_{N=O(\text{in A})}^{Mwt_A}}{\gamma_{N=O(\text{in B})}^{Mwt_B}} \right] \quad (7.24)$$

where Mwt is the molecular weight of the solvent. Equations 7.21 and 7.24 are applicable only if the electroactive species on both sides of the cell are identical ions.

The case of non-identical electroactive species in a cell containing a common solvent throughout has been discussed by Laitinen and Liu (206); however, they did not account for changing activity coefficients. Since the three scales use a common standard state for the gaseous components, i.e., 1 atmosphere of pressure, a change in concentration scale will not affect a gas electrode. The change in standard electrode potentials between the concentration scales must be calculated separately and then combined to find the total change for the cell. The activity, a , of an ion in an infinitely dilute solution is given by $(\gamma_{N=0})^N$, m and M for the three concentration scales. Using the dilute relationships in Table 7.1 and the Nernst equation,

$$E = E^{\circ} + \frac{RT}{nF} \ln a \quad (7.25)$$

the two interrelationships for the electrode reaction



are

$$E_m^{\circ} = E_M^{\circ} + \frac{RT}{nF} \ln [D_{(\text{solvent})}] \quad (7.27)$$

$$E_N^{\circ} = E_M^{\circ} + \frac{RT}{nF} \ln \left[\frac{1000 D_{(\text{solvent})}}{\gamma_{N=0}^{Mwt}(\text{solvent})} \right] \quad (7.28)$$

and for gaseous electrodes

$$E_M^{\circ} = E_m^{\circ} = E_N^{\circ} \quad (7.29)$$

Equations 7.27 to 7.29, which are more general statements of equations 7.21 and 7.24, are not restricted by the types of electrodes

or solvents.

7.3 Calculation of Liquid Junction Potentials

The liquid junction potentials, E_J , for several nitrate systems were calculated as a function of temperature using the specific conductance of the melts (265) and the method proposed by Klemm (63). The relative mobility between a cation and an anion was assumed to be independent of the concentration; the validity of this assumption has been demonstrated for the nitrate (68) and nitrite (70) systems. The derivation of equations and the methods used to calculate the E_J values are given in Appendix B. The liquid junction potentials at 300, 350 and 400°C were calculated for the cell



where Me was either one of the first three alkali metals or one of their binary mixtures. The results are tabulated in Table 7.2 and plotted in Figures 7.1 to 7.6 for the mole fraction of silver nitrate from 1.0 to 10^{-4} . (The points have been omitted from the plots for clarity.) The values range from +25 mV for potassium nitrate at 300°C to 0.1 mV for lithium nitrate at 400°C. In all the systems, as the silver nitrate concentration decreased the liquid junction potential rapidly increased; when the concentration reached 0.01 mole fraction the liquid junction potential remained constant. This behavior was expected, for even if the system were behaving ideally, a change in the E_J value would cause an error in the slope of a Nernst plot at low concentrations. For a cell which does not contain pure

silver nitrate the liquid junction potential can be determined using two silver concentration cells as shown below:

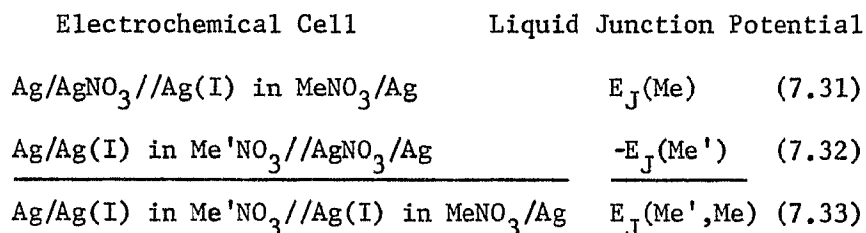


TABLE 7.2

CALCULATED LIQUID JUNCTION POTENTIALS, E_J ,
FOR THE CELL: $\text{Ag}/\text{AgNO}_3//\text{Ag(I) in MeNO}_3/\text{Ag}$

$N_{\text{Ag(I)}}$		10^{-4}	10^{-3}	10^{-2}	0.05	0.1	0.2	0.4	0.6	0.8	0.9
$-\text{Log } N_{\text{Ag(I)}}$		4.00	3.00	2.00	1.30	1.00	0.70	0.40	0.22	0.10	0.05
MeNO ₃	T°C	E_J (mV)									
LiNO ₃	300	5.4	5.4	5.4	5.1	4.9	4.3	3.2	2.1	1.0	0.4
	350	2.9	2.9	2.9	2.8	2.6	2.3	1.7	1.2	0.6	0.2
	400	0.6	0.6	0.6	0.6	0.5	0.5	0.4	0.2	0.1	0.1
NaNO ₃	300	5.1	5.1	5.0	4.8	4.6	4.0	3.0	2.0	1.0	0.5
	350	3.7	3.7	3.7	3.5	3.3	3.0	2.2	1.5	0.7	0.4
	400	2.6	2.6	2.6	2.5	2.3	2.1	1.5	1.0	0.5	0.3
KNO ₃	300	25.7	25.7	25.4	24.1	22.5	19.4	13.8	8.8	4.2	2.0
	350	23.5	23.5	23.3	22.1	20.7	17.9	12.9	8.2	4.0	1.9
	400	22.3	22.0	22.0	21.0	19.7	17.1	12.3	7.9	3.8	1.9
0.54 LiNO ₃ 0.46 NaNO ₃	300	5.3	5.3	5.3	5.0	4.8	4.2	3.1	2.1	1.0	0.5
	350	3.3	3.3	3.3	3.2	3.0	2.6	2.0	1.3	0.6	0.3
	400	1.5	1.5	1.5	1.5	1.4	1.2	0.9	0.6	0.3	0.2
0.59 LiNO ₃ 0.41 KNO ₃	300	12.7	12.7	12.6	12.0	11.3	9.9	7.2	4.7	2.3	1.1
	350	10.3	10.3	10.2	9.8	9.2	8.1	6.0	3.9	1.9	0.9
	400	8.3	8.3	8.2	7.9	7.4	6.6	4.8	3.2	1.6	0.8
0.45 NaNO ₃ 0.55 KNO ₃	300	15.5	15.4	15.3	14.6	13.7	12.0	8.7	5.6	2.7	1.3
	350	13.7	13.7	13.5	12.9	12.1	10.6	7.8	5.1	2.5	1.2
	400	12.5	12.5	12.4	11.8	11.2	9.8	7.2	4.7	2.3	1.1

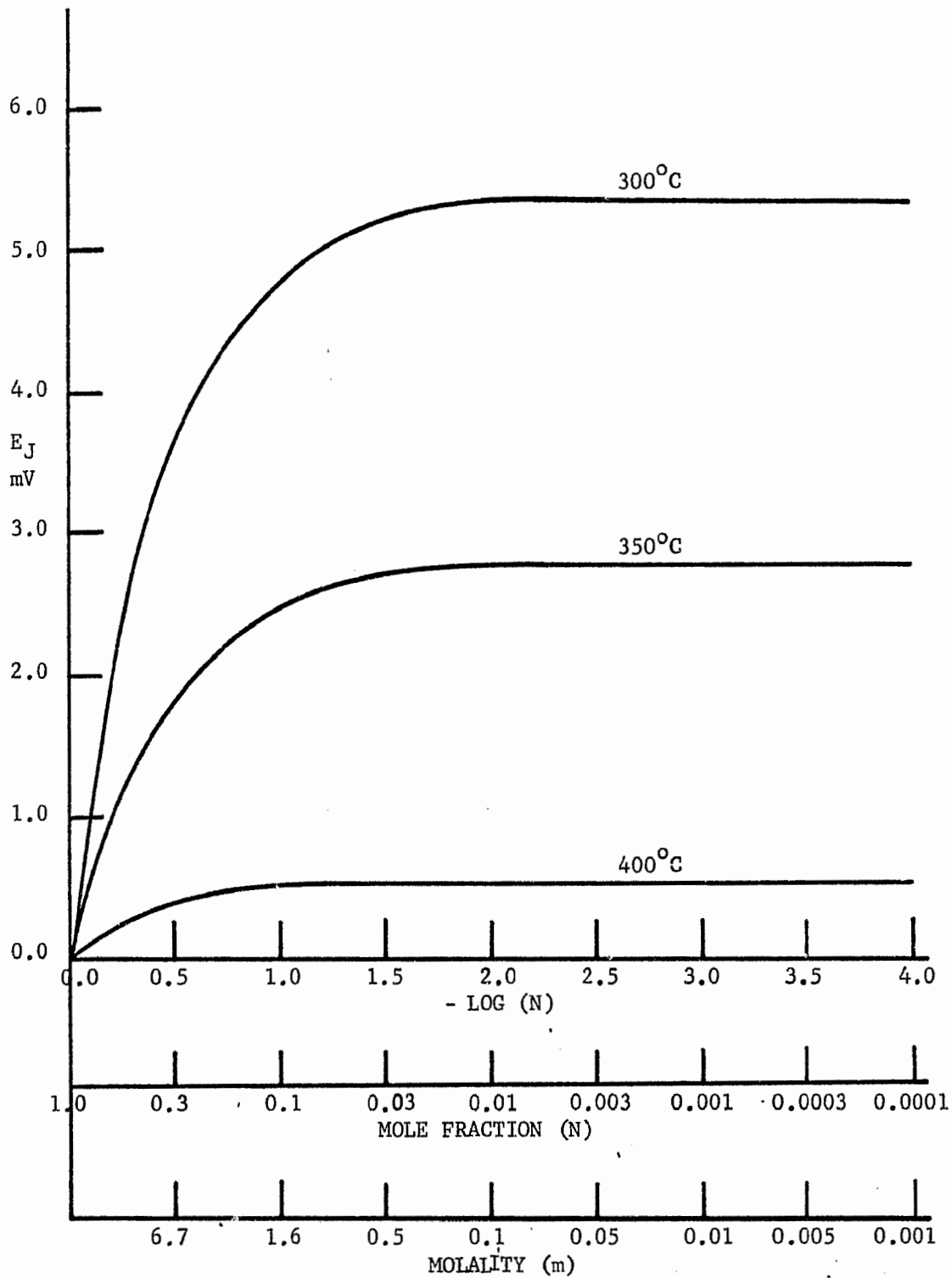
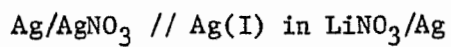


Figure 7.1 Calculated Liquid Junction Potentials, E_J , for a Ag(I) in LiNO_3 Concentration Cell



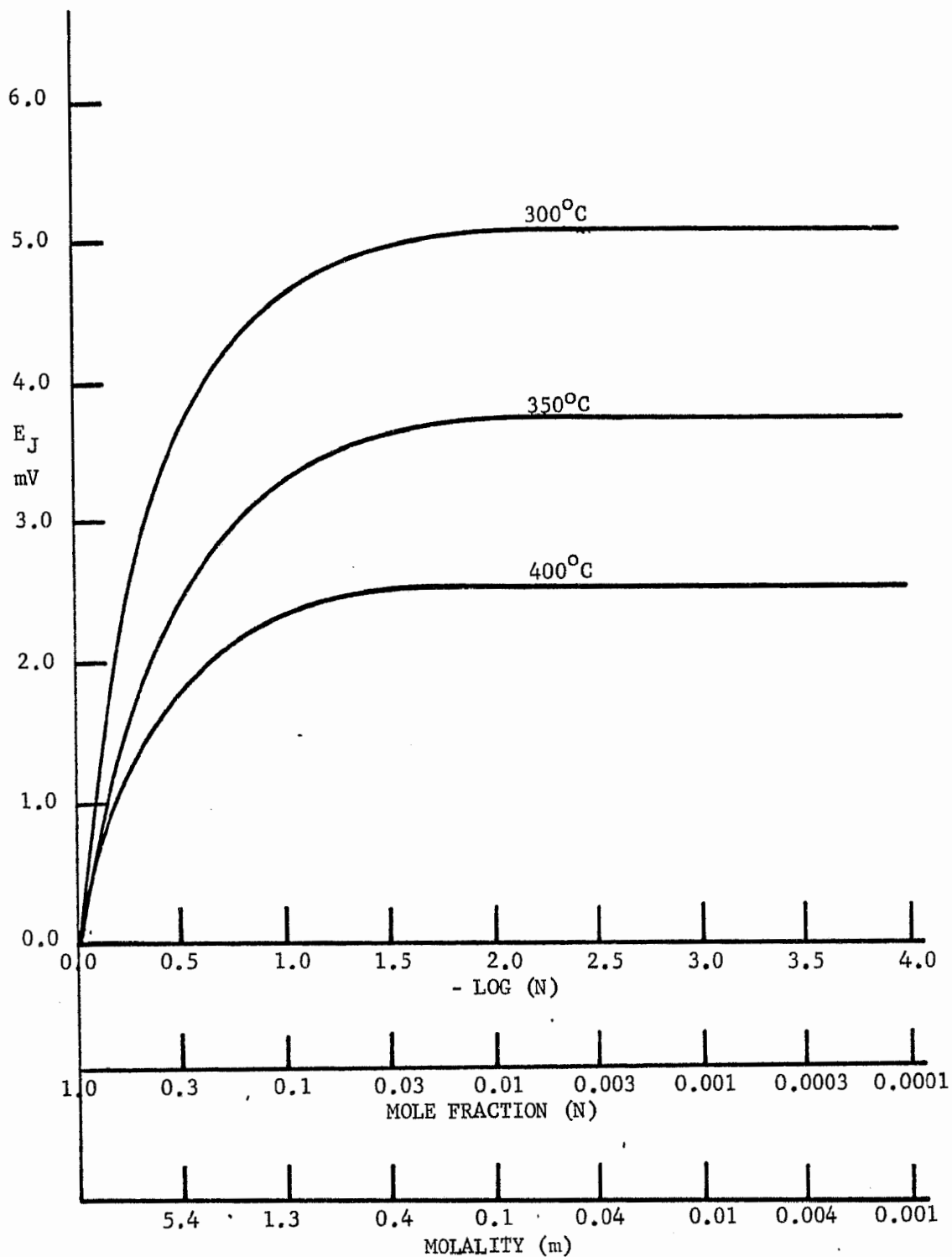
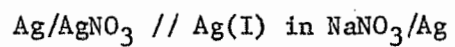


Figure 7.2 Calculated Liquid Junction Potentials, E_J , for a Ag(I) in NaNO_3 Concentration Cell.



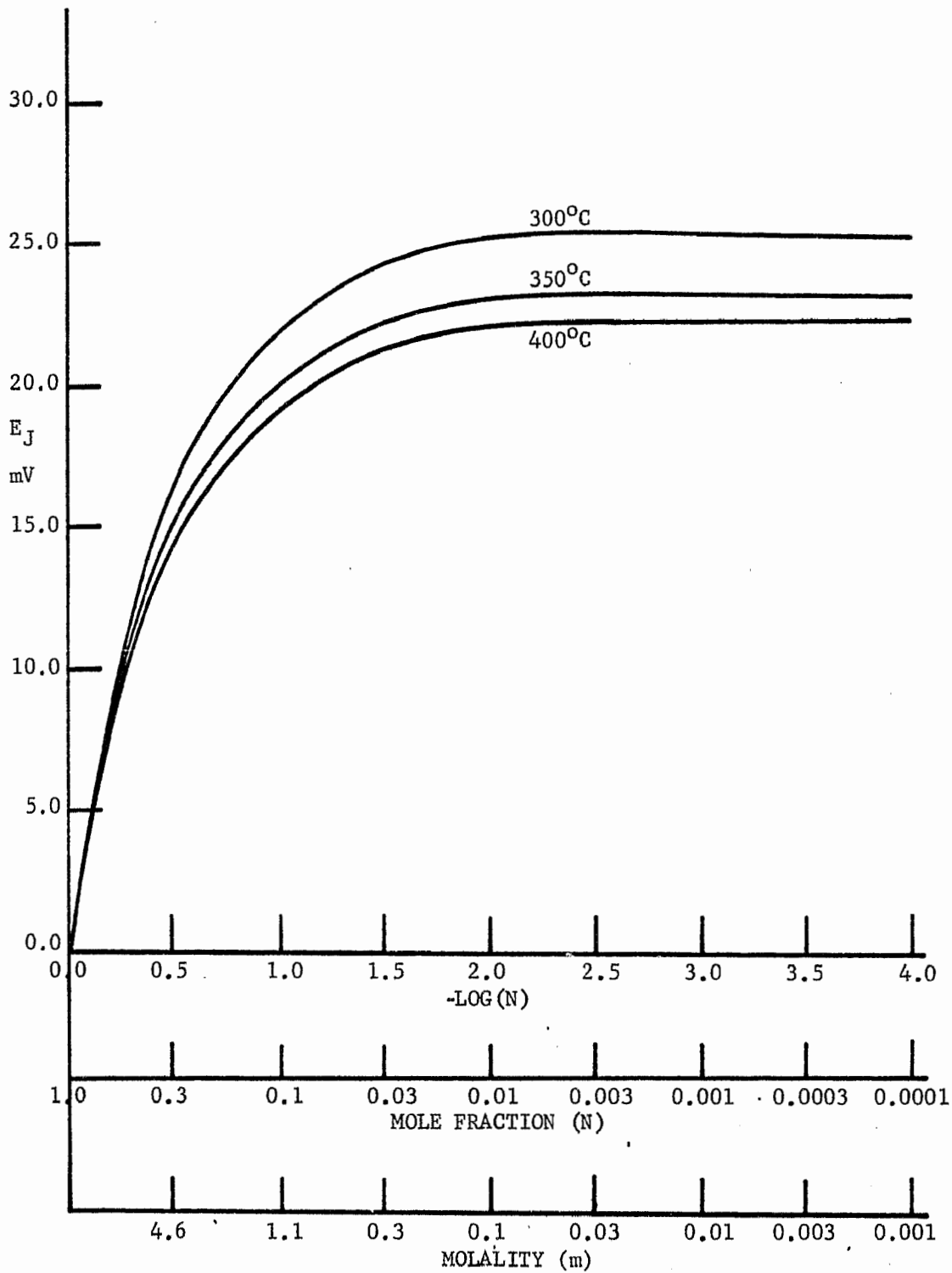
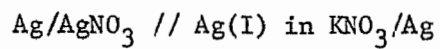


Figure 7.3 Calculated Liquid Junction Potentials, E_J , for a Ag(I) in KNO_3 Concentration Cell.



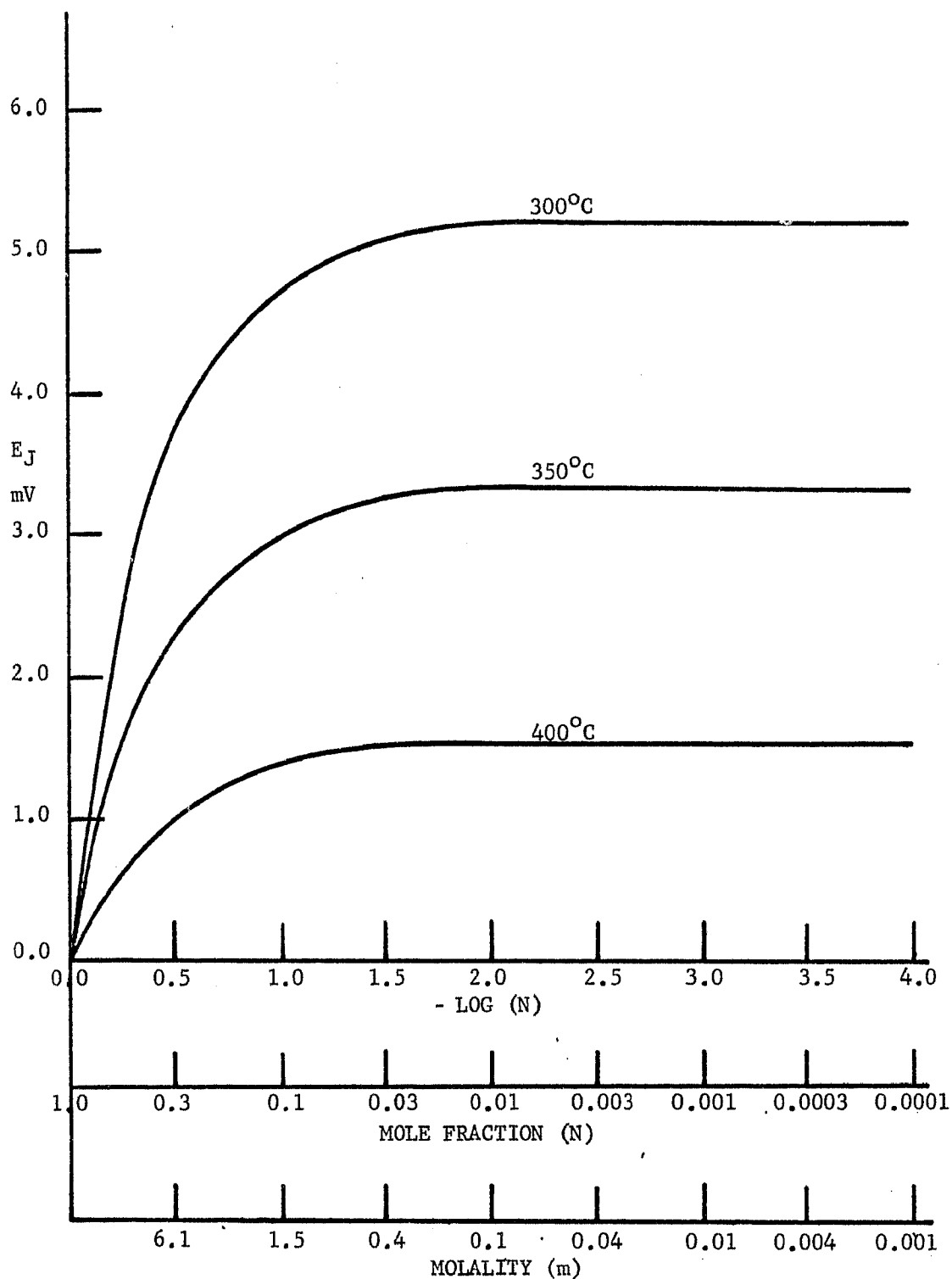


Figure 7.4 Calculated Liquid Junction Potentials, E_J , for a Ag(I) in (0.54 Li, 0.46 Na)NO₃ Concentration Cell.

Ag/AgNO₃ // Ag(I) in (0.54 Li, 0.46 Na)NO₃/Ag

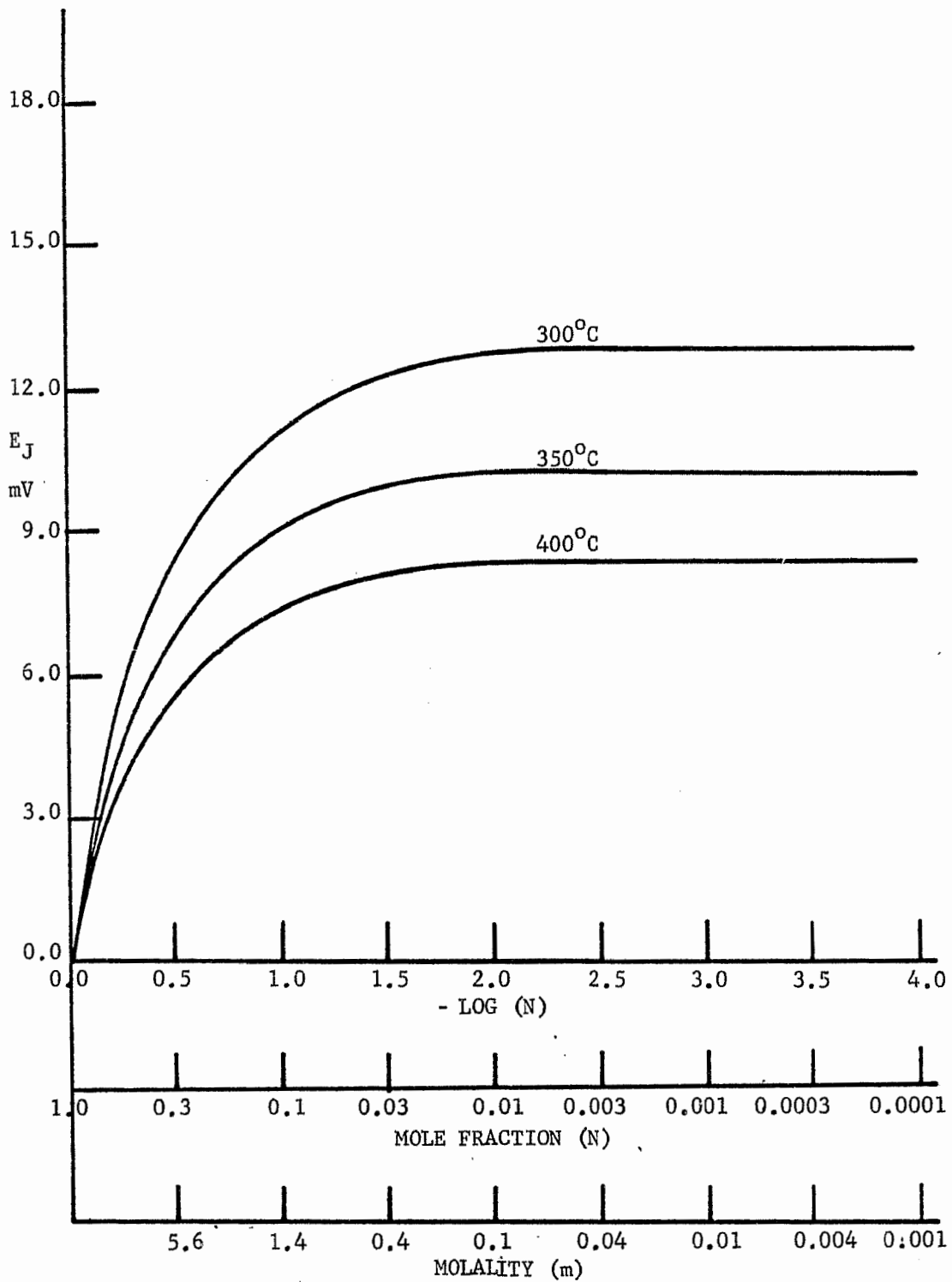


Figure 7.5 Calculated Liquid Junction Potentials, E_J , for a Ag(I) in (0.59 Li, 0.41 K)NO₃ Concentration Cell.

Ag/AgNO₃ //Ag(I) in (0.59 Li, 0.41 K)NO₃/Ag

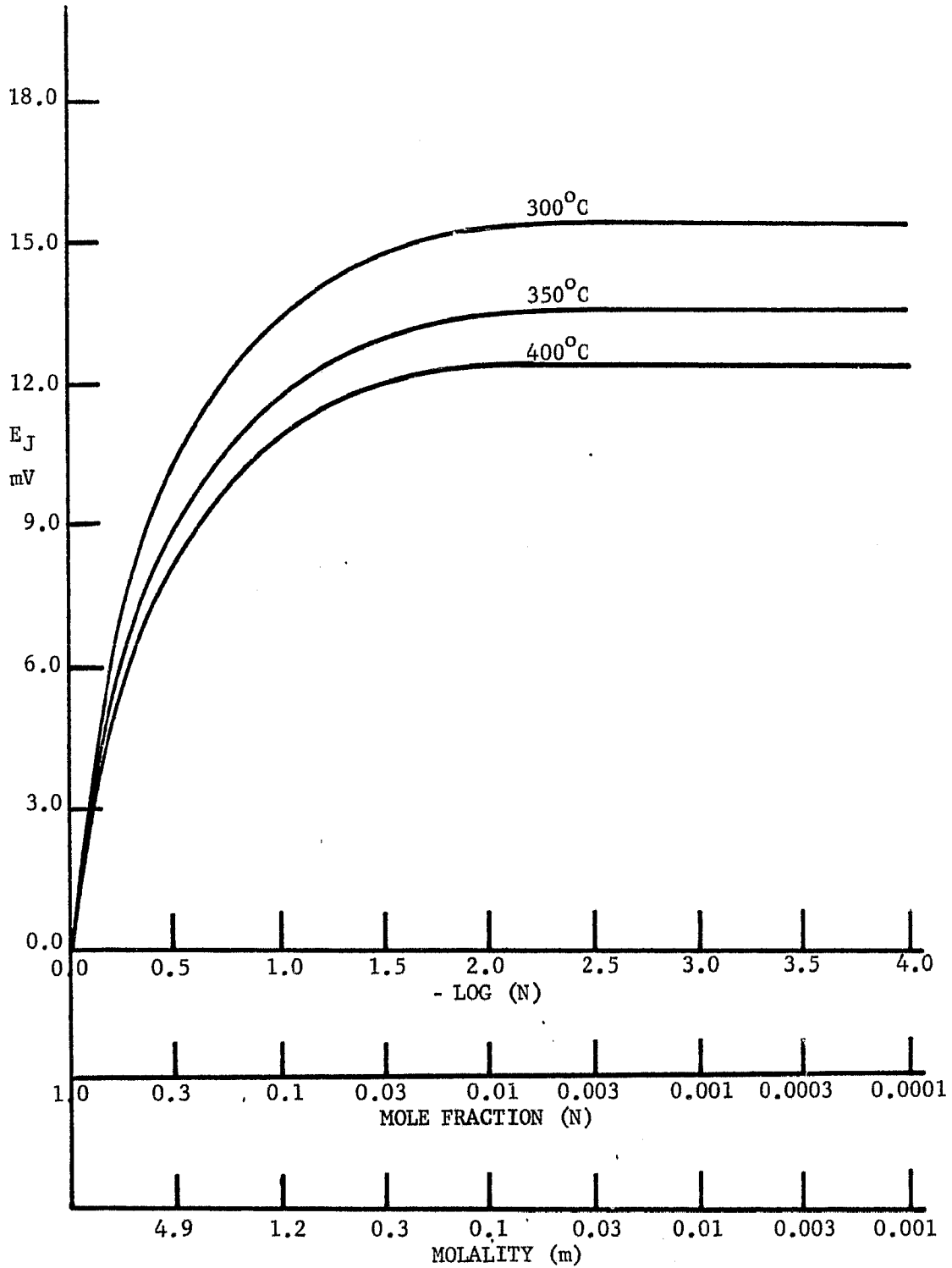
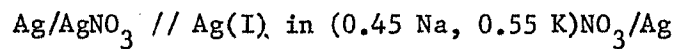


Figure 7.6 Calculated Liquid Junction Potentials, E_J , for a Ag(I) in (0.45 Na, 0.55 K)NO₃ Concentration Cell.



7.4 Densities of Nitrate and Sulfate Melts

The bouyancy method was used to determine the density, as a function of temperature, of several binary nitrate melts and the ternary sulfate eutectic. Using pure sodium nitrate as a standard, the volume of a silver bob (suspended from an electric balance so that its weight could be recorded before and after immersion in a thermostated melt) was calibrated from 325°C to 475°C. The density, D , of the sodium nitrate melt is given as a function of the temperature by the following equation (2):

$$D = 2.320 - 7.5 \times 10^{-4} T \text{ (gms cm}^{-3}\text{)} \quad (7.34)$$

where T is in degrees Kelvin. The volume of the bob immersed in the melt was calculated by dividing the bob's loss of weight, upon immersion in the melt, by the density of the melt at the given temperature. The results for the calibration of the volume of the silver bob are summarized in Table 7.3 and plotted in Figure 7.7. Figure 7.7 shows no significant difference in the results obtained between the heating and cooling portion of the temperature cycle, demonstrating that complete temperature equilibrium had been reached at each measurement. The equation for a least squares straight line fit of the data is

$$\text{Volume} = 3.6916 + 3.2 \times 10^{-4} T^{\circ}\text{C} \text{ (cm}^3\text{)} \quad (7.35)$$

with a standard deviation of 0.0018 cm^3 . The loss of weight by the silver bob at 550°C in the lithium ~~potassium~~ sulfate eutectic (density = $2.120 \text{ gms cm}^{-3}$) (58) was 8.1877 gms which corresponds to a volume of 3.8621 cm^3 ; this compares favorably to the value of 3.8676 cm^3 predicted

by equation 7.35.

TABLE 7.3
VOLUME OF SILVER BOB AS FUNCTION OF TEMPERATURE

Temperature °C	Loss of Weight gms	Density of NaNO ₃ gms cm ⁻³	Volume of Bob cm ³
327.3	7.1818	1.891	3.7981
348.6	7.1365	1.876	3.8045
355.1	7.1143	1.871	3.8024
371.1	7.0877	1.860	3.8106
376.4	7.0752	1.856	3.8125
395.0	7.0387	1.842	3.8208
397.4	7.0300	1.841	3.8190
402.0	7.0175	1.838	3.8180
425.7	6.9682	1.820	3.8287
428.5	6.9601	1.819	3.8272
446.8	6.9233	1.805	3.8354
448.1	6.9261	1.805	3.8372
470.7	6.8684	1.789	3.8401

The densities were determined for four binary nitrate melts between the temperatures of 200°C and 400°C and the ternary sulfate eutectic at 550°C. The density results for the five melts are tabulated in Tables 7.4 to 7.8 and the nitrate densities are plotted in Figures 7.8 to 7.11. The data in the nitrate plots (Figures 7.8 to

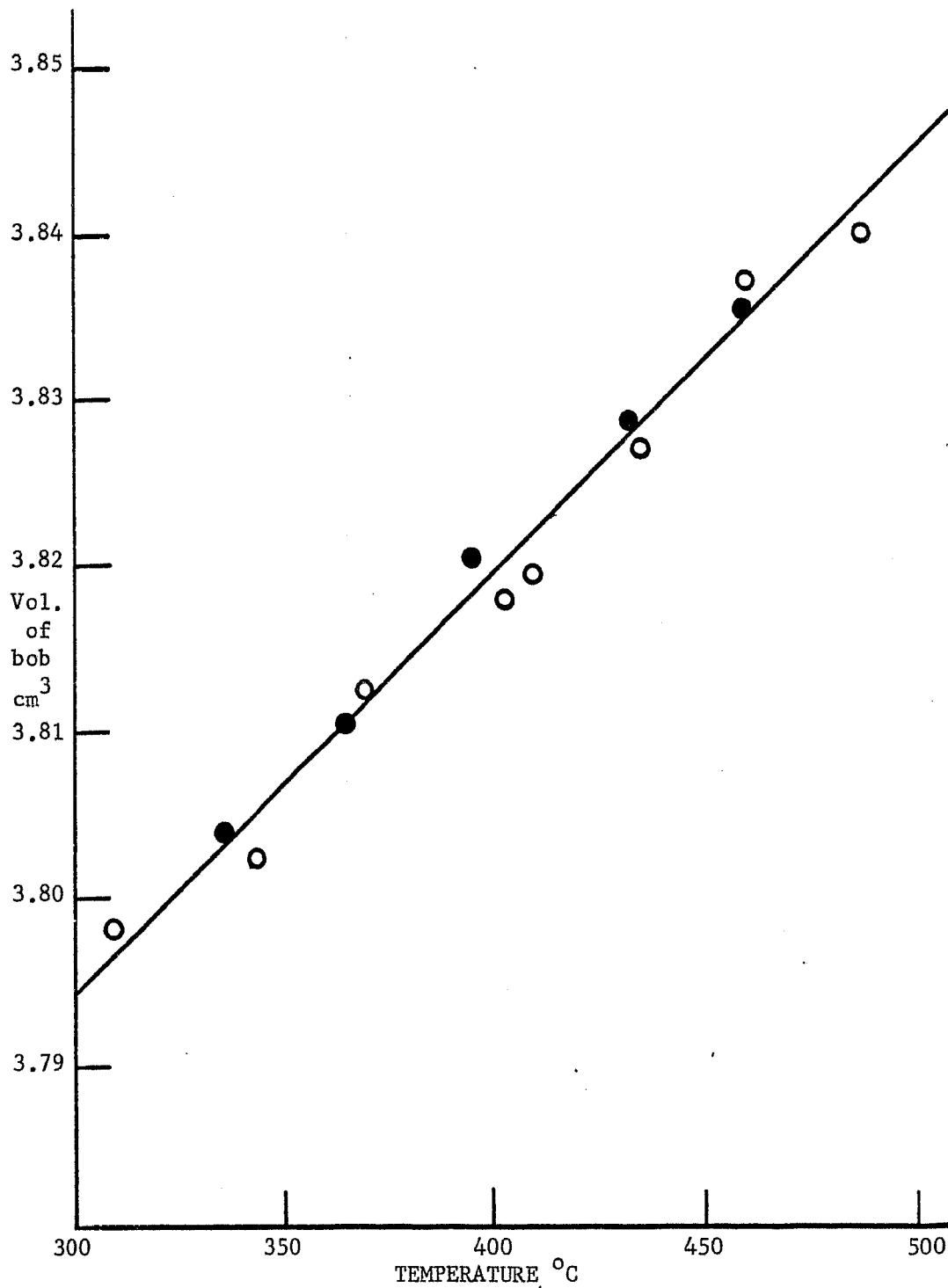


Figure 7.7 Calibration of Silver Bob for Density Measurements.

The open points were obtained from heating portion of calibration procedure and the solid points from the cooling portion.

7.11) were fitted by a least squares method to the linear equation

$$D = a - b \times 10^{-4} T^{\circ}\text{C} \quad (7.36)$$

where D is the density of the melt at $T^{\circ}\text{C}$. The values of the parameters (a and b) are given in Table 7.9 along with the standard deviation and the temperature range for each system.

TABLE 7.4

DENSITY OF (0.54 Li, 0.46 Na)NO₃ EUTECTIC

Temperature $^{\circ}\text{C}$	Loss of Weight gms	Volume of Bob cm^3	Density of Melt gms cm^{-3}
207.6	7.0977	3.7580	1.8887
228.1	7.0500	3.7646	1.8727
263.9	6.9731	3.7760	1.8467
284.9	6.9290	3.7828	1.8317
313.1	6.8745	3.7918	1.8130
315.0	6.8551	3.7924	1.8076
334.4	6.8314	3.7986	1.7984
361.5	6.7583	3.8073	1.7751
391.0	6.6815	3.8167	1.7506

TABLE 7.5

DENSITY OF (0.41 Li, 0.59 K)NO₃ EUTECTIC

Temperature °C	Loss of Weight gms	Volume of Bob cm ³	Density of Melt gms cm ⁻³
158.8	7.3497	3.7424	1.9639
182.0	7.2769	3.7498	1.9406
208.9	7.2387	3.7584	1.9260
244.0	7.1530	3.7697	1.8975
257.8	7.1215	3.7740	1.8870
293.7	6.9905	3.7856	1.8466
317.4	6.9256	3.7932	1.8258
344.2	6.8495	3.8017	1.8017
365.1	6.8231	3.8084	1.7916
399.7	6.7475	3.8195	1.7666

TABLE 7.6

DENSITY OF (0.59 Li, 0.41 K)NO₃ MIXTURE

Temperature °C	Loss of Weight gms	Volume of Bob cm ³	Density of Melt gms cm ⁻³
209.7	7.1254	3.7587	1.8957
232.1	7.0626	3.7659	1.8754
265.0	7.0184	3.7764	1.8585
286.6	6.9049	3.7833	1.8251
314.4	6.8502	3.7922	1.8064
344.3	6.7923	3.8018	1.7866
350.2	6.7596	3.8037	1.7771
391.8	6.6916	3.8170	1.7531
418.0	6.6355	3.8254	1.7346

TABLE 7.7

DENSITY OF (0.45 Na, 0.55 K)NO₃ EUTECTIC

Temperature °C	Loss of Weight gms	Volume of Bob cm ³	Density of Melt gms cm ⁻³
252.2	7.2911	3.7723	1.9328
260.0	7.2725	3.7748	1.9266
268.5	7.2479	3.7775	1.9187
287.0	7.1956	3.7834	1.9019
318.2	7.1198	3.7934	1.8769
357.2	7.1168	3.8059	1.8481
374.6	6.9880	3.8115	1.8334
375.6	6.9954	3.8118	1.8352
401.9	6.9264	3.8202	1.8131
428.3	6.8756	3.8287	1.7958
449.8	6.8088	3.8355	1.7752
476.5	6.7677	3.8440	1.7606
501.7	6.1769	3.8521	1.7437

TABLE 7.8

DENSITY OF (0.78 Li, 0.085 Na, 0.135 K)₂SO₄ EUTECTIC

Temperature °C	Loss of Weight gms	Volume of Bob cm ³	Density of Melt gms cm ⁻³
549.8	8.2135	3.8621	2.1267
549.9	8.1963	3.8621	2.1222
550.0	8.2012	3.8621	2.1235
550.1	8.2064	3.8621	2.1248
550.2	8.2184	3.8621	2.1280

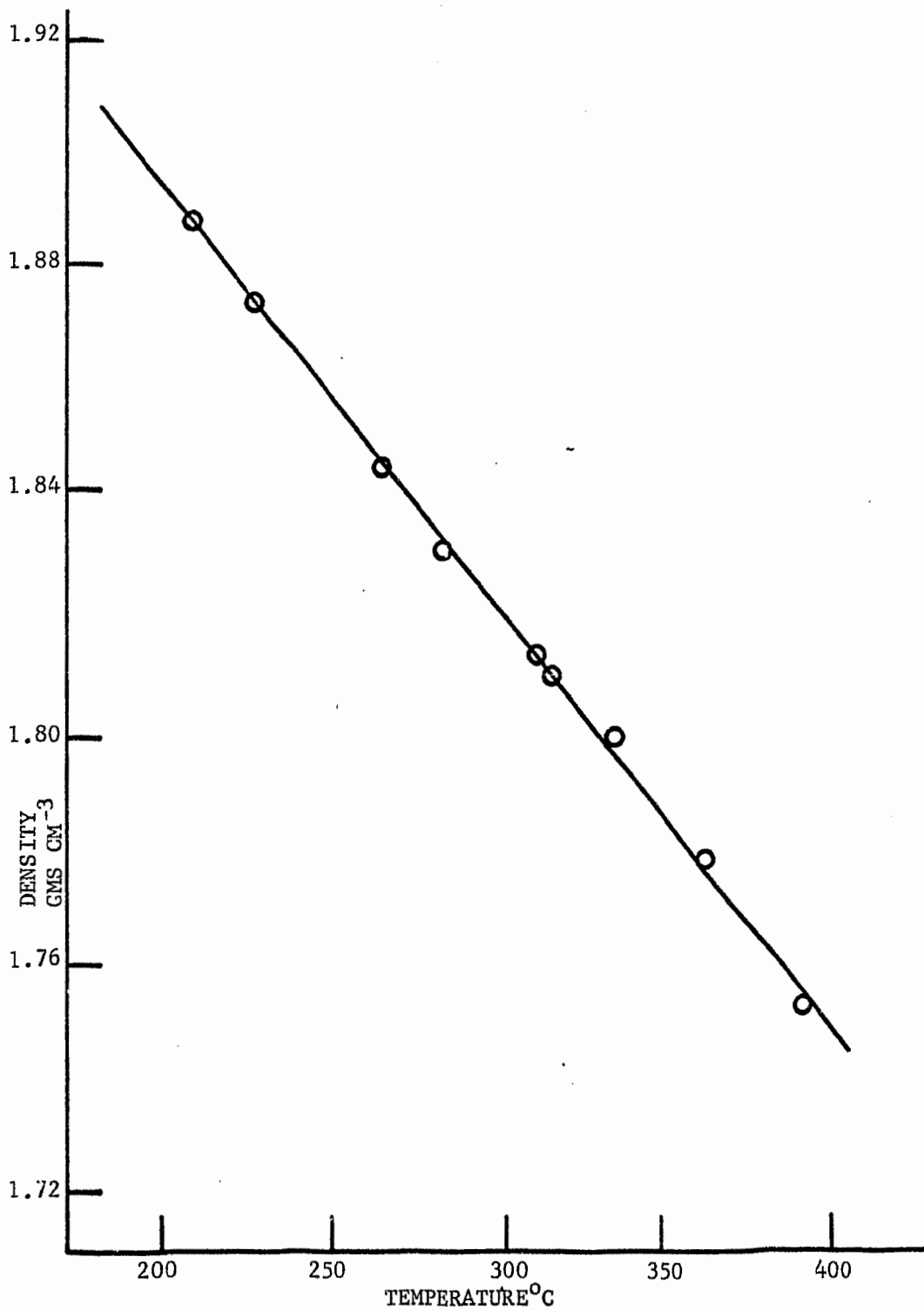


Figure 7.8 Density of (0.54 Li, 0.46 Na)NO₃ Eutectic Versus Temperature

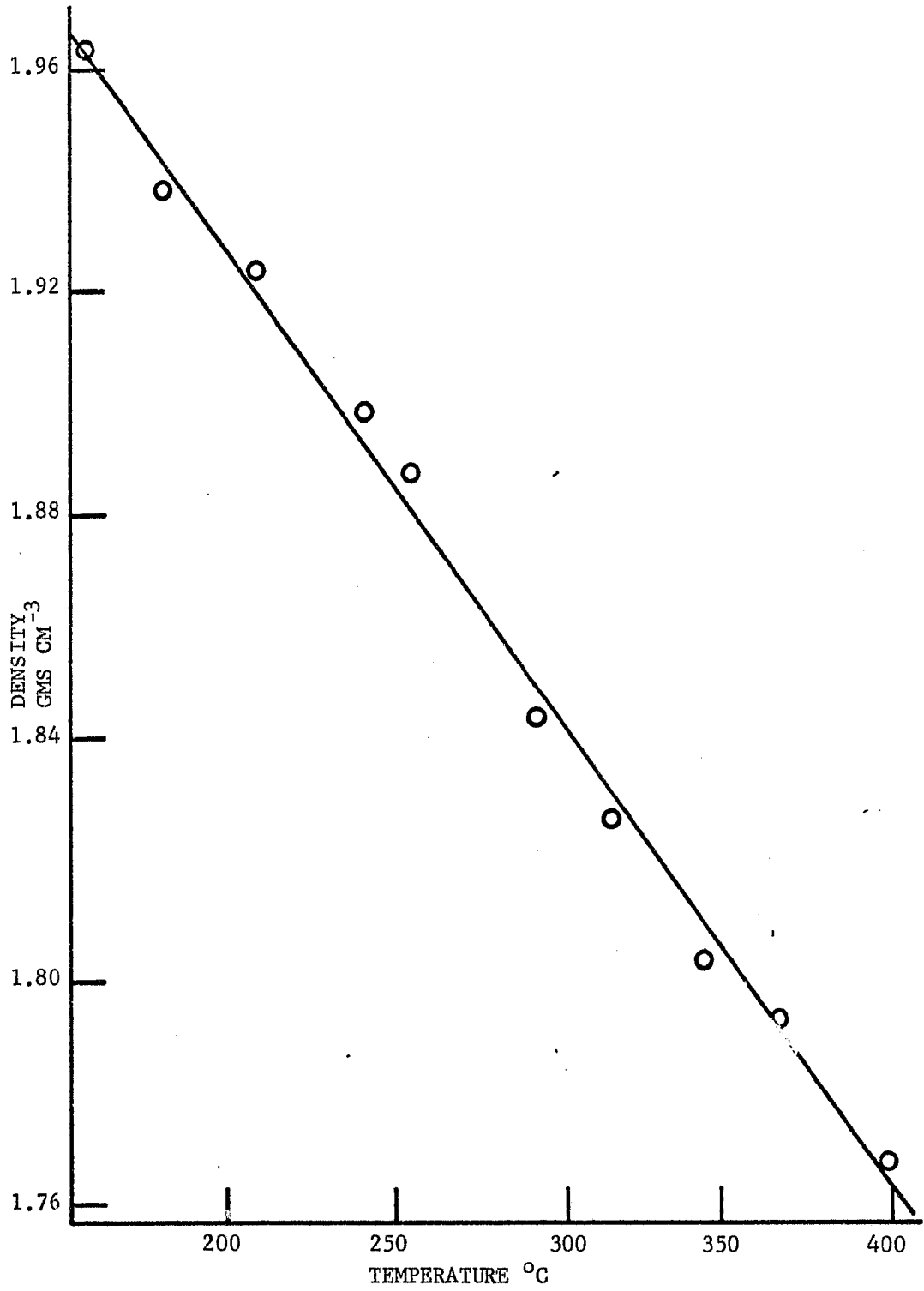


Figure 7.9 Density of (0.41 Li, 0.59 K)NO₃ Eutectic Versus Temperature

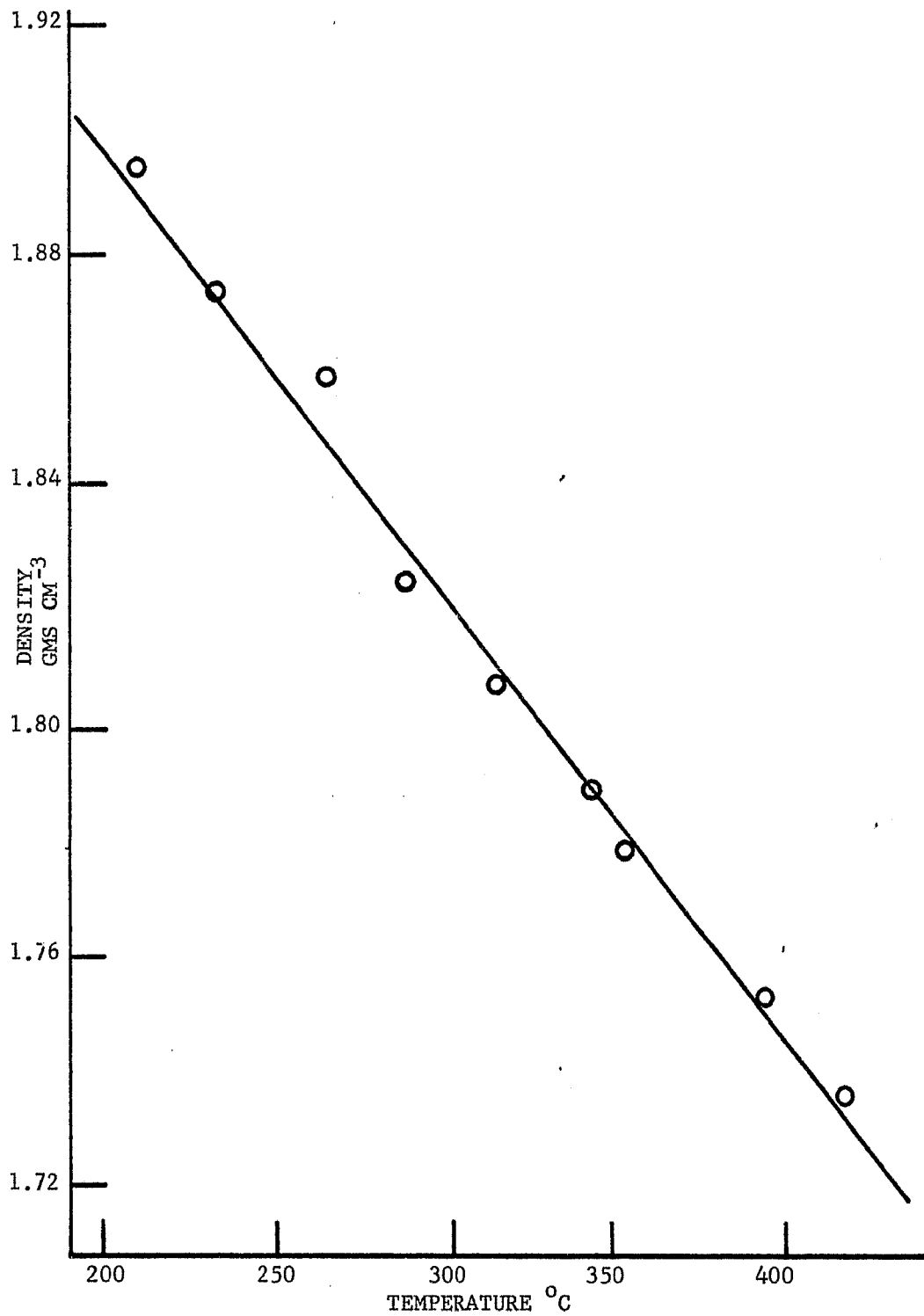


Figure 7.10 Density of (0.59 Li, 0.41 K)NO₃ Mixture Versus Temperature

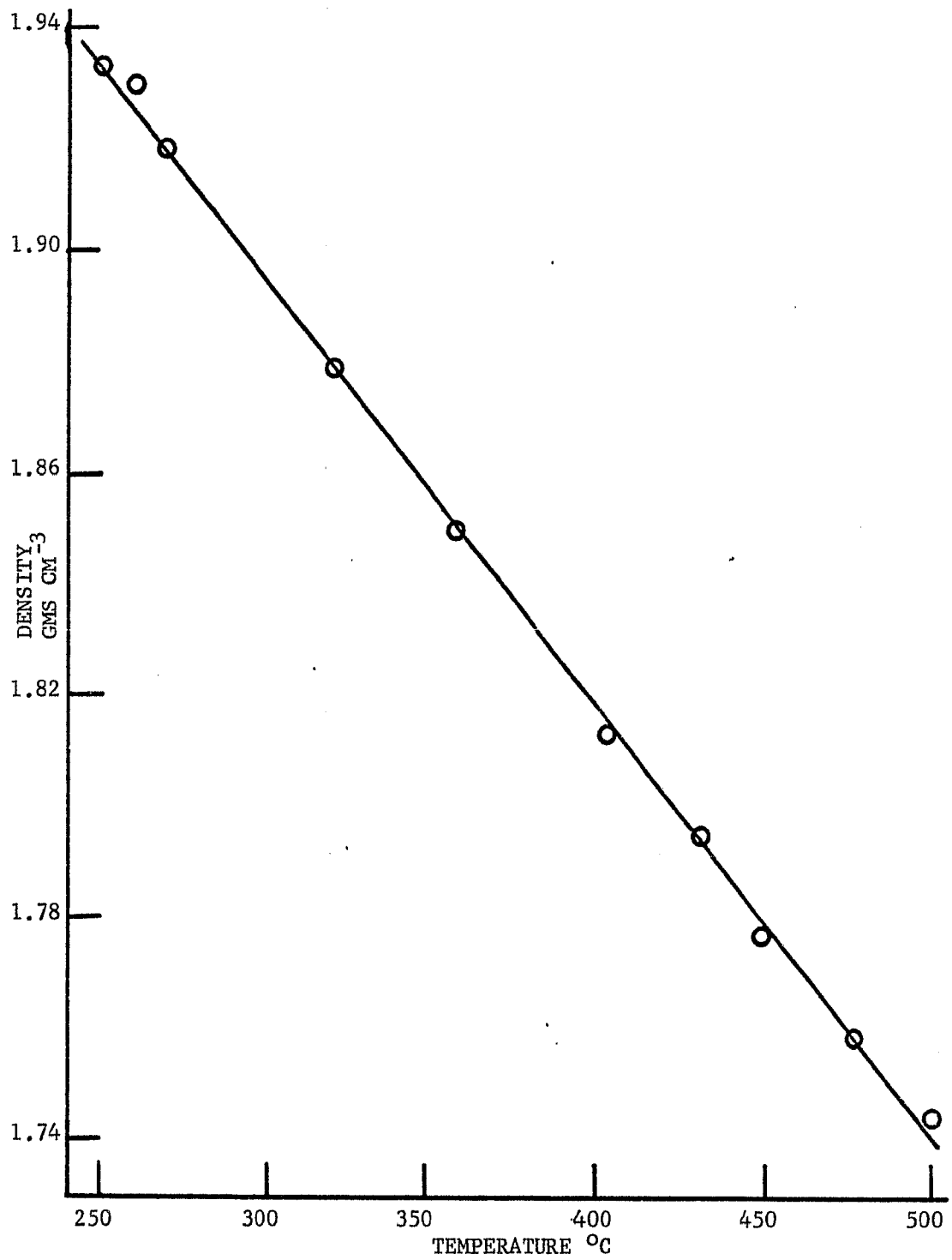


Figure 7.11 Density of (0.45 Na, 0.55 K)NO₃ Eutectic Versus Temperature

TABLE 7.9

DENSITY PARAMETERS FOR THE EQUATION

$$D = a - b \times 10^{-4} T^{\circ}\text{C} \text{ (gms cm}^{-3}\text{)}$$

Melt	a	b	St. Dev.	Temperature Range °C
0.45 NaNO ₃ 0.55 KNO ₃	2.122	7.648	0.002	250 - 500
0.46 NaNO ₃ 0.54 LiNO ₃	2.042	7.399	0.002	200 - 400
0.41 LiNO ₃ 0.59 KNO ₃	2.099	8.436	0.005	150 - 400
0.59 LiNO ₃ 0.41 KNO ₃	2.058	7.842	0.005	200 - 425
0.78 Li ₂ SO ₄ 0.085 Na ₂ SO ₄ 0.135 K ₂ SO ₄	2.125	—	0.002	550

For systems of simple solutions where complexes do not form, molar volumes have been found to show only small deviations from additivity (57, 58, 70, 318). This fact can be used in the estimation of densities for systems where experimental data are lacking. The average molecular weight, M_m , of a mixture composed of two salts of molecular weights M_x and M_y with a common anion or cation is given by

$$M_m = N_x M_x + N_y M_y \quad (7.37)$$

where N is the mole fraction of the respective salts. The molar

volume, V° , of a salt is calculated by dividing its molecular weight by its density,

$$V^{\circ} = M/D \quad (7.38)$$

and the molar volume of the mixture, V_m° , is given by:

$$V_m^{\circ} = N_x V_x^{\circ} + N_y V_y^{\circ} \quad (7.39)$$

Equations 7.37 and 7.39 are combined and simplified to give the density of the mixture by the equation:

$$D_m = \frac{D_x D_y (N_x M_x + N_y M_y)}{D_x N_x M_x + D_y N_y M_y} \quad (7.40)$$

The main objections to this method of calculating the density of mixtures is the need to assume ideal behavior (i.e., no complexes formed) and to extrapolate the densities of the pure components to temperatures below their melting points. For the simple systems the deviations between the calculated and experimental densities are usually less than $\pm 1\%$ (58). The experimental, calculated and literature densities for the nitrate mixtures at 300, 350 and 400°C are tabulated in Table 7.10. Similar calculations and tabulations for two sulfate eutectics at 550°C are also presented in Table 7.10. All densities determined experimentally are within 1% of the densities calculated from the additivity of molar volumes with the experimental densities tending to be slightly lower than the calculated values; this was taken as an indication of some interaction between the different types of cations disrupting the packing symmetry of the ions in the melt.

TABLE 7.10

DENSITIES OF NITRATE AND SULFATE MELTS AT SELECTED TEMPERATURES

Melt	Temperature °C	Densities			Ref.
		Experimental	Calculated	Literature	
0.54 LiNO ₃ 0.46 NaNO ₃	300	1.820	1.832	1.854*	60
	350	1.783	1.800	1.822*	60
	400	1.746	1.769	1.790*	60
0.41 LiNO ₃ 0.59 KNO ₃	300	1.846	1.849	1.877 [▲]	59
	350	1.804	1.816	1.838 [▲]	59
	400	1.762	1.783	1.799 [▲]	59
0.59 LiNO ₃ 0.41 KNO ₃	300	1.823	1.824	1.836**	60
	350	1.784	1.793	1.802**	60
	400	1.744	1.761	1.765**	60
0.45 NaNO ₃ 0.55 KNO ₃	300	1.893	1.903	1.891 ^{▲▲}	59
	350	1.854	1.867	1.825 ^{▲▲}	59
	400	1.816	1.830	1.758 ^{▲▲}	59
0.50 NaNO ₃ 0.50 KNO ₃	300	—	1.904	1.902	58
	350	—	1.868	1.864	58
	400	—	1.834	1.825	58
0.78 Li ₂ SO ₄ 0.085 Na ₂ SO ₄ 0.135 K ₂ SO ₄	550	2.125	2.147	2.2	320
0.80 Li ₂ SO ₄ 0.20 K ₂ SO ₄	550		2.141	2.120	58

* (0.60 Li, 0.40 Na)NO₃** (0.60 Li, 0.40 K)NO₃▲ (0.43 Li, 0.57 K)NO₃▲▲ (0.47 Na, 0.53 K)NO₃

These results are consistent with the measurements made by Powers et al. (319) on several binary alkali metal nitrate mixtures. They reported that the deviations, Δv^E , from the additivity of molar volumes were positive and obeyed the approximate equation

$$\Delta v^E = N_1 N_2 v^1 \delta^4 \quad (7.41)$$

where $v^1 \approx 22,000 \text{ cm}^3 \text{ mole}^{-1}$ (7.42)

$$\delta = \frac{(d_1 - d_2)}{(d_1 + d_2)} \quad (7.43)$$

$$d_1 = \text{radius of cation} + \text{radius of anion of salt 1} \quad (7.44)$$

$$d_2 = \text{radius of cation} + \text{radius of anion of salt 2} \quad (7.45)$$

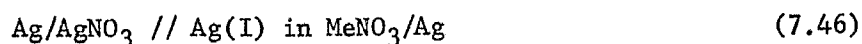
The value of Δv^E for the sodium-potassium-nitrate eutectic was reported to be $1.05 \pm 0.32 \text{ cm}^3 \text{ mole}^{-1}$; without applying the Δv^E correction the calculated density of the eutectic at 400°C was $1.830 \text{ gms cm}^{-3}$, but after correction had been applied it was $1.793 \pm 0.011 \text{ gms cm}^{-3}$ (a difference of $2.0 \pm 1.4\%$ between the two calculated densities). The application of the Δv^E correction term to the calculations in this study eliminates the tendency for the results to be slightly lower than the calculated values.

The only serious disagreement between the literature and the experimental values for the nitrate melts was in the density of the sodium-potassium-nitrate eutectic. The density reported by Papaioannou and Harrington (59) at 400°C is 4% below the calculated value and 3.2% below the value obtained from the current investigation; no

apparent reason for this discrepancy could be ascertained from their paper. As the experimental results of this study have conformed closely to the calculated density, and as the densities in the other nitrate melts have agreed with the calculated values, the validity of their results must be questioned.

7.5 Silver Nitrate Activity Coefficients

The activity coefficients for silver nitrate in several single and binary alkali nitrate melts at 300, 350 and 400°C were determined by measuring the emf of the concentration cell:



The emf of the cell is given by:

$$E = \frac{RT}{F} \ln (N \gamma_N) + E_J \quad (7.47)$$

where the mole fraction, N , and activity coefficient, γ_N , refer to the silver nitrate in the right-hand portion of the cell, and the liquid junction potential, E_J , was estimated from the data in Figures 7.1 to 7.6. Equation 7.47 is solved in terms of γ_N to give

$$\gamma_N = \exp \left[\frac{F(E - E_J)}{RT} - \ln(N) \right] \quad (7.48)$$

Several other workers have used this approach to obtain values for the activity coefficient of silver nitrate in nitrate melts; however, their studies were limited to high concentrations of silver nitrate ($N > 0.05$) and they assumed that the liquid junction potential was zero (cf. chapter 3.4, page 44). Low concentrations of silver nitrate ($10^{-4} \leq N \leq 10^{-2}$) were used in this study for three

reasons: firstly, most electrochemical studies are made in this concentration region; secondly, the probability of ideal behavior is greater; and, thirdly, whereas at higher concentrations the value of the activity coefficient is continually changing, in this region it should be a constant.

At very low silver nitrate concentrations, corrosion of the silver electrode in the nitrate melts becomes a serious problem (as shown by the deviation from the Nernst slope in Figure 7.12). A very small amount of corrosion in very dilute solutions will produce a relatively large change in the silver concentrations. A computer program which simulated the corrosion occurring during the experiment was used to correct the raw data from the experimental cell for corrosion. In the computation the activity coefficient was assumed to be constant for the concentration range of each calculation; such an assumption is justified with the low concentrations. A change in concentration from N_1 to N_2 produces a corresponding emf change from E_1 to E_2 according to the following equations:

$$E_1 = \frac{RT}{F} \ln N_1 \gamma_N \quad (7.49)$$

$$E_2 = \frac{RT}{F} \ln N_2 \gamma_N \quad (7.50)$$

$$\exp \left[\frac{F(E_2 - E_1)}{RT} \right] = \frac{N_2}{N_1} = \frac{N_1 + (N_2 - N_1)}{N_1} \quad (7.51)$$

$$N_1 = \frac{N_2 - N_1}{\exp \left[\frac{F(E_2 - E_1)}{RT} \right] - 1} \quad (7.52)$$

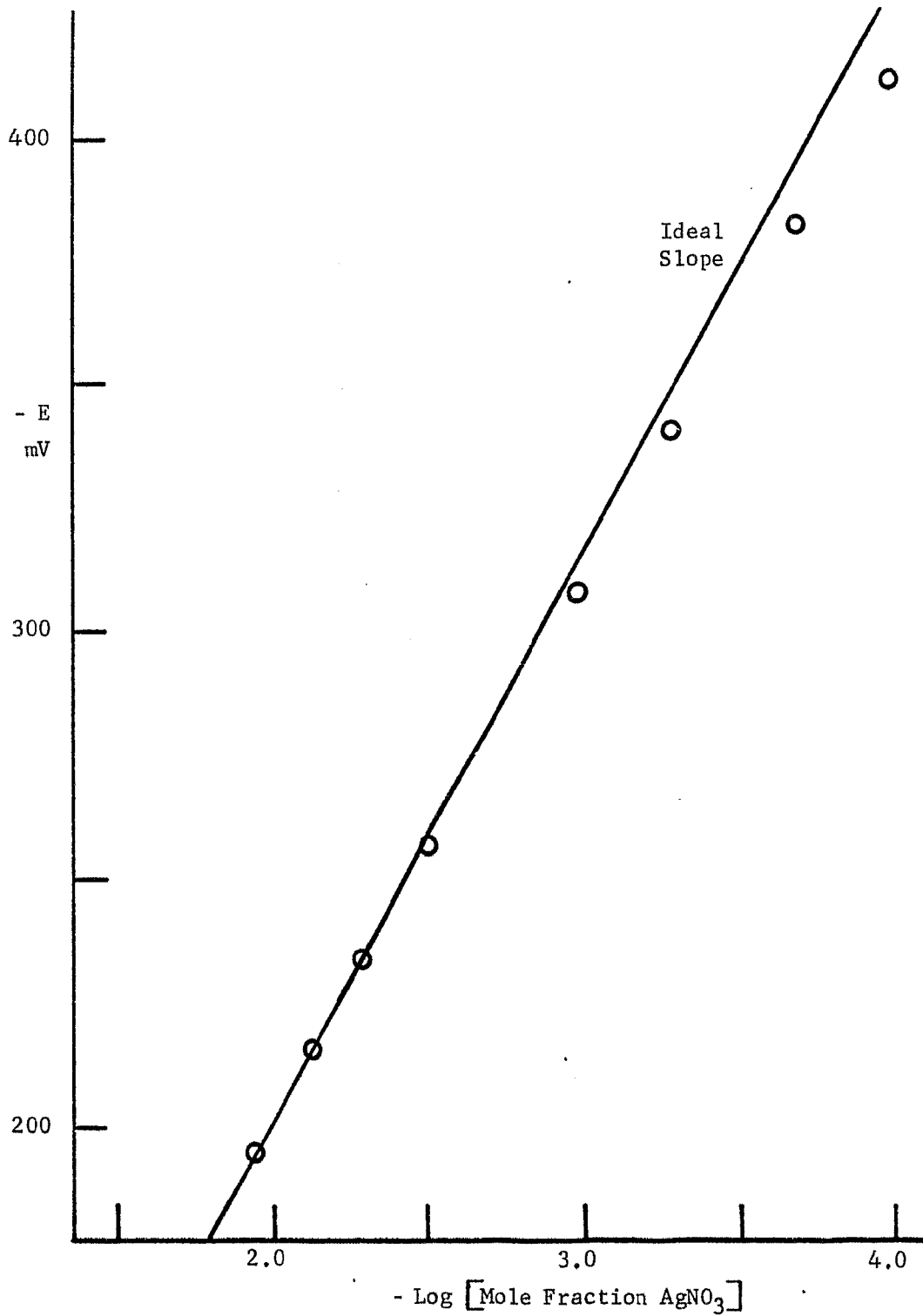
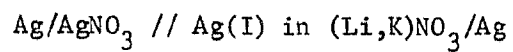


Figure 7.12 Nernst plot at 300°C for the cell:



The data have not been corrected for corrosion of the silver electrode.

The observed change in the emf, $(E_2 - E_1)$, which results from a change in concentration, $(N_2 - N_1)$, can be used to calculate the initial concentration, N_1 , using equation 7.52.

In the actual experiment the change in concentration is the sum of the amount of silver(I) generated, G , by coulometric oxidation of the silver electrode and the amount, C , due to corrosion. The entire corrosion, silver(I) generation and emf measurement cycle is presented as a function of time in Figure 7.13.

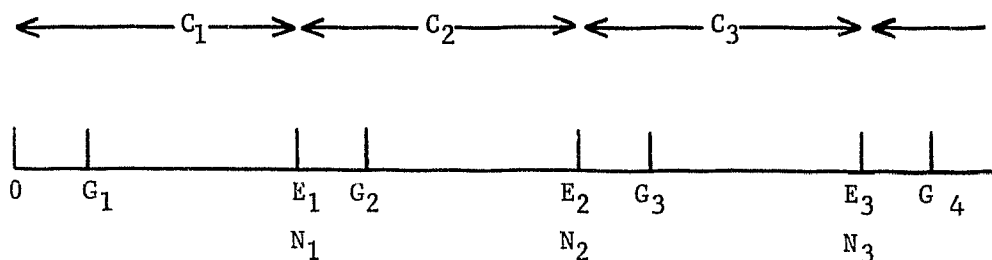


Figure 7.13 Time Scale for Calculation of
Silver Corrosion in Nitrate Melts

At time G_1 a concentration of silver nitrate equivalent to a mole fraction of G_1 is generated coulometrically. After stabilization, a potential of E_1 is measured at time E_1 ; however, during this time period the increase in the silver(I) concentration due to corrosion is an amount equivalent to a mole fraction of C_1 . The true silver concentration, N_1 , at time E_1 is given by $N_1 = G_1 + C_1$ since in very dilute solutions mole fractions are additive. At time G_2 , additional silver(I) is generated to give a total generated silver(I) concentration equivalent to a mole fraction of G_2 . This entire sequence is

repeated until the end of the experiment.

The change in potential, $(E_2 - E_1)$, is produced by a concentration change of $(N_2 - N_1)$ which is given by:

$$\begin{aligned} N_2 - N_1 &= G_2 + C_1 + C_2 - G_1 - C_1 \\ &= G_2 - G_1 + C_2 \end{aligned} \quad (7.53)$$

The value of C_2 is unknown; however, it can be by-passed by examining the potential difference between E_3 and E_2 and by assuming C_3 to be zero.

$$\begin{aligned} N_3 - N_2 &= G_3 + C_1 + C_2 - G_2 - C_1 - C_2 \\ &= G_3 - G_2 \end{aligned} \quad (7.54)$$

A value for N_2 is calculated using equation 7.52 and then substituted into equation 7.51 to obtain a value for N_1 . By assuming C_3 , instead of C_2 , is zero a second order approximation is made instead of a first order. This procedure can be extended to higher orders of approximation, but calculations have shown that anything beyond second order has very little effect on the final answer. The value of C_1 is given by

$$C_1 = N_1 - G_1 \quad (7.55)$$

The entire procedure is repeated for each of the points in the experimental run except for the last two data points, N_{k-1} and N_k . Since a third data point is not available for the calculation, it is assumed that C_k is zero and the values for N_{k-1} and N_k are calculated using equation 7.51.

The rate of corrosion for the silver electrode was found to be greatly enhanced by the presence of the lithium ion and to be moderately

increased by an increase in temperature with the least corrosion occurring in the sodium-potassium nitrate eutectic at 300°C. The results from the computer program for a typical run are given in Table 7.11 and a comparison of the amount of corrosion for several systems, as predicted by the computer program and the amount determined by atomic adsorption is given in Table 7.12.

TABLE 7.11

COMPUTER CORRECTION FOR CORROSION OF SILVER ELECTRODE
IN (0.59 Li, 0.41 K)NO₃ MIXTURE AT 300°C

$E - E_J$ (volts)	$G \times 10^4$	$\chi(C = 0)$	Total C $\times 10^4$	$\chi(C \neq 0)$	$\frac{\text{Total C}}{G} \times 100$
-0.4151	1.06	2.11	0.298	1.64	28%
-0.3832	2.12	2.00	0.347	1.72	16%
-0.3420	5.26	1.86	0.861	1.61	16%
-0.3094	10.52	1.81	0.832	1.67	8%
-0.2576	31.56	1.72	2.734	1.58	9%
-0.2329	52.58	1.70	3.401	1.60	6%
-0.2168	73.64	1.67	2.482	1.62	3%
-0.1951	115.7	1.66	2.482	1.62	2%

G = Total mole fractions of silver(I) generated coulometrically

C = Total mole fractions of silver(I) calculated due to corrosion

TABLE 7.12

CORROSION OF SILVER IN NITRATE MELTS

Melt	Temperature °C	G x 10 ⁴	$\frac{C \times 100}{G}$	$\frac{C_{AA} \times 100}{G}$
0.59 LiNO ₃ 0.41 KNO ₃	300	115.7 127.1	2.1% 2.5%	3.0% 2.0%
LiNO ₃	400	92.4 105.3	3.5% 5.3%	3.9% 4.5%
0.45 NaNO ₃ 0.55 KNO ₃	300	76.0 97.5	0.3% 0.1%	0.2% -0.3%

G = total silver(I) generated according to coulometer expressed in mole fractions of silver(I)

C = total silver(I) added to system by corrosion expressed in mole fractions of silver(I) as estimated by the computer program

C_{AA} = total silver(I) added to system by corrosion expressed in mole fractions of silver(I) as determined by Atomic Absorption.

Measurement of the rate of silver corrosion in several nitrate melts has verified the highly acidic character of the lithium ion (380). The present investigation used an experimental cell where the average area of the silver electrodes was about 0.8 cm² and the average length of time for the contact of silver with the melt was six hours. From these values and the corrosion rates reported by Conte and Ingram (98), the total number of mole fractions of silver(I) introduced into an average cell at 325°C were calculated to

be 0.37×10^{-4} and 8000×10^{-4} for the sodium-potassium nitrate eutectic and the lithium nitrate melts, respectively. For the sodium-potassium nitrate melt at 300°C the amount of corrosion estimated by the computer (0.23×10^{-4}) was close to the literature value; however, for lithium nitrate the computer estimate of corrosion (3.2×10^{-4}) was considerably smaller than the value calculated from the literature. Since the rate of corrosion will decrease as the silver(I) concentration increases, the difference in the amount of corrosion between the two studies is partially accounted for in that Conte and Ingram (380) used a larger volume of melt and did not add extra silver(I) to their system. Also, the particularly large difference for the lithium nitrate melt indicates either the presence of impurities in the melt used by Conte and Ingram or a strong dependence of the corrosion rate in the lithium nitrate melt on the concentration of silver(I) ion in the melt.

The activity coefficient for silver nitrate at 300, 350 and 400°C in the various nitrate melts (the experimental concentrations having been corrected for corrosion) was calculated according to equation 7.48 and then plotted in Figures 7.14 to 7.31. Each plot in a given solvent and at a given temperature presents the data for three to five individual runs with a maximum fluctuation of temperature of $\pm 1^{\circ}\text{C}$ from that given between all the runs. The applicable results of previous workers were first corrected for the non-zero value of the liquid junction potential and then included in the plots of Figures 7.14 through 7.31.

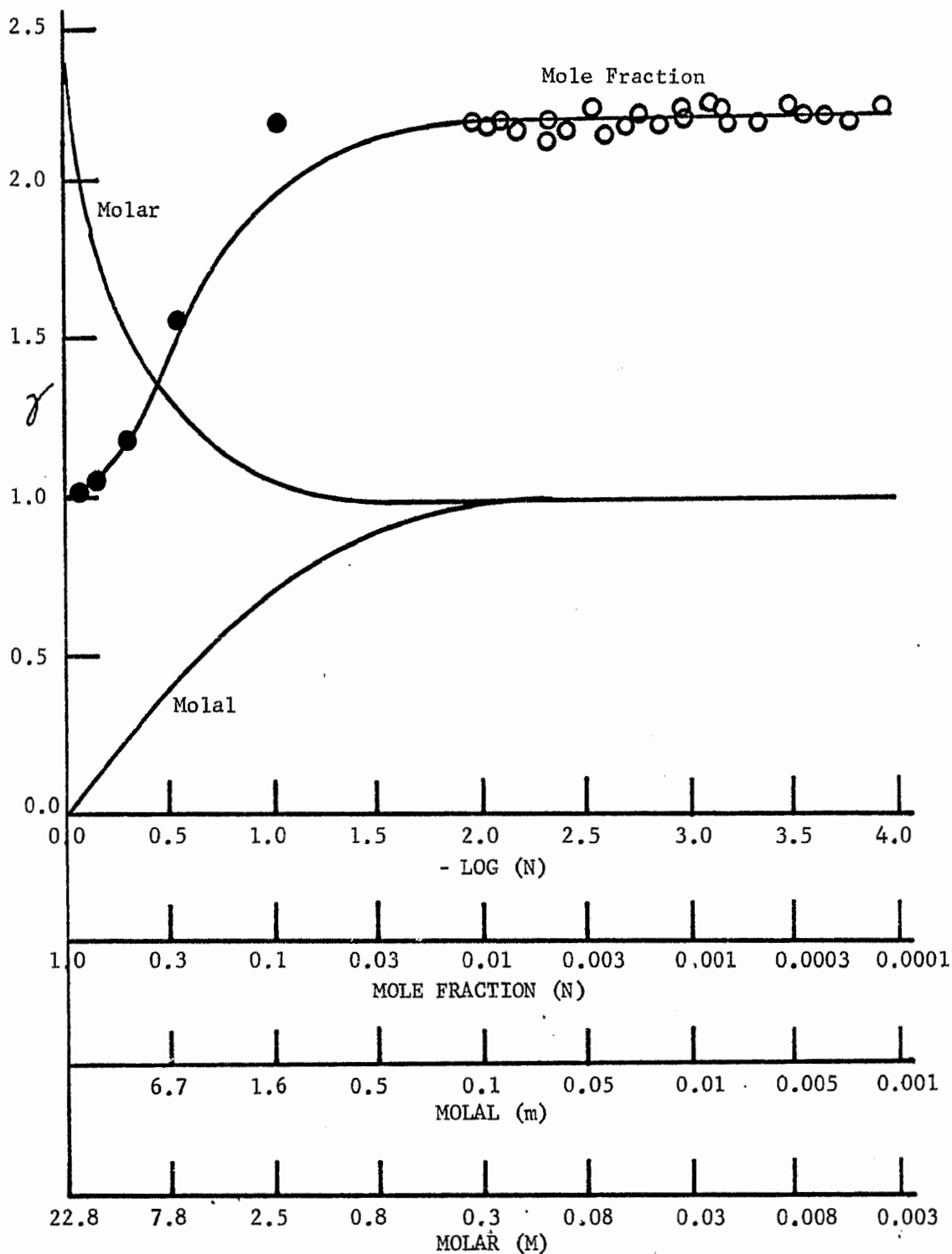


Figure 7.14 Activity Coefficient, γ , for Ag(I) in LiNO_3 at 300°C .

The γ values on the molal and molar scales were calculated from the experimental values on the mole fraction scale, \circ - this investigation, \bullet - reference (86).

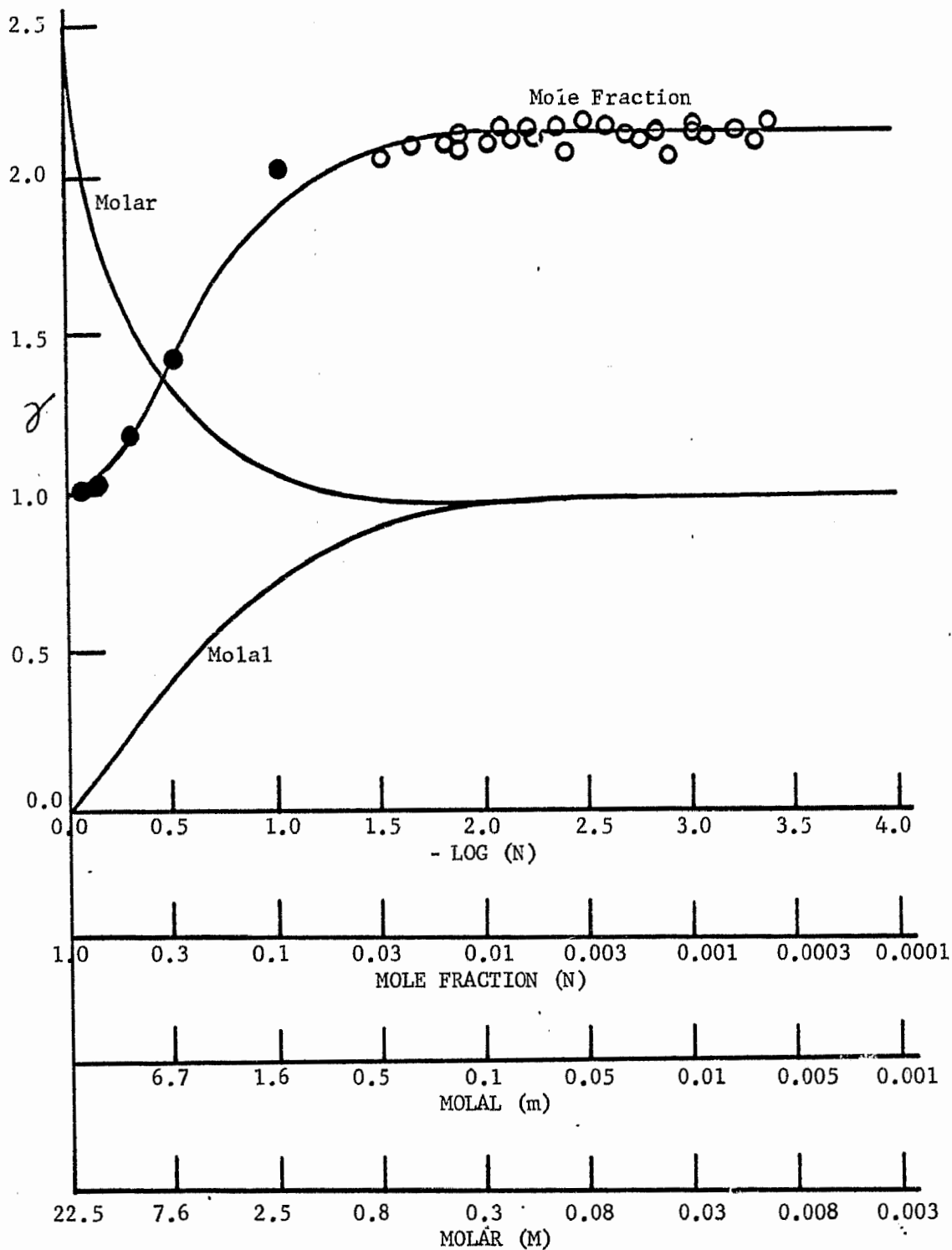


Figure 7.15 Activity Coefficient, γ , for Ag(I) in LiNO_3 at 350°C

The γ values on the molal and molar scales were calculated from the experimental values on the mole fraction scale, \circ - this investigation, \bullet - reference (86).

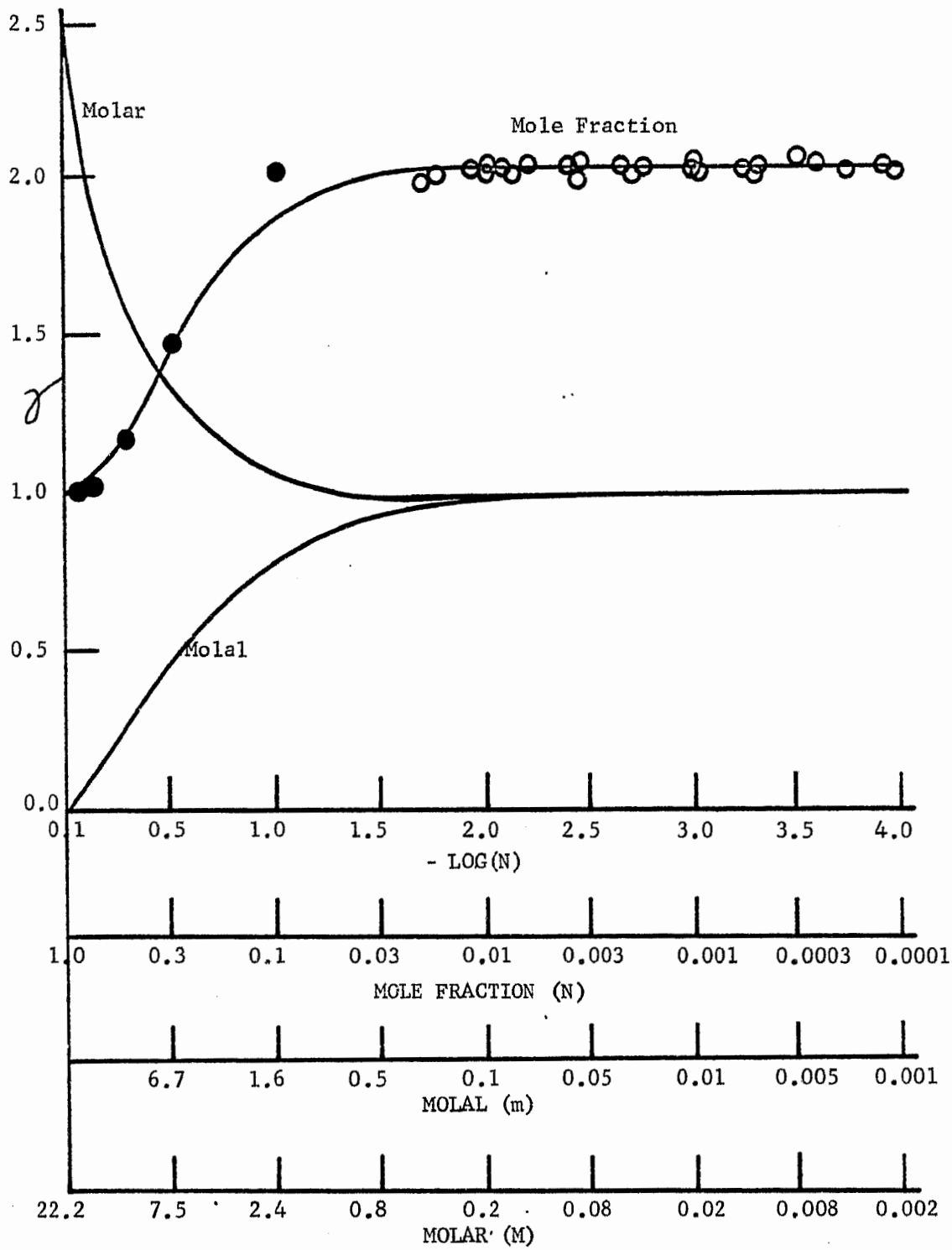


Figure 7.16

Activity Coefficient, γ , for Ag(I) in LiNO_3 at 400°C

The γ values on the molal and molar scales were calculated from the experimental values on the mole fraction scale,

○ - this investigation, ● - reference (86)

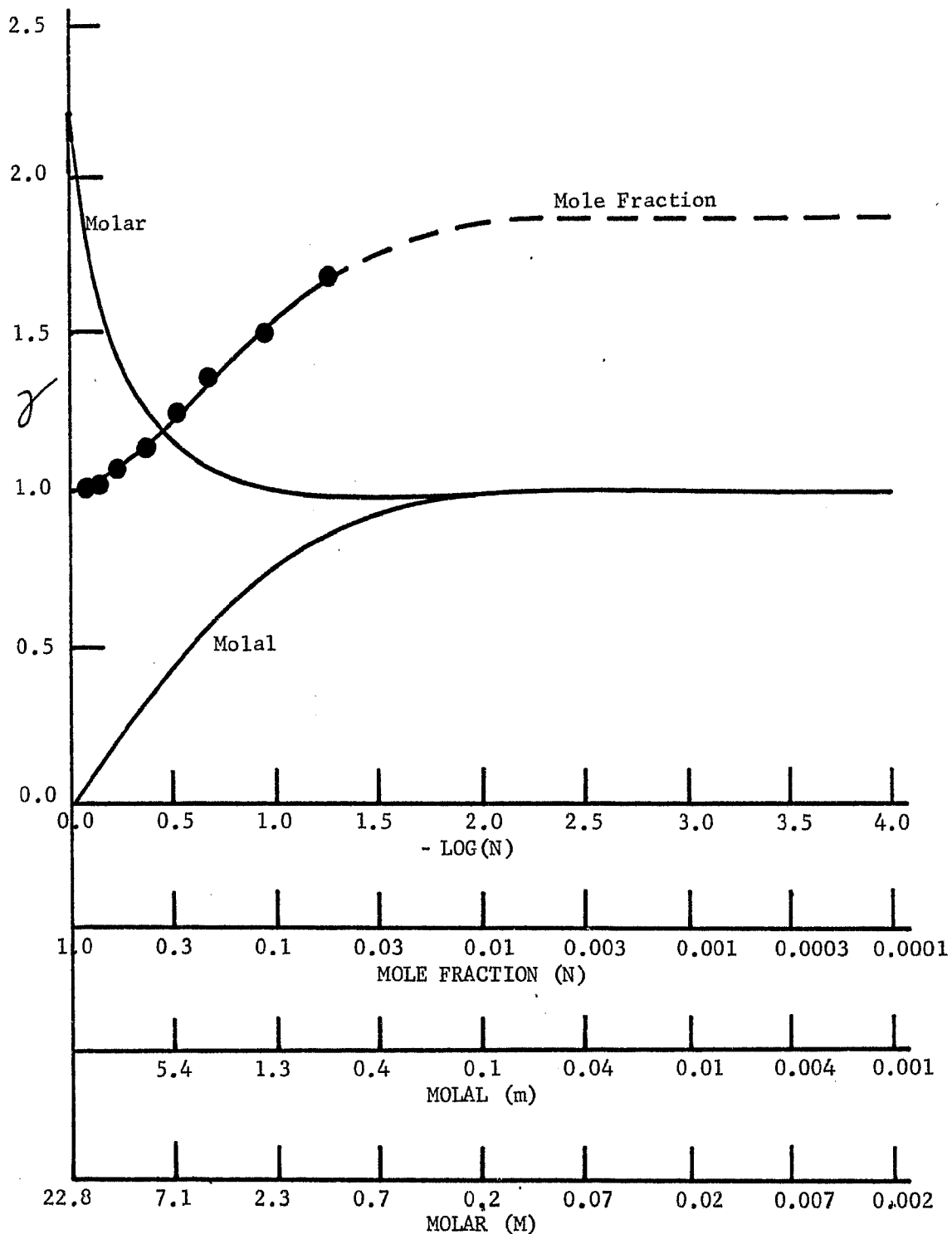


Figure 7.17 Activity Coefficient, γ , for Ag(I) in NaNO₃ at 300°C.

The γ values on the molal and molar scales were calculated from the experimental values on the mole fraction scale, -- estimated, ● - reference (56).

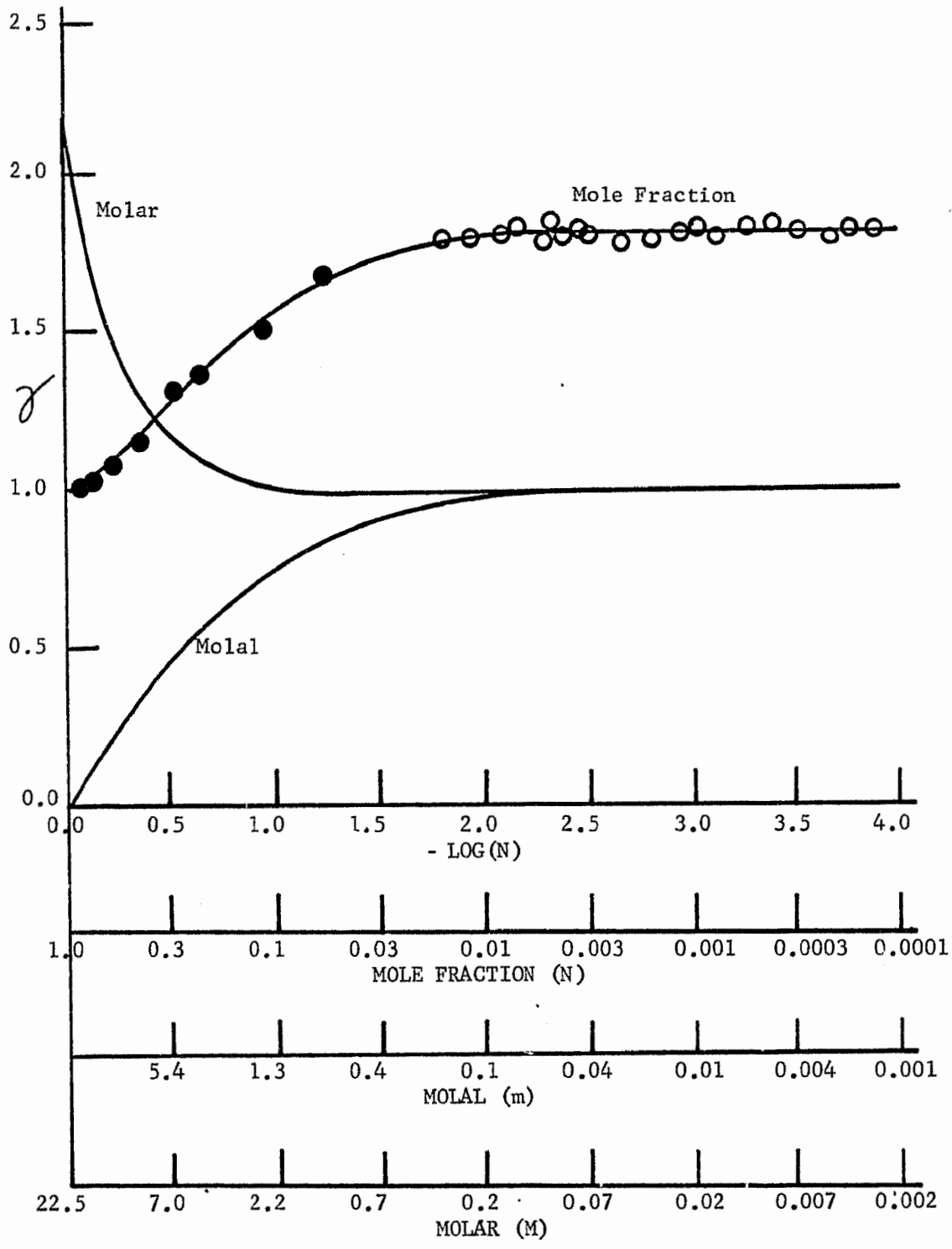


Figure 7.18 Activity Coefficient, γ , for Ag(I) in NaNO_3 at 350°C .

The γ values on the molal and molar scales were calculated from the experimental values on the mole fraction scale, \circ - this investigation, \bullet - reference (56).

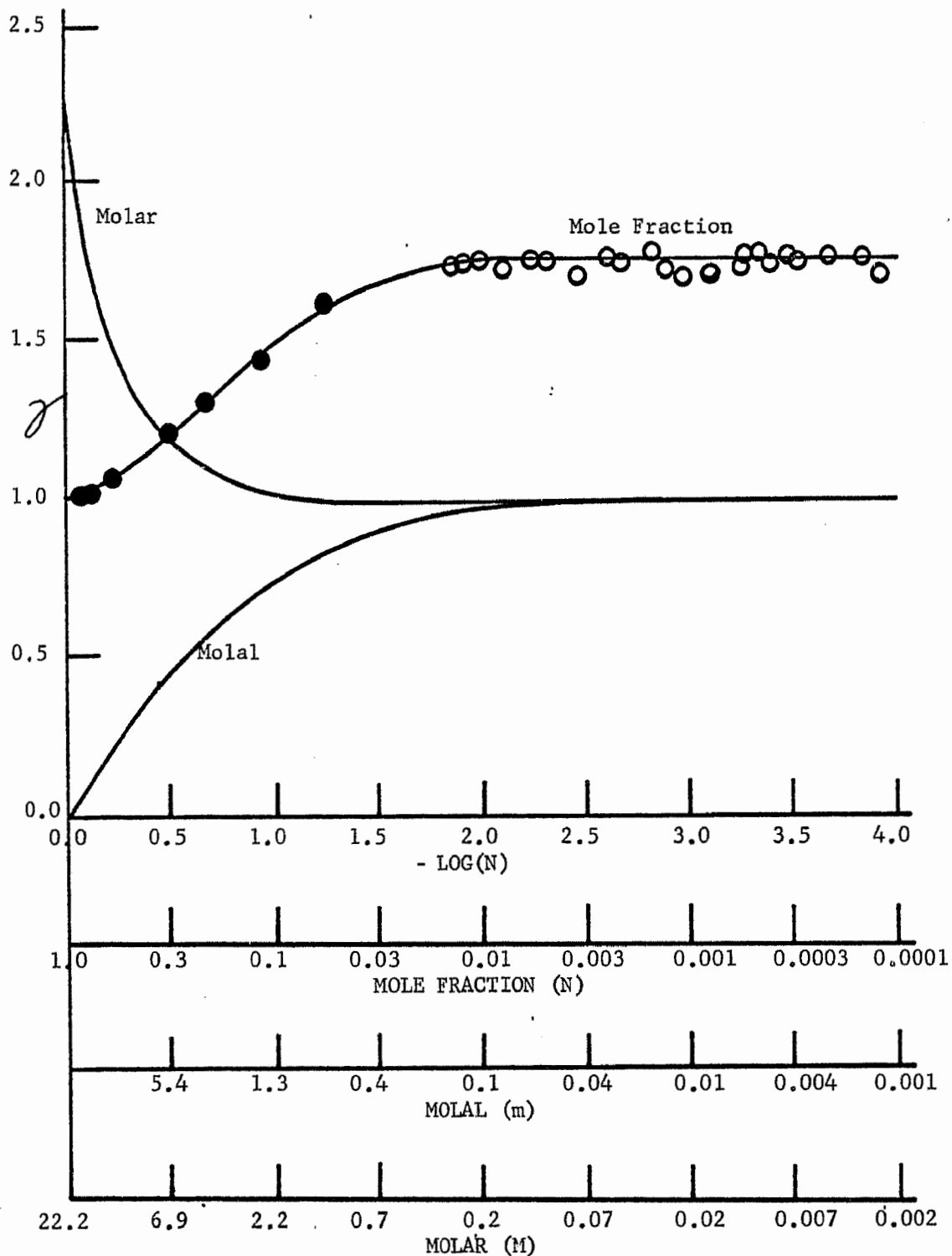


Figure 7.19 Activity Coefficient, γ , for Ag(I) in NaNO₃ at 400°C.

The γ values on the molal and molar scales were calculated from the experimental values on the mole fraction scale, \circ - this investigation, \bullet - reference (56).

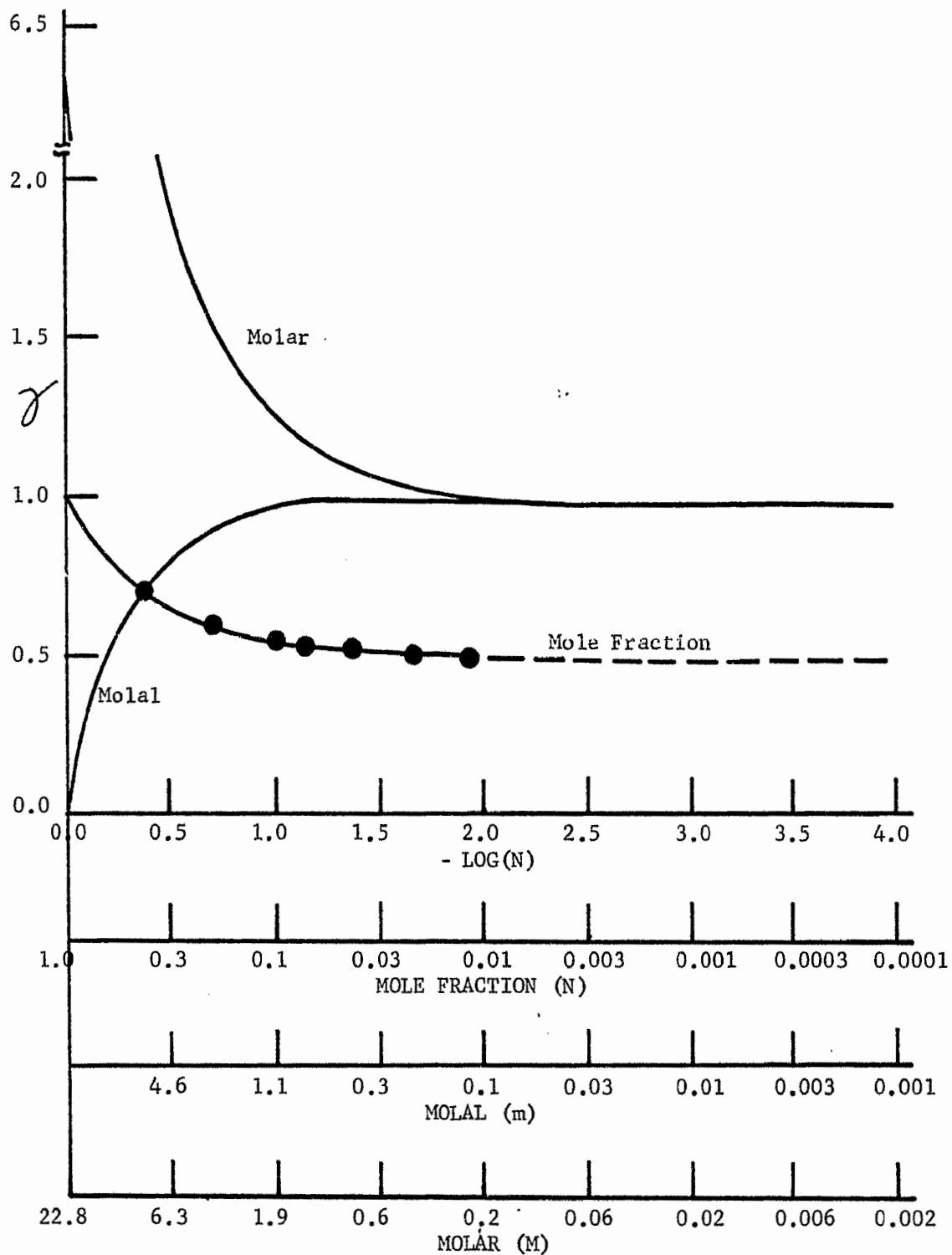


Figure 7.20 Activity Coefficient, γ , for Ag(I) in KNO₃ at 300°C.

The γ values on the molal and molar scales were calculated from the experimental values on the mole fraction scale, --- estimated, ● - reference (136).

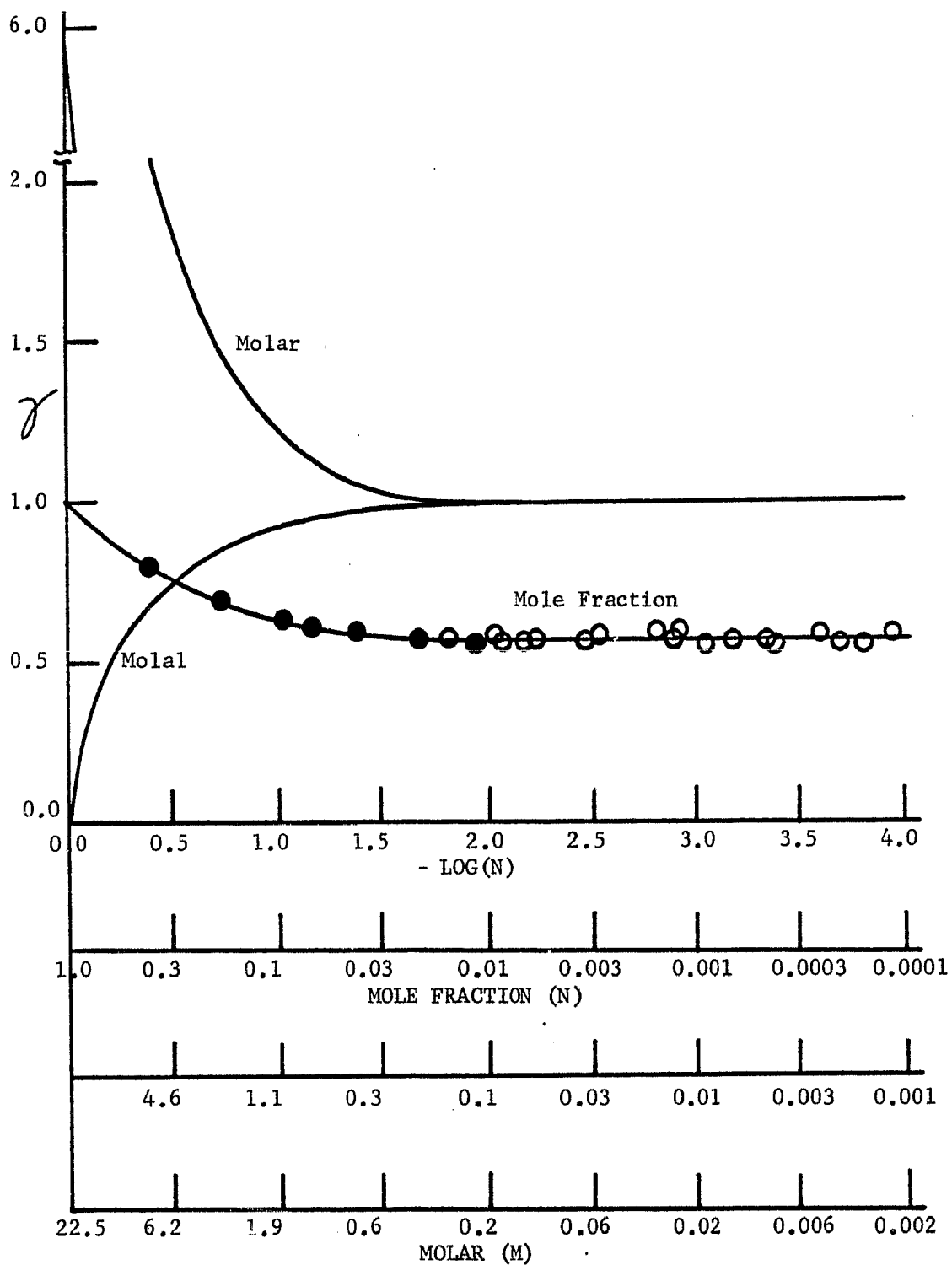


Figure 7.21 Activity Coefficient, γ , for Ag(I) in KNO_3 at 350°C .

The γ values on the molal and molar scales were calculated from the experimental values on the mole fraction scale,
 ○ - this investigation, ● - reference (136).

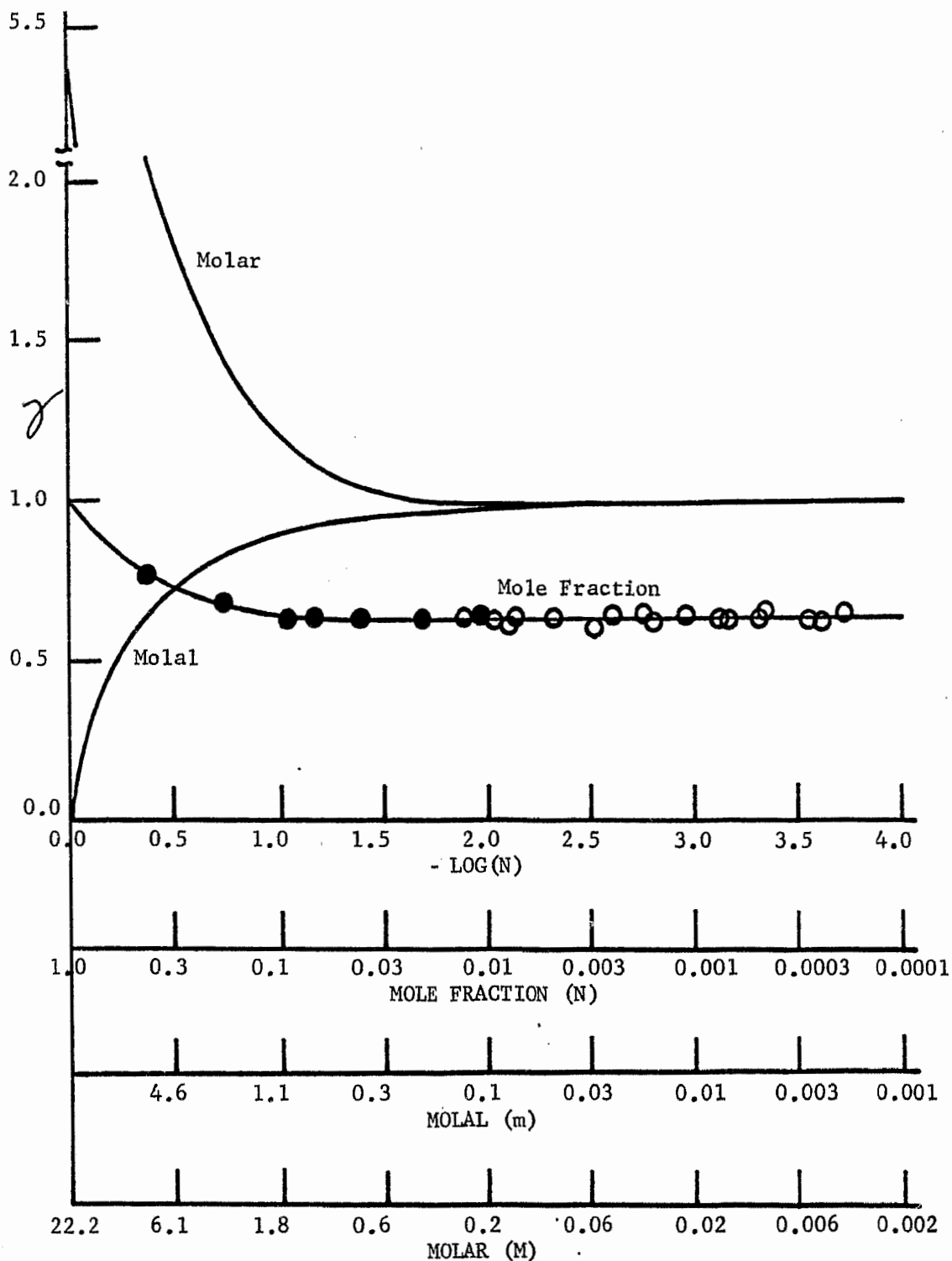


Figure 7.22 Activity Coefficient, γ , for Ag(I) in KNO_3 at 400°C .

The γ values on the molal and molar scales were calculated from the experimental values on the mole fraction scale,
 ○ - this investigation, ● - reference (136).

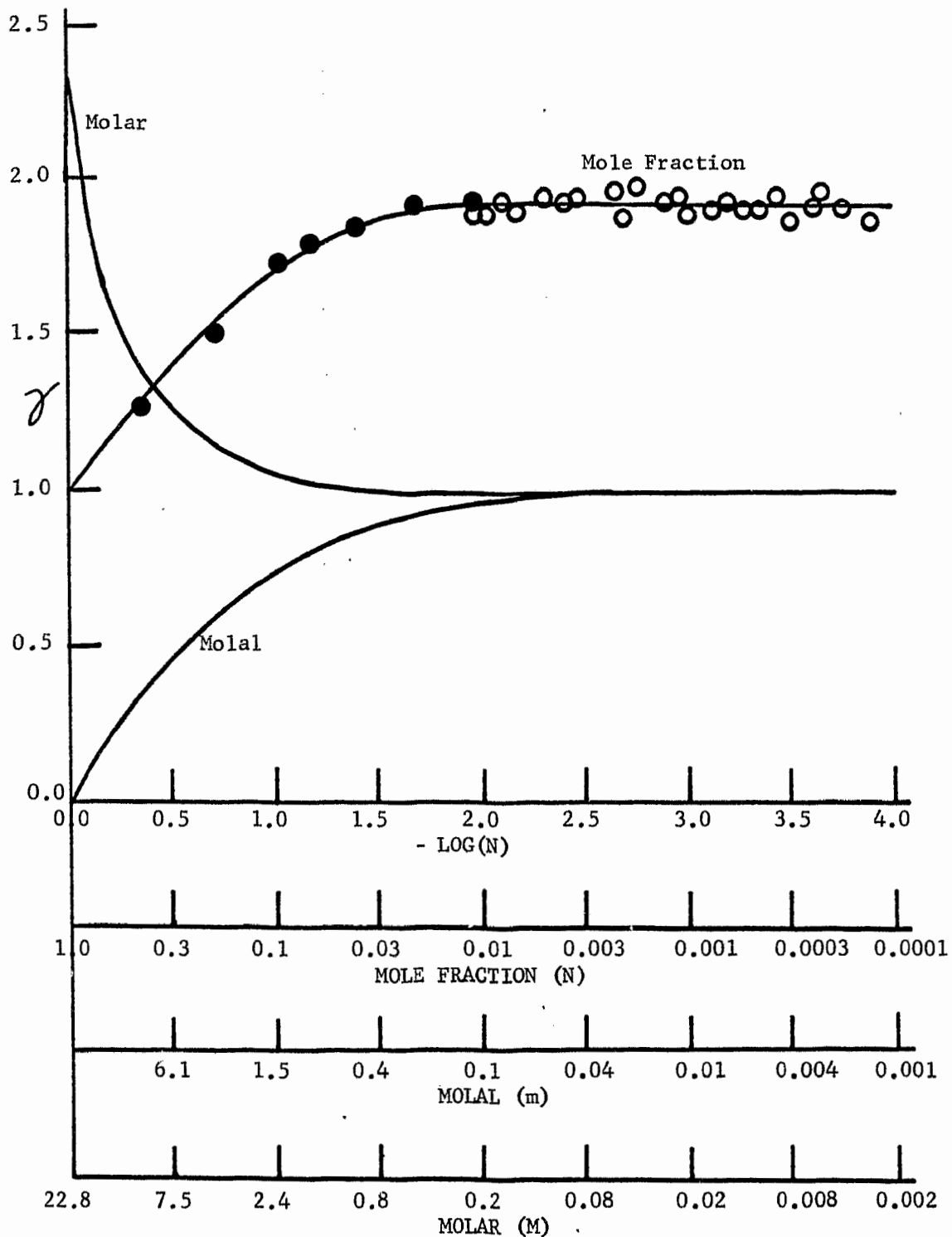


Figure 7.23 Activity Coefficient, γ , for Ag(I) in $(\text{Li,Na})\text{NO}_3$ at 300°C .

The γ values on the molal and molar scales were calculated from the experimental values on the mole fraction scale, \circ - this investigation, \bullet - reference (136).

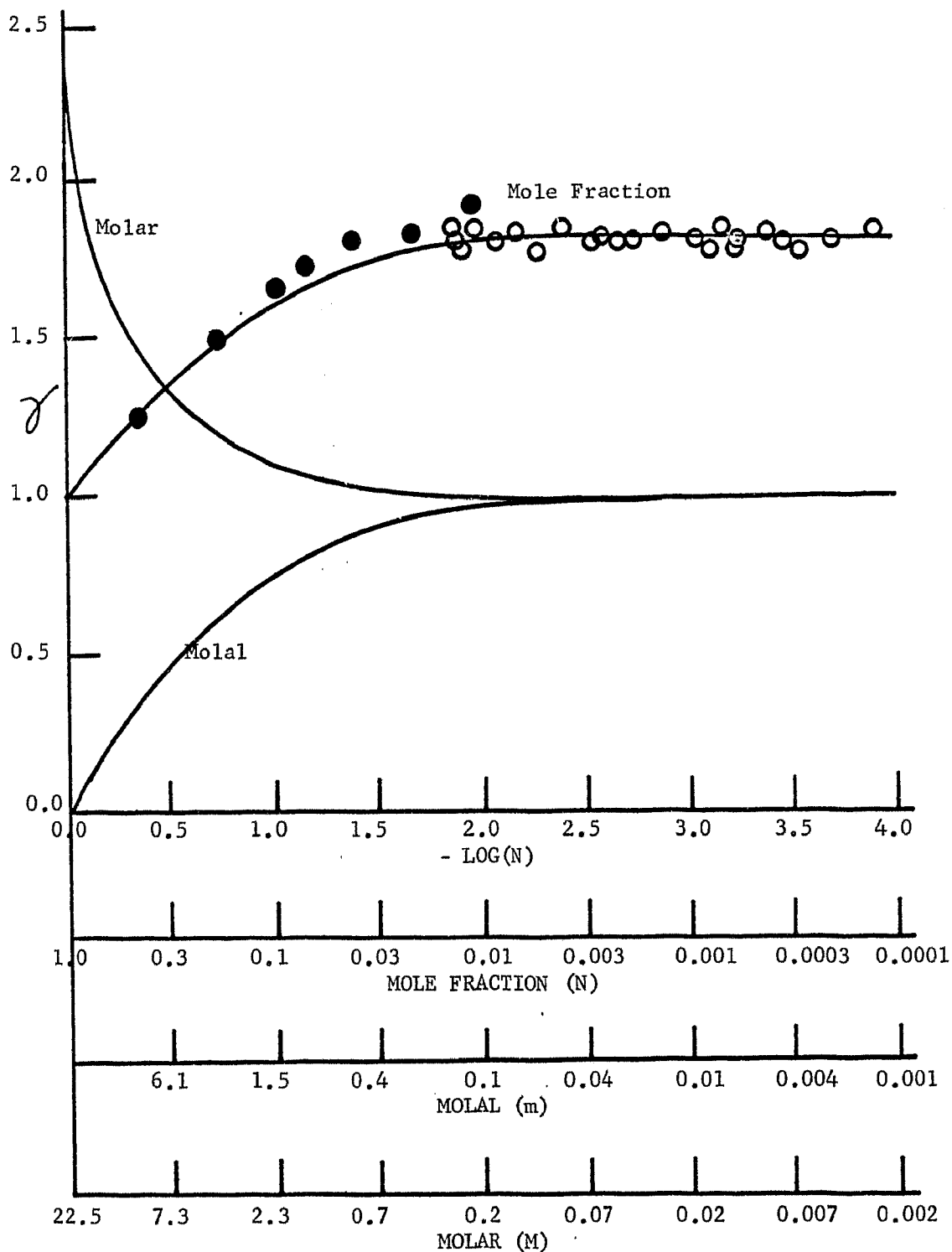


Figure 7.24 Activity Coefficient, γ , for Ag(I) in $(\text{Li,Na})\text{NO}_3$ at 350°C .

The γ values on the molal and molar scales were calculated from the experimental values on the mole fraction scale,
 ○ - this investigation, ● - reference (136).

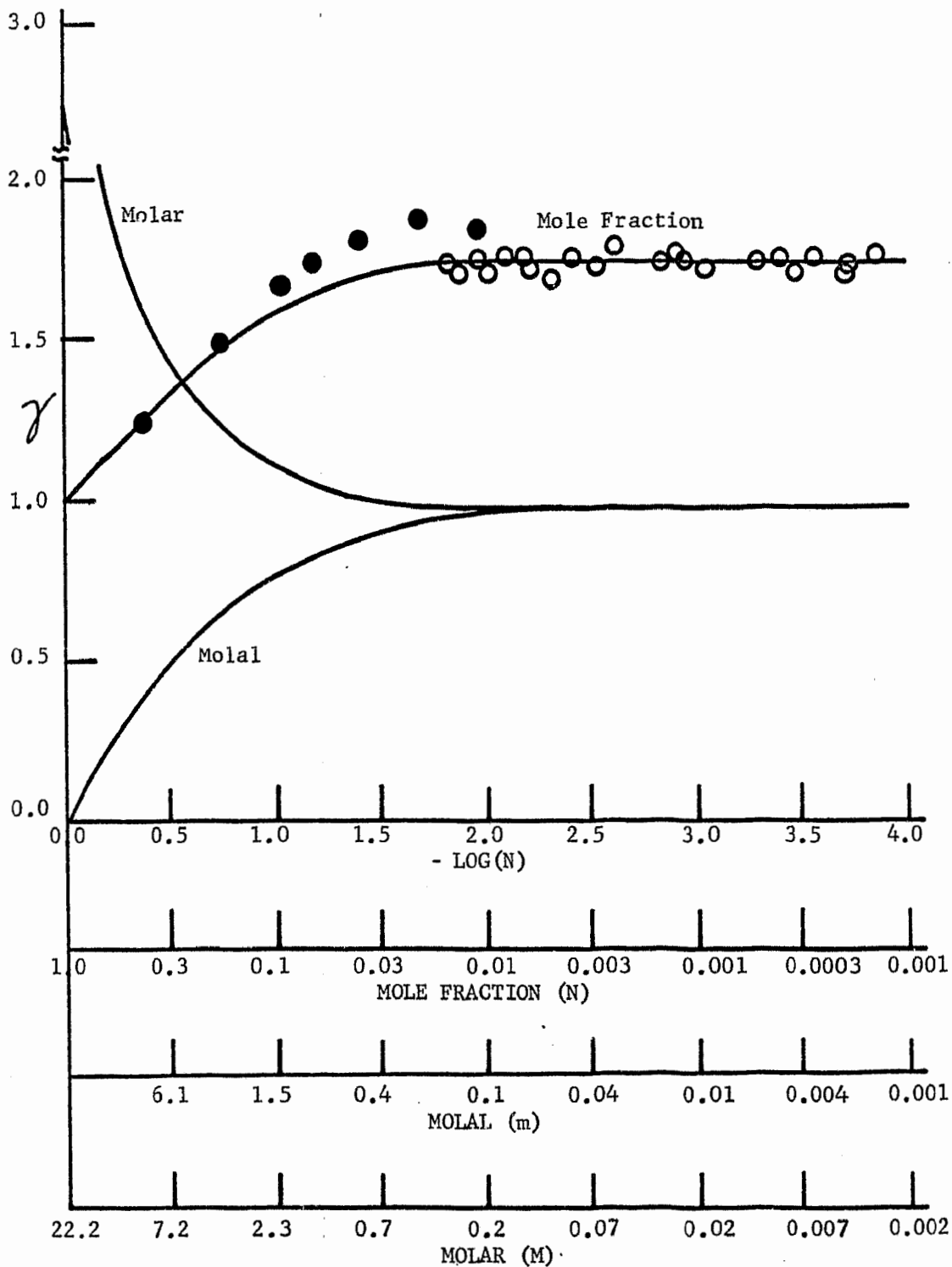


Figure 7.25 Activity Coefficient, γ , for Ag(I) in (Li,Na)NO₃ at 400°C.

The γ values on the molal and molar scales were calculated from the experimental values on the mole fraction scale,
 ○ - this investigation, ● - reference (136).

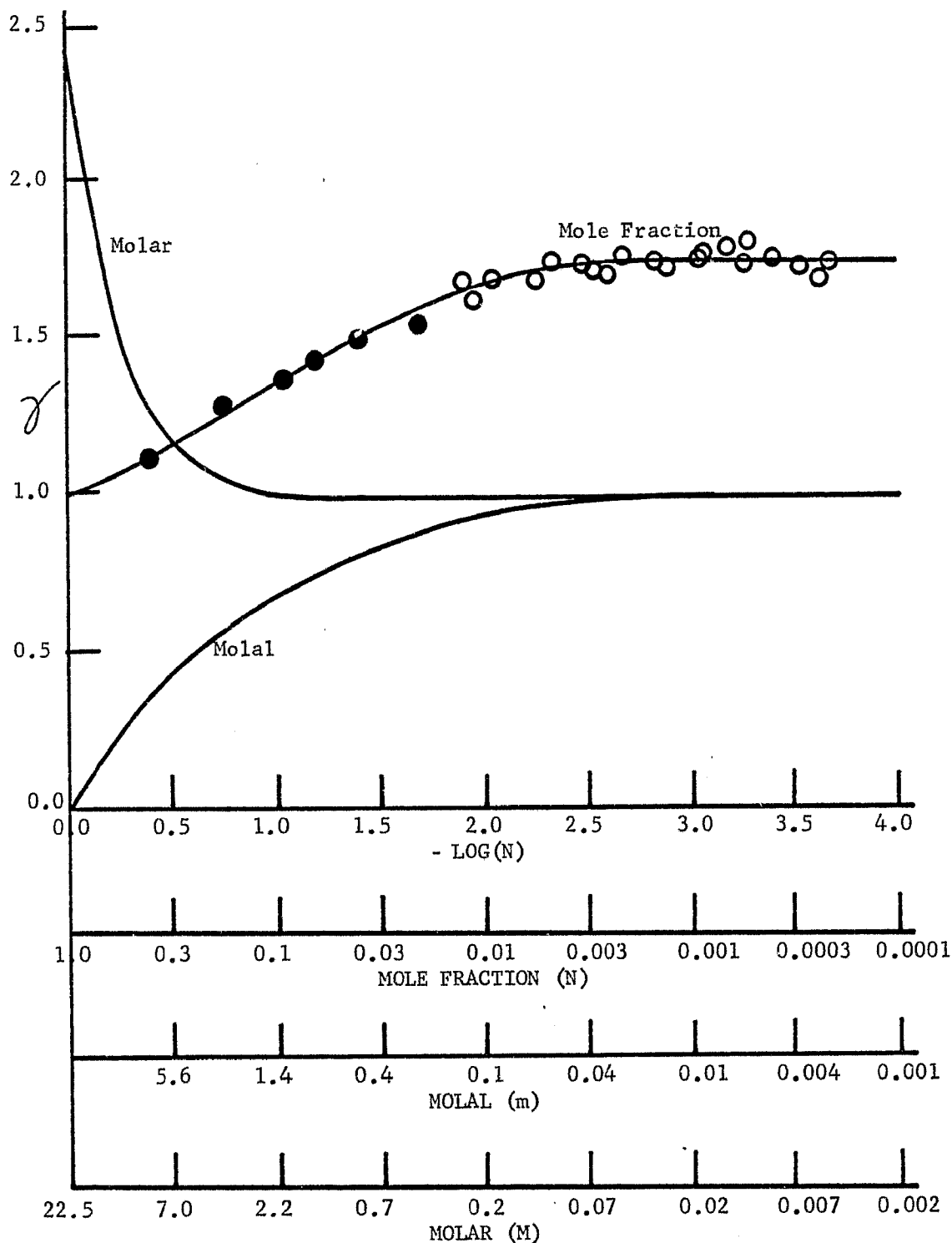


Figure 7.27 Activity Coefficient, γ , for Ag(I) in $(Li,K)NO_3$ at $350^\circ C$.

The γ values on the molal and molar scales were calculated from the experimental values on the mole fraction scale,
 ○ - this investigation, ● - reference (136).

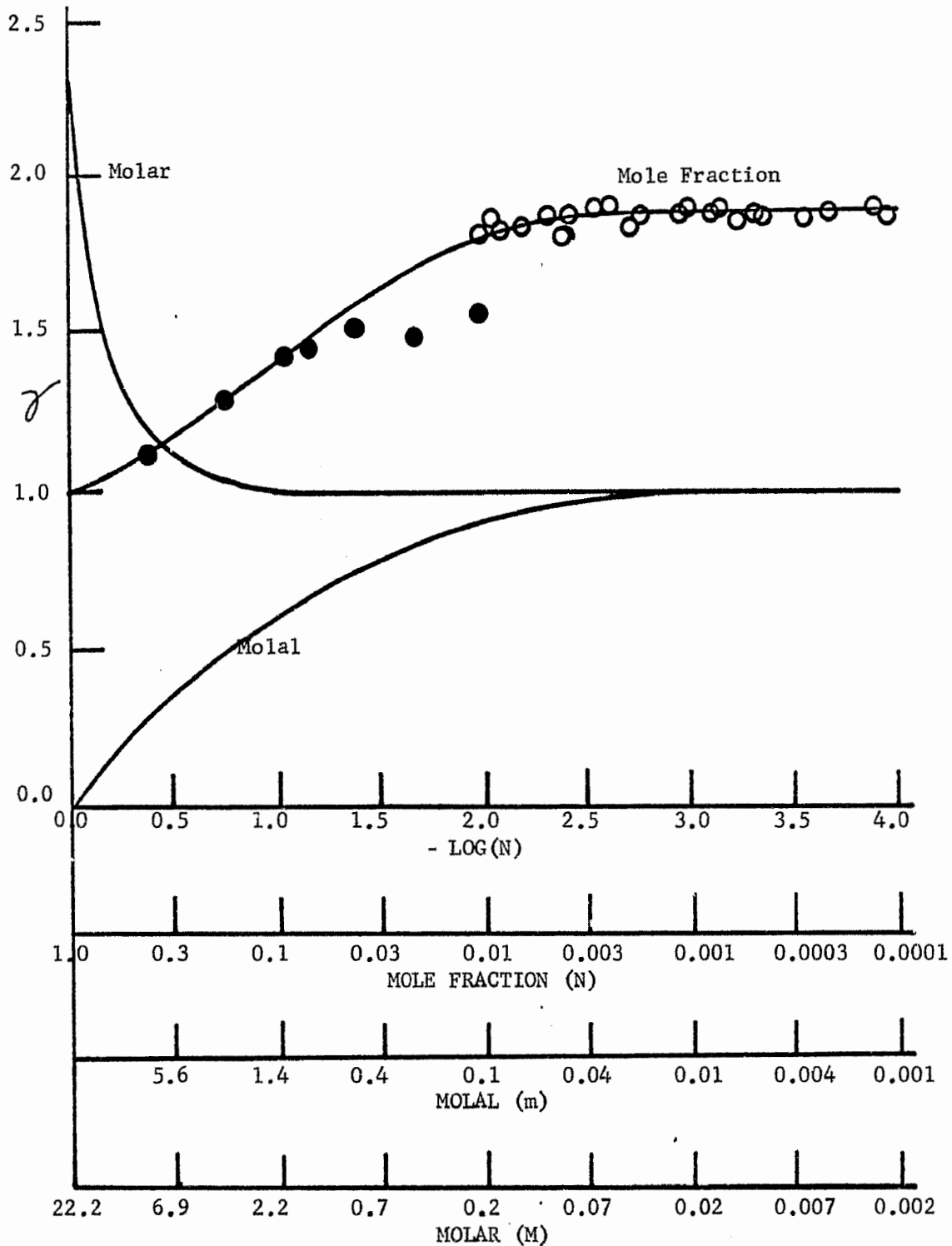


Figure 7.28 Activity Coefficient, γ , for Ag(I) in $(\text{Li,K})\text{NO}_3$ at 400°C ;

The γ values on the molal and molar scales were calculated from the experimental values on the mole fraction scale,
 ○ - this investigation, ● - reference (136).

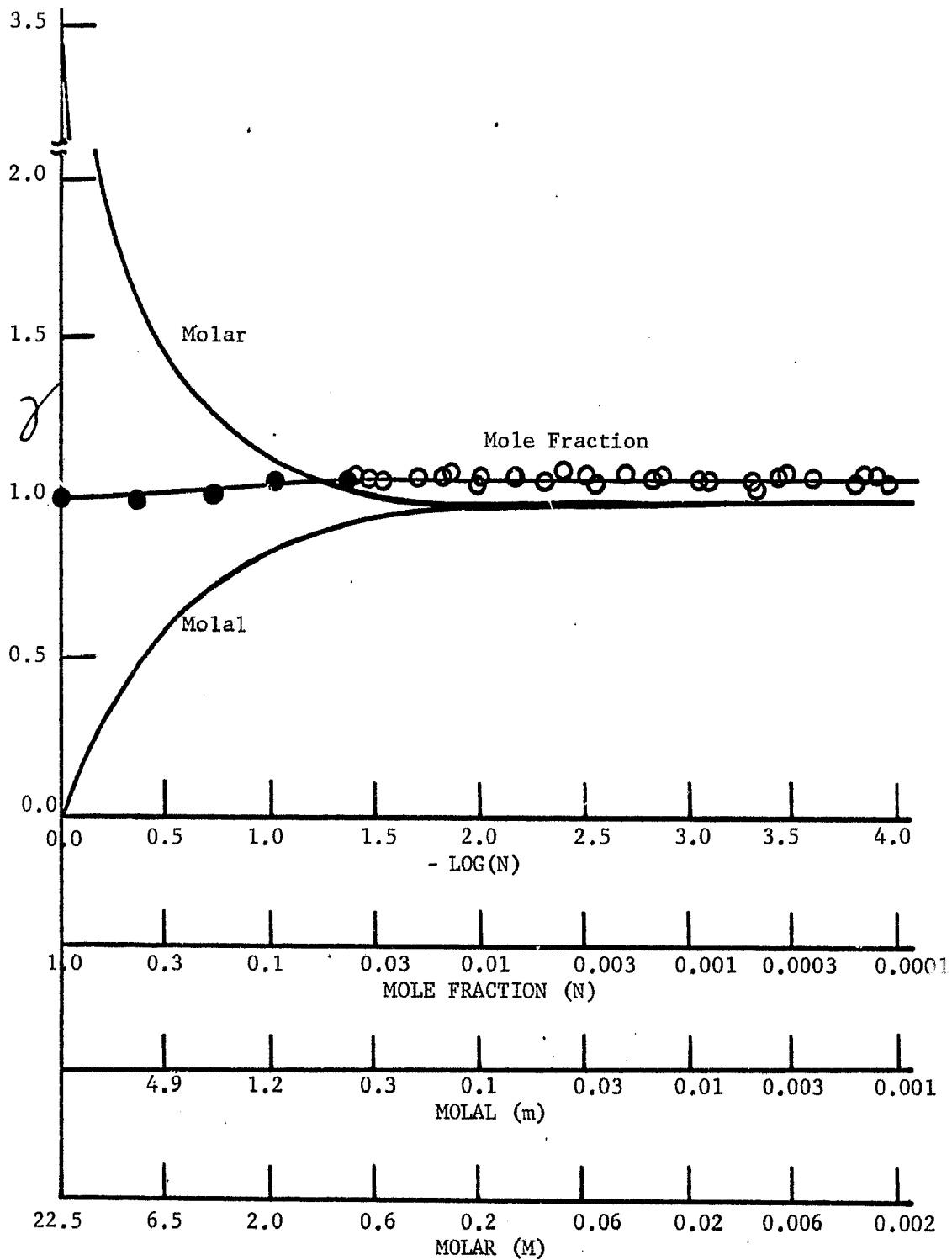


Figure 7.30 Activity Coefficient, γ , for Ag(I) in $(\text{Na,K})\text{NO}_3$ at 350°C .

The γ values on the molal and molar scales were calculated from the experimental values on the mole fraction scale,
 ○ - this investigation, ● - reference (136).

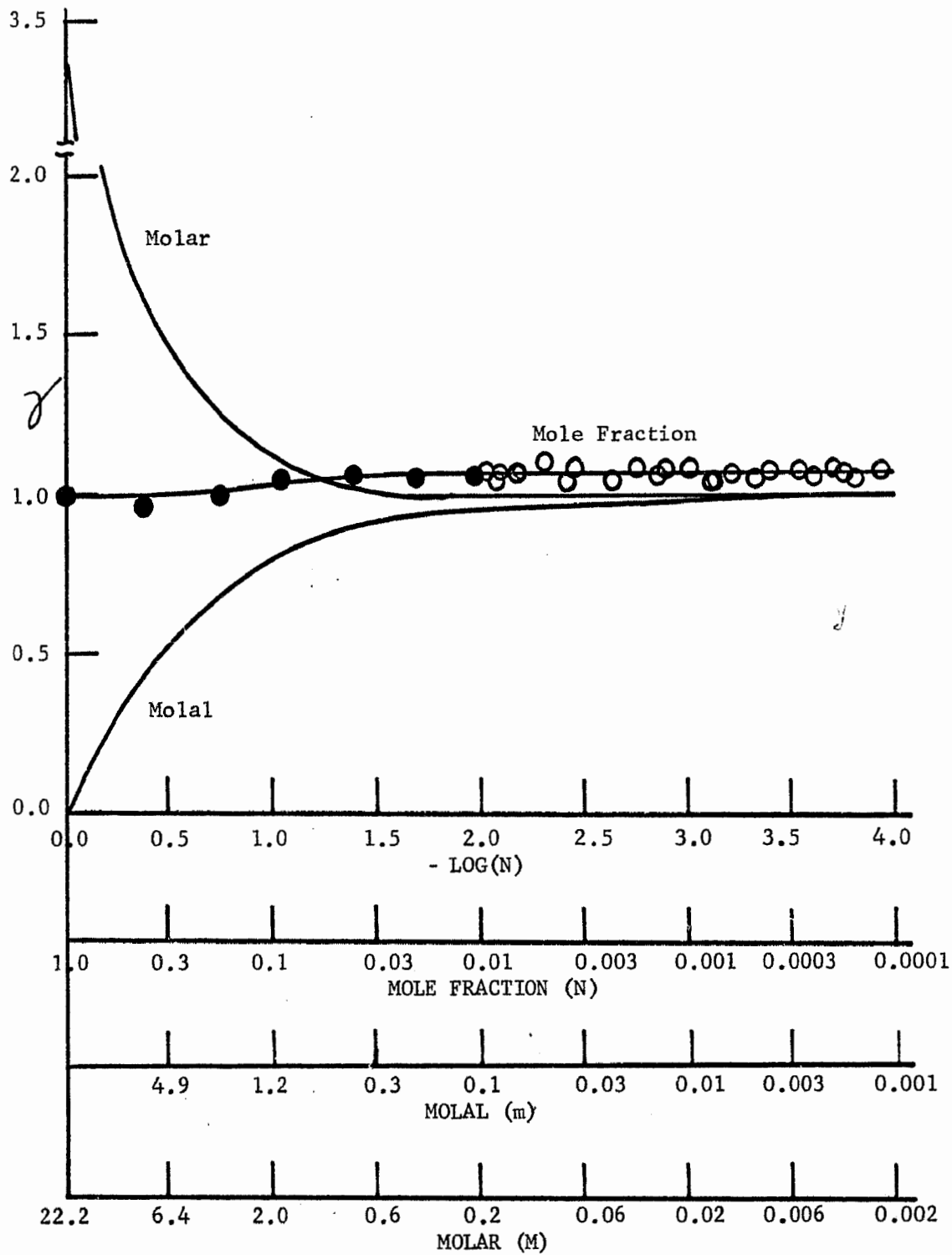


Figure 7.31 Activity Coefficient, γ , for Ag(I) in $(\text{Na,K})\text{NO}_3$ at 400°C .

The γ values on the molal and molar scales were calculated from the experimental values on the mole fraction scale,
 ○ - this investigation, ● - reference (136).

All the plots of γ_N vs. $\log(N)$ reached a limit as $N \rightarrow 0$ and these values for $\gamma_{N=0}$ are summarized in Table 7.13. The activity coefficients on the molal and molar concentration scales were calculated using equation 7.16, the $\gamma_{N=0}$ values in Table 7.13 and the data from Figures 7.14 to 7.31 and then plotted with the mole fraction activity curves in Figures 7.14 to 7.31. Since it has been shown that molar volumes are additive to $\pm 1\%$, this characteristic of the pure salts plus the density data given by Janz (2) were used to obtain the density values required in all the calculations.

TABLE 7.13
ACTIVITY COEFFICIENT, * $\gamma_{N=0}$, OF AgNO_3
ON MOLE FRACTION SCALE AT INFINITE DILUTION

Melt	Temperature $\pm 2^\circ\text{C}$	$\gamma_{N=0}$ $E_J = 0$	$\gamma_{N=0}$ $E_J \neq 0$	W^0 cal mole ⁻¹ $E_J = 0$	W cal mole ⁻¹ $E_J \neq 0$	W^{0**} cal mole ⁻¹ $E_J = 0$
LiNO_3	300	2.50	2.24	1043	919	850
	350	2.27	2.15	1015	948	850
	400	2.10	2.08	994	980	850
NaNO_3	300	(2.09)	(1.89)	(841)	(725)	840
	350	1.97	1.84	840	755	840
	400	1.86	1.78	832	772	840
KNO_3	300	(0.91)	(0.54)	(-113)	(-702)	-75
	350	0.91	0.59	-113	-653	-75
	400	0.93	0.64	-89.1	-597	-75
0.46 LiNO_3 0.54 NaNO_3	300	2.16	1.94	877	755	930
	350	1.97	1.85	838	762	930
	400	1.82	1.77	799	764	930

TABLE 7.13--Continued

Melt	Temperature $\pm 2^\circ\text{C}$	$\gamma_{N=0}^{\circ}$ $E_J = 0$	$\gamma_{N \neq 0}$ $E_J \neq 0$	W° cal mole $^{-1}$ $E_J = 0$	W cal mole $^{-1}$ $E_J \neq 0$	W^{**} cal mole $^{-1}$ $E_J = 0$
0.59 LiNO ₃	300	2.11	1.64	853	564	—
0.41 KNO ₃	350	2.14	1.77	942	707	—
	400	2.20	1.91	1057	865	—
0.45 NaNO ₃	300	1.38	1.01	367	11.3	440
0.55 KNO ₃	350	1.39	1.08	409	95.3	440
	400	1.39	1.12	440	152.	440

* Values in brackets are estimated values due to temperatures below the melting point of the solvent.

** Reference (136).

7.6 Comparison of Results with Published Results

According to the theory of regular solutions, the work constant, W , relates the activity coefficient to the mole fraction of the solute as expressed by equation 3.80 for values of $N \leq 0.5$.

$$(1 - N)^2 W = RT \ln \gamma_N \quad (7.56)$$

At infinite dilution $N = 0$, and equation 7.56 reduces to

$$W = RT \ln \gamma_{N=0} \quad (7.57)$$

The values for γ and W for the systems in which the liquid junction potential, E_J , is not assumed to be zero are related to the corresponding values γ° and W° when E_J is assumed to be zero in the following derivation.

From equation 7.48

$$\gamma_N = \exp \left[\frac{F}{RT} (E - E_J) - \ln N \right] \quad (7.58)$$

$$\gamma_N^0 = \exp \left[\frac{F}{RT} (E) - \ln N \right] \quad (7.59)$$

These two equations are combined and simplified to give the relationship between γ_N and γ_N^0 in the form of

$$\gamma_N^0 = \gamma_N \exp \left[\frac{E_J F}{RT} \right] \quad (7.60)$$

Equations 7.56 and 7.60 are combined and simplified to relate W^0 to W by the equation

$$W^0 = W + \frac{F E_J}{(1 - N)^2} \quad (7.61)$$

At infinite dilution ($N = 0$) equation 7.61 simplifies to

$$W^0 = W + E_J F = W + 23086 E_J \quad (7.62)$$

Equations 7.57, 7.60 and 7.62 were used to calculate W , W^0 and

$\gamma_{N=0}^0$ for the nitrate melts in this study and the results are

tabulated in Table 7.13 with representative values of W^0 from the literature. The experimental values of W^0 agree with the values given by Bakes et al. (136) except those of the lithium nitrate and the potassium nitrate solvent systems. Murgulescu and Marchidan (138) report a W^0 value of 1245 cal mole⁻¹ for the lithium nitrate system and Bakes and Guion (137) report a W^0 value of -150 cal mole⁻¹ for the potassium nitrate system. These values indicate that all of the experimental values of W^0 are well within the range of the W^0 values reported in the literature. The assumption by

most of the previous workers that W^0 was independent of the temperature was shown to be incorrect in this work. Ketelaar and Dammers-de Klerk (120) reported that the value of the work constant in dilute solutions of silver nitrate is given by:

$$W = a - \alpha T \quad (7.63)$$

The values for "a" and " α " can be obtained from the equations reported by Kleppa et al. (122) for the total heat of mixing, ΔH^M , and the entropy of mixing, S^E , in binary melts.

$$\Delta H^M = (a + bN_1 + cN_1N_2)N_1N_2 \quad (7.64)$$

$$S^E = \alpha N_1N_2 \quad (7.65)$$

Ketelaar and Dammers-de Klerk (120) used a reversible gaseous nitrate electrode to eliminate the liquid junction error and their values for α and W are compared with the values from this study in Table 7.14; also included are the temperature independent values of W based on the heats of mixing determined by Kleppa et al. (122).

The main difficulty with the approach used by Ketelaar and Dammers-de Klerk is the instability of the gaseous nitrate electrode since a change of ΔE in the measured emf will produce a change in W , according to the equation

$$\Delta W = \frac{23.086}{(1-N)^2} \Delta E \text{ cal mole}^{-1} \text{ mV}^{-1} \quad (7.66)$$

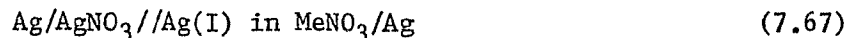
which was derived from equation 7.61. The estimation of the liquid junction potential may be a major source of error in the current investigation.

TABLE 7.14

WORK CONSTANT W (CAL MOLE⁻¹) AND COEFFICIENT α (CAL MOLE⁻¹ DEG⁻¹)
FOR BINARY NITRATE MIXTURES AT 350°C

$W = a - \alpha T$					
Melt AgNO ₃ in	α Reference (120)	α This Work	W Reference (120)	W This Work	W $\alpha = 0$ Reference (122)
LiNO ₃	-0.37 ± 0.08	-0.61 ± 0.05	933 ± 50	948	702
NaNO ₃	-0.64 ± 0.12	-0.47 ± 0.15	1076 ± 75	755	677
KNO ₃	-0.35 ± 0.15	-1.05 ± 0.10	-85 ± 94	-653	-303
0.46 LiNO ₃ 0.54 NaNO ₃		-0.09 ± 0.05		762	
0.59 LiNO ₃ 0.41 KNO ₃		-3.01 ± 0.15		707	
0.45 NaNO ₃ 0.55 KNO ₃		-1.41 ± 0.20		95.3	

Equation 7.61 combined with the fact that previous workers found W to be independent of the silver ion concentration for $N < 0.5$ indicates that $E_J F / (1 - N)^2$ should be a constant for $N < 0.5$. There is no reason why the correction for the liquid junction potential should change the behavior of the system from that of a regular solution to that of a non-regular solution (i.e., $W = f(N)$); therefore, a plot of E_J versus $(1 - N)^2$ should yield a straight line. The calculated liquid junction potentials for the cell



at 350°C where Me represents the first three alkali metal cations were plotted in Figure 7.32 as a function of $(1 - N)^2$ where N is the mole fraction of the silver(I) in the right half-cell. The three plots exhibited a linear relationship for values of $N < 0.5$ and a high degree of curvature for mole fractions of silver nitrate greater than 0.5. The curves became linear again for dilute solutions of alkali metal nitrate in silver nitrate. These results were expected since the degree of ideal behavior exhibited by each ion and its liquid junction potential is directly proportional to its concentration in the system. This evidence supports the validity of this method for estimating the liquid junction potential in highly ionized dilute melts.

The determination of the activity coefficients for several metals in halide melts has been reviewed by Blander (1) and Yang and Hudson (207). The liquid junction potential was eliminated in

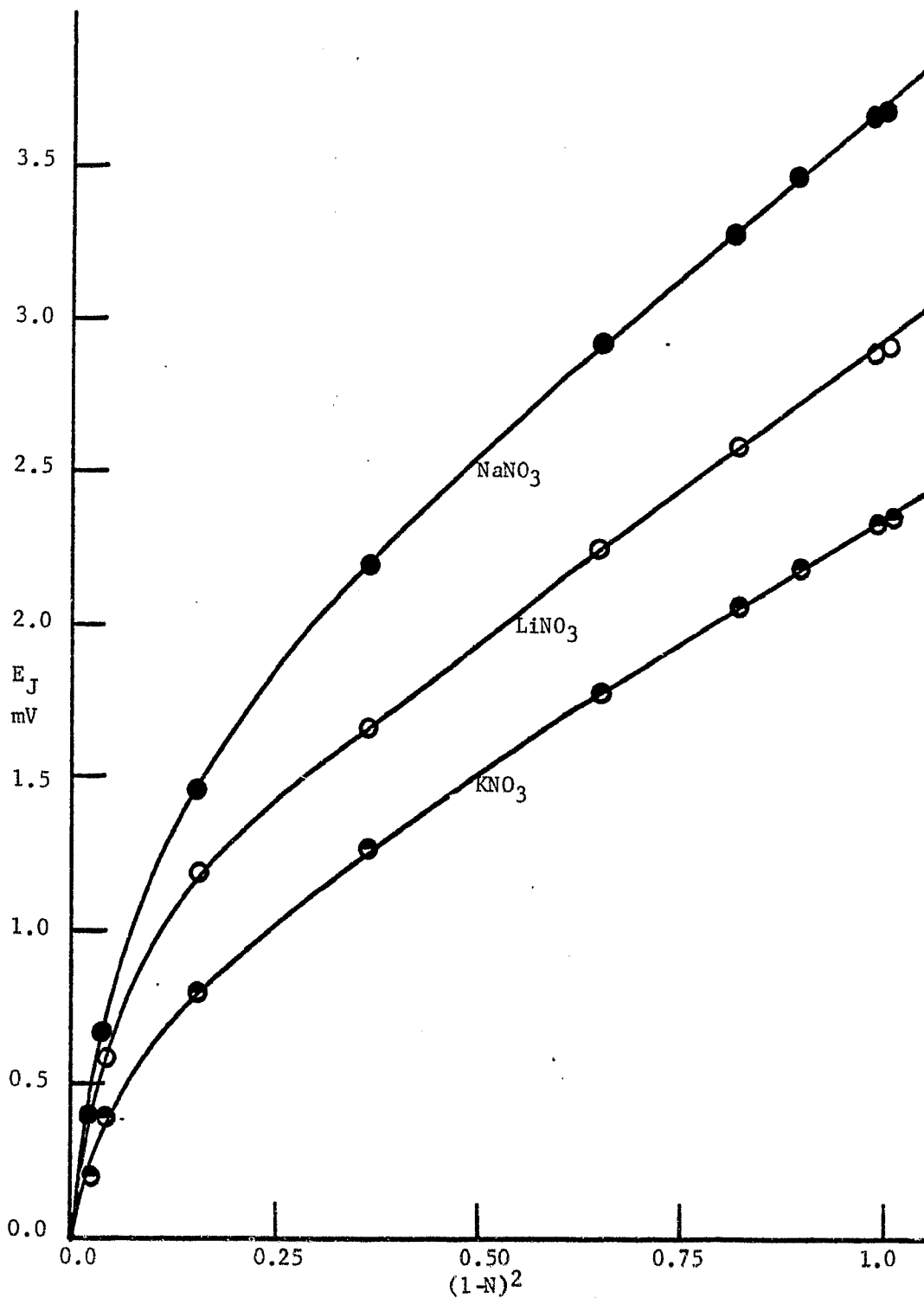


Figure 7.32 The Calculated Liquid Junction Potential, E_J , versus $(1-N)^2$ at 350°C.

N = mole fraction Ag(I) in a concentration cell of the type $\text{Ag/AgNO}_3 // \text{Ag(I) in MeNO}_3/\text{Ag}$
 For KNO_3 multiply E_J by 10.

the evaluation of the activity coefficients using the well-established halogen gas electrodes in a formation cell of the following type:



The large scatter in the published results is due to the high degree of sensitivity of γ to the measured potential and stability of the halogen gas electrodes, which are dependent upon the pretreatment of the electrode and the experimental conditions. The value for the work constant, W , for silver chloride in sodium chloride is approximately $800 \text{ cal mole}^{-1}$ which compares well with the $772 \text{ cal mole}^{-1}$ measured for silver nitrate in sodium nitrate. The value of W for silver chloride in the lithium-potassium chloride eutectic is reported by Yang and Hudson (207) to be $400 \text{ cal mole}^{-1}$ at 550°C and $415 \text{ cal mole}^{-1}$ at 400°C . The value for W in the corresponding nitrate system at 400°C is $865 \text{ cal mole}^{-1}$ which represents a change for $\gamma_{\text{N=O}}$ from 1.91 for the nitrate system to 1.76 for the chloride system or a change of 8.2%. This difference in the two values for $\gamma_{\text{N=O}}$ is equivalent to 4.8 millivolts at 400°C .

The activity coefficient, γ , is proportional to the degree of interaction between the solute ions and the solvent ions. The thermodynamic quantities involved in the system are interrelated by the equation

$$RT \ln a = RT \ln N \gamma = \Delta \bar{H}^M - T \Delta \bar{S}^M \quad (7.69)$$

where $\Delta \bar{H}^M$, the partial molar heat of mixing, is related to the

difference in the binding energies between the ions in the solution and in the pure melts. The partial molar entropy of mixing, $\Delta \bar{S}^M$, is related to the distribution of the various ions in the solution. In an ideal solution $\Delta \bar{H}^M = 0$ and $\Delta \bar{S}^M = -R \ln N$; therefore, γ is unity at all times. Systems of this nature are very rare. If $\Delta \bar{H}^M \neq 0$ and the ions of the same sign are randomly distributed in the solution, as in the Temkin model (124), then the solution is a regular solution in which $\Delta \bar{S}^M = -R \ln N$, and $RT \ln \gamma = \Delta \bar{H}^M$. It is in this type of system that calorimetric and cryoscopic measurements have been used by many workers to determine activity coefficients.

In a real system, $\Delta \bar{H}^M \neq 0$ and $\Delta \bar{S}^M \neq -R \ln N$ making it necessary to know a great deal about the nature and structure of the melt in order to accurately predict the activity coefficients for the system.

The interaction between the ions in the solution (i.e., the activity coefficient) can be interpreted qualitatively in terms of the polarizability and polarizing power of each ion. The polarizability of most of the anions is much greater than that of the cations in the solution. When two metal ions (Me_1 and Me_2) with a common anion are mixed and if the polarizing power of each is about the same, the cloud of electrons from the anion will be evenly distributed around the two metals with approximately the same electron density as in the individual pure melts. γ will be approximately unity in this case since no stable complexes were formed in the mixture as

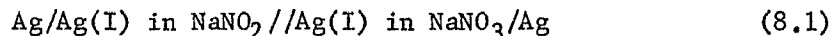
compared to individual pure melts. If Me_1 has a greater polarizing power than Me_2 , then the electron cloud from the anions will be concentrated around the Me_1 ions and may form a stable complex. The complexed Me_1 ion will be more stable in the solution than in its pure melt and it will have a γ value less than unity. The other cation, Me_2 , will be less stable in the mixture than in its pure melt and will have a γ value greater than unity. The addition of a third cation will complicate the interpretation of the system since there would be three cations competing for the electron cloud around the anions. Normally a weighted averaging effect is observed for these systems and the possibility of uneven repulsion energies between the cations may cause an uneven distribution of the different cations among themselves.

The polarizing power of an ion is determined primarily by its charge, size and electronic configuration. For a given solvent, the greater the charge and the smaller the size of the solute ion, the greater is its polarizing power and the smaller is its γ value. The stability of the complex ions decreases with an increase in temperature and the environment of the cation approaches that of the pure melt as its concentration increases in the solution. It has been well verified experimentally that the value of γ , as would be expected, approaches unity for both of these conditions. Very little work has been done on systems which contain several different cations and several different anions, but it would be expected that a similar treatment could be applied to those systems.

8. RESULTS AND DISCUSSION
MIXED SOLVENT JUNCTION POTENTIALS

8.1 Nitrite//Nitrate Solvent Junction Potential

The relationship between the emf series in nitrite and nitrate melts was determined by examining the following cell at $309 \pm 2^\circ\text{C}$:



A 0.001 to 0.05 molal silver nitrite in sodium nitrite concentration cell was set up to check the behavior and stability of the silver electrode. Analysis of the electrode compartments showed 100% current efficiency in the coulometric generation of silver(I) in the sodium nitrite melt. The Nernst plot for the concentration cell is compared to the theoretical slope in Figure 8.1. For temperatures less than 320°C and silver concentrations less than 0.015 m, the silver electrode was found to be stable and to exhibit ideal behavior. Once decomposition started the reaction became fairly rapid accompanied by the evolution of a brown gas (nitrogen dioxide) and the formation of a gray precipitate which analysis identified as silver metal. The results for the silver nitrite electrode agreed with those of Bartlett and Johnson (32).

The results for a similar check on the silver nitrate in sodium nitrate concentration cell are presented in Figure 8.2. The coulometric generation of silver(I) in sodium nitrate was found to be

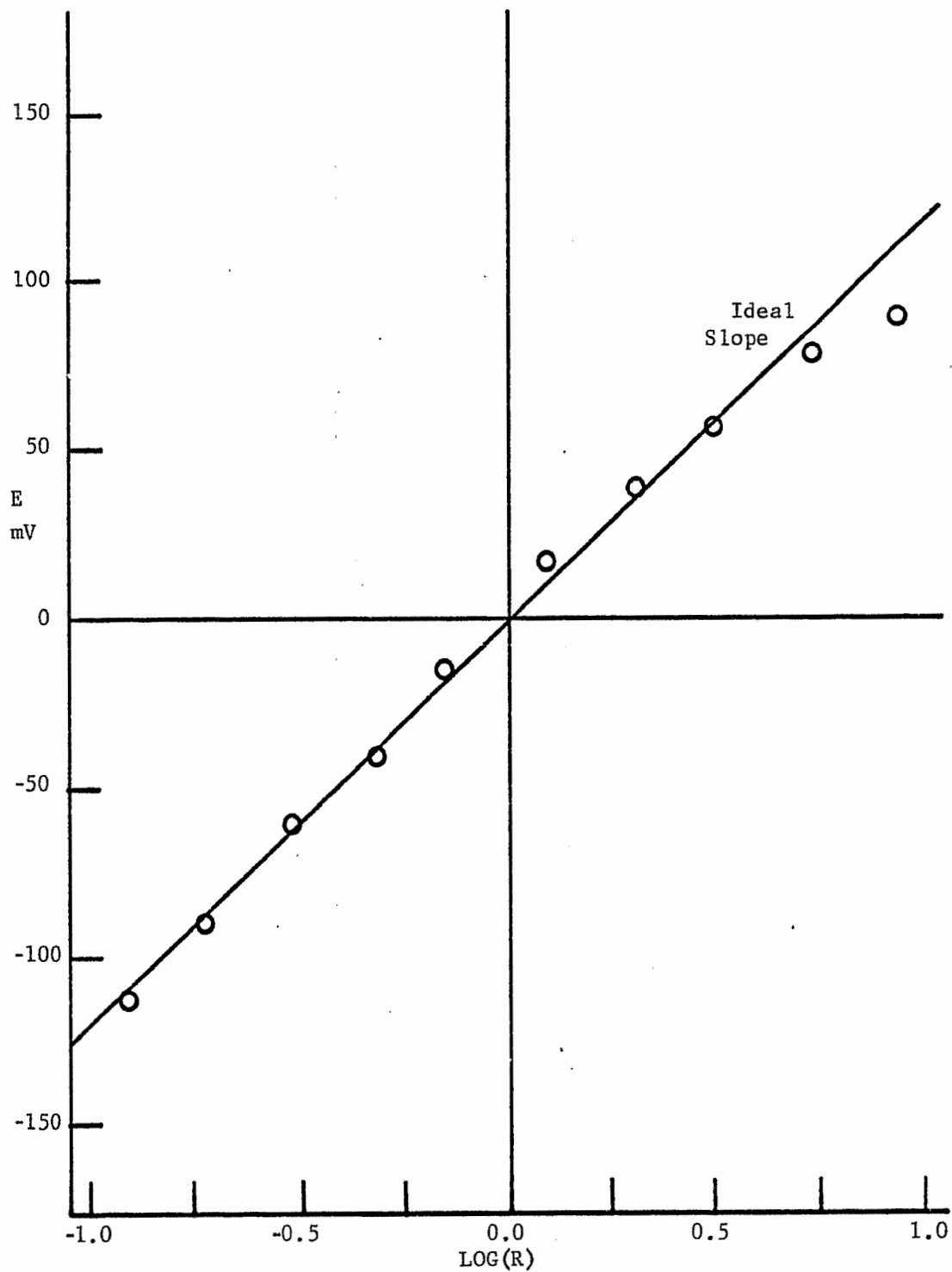


Figure 8.1 AgNO_2 in NaNO_2 Concentration Cell at $309 \pm 2^\circ\text{C}$.

$R = \frac{[\text{AgNO}_2] \text{ right half cell}}{[\text{AgNO}_2] \text{ reference half cell}}$,
 $[\text{AgNO}_2] \text{ reference} = 0.00613 \text{ molal}$.

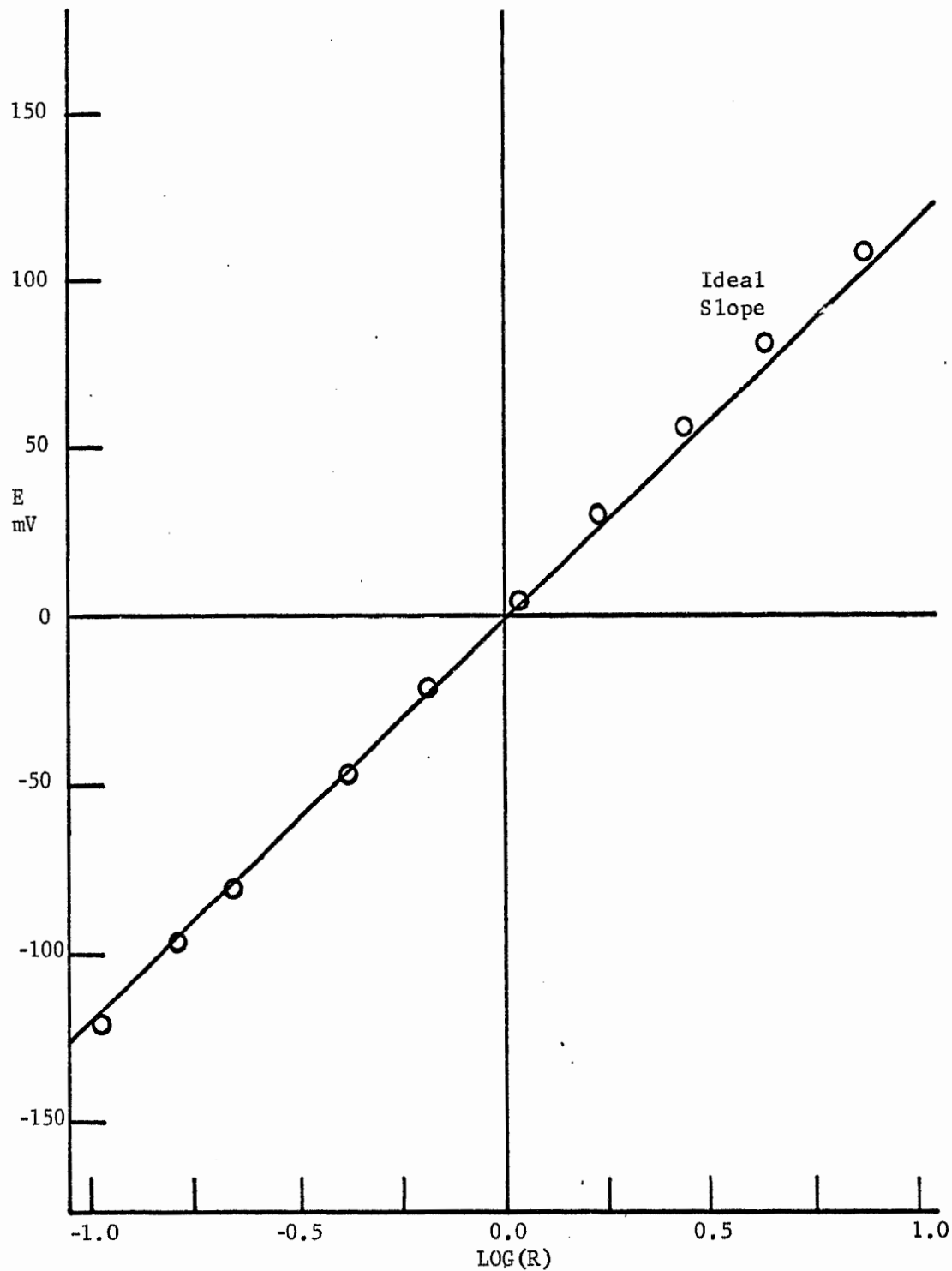


Figure 8.2 AgNO_3 in NaNO_3 Concentration Cell at $309 \pm 2^\circ\text{C}$.

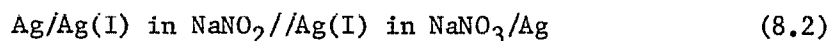
$$R = \frac{[\text{AgNO}_3] \text{ right half cell}}{[\text{AgNO}_3] \text{ reference half cell}},$$

$$[\text{AgNO}_3] \text{ reference} = 0.01719 \text{ molal}$$

100% efficient and the emf showed ideal Nernst behavior for concentrations of 0.001 to 0.15 molal at $309 \pm 2^\circ\text{C}$.

Four sintered glass frits of fine porosity were filled with sodium nitrite and placed in a sodium nitrate melt to check for diffusion through the frit. At staggered time intervals the frits were removed from the melt and analyzed for nitrite content with a standard oxidation-reduction titration technique. The loss of nitrite after four hours was 1% and after 16 hours was 4%; therefore, since an average run lasted only three to four hours, it was assumed that there was no diffusion of the nitrite through the frit.

The combined data for four trials at $309 \pm 2^\circ\text{C}$ for the cell



are tabulated in Table 8.1 and plotted in the form of a Nernst plot in Figure 8.3. All the cell potentials are given with reference to a common reference electrode of 0.030 molal silver(I) in sodium nitrate. The experimental slope of 0.1163 V compares well with the theoretical slope of 0.1155 V. The standard deviation of the data from the theoretical slope is 0.0033 V and the measured standard cell potential on the molality scale is 0.2455 V for the cell. The estimated liquid junction potential was subtracted from the measured standard potential to give the chemical standard potential for the cell before calculating the chemical standard cell potential on the molar and mole fraction scales using equations 7.21 and 7.24, respectively. The densities of the solvents were given by Janz (2) and due to the lack of data on the nitrite system, it was necessary to

assume that the activity coefficient, $\gamma_{N=0}$, for silver(I) was the same in each solvent. This assumption was warranted since the cations in both systems are the same and the nature of the anion undergoes only a minor change (cf. chapter 7.5, page 142). The final results are summarized in Table 8.2.

TABLE 8.1
 POTENTIALS FOR THE SOLVENT CELL
 Ag/Ag(I) in NaNO₂//Ag(I) in NaNO₃/Ag
 AT 309 ± 2°C

$-\log [\text{AgNO}_2]$ molal	$-\log [\text{AgNO}_3]$ molal	ΔE^* mV	E mV
2.648	1.697	20.4	373.1
2.548			361.1
2.449			349.9
2.333			336.6
2.246			326.9
2.149			315.4
2.049			304.3
1.949			292.4
3.038	1.649	14.6	421.2
2.938			410.2
2.837			399.0
2.738			388.0
2.637			376.7
2.538			365.4
2.438			353.2
2.337			340.9
2.237			329.8

TABLE 8.1--Continued

$-\log [\text{AgNO}_2]$ molal	$-\log [\text{AgNO}_3]$ molal	ΔE^* mV	E mV
2.138			318.6
2.039			306.8
1.939			294.7
1.838			283.1
1.737			271.2
1.636			259.3
1.537			247.9
2.880	1.477	-5.4	403.6
2.780			392.7
2.679			381.6
2.580			370.6
2.480			359.7
2.379			348.3
2.280			336.9
2.180			325.1
2.081			314.9
2.701	1.509	1.5	385.2
2.602			374.1
2.500			362.0
2.403			350.5
2.301			338.3
2.202			327.0
2.098			314.5
2.001			303.4

* potential added to cell value to convert to 0.030 molal AgNO_3 reference.

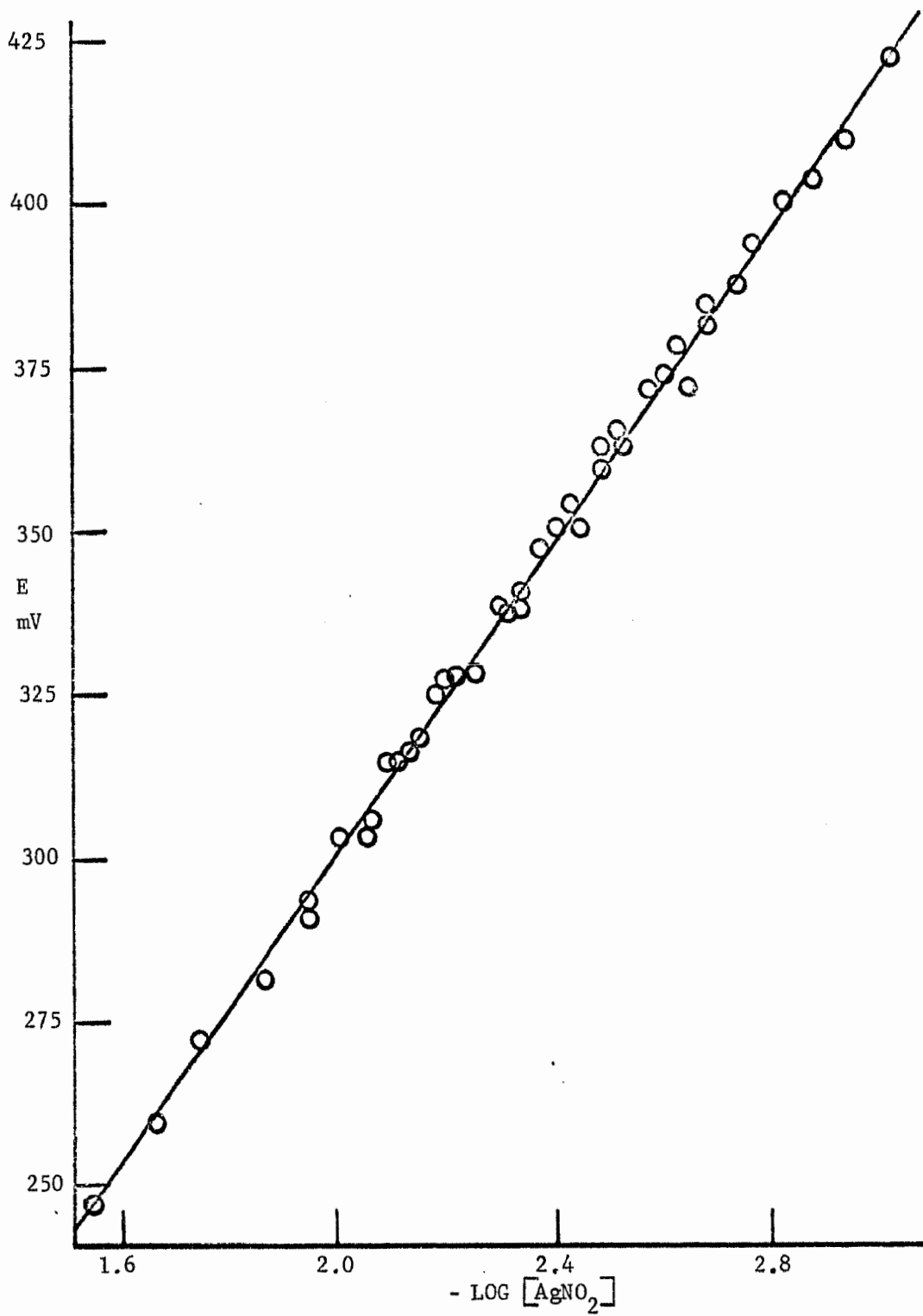


Figure 8.3 Nernst Plot at 309°C for the Solvent Cell

Ag/Ag(I) in NaNO₂//Ag(I) in NaNO₃/Ag

[AgNO₃] = 0.030 molal

TABLE 8.2

POTENTIALS AT $309 \pm 2^\circ\text{C}$ FOR THE CELL:
 $\text{Ag}/\text{Ag(I)} \text{ in } \text{NaNO}_2 // \text{Ag(I)} \text{ in } \text{NaNO}_3 / \text{Ag}$

Number of individual runs	4
Experimental slope for Nernst plot, V	0.1163
Standard deviation from theoretical slope of 0.1155, V	0.0033
E_m° (measured), V	0.2455
Calculated liquid junction potential, E_J , V	0.0160
E_m° (chemical), V	0.230 ± 0.003
E_M° (chemical), V	0.226 ± 0.003
E_N° (chemical), V	0.219 ± 0.003

The cation effect on the cell potential was studied by changing the solvent from pure sodium nitrate to an equimolar sodium-potassium nitrate mixture. The results for the different cells (A and B) at $309 \pm 2^\circ\text{C}$ are summarized in Table 8.3, and the result of the combination of the two cells, i.e., cell (A + B), is the same as the pure nitrite-nitrate experimental cell. The combined E° equals 0.238 ± 0.003 V which differs from the directly determined value by 0.008 V or 3.5%.

The standard molar chemical cell potential, 0.226 ± 0.003 V, expressed as ΔG° , the change in Gibbs free energy, is -5.22 ± 0.07 kcal mole⁻¹ for the cell reaction

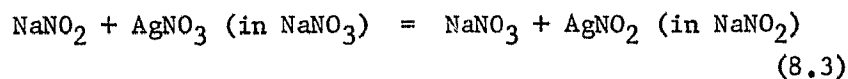
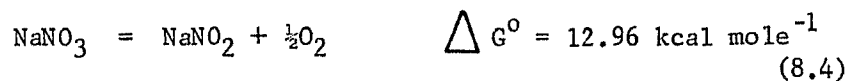


TABLE 8.3

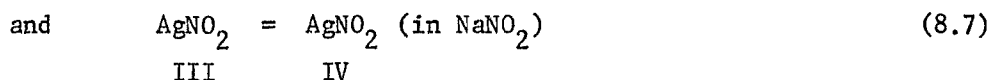
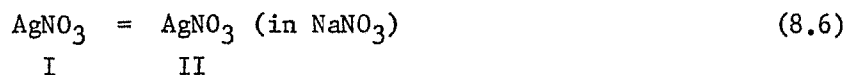
SILVER CONCENTRATION CELL WITH DIFFERENT CELL SOLVENTS AT $309 \pm 2^\circ\text{C}$.
 NaKNO_3 represents a 1:1 mole mixture of NaNO_3 - KNO_3 .

Cell	A	B	A+B
Cell solvents	$\text{NaKNO}_3//\text{NaNO}_3$	$\text{NaNO}_2//\text{NaKNO}_3$	$\text{NaNO}_2//\text{NaNO}_3$
Number of individual cells	3	3	
Experimental slope for Nernst plot, V	0.1102	0.1210	
Standard deviation from theoretical slope of 0.1155, V	0.0009	0.0018	
E_m^0 (measured), V	+0.0161	+0.2380	+0.2541
Calculated liquid junction potential, E_J , V	-0.0153	+0.0318	+0.0165
E_m^0 (chemical), V	+0.0314 \pm 0.0009	+0.2062 \pm 0.0018	+0.2376 \pm 0.0027

The following information is taken from papers by Bartlett and Johnson (74) and Triaca and Arvia (96), respectively, at a temperature of 309°C:



The former value is estimated, whereas the latter is calculated from thermodynamic tables. As no estimate for the error in these two values was given in the literature, a maximum of ± 0.1 kcal mole⁻¹ was used in the following calculations. The thermodynamic tables deal with pure salts and the electrochemical cell measures the properties of dilute solutions of the silver salts; therefore, the two additional dilution equations must be considered:



The ΔG value for reaction 8.6 is given by

$$\Delta G = RT \ln \left[\frac{\gamma_{\text{M}_{\text{II}}}^{\text{M}_{\text{II}}}}{\gamma_{\text{M}_{\text{I}}}^{\text{M}_{\text{I}}}} \right] \quad (8.8)$$

where I represents pure silver nitrate and II represents a very dilute solution of silver nitrate in sodium nitrate. The molarity, M_{I} , of pure silver nitrate is given by

$$M_{\text{I}} = \frac{1000 D}{\text{Mwt}} \quad (8.9)$$

where Mwt is the molecular weight and D is the density of the silver

nitrate at the given temperature T. The value of $\gamma_{M_{II}}$ is given by the definition

$$\gamma_{M_{II}} = 1 \quad (8.10)$$

and γ_{M_I} is given by equation 7.16 which is simplified to

$$\frac{1}{\gamma_{N=0}} = \frac{\gamma_{M_I}^D \text{Mwt}(\text{solvent})}{D(\text{solvent})^{\text{Mwt}}} \quad (8.11)$$

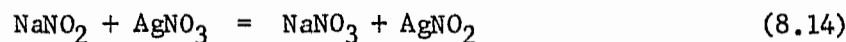
when I is pure silver nitrate. Equations 8.9 and 8.11 are substituted into 8.8 to give

$$\Delta G_{(8.6)} = RT \ln \left[\frac{M_{II} \gamma_{N=0} (\text{in NaNO}_3)^{\text{Mwt}(\text{NaNO}_3)}}{1000 D(\text{NaNO}_3)} \right] \quad (8.12)$$

and by a similar argument the ΔG for reaction 8.7 is given by

$$\Delta G_{(8.7)} = RT \ln \left[\frac{M_{IV} \gamma_{N=0} (\text{in NaNO}_2)^{\text{Mwt}(\text{NaNO}_2)}}{1000 D(\text{NaNO}_2)} \right] \quad (8.13)$$

The combination of reactions (8.3) + (8.6) - (8.7) gives the reaction



and a ΔG° value of

$$\Delta G_{(8.14)}^\circ = \Delta G_{(8.3)}^\circ + \Delta G_{(8.6)} - \Delta G_{(8.7)} \quad (8.15)$$

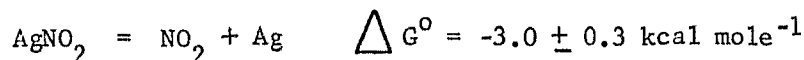
$$\Delta G_{(8.14)}^\circ = \Delta G_{(8.3)}^\circ + RT \ln \left[\frac{\gamma_{N=0} (\text{in NaNO}_3)^{\text{Mwt}(\text{NaNO}_3)} D(\text{NaNO}_2^-)}{\gamma_{N=0} (\text{in NaNO}_2)^{\text{Mwt}(\text{NaNO}_2)} D(\text{NaNO}_3^-)} \right] \quad (8.16)$$

where $M_{II} = M_{IV}$ since $\Delta G_{(8.3)}^{\circ}$ is used to represent the observed free energy change in reaction 8.3. By combining the two equations (7.21 and 7.24) used to interrelate the standard cell potentials with equation 8.15 it can be shown that

$$\Delta G_{(8.14)}^{\circ} = -n F E_N^{\circ} \quad (8.17)$$

where E_N° is the standard chemical cell potential on the mole fraction scale. Therefore, $\Delta G_{(8.14)}^{\circ}$ is -5.05 ± 0.07 kcal mole⁻¹ at $309 \pm 2^{\circ}\text{C}$.

Using equations 8.4 and 8.5 in conjunction with the equation for the experimental nitrite-nitrate cell (8.14), ΔG° can be estimated for the decomposition of silver nitrite at 309°C



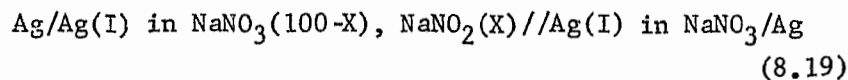
Since the cell temperature was approximately 170°C above the listed decomposition temperature, a small negative value was anticipated. Unfortunately, there were no data available in the literature with which to compare the new value for the decomposition of silver nitrite.

No attempt was made to determine the temperature dependence of the nitrite-nitrate cell emf since the temperature range from the melting point of sodium nitrate (302°C) to the upper limit of the silver nitrite/silver electrode (approximately 320°C) was very limited. The lower temperature limit could have been decreased to 220°C by replacing the sodium nitrate with the sodium-potassium nitrate eutectic; however, this would have introduced a change in

cations across the solvent junction and invalidated the assumption that $\gamma_{N=0}$ for dilute solutions of silver(I) is the same in both melts, thereby preventing any thermodynamic calculations.

8.2 Nitrite-Nitrate/Nitrate Solvent Junction Potential

A series of cells were examined in which the solvent was pure sodium nitrate in one electrode compartment and a mixture of sodium nitrate and sodium nitrite in the other. The standard potentials at $309 \pm 2^\circ\text{C}$ based on the molality scale for the cell



are summarized in Table 8.4 where X is the mole percent of sodium nitrite in the working electrode compartment. The results are plotted in Figure 8.4 in two forms: line 1 was potential versus mole percent sodium nitrite and line 2 was potential versus $\log(\text{mole percent sodium nitrite})$. The solid points represent experimental points and the open points in line 2 were obtained by interpolation of the data on line 1. The portion of line 2 between 10 and 80 mole percent of sodium nitrite was fitted to a least squares straight line with a standard deviation of ± 0.003 volts.

$$E_m^0 = +0.119 - 0.170 \log(X) \quad 10 \leq X \leq 80 \quad (8.20)$$

It is interesting to note that the slope 0.170 has the same value as $2.303 RT/\beta F$ at 309°C with $\beta = 2/3$. That β is the same simple ratio as that of the oxygen atoms in nitrite to nitrate may be merely a fortuitous coincidence or it may indicate some

TABLE 8.4

STANDARD POTENTIALS AT $309 \pm 2^\circ\text{C}$ FOR THE CELL:Ag/Ag(I) in $\text{NaNO}_3(100-X)$, $\text{NaNO}_2(X)$ //Ag(I)(0.030 m) in NaNO_3/Ag X is the mole percent NaNO_2 in the left half cell.

Mole percent (X)	0	10	25	50	73	100
Number of individual cells	1	3	3	3	2	4
Experimental slope for Nernst plot, V	0.1160	0.1256	0.1224	0.1113	0.1140	0.116
Standard deviation from theoretical slope of 0.1155, V	0.0001	0.0023	0.0026	0.0011	0.0008	0.0033
E_m^0 (measured), V	0.0000	0.0550	0.1229	0.1739	0.2067	0.2455
Calculated liquid junction potential, E_J , V	0.0000	0.0017	0.0042	0.0086	0.0117	0.0160
E_m^0 (chemical), V	0.0000	0.0533	0.1187	0.1653	0.1950	0.2295

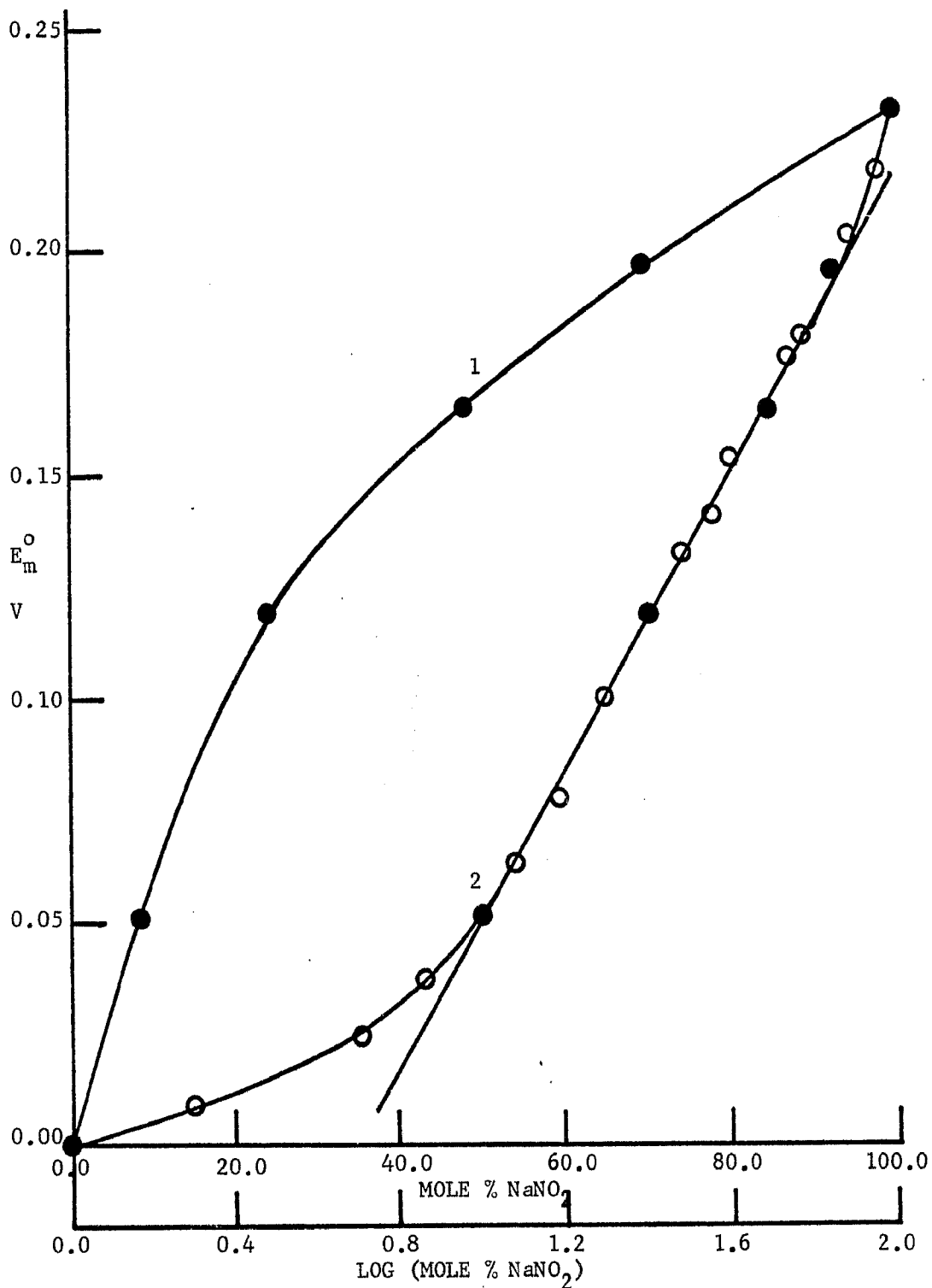


Figure 8.4 Standard Potential at 309°C for the Solvent Cell:
 $\text{Ag}/\text{Ag}(\text{I})$ in $(N)\text{NaNO}_2 + (100-N)\text{NaNO}_3 // \text{Ag}(\text{I})$ in NaNO_3/Ag

1 - Potential versus mole percent NaNO_2 , (N)

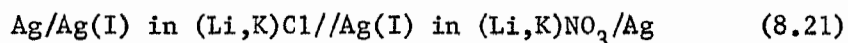
2 - Potential versus $\text{log}(\text{Mole percent NaNO}_2)$

● - experimental points, ○ - interpolated from line 1

underlying relationship, not apparent at present. This relationship would make possible the determination of large concentrations of nitrite in a nitrate melt by using a silver nitrate reference electrode and a silver electrode in the unknown melt.

8.3 Chloride//Nitrate Solvent Junction Potential

The emf series in the chloride and nitrate melts were correlated at $400 \pm 2^\circ\text{C}$ by examining the cell:



The lithium ion:potassium ion ratio was 0.59:0.41 in both melts and is the same as that in the lithium-potassium chloride eutectic. A procedure similar to that used in chapter 8.1 was used to check the behavior of the silver(I)/silver electrode in each of the melts at 400°C . The Nernst plot for the silver chloride concentration cell (Figure 8.5) and the silver nitrate concentration cell (Figure 8.6) exhibited ideal behavior for both melts for molal concentrations of 0.001 to 0.1. Analysis for silver(I) in the electrode compartments showed 100% current efficiency in the coulometric generation of silver(I) in both melts. Due to the higher initial silver concentrations (approximately a factor of 10) in these cells compared to those used in the activity coefficient measurements (chapter 7.5, page 142) and absence of the long periods (two to three hours) of contact between the silver electrode and very dilute silver nitrate solutions, the corrosion of the silver electrodes did not present a problem in these measurements as it did in the previous measurements (chapter 7.5).

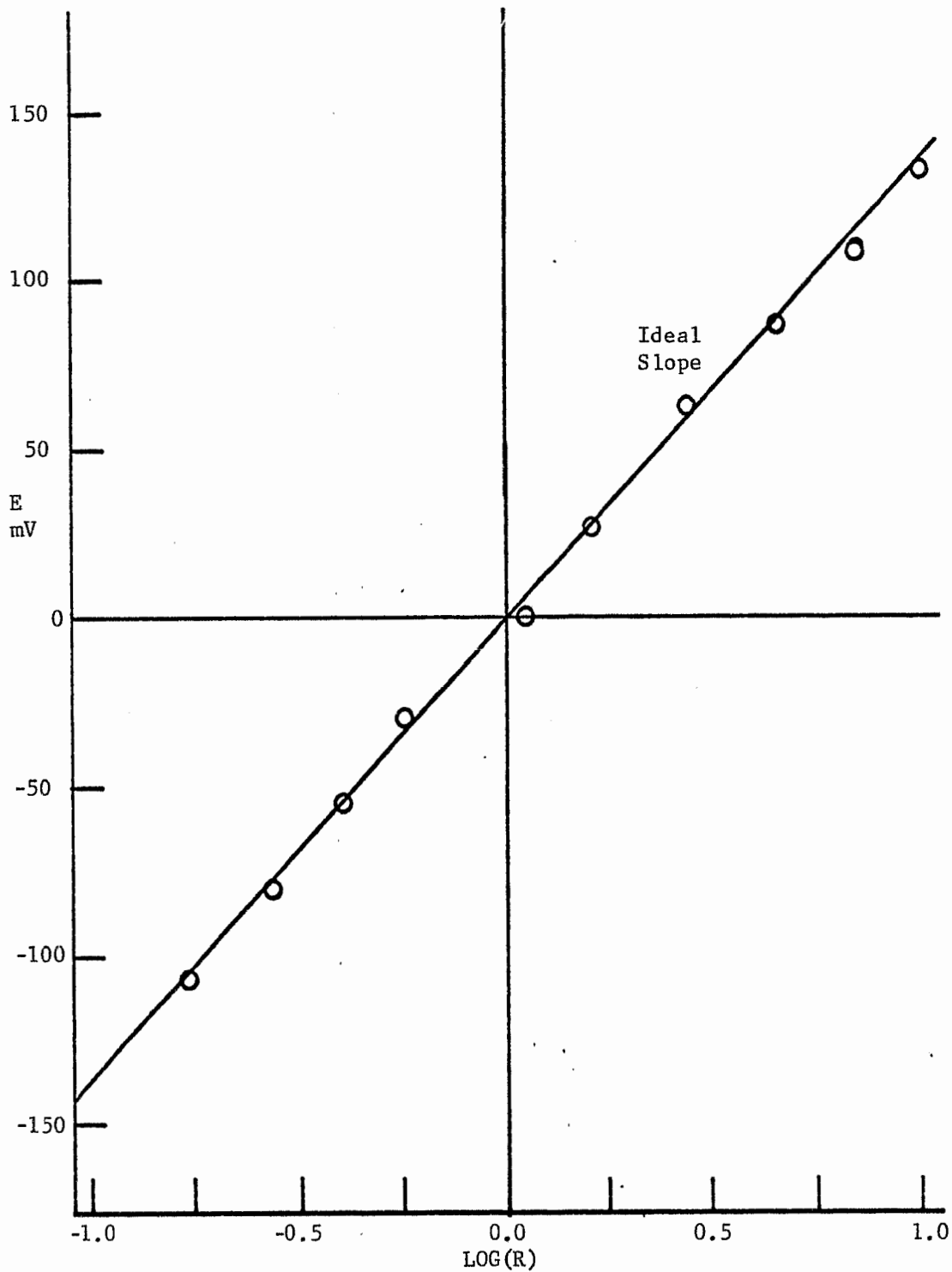


Figure 8.5 AgCl in (Li,K)Cl Concentration Cell at $400 \pm 2^\circ\text{C}$.

$$R = \frac{[\text{AgCl}] \text{ right half cell}}{[\text{AgCl}] \text{ reference half cell}},$$

$$[\text{AgCl}] \text{ reference} = 0.00987 \text{ molal.}$$

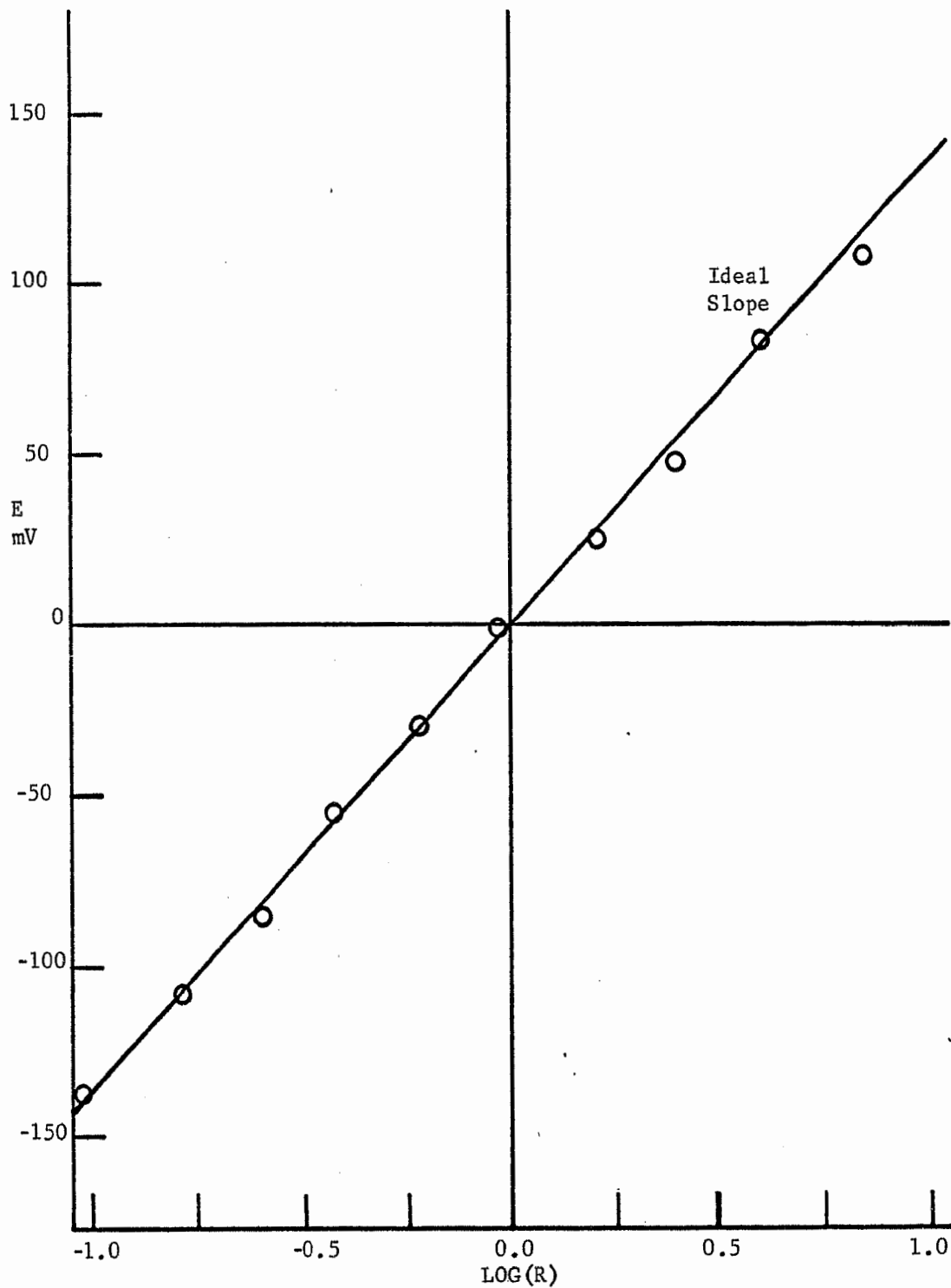
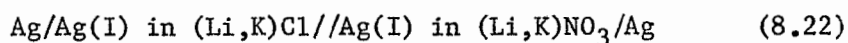


Figure 8.6 AgNO_3 in $(\text{Li},\text{K})\text{NO}_3$ Concentration Cell at $400 \pm 2^\circ\text{C}$

$R = \frac{[\text{AgNO}_3] \text{ right half cell}}{[\text{AgNO}_3] \text{ reference half cell}}$,
 $[\text{AgNO}_3] \text{ reference} = 0.02212 \text{ molal}$

Analysis of the chloride electrode compartment found from 10 to 15 mole percent nitrate in the chloride melt after three to four hours when the two melts were separated by a single sintered glass frit of fine porosity. The mole percent of nitrate was reduced to less than 1% when a double fritted chloride electrode compartment was used and the small compartment between the two frits was initially filled with just the chloride melt.

The observed potentials at $400 \pm 2^\circ\text{C}$ for the cell



with respect to a common 0.030 molal silver nitrate reference electrode have been tabulated in Table 8.5 for five of the individual runs made on the cell. The data presented in Figure 8.7 in the form of a Nernst plot and with a least squares slope of 0.1338 volts shows a close agreement with the theoretical value of 0.1336 volts.

The results for the chloride-nitrate cell are summarized in Table 8.6 and the activity coefficients used in the calculation of E_N^0 were $\gamma_{\text{N=0}} = 2.04$ (207) for the chloride melt and $\gamma_{\text{N=0}} = 1.91$ (Table 7.13, page 168) for the nitrate melt. The density for the chloride melt was given by Janz (2) and the density for the nitrate melt was taken from Table 7.10 (page 140).

The temperature dependence of the cell was calculated by determining the standard cell potentials from 365°C (5°C above the melting point of the chloride eutectic) to 450°C ; at higher temperatures the nitrate cell became unstable. The results are summarized in Table 8.7 and plotted in Figure 8.8. dE/dT at 400°C has the same

value on all of the concentration scales and is $(4.4 \pm 0.5) \times 10^{-4}$ volt deg⁻¹.

TABLE 8.5

POTENTIALS AT $400 \pm 2^\circ\text{C}$ FOR THE SOLVENT CELL:

Ag/Ag(I) in (Li,K)Cl//Ag(I) in (Li,K)NO₃/Ag

$-\log [\text{AgCl}]$ molal	$-\log [\text{AgNO}_3]$ molal	ΔE^* mV	E mV
1.9133	1.4165	-14.2	739.1
1.8128			726.7
1.7127			713.6
1.6112			700.1
1.0447			621.9
0.9451			609.0
0.8445			595.4
0.7474			582.7
1.5297	1.6715	19.9	688.1
1.4288			675.1
1.3281			662.7
1.2280			648.2
1.1288			635.9
1.0275			621.6
2.0145			1.5003
1.9144	738.4		
1.8157	725.6		
1.7161	710.6		
1.6151	696.3		

TABLE 8.5--Continued

$-\log [\text{AgCl}]$ molal	$-\log [\text{AgNO}_3]$ molal	ΔE^* mV	E mV
1.5145			682.6
1.4146			670.0
1.3137			657.1
1.2146			644.0
1.9967	1.6017	10.5	752.4
1.8970			736.4
1.6966			708.9
1.5967			696.2
1.6130	1.9131	52.1	699.6
1.6130	1.8076	38.0	699.1
1.6130	1.7105	25.1	698.6
1.6130	1.5998	10.3	697.6
1.6130	1.4033	-16.0	697.9
1.6130	1.2146	-41.2	698.0
1.6130	1.0038	-69.4	698.5

* potential added to cell value to convert to 0.030 molal AgNO_3 reference

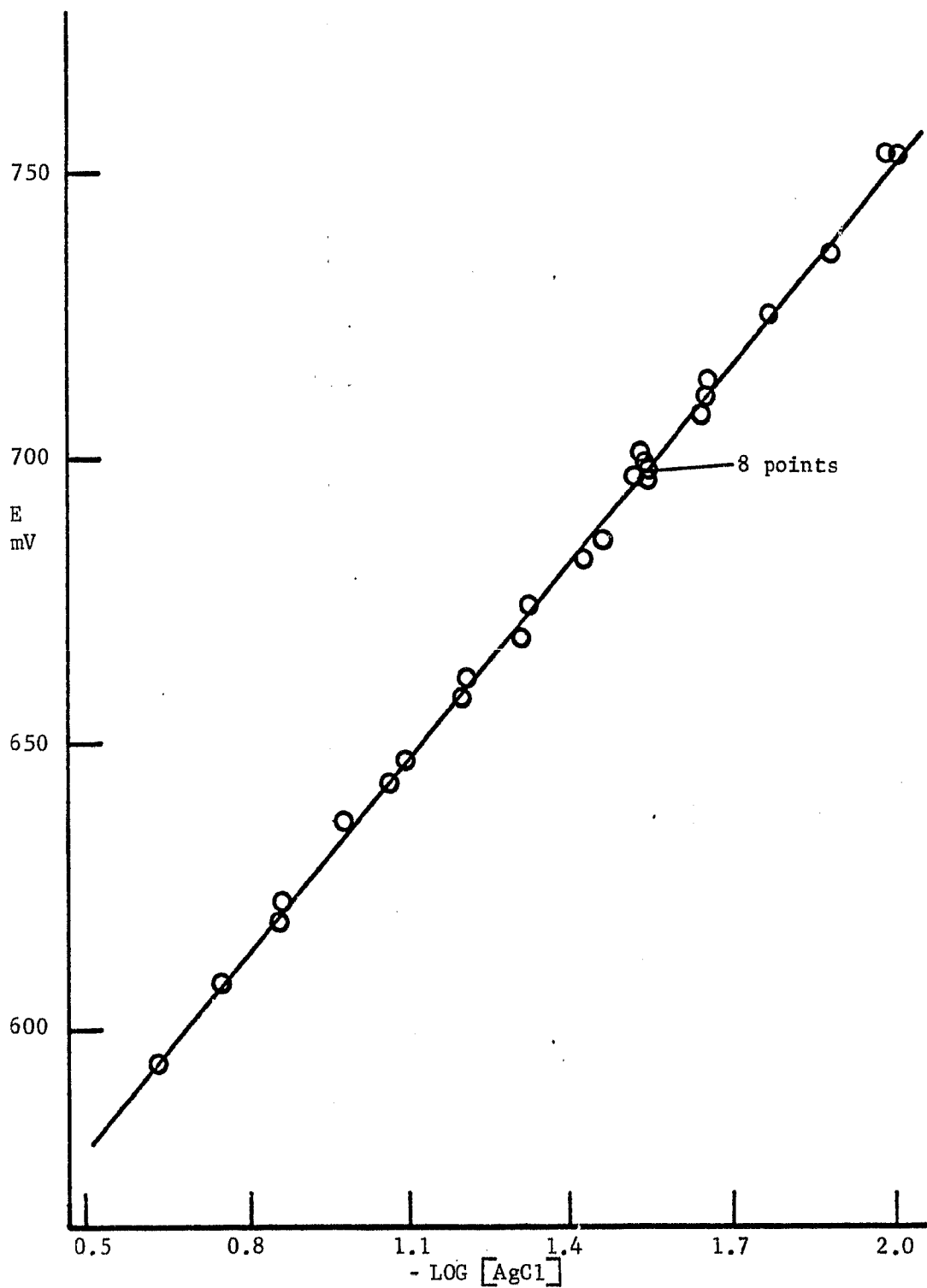


Figure 8.7 Nernst Plot at 400°C for the Solvent Cell:
 $\text{Ag}/\text{Ag}(\text{I})$ in $(\text{Li},\text{K})\text{Cl}$ // $\text{Ag}(\text{I})$ in $(\text{Li},\text{K})\text{NO}_3/\text{Ag}$

$[\text{AgNO}_3] = 0.030$ molal

TABLE 8.6

POTENTIALS AT $400 \pm 2^\circ\text{C}$ FOR THE CELL:
 $\text{Ag}/\text{Ag(I)}$ in $(\text{Li,K})\text{Cl}/\text{Ag(I)}$ in $(\text{Li,K})\text{NO}_3/\text{Ag}$

Number of individual runs	5
Experimental slope for Nernst plot, V	0.1338
Standard deviation from theoretical slope of 0.1336, V	0.0015
E_m° (measured), V	0.687
Calculated liquid junction potential, E_J , V	-0.003
E_m° (chemical), V	0.690 ± 0.002
E_M° (chemical), V	0.682 ± 0.002
E_N° (chemical), V	0.668 ± 0.002

TABLE 8.7

TEMPERATURE DEPENDENCE OF THE POTENTIAL OF THE SOLVENT CELL:
 $\text{Ag}/\text{Ag(I)}$ in $(\text{Li,K})\text{Cl}/\text{Ag(I)}$ in $(\text{Li,K})\text{NO}_3/\text{Ag}$

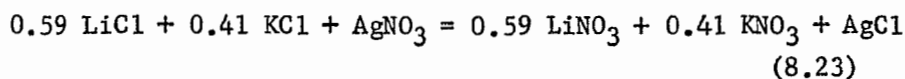
Number of trials	Temperature ($\pm 2^\circ\text{C}$)	E_m° (mV)
2	365	674 ± 5
3	380	683 ± 2
5	400	690 ± 2
2	425	697 ± 5
1	450	717 ± 8

TABLE 8.7--Continued

$$\frac{dE_m^{\circ}}{dT} = (4.7 \pm 1.2) \times 10^{-4} \text{ volt deg}^{-1}$$

$$\frac{dE_M^{\circ}}{dT} = \frac{dE_N^{\circ}}{dT} = \frac{dE_m^{\circ}}{dT} \text{ at } 400^{\circ}\text{C}$$

The electrolytic cell represents the chemical reaction:



which has a standard chemical cell potential, E_N° , of 0.668 ± 0.002 volts at $400 \pm 2^{\circ}\text{C}$ or a change in Gibbs free energy, ΔG° , of $-15.4 \pm 0.05 \text{ kcal mole}^{-1}$. The use of the cell potential based on the mole fraction scale has been discussed and justified in chapter 8.1. It was assumed that the free energies of mixing in the formation of the alkali nitrate solvent and the alkali chloride solvent are identical. The data required to check this assumption are not available in the literature. A value for ΔG_{673}° was calculated from published thermodynamic values (96, 117, 172, 209) and found to be $-16.0 \pm 1.0 \text{ kcal mole}^{-1}$. The large error in the calculated value comes from the estimation of ΔG_f° for lithium nitrate (117) since there are no exact thermodynamic measurements available. The experimental dE/dT of $(4.7 \pm 1.2) \times 10^{-4}$ volts for the cell agreed well with the calculated value of $(5.0 \pm 4.0) \times 10^{-4}$ volts (96, 117, 172, 209) for the temperature interval from 350 to 400°C .

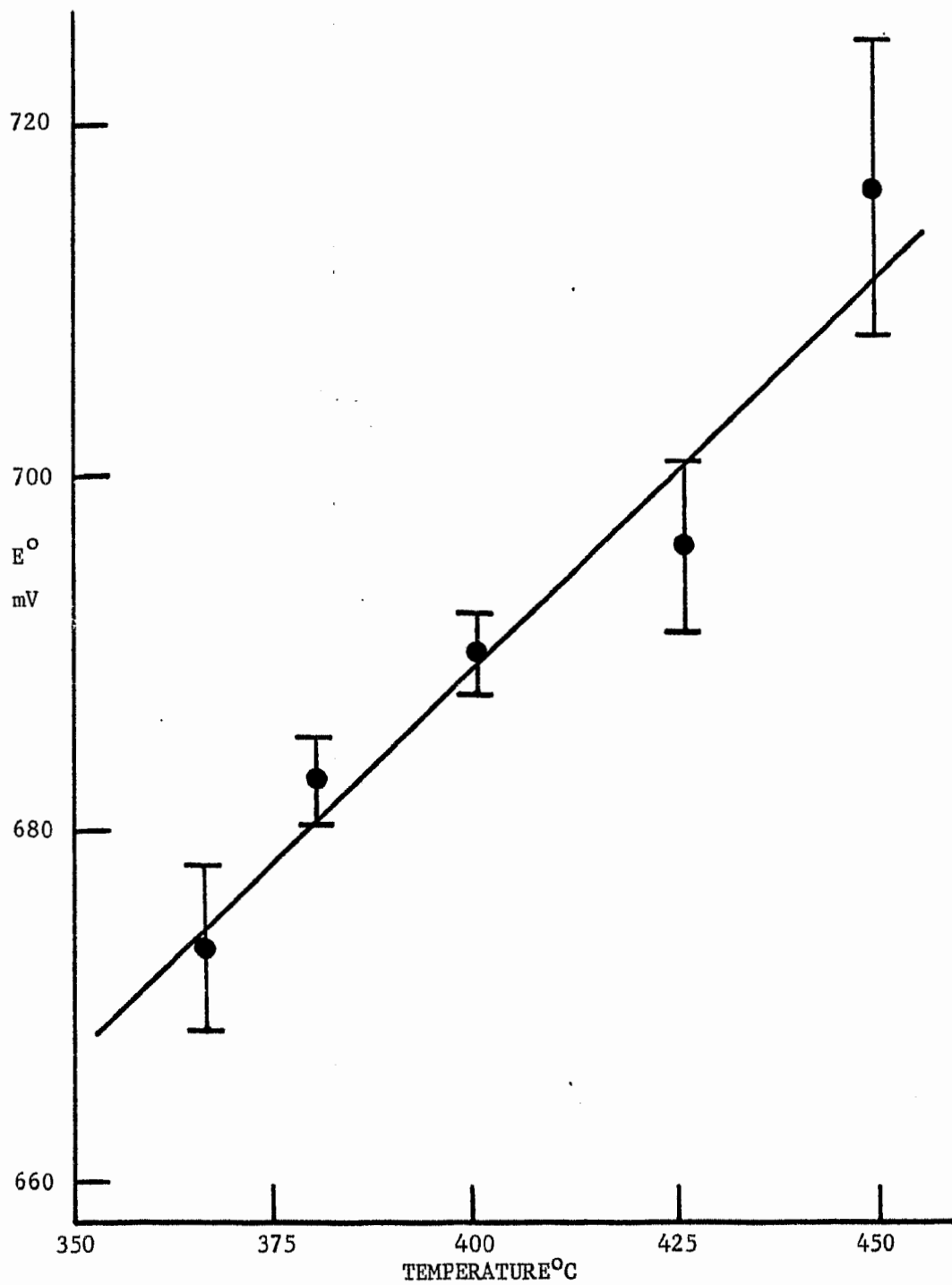


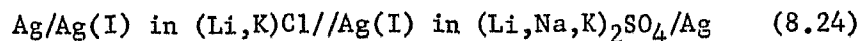
Figure 8.8 Temperature Dependence of the Potential for the Solvent Cell:



Several attempts were made to measure the potential of a cell containing alkali nitrate as one solvent and a mixture of alkali nitrate and alkali chloride as the solvent in the other compartment. The Nernst plot of the data from these cells exhibited a slope far below the theoretical value of 0.1336 volts at 400°C. The initially clear mixed chloride nitrate melt became cloudy when silver(I) was added to the melt and the intensity of the cloudiness increased as the amount of silver(I) was increased. This precipitate was attributed to the formation of insoluble silver chloride and since the field of silver halide complexes in molten nitrates have been extensively reported in the literature (99, 103, 118, 127, 142, 144-147), the investigations on this system were discontinued.

8.4 Chloride//Sulfate Solvent Junction Potential

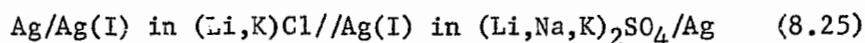
The solvent junction potential between the chloride and the sulfate melts at 550°C was determined by examining the cell:



The binary chloride eutectic (0.59 LiCl, 0.41 KCl) and the ternary sulfate eutectic (0.78 Li₂SO₄, 0.085 Na₂SO₄, 0.135 K₂SO₄) were used despite the slight difference in the ratios between the cations in the two melts. The low melting points of the two eutectics permitted the use of Pyrex glass (annealing point: approximately 565°C) throughout the system without necessitating a more elaborate system made of Vycor or quartz. In order to check for ideal behavior of the silver electrode in each of the melts, concentration cells were

set up and the data plotted in Figures 8.9 and 8.10 confirm this property according to the Nernst equation. Analysis for silver(I) in the electrode compartments verified 100% current efficiency in the coulometric generation of the silver(I) in each of the melts. Analysis also showed no appreciable diffusion of the sulfate melt had occurred through a sintered glass frit of fine porosity into the chloride melt after four to five hours.

The data for the cell



at $550 \pm 2^\circ\text{C}$ are summarized in Table 8.8 and plotted in the form of a Nernst plot in Figure 8.11. All the potentials are expressed in terms of a common 0.030 molal silver(I)/silver reference electrode in the alkali sulfate melt. The results for the chloride-sulfate cell are summarized in Table 8.9. The conductivity data required for the calculation of the liquid junction potential for the ternary sulfate and the silver sulfate melts were not available in the literature, thus only the measured standard cell potentials could be reported. The values for the silver activity coefficients used in the conversion of the standard cell potential to the mole fraction scale were $\gamma_{\text{N=0}} = 1.76$ for the chloride melt (207) and unity for the sulfate melt. The assumption that the silver ion exhibits ideal behavior in the sulfate melt was necessitated by a lack of the required activity data in the literature. A value of $\gamma_{\text{N=0}} = 0.85$ has been measured in the binary sulfate eutectic ($0.8 \text{ Li}_2\text{SO}_4 + 0.2 \text{ K}_2\text{SO}_4$) (321) by adding potassium chloride to a dilute silver sulfate solution

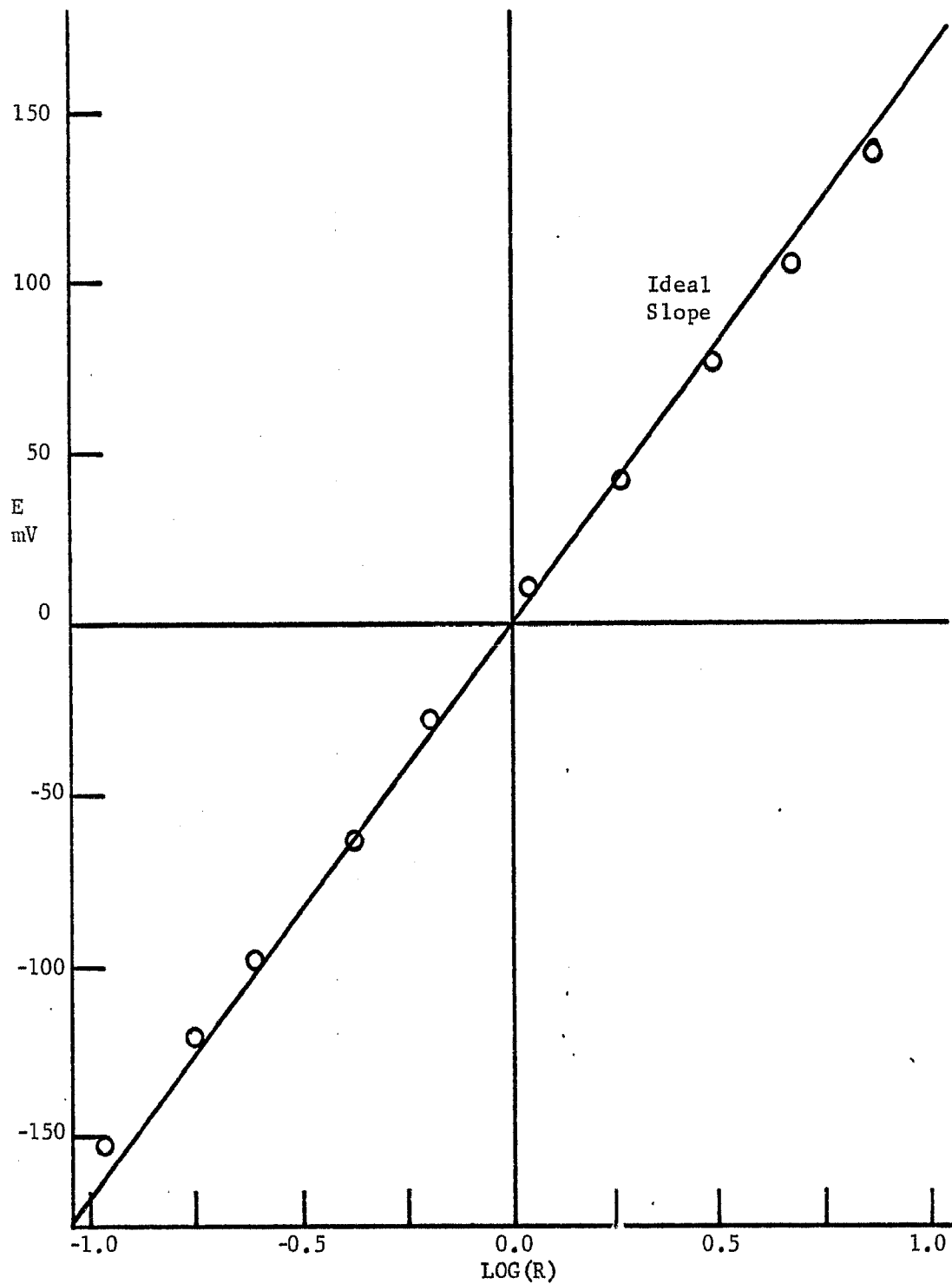


Figure 8.9 AgCl in (Li,K)Cl Concentration Cell at $550 \pm 2^\circ\text{C}$

$$R = \frac{[\text{AgCl}]_{\text{right half cell}}}{[\text{AgCl}]_{\text{reference half cell}}}$$

$[\text{AgCl}]_{\text{reference}} = 0.01362 \text{ molal}$

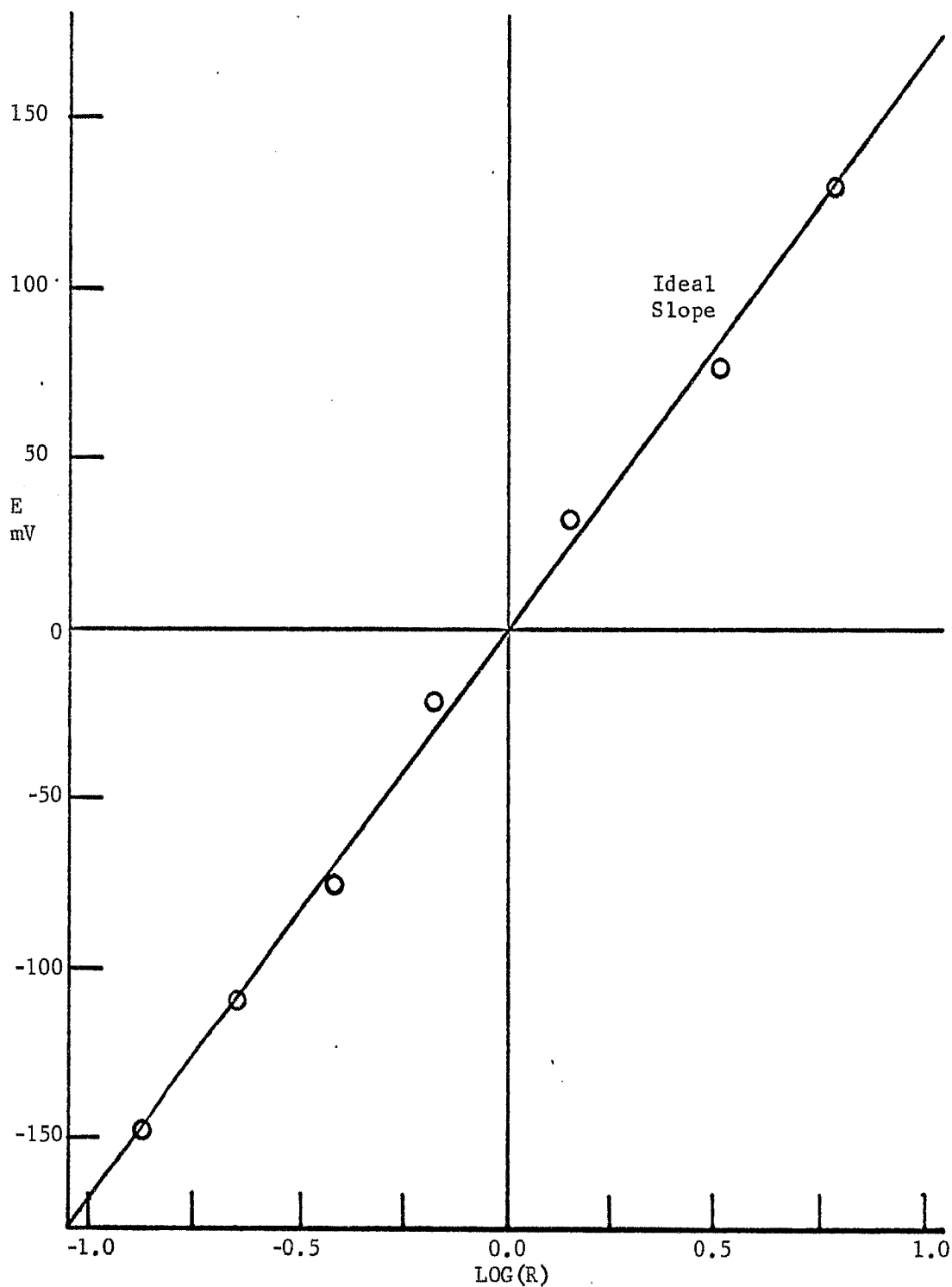


Figure 8.10 Ag_2SO_4 in $(\text{Li},\text{Na},\text{K})_2\text{SO}_4$ Concentration Cell at $550 \pm 2^\circ\text{C}$

$$R = \frac{[\text{Ag}_2\text{SO}_4] \text{ in right half cell}}{[\text{Ag}_2\text{SO}_4] \text{ reference half cell}}$$

$[\text{Ag}_2\text{SO}_4] \text{ reference} = 0.00716 \text{ molal}$

at 600 to 700°C. The dissimilarities between the system used in this study and the system used by Woolner and Hill (321) prevented the use of their γ value in this study.

TABLE 8.8

POTENTIALS AT 550 \pm 2°C FOR THE SOLVENT CELL:
 Ag/Ag(I) in (Li,K)Cl//Ag(I) in (Li,Na,K)₂SO₄/Ag

$-\log [\text{AgCl}]$ molal	$-\log(2 [\text{Ag}_2\text{SO}_4])$ molal	ΔE^* mV	E mV
1.4838	1.3819	-23.0	710.5
1.3830			695.7
1.2821			679.2
1.1829			661.8
1.0807			645.2
0.9556			625.4
0.9556	1.2061	-51.7	625.4
2.0558	1.5627	6.5	801.2
1.9555			787.1
1.8538			771.9
1.7558			755.5
1.6561			739.3
1.5555			720.4
1.4559			704.5
1.3552			686.1
1.2454			669.5
2.0297	1.3164	33.7	801.5
1.9290			785.7

TABLE 8.8--Continued

$-\log [\text{AgCl}]$ molal	$-\log(2 [\text{Ag}_2\text{SO}_4])$ molal	ΔE^* mV	E mV
1.8294			768.2
1.7293			752.2
1.6294			734.9
1.5283			718.8
1.4263			701.5
1.3285			686.4
2.0015	1.2983	36.7	798.9
1.9010			782.3
1.8006			765.5
1.7016			749.5
1.6015			733.1
1.5005			715.0
1.4010			699.7
1.3007			683.6
1.6213	1.8593	54.9	733.0
1.6213	1.7589	38.5	732.8
1.6213	1.6499	20.7	732.1
1.6213	1.5525	4.8	733.0
1.6213	1.4532	11.4	734.0
1.6213	1.3493	28.3	734.8
1.6213	1.2501	44.5	733.9

* potential added to cell value to convert to 0.015 molal Ag_2SO_4 reference

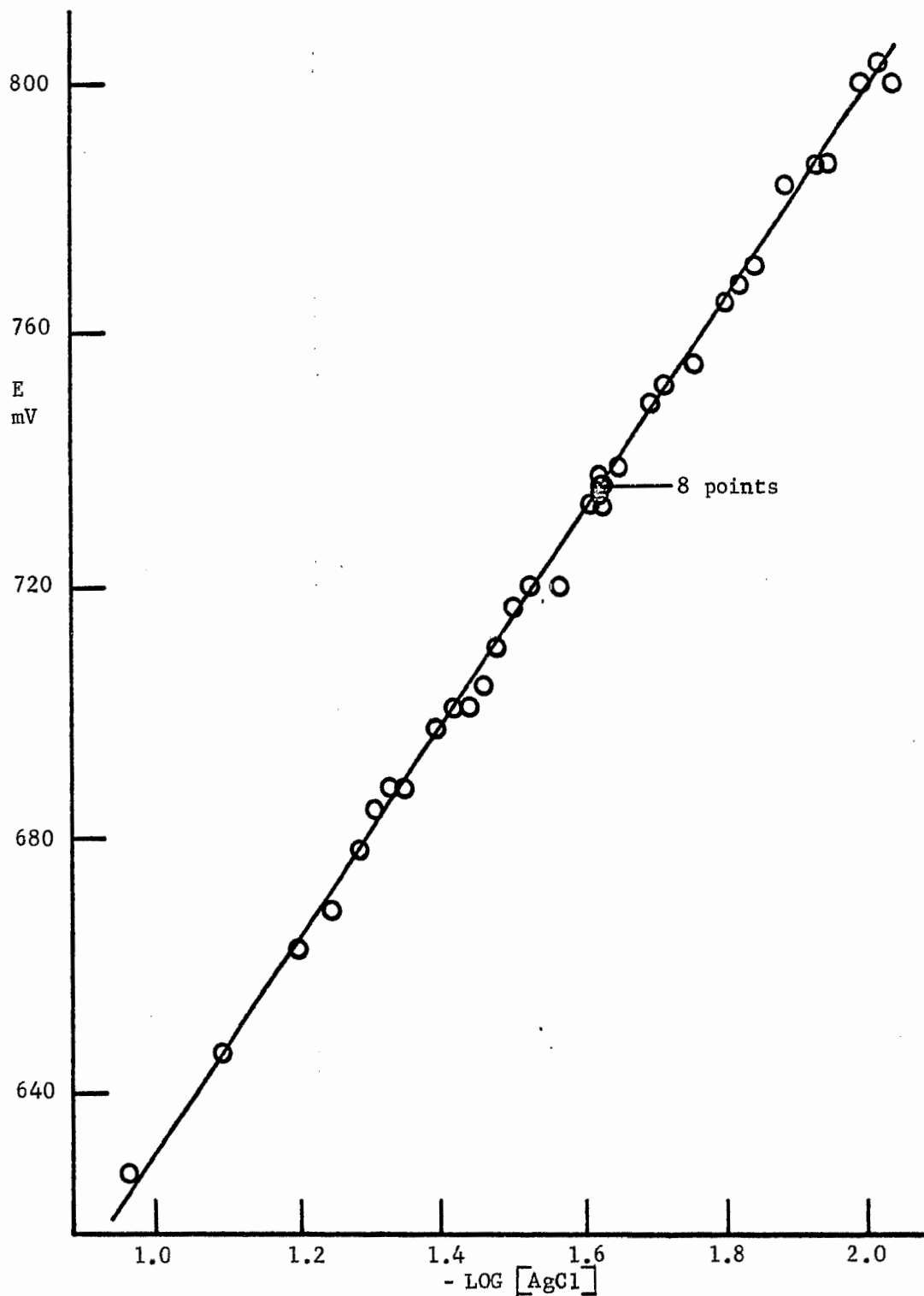
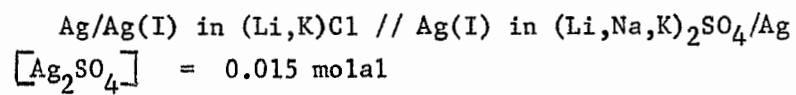


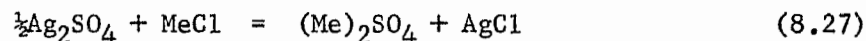
Figure 8.11 Nernst Plot at 550°C for the Solvent Cell:



The standard measured cell potential on the mole fraction scale, expressed as the change in Gibbs free energy, is

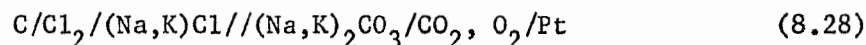
$$\Delta G^{\circ} = -17.5 \pm 0.5 \text{ kcal mole}^{-1} \quad (8.26)$$

and represents the change in free energy at $550 \pm 2^{\circ}\text{C}$ for the chemical reaction

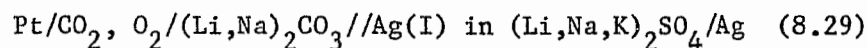


where Me is a mixture of the first three alkali metals. In the literature on sulfate melts there are insufficient thermodynamic data to permit the calculation of ΔG for the cell reaction.

Ozeryanaya *et al.* (309) studied the cell



for temperatures from 770 to 1000°C and the extrapolation of their results to 550°C gives a potential of -0.973 volts. Bartlett and Johnson (287) report the potential of the cell



is +0.727 volts on the mole fraction scale.

TABLE 8.9

POTENTIALS AT $550 \pm 2^{\circ}\text{C}$ FOR THE CELL:

$\text{Ag}/\text{Ag(I)} \text{ in } (\text{Li,K})\text{Cl}/\text{Ag(I)} \text{ in } (\text{Li,Na,K})_2\text{SO}_4/\text{Ag}$

Number of individual runs	5
Experimental slope for Nernst plot, V	0.1642
Standard deviation from theoretical slope of 0.1633 volts, V	0.0018
E_m° (measured), V	0.7178

TABLE 8.9--Continued

Calculated liquid junction potential, E_J , V	Data not available
E_m^O (measured), V	0.717 ± 0.002
E_M^O (measured), V	0.690 ± 0.002
E_N^O (measured), V	0.757 ± 0.002

The potential at 550°C of the cell



is reported to be +0.8855 volts by Yang and Hudson (207, 208). The combination of these three cells (8.28, 8.29 and 8.30) is equivalent to the chloride-sulfate solvent cell measured in this investigation. The potential from the three combined cells is 0.640 volts as compared to the 0.757 volts given in Table 8.9. The difference between the two values may be due to the extrapolation of the results for cell 8.28 to a temperature 220 C° below the experimental temperatures involved in the original experiment.

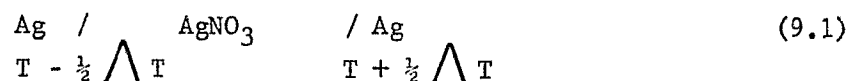
Preliminary tests showed that the silver, alkali metal-chloride, sulfate system formed two immiscible layers in the liquid state, which was consistent with previous reports (274, 322); therefore, no attempt was made to study a cell using a mixture of sulfate and chloride melts as one of the solvents. The melting point of 512°C for the sulfate eutectic and the upper limit of 560°C for the useful working temperature range for Pyrex glass prevented any meaningful dE/dT studies on this system.

9. RESULTS AND DISCUSSION

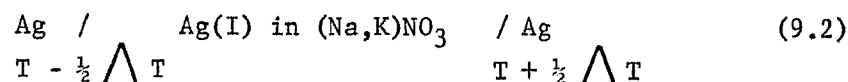
NITRATE THERMOCELLS

9.1 Seebeck Coefficient for Silver Nitrate

The Seebeck coefficient, \mathcal{E}_T° , for pure silver nitrate at temperature T is given by $\mathcal{E}_T^{\circ} = (dE/dT)_T$ (the initial thermoelectric power) for the cell



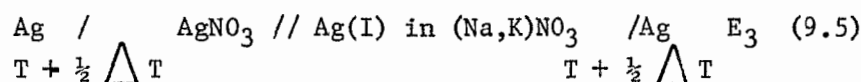
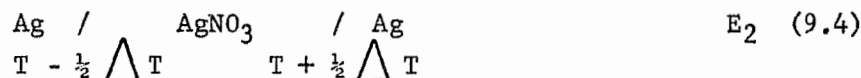
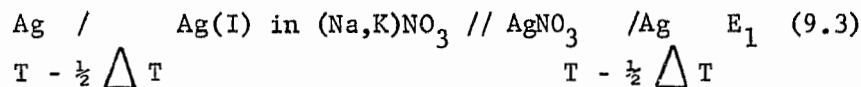
where the sign of \mathcal{E}_T° is the same as that of the hot electrode. The Seebeck coefficient, \mathcal{E}_T , at temperature T for the cell



is also given by $\mathcal{E}_T = (dE/dT)_T$ except that the data must be extrapolated back to time equals zero to avoid including the emf due to the Soret effect in the measured \mathcal{E}_T value. To avoid the Soret effect a special cell was used which maintained two isothermal fritted compartments at $T - \frac{1}{2} \Delta T$ and $T + \frac{1}{2} \Delta T$ so that the temperature gradient occurred only in the melt between the two half cells. The potential of several cells of uniform composition with a 25 to 50°C temperature gradient were monitored for periods of six to ten hours and the emf remained constant to ± 0.05 millivolts, thus illustrating the absence of any Soret effect.

The measured \mathcal{E}_T for the dilute silver nitrate thermocell can

be related to the \mathcal{E}_T° for the pure silver nitrate thermal cell by considering the sum of the following three cells:



$$E_1 = \frac{-R(T - \frac{1}{2} \Delta T)}{F} \ln N \gamma^- \quad (9.6)$$

$$E_2 = \mathcal{E}_T^{\circ} \Delta T \quad (9.7)$$

$$E_3 = \frac{R(T + \frac{1}{2} \Delta T)}{F} \ln N \gamma^+ \quad (9.8)$$

N is the mole fraction of silver nitrate in the dilute thermal cell; γ^- is the silver nitrate activity coefficient at concentration N and temperature $T - \frac{1}{2} \Delta T$ and γ^+ is the corresponding coefficient at the hot electrode at the temperature $T + \frac{1}{2} \Delta T$. The observed emf for the dilute thermal cell, $\mathcal{E}_T \Delta T$, is given by the sum of the potentials for the three cells (9.3 to 9.5).

$$\mathcal{E}_T \Delta T = E_1 + E_2 + E_3 \quad (9.9)$$

$$\mathcal{E}_T \Delta T = \mathcal{E}_T^{\circ} \Delta T - \frac{R(T - \frac{1}{2} \Delta T)}{F} \ln N \gamma^-$$

$$+ \frac{R(T + \frac{1}{2} \Delta T)}{F} \ln N \gamma^+ \quad (9.10)$$

$$\begin{aligned} \varepsilon_T \Delta T = \varepsilon_T^o \Delta T + \frac{R \Delta T \ln N}{F} - \frac{R(T - \frac{1}{2} \Delta T)}{F} \ln \gamma^- \\ + \frac{R(T + \frac{1}{2} \Delta T)}{F} \ln \gamma^+ \end{aligned} \quad (9.11)$$

At low silver nitrate concentrations ($N < 0.5$) the following relations hold (equations 3.101 and 3.102, page 54):

$$RT \ln \gamma = (1 - N)^2 W_T \quad (9.12)$$

$$RT \ln \gamma = (1 - N)^2 (a - \alpha T) \quad (9.13)$$

and equation 9.11 simplifies to:

$$\varepsilon_T \Delta T = \varepsilon_T^o \Delta T + \frac{R}{F} \Delta T \ln N - \frac{\Delta T \alpha (1 - N)^2}{F} \quad (9.14)$$

or

$$\varepsilon_T^o = \varepsilon_T - \frac{R \ln N}{F} + \frac{\alpha (1 - N)^2}{F} \quad (9.15)$$

The activity coefficient, γ_i , is related to the partial excess free energy of mixing $\Delta \bar{G}_i^M$ by the relationship

$$RT \ln \gamma_i = \Delta \bar{G}_i^M \quad (9.16)$$

The definition of Gibbs free energy at constant temperature

$$\Delta \bar{G}_i^E = \Delta \bar{H}_i^M - T \Delta \bar{S}_i^E \quad (9.17)$$

is used with equation 9.16 to relate γ with the partial enthalpy of mixing, $\Delta \bar{H}_i^M$, and the partial excess entropy of mixing, \bar{S}_i^E .

$$R \ln \gamma_i - \frac{\Delta \bar{H}_i^M}{T} = - \Delta \bar{S}_i^E \quad (9.18)$$

The partial excess entropy is related to the concentrations (120)

by

$$\Delta \bar{s}_i^E = \alpha (1 - N)^2 \quad (9.19)$$

and when equations 9.15, 9.18 and 9.19 are combined, the result

$$\mathcal{E}_T^o = \mathcal{E}_T - \frac{R \ln N}{F} - \frac{R}{F} \ln \gamma + \frac{\Delta \bar{H}^M}{FT} \quad (9.20)$$

is identical to that derived by Dupuy (166) from the theory of thermoelectric cells.

The value of α in the sodium-potassium nitrate eutectic is -1.41 (Table 7.14, page 172) and according to equation 9.15 the \mathcal{E}_T should vary with the silver nitrate concentration according to

$$\mathcal{E}_T = \mathcal{E}_T^o + \frac{R \ln N}{F} + \frac{1.41 (1 - N)^2}{F} \quad (9.21)$$

9.2 Dependence of Seebeck Coefficient on Concentration and Temperature

Each run consisted of taking ΔT through the cycle $0 \rightarrow + 50 \rightarrow 0 \rightarrow - 50 \rightarrow 0^\circ\text{C}$ where ΔT was defined as the temperature of the right-hand electrode less that of the left-hand electrode. The temperature controllers were adjusted such that the average temperature of the cell kept constant to $\pm 2^\circ\text{C}$ with an average of eight to ten points being recorded per run. The temperatures and emf were recorded only after they had remained stable at $\pm 0.5^\circ\text{C}$ and 0.05 mV, respectively, for a period of 15 minutes.

The results from two runs at $275 \pm 2^\circ\text{C}$ and a 0.2 mole fraction silver nitrate are presented in Figure 9.1. The least squares fit

of the data in Figure 9.1 has a slope of $-315 \mu\text{V deg}^{-1}$ and a standard deviation in the measured emf of 0.62 mV. The results for the determination of \mathcal{E}_T as a function of the silver nitrate concentration at $350 \pm 2^\circ\text{C}$ are given in Table 9.1 and plotted in Figure 9.2 along with the results for dilute solutions of silver nitrate in sodium nitrate (170, 324) and in potassium nitrate (324). The curve predicted by equation 9.21 using a value of $-325 \mu\text{V deg}^{-1}$ for \mathcal{E}_T^0 was compared with the results in Figure 9.2. The \mathcal{E}_T^0 value was obtained by the extrapolation of the results in Figure 9.2 to $N = 1$. The experimental curve remained constant for values of N greater than 0.2 and it was only for the very dilute solutions ($N < 0.1$) that the experimental curve began to rise as predicted by the theoretical curve. The results for the sodium-potassium nitrate eutectic lie about mid-way between the published results for the two single salt solvents. The results for silver nitrate in lithium nitrate (164) were closer to the theoretical curve (equation 9.15) than those for any of the previously mentioned systems; however, Dupuy (166) did not state how the activity coefficient values used in the calculations were obtained. No apparent reason for these discrepancies could be formulated or found in the literature. Several runs were made in which the silver nitrate in the cell was restricted to the fritted electrode compartments and the thermal gradient was applied to the pure solvent. The thermal emfs were unstable and irreproducible with an average value of $-90 \pm 50 \mu\text{V deg}^{-1}$ for the initial thermoelectric power for the system. The small negative value for \mathcal{E} in

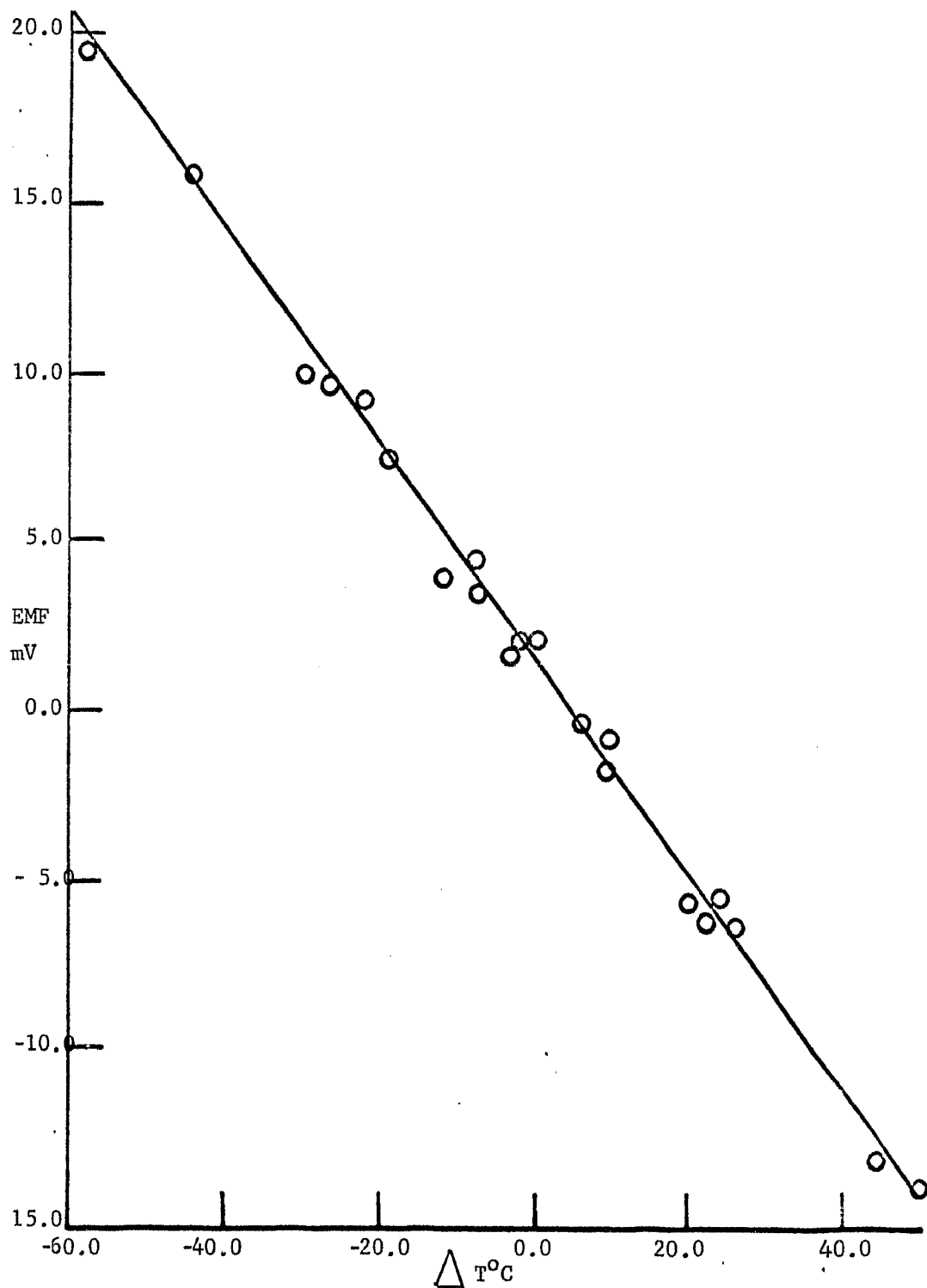


Figure 9.1 EMF of Dilute Silver Nitrate Thermal Cell

$[AgNO_3]$ = 0.20 mole fraction

Solvent = (Na,K)NO₃

Average Temperature = $275 \pm 2^\circ C$

the pure solvent may account for some of the deviations from the theoretical values for the dilute silver nitrate solutions. Fortunately, only the \mathcal{E}_T° for pure silver nitrate was required for the correlation of the emf series at different temperatures and there was substantial agreement in the published work (169) on the value of \mathcal{E}_T° .

TABLE 9.1

SEEBECK COEFFICIENT AS A FUNCTION OF SILVER NITRATE CONCENTRATION AT $350 \pm 2^{\circ}\text{C}$

Number of Runs	N_{AgNO_3}	$-\mathcal{E}_{350}$ $\mu\text{V deg}^{-1}$
2	0.852	324
2	0.698	323
3	0.560	320
3	0.401	317
3	0.309	320
4	0.200	315
4	0.110	345

It has been reported in several papers that \mathcal{E}_T° increases by as much as $0.05\% \text{ deg}^{-1}$ with an increase in the average temperature of the thermocell (169). The results for the determination of \mathcal{E}_T° as a function of temperature are given in Table 9.2. The maximum possible error in the experimental values of \mathcal{E}_T° was estimated to be $\pm 5 \mu\text{V deg}^{-1}$.

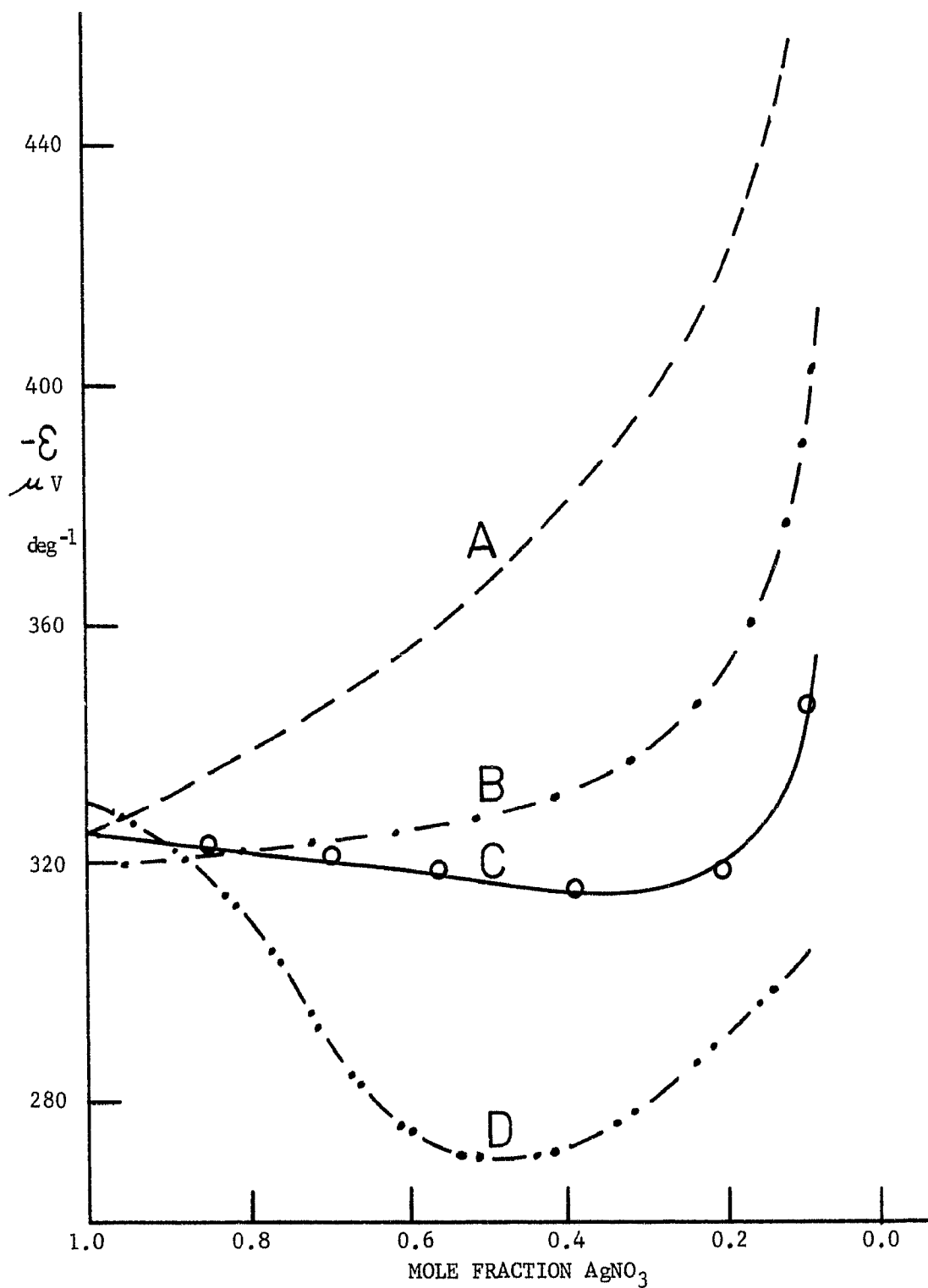


Figure 9.2 Seebeck Coefficient at $350 \pm 2^\circ\text{C}$ Versus Silver(I) Concentration

- A Ag(I) in $(\text{Na},\text{K})\text{NO}_3$ (Theoretical)
- B Ag(I) in NaNO_3 (170,324)
- C Ag(I) in $(\text{Na},\text{K})\text{NO}_3$ (This Study)
- D Ag(I) in KNO_3 (324)

The linear equation of least squares best fit for the data is

$$\mathcal{E}_T^{\circ} = -277.5 - 0.136 T^{\circ}\text{C} \quad (\mu\text{V deg}^{-1}) \quad (9.22)$$

with a standard deviation of $1.4 \mu\text{V deg}^{-1}$. The experimental increase, in \mathcal{E}_T° of $0.042\% \text{ deg}^{-1}$ agreed with the previously determined values (169).

TABLE 9.2

VALUES OF \mathcal{E}_T° AS A FUNCTION OF TEMPERATURE

Temperature $\pm 2^{\circ}\text{C}$	$-\mathcal{E}_T^{\circ}$ $\pm 5 \mu\text{V deg}^{-1}$
275	314
300	320
325	321
350	325

9.3 Calculation of Thermoelectric emfs in Nitrate and Chloride

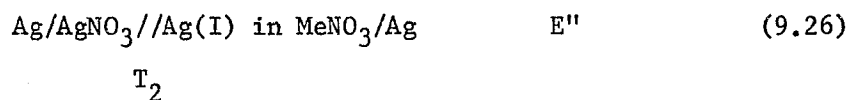
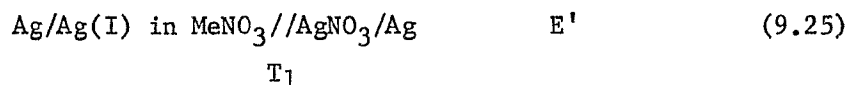
Melts

In order to evaluate the thermal emf, E_{T_1/T_2} , of the silver nitrate cell between temperatures T_1 and T_2 , the dependence of \mathcal{E}_T° on the temperature as given in equation 9.22 necessitates the following integration:

$$E_N(T_1/T_2)(\text{AgNO}_3) = \int_{T_2}^{T_1} \mathcal{E}_T^{\circ} dT \quad (9.23)$$

$$E_N(T_1/T_2)(\text{AgNO}_3) = (-277.5 (T_1 - T_2) - 0.0680 (T_1^2 - T_2^2)) \times 10^{-6} \text{ V (}^\circ\text{C)} \quad (9.24)$$

The $E_N(T_1/T_2)(\text{AgNO}_3)$ potential is based on the mole fraction scale and the conversion of the thermal emf to the molal and molar scales requires consideration of the following concentration cells at T_1 and T_2 where the silver(I) concentrations are unity on the concentration scale being considered.



From the interrelationships between the concentration scales in Table 7.1 (page 114) and the Nernst equation for concentration cells, the potentials E' and E'' are given by

$$E'_m = - \frac{RT_1}{F} \ln N_{m_1} \gamma_{N_{m_1}} \quad (9.27)$$

$$E''_m = \frac{RT_2}{F} \ln N_{m_1} \gamma_{N_{m_2}} \quad (9.28)$$

for the molality scale and

$$E'_M = - \frac{RT_1}{F} \ln N_{M_1} \gamma_{N_{M_1}} \quad (9.29)$$

$$E''_M = \frac{RT_2}{F} \ln N_{M_2} \gamma_{N_{M_2}} \quad (9.30)$$

for the molarity scale. The values of N_{m_1} and N_{M_1} at temperature T_1 are given by:

$$N_{m_1} = \frac{Mwt}{1000 + Mwt} \quad (9.31)$$

and

$$N_{M_1} = \frac{Mwt}{1000 D_{T_1} + Mwt - Mwt^*} \quad (9.32)$$

where D_{T_1} is the density of the solution at T_1 , Mwt is the molecular weight of the solvent and Mwt^* is the molecular weight of the solute. $\gamma_{N_{M_1}}$ represents the activity coefficient of the electroactive solute in the given solvent at concentration N and temperature T_1 .

The thermal emf on the molal scale is given by

$$E_m(T_1/T_2) (\text{Ag(I) in MeNO}_3) = E_N(T_1/T_2) (\text{AgNO}_3) + E_m^I + E_m^{II} \quad (9.33)$$

and by

$$E_M(T_1/T_2) (\text{Ag(I) in MeNO}_3) = E_N(T_1/T_2) (\text{AgNO}_3) + E_M^I + E_M^{II} \quad (9.34)$$

for the molarity scale.

Metz and Seifert (168) reported that the Seebeck coefficient for a pure silver chloride cell using silver electrodes was given by

$$\mathcal{E}_T^{\circ} = -381 + 7.89 \times 10^{-3} T \text{ (}^{\circ}\text{C)} \mu\text{V deg}^{-1}$$

The thermal emf of the silver chloride cell operating between the temperatures of T_1 $^{\circ}\text{C}$ and T_2 $^{\circ}\text{C}$ is given by

$$E_N(T_1/T_2) (\text{AgCl}) = \int_{T_2}^{T_1} \mathcal{E}_T^{\circ} dT \quad (9.36)$$

$$E_N(T_1/T_2) (\text{AgCl}) = (-381 (T_1 - T_2) - 0.00394 (T_1^2 - T_2^2)) \times 10^{-6} \text{ V (T}^{\circ}\text{C)} \quad (9.37)$$

A set of equations similar to those used for the nitrate melts (9.27 to 9.34) must be used to calculate the thermal emfs on the molal and molar scales for the chloride melt.

If it should be necessary to use the thermal equations at temperatures below the melting point of the pure silver salt, the salt is assumed to be a super-cooled liquid at the low temperature. This assumption is valid since the same assumption was made in the case of the mole fraction scale in the isothermal cells at the same temperature. The use of these equations will permit the correlation of all the melts studied over the temperature range from 86°C to 550°C.

As pointed out by Schnelbaum and Sundheim (165), the determination of the transported entropy and heat of transport of the silver ion requires both the initial thermoelectric power and the Seebeck coefficient, as well as the final thermoelectric emf which is realized after the Soret effect reaches equilibrium. Since only the initial thermal emf was required in this study, the work on the thermal cell was not expanded to include the Soret effect.

10. RESULTS AND DISCUSSION

GAS ELECTRODES

10.1 The Emf of the Silver-Platinum Thermocouple in the Gas Electrode Systems

A determination was made of the thermoelectric power, $\mathcal{E}_{(Ag-Pt)}$, of the silver-platinum thermocouple in order to correct for the silver-platinum thermoelectric emf present in the silver(I)/silver gas electrode (platinum) circuit (168). The thermoelectric emf was not present in previous silver concentration cells because identical material was used for both electrodes; however, silver and platinum were used in the gas electrode cells to connect the external electrical circuit at room temperature with the electrodes immersed in the melt. This produces a thermoelectric emf equivalent to a silver-platinum-silver thermocouple with one junction at room temperature ($25 \pm 3^{\circ}\text{C}$) and the other at the temperature of the melt. A thermostated sodium-potassium nitrate eutectic melt and a calibrated chromel-alumel thermocouple were used to calibrate a silver-platinum thermocouple with a reference junction at 0°C . The data from the silver-platinum thermocouple (Figure 10.1) were fitted using five different polynomials varying in order from one to five. The standard deviation for each fit is given in Table 10.1.

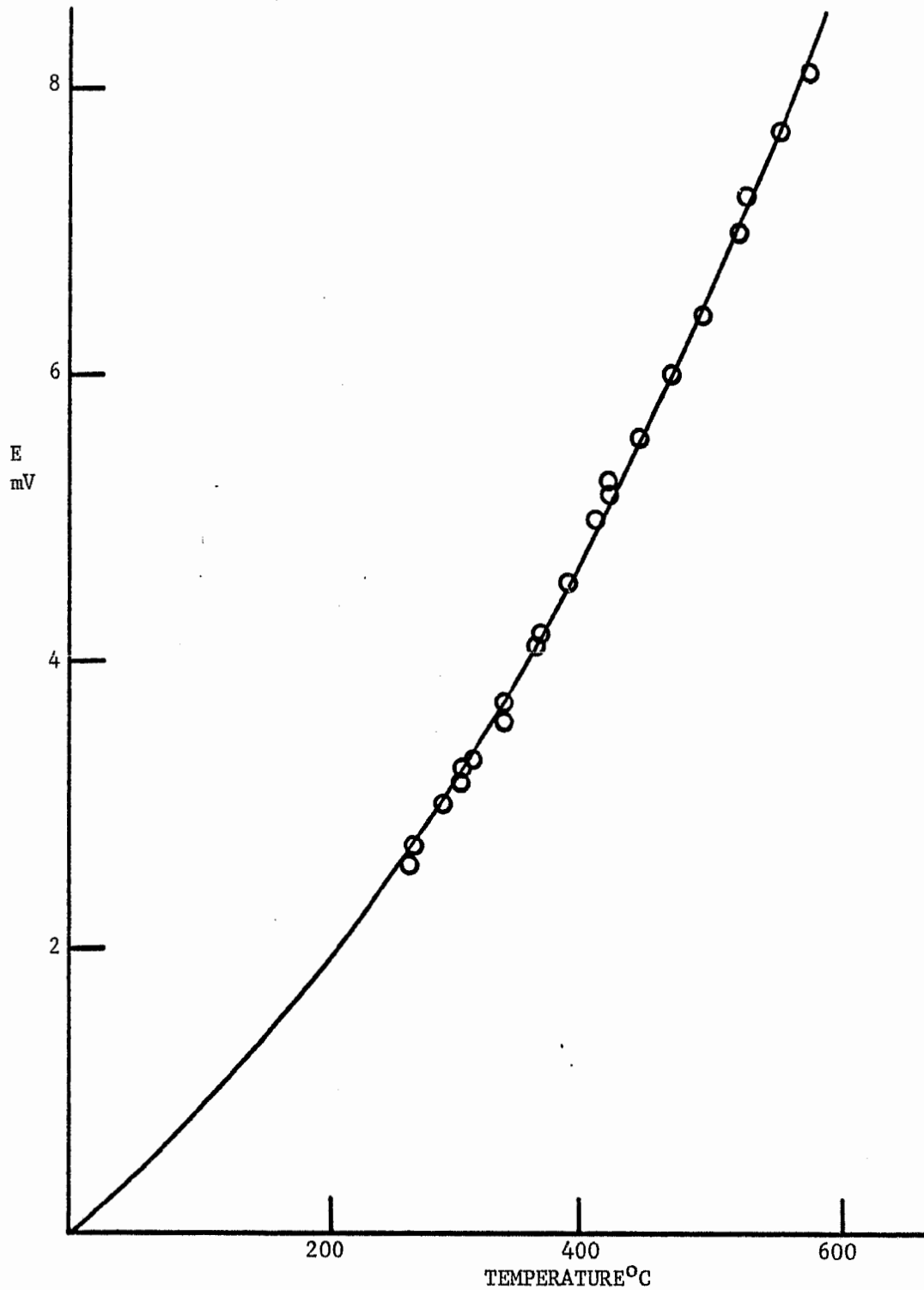


Figure 10.1 EMF of Ag-Pt Thermocouple versus Temperature
Reference Junction at 0°C

TABLE 10.1

POLYNOMIAL FIT FOR THE EMF OF THE Ag-Pt THERMOCOUPLE
AS A FUNCTION OF THE TEMPERATURE

Order	Standard Deviation (mV)
1	0.381
2	0.040
3	0.021
4	0.021
5	33.86

The third and fourth order polynomials gave the best fits for the data and for convenience the third order polynomial was chosen to interpolate the emf of the silver-platinum thermocouple by the equation:

$$\text{emf (mV, Ag "+")} = 0.0004 + 5.11 \times 10^{-3} (T) + 2.09 \times 10^{-5} (T^2) - 9.74 \times 10^{-9} (T^3), (^\circ\text{C}) \quad (10.1)$$

The emf of the thermocouple at temperatures relative to the gas electrode systems were calculated and are summarized in Table 10.2.

TABLE 10.2

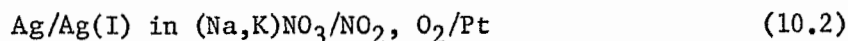
THE EMF OF THE Ag - Pt THERMOCOUPLE
WITH A REFERENCE JUNCTION AT 0°C

Temperature (C°)	Emf (Ag "+") mV
25	0.14
250	2.43
270	2.71
300	3.15
350	3.93
400	4.76
550	7.51

The tabulated results (Table 10.2) are consistently about 0.1 mV greater than the published values (325) which were given only at 100 degree intervals.

The value of dE/dT for the thermocouple is $5.6 \mu\text{V deg}^{-1}$ at 25°C and $16.6 \mu\text{V deg}^{-1}$ at 400°C ; therefore, any fluctuation of 2 or 3 degrees in the room temperature or cell temperature can be neglected in the calculation of the thermocouple emf.

The observed emf, E' , for the cell



operating at the temperature, T , is equal to the sum of the potentials of the chemical cell, E , and the silver-platinum thermocouple, $E_{(\text{Ag-Pt})}$, at the temperature, T , and a reference junction at room temperature (25°C). For a cell at 400°C , $E_{(\text{Ag-Pt})} = -4.62 \text{ mV}$ and the chemical potential of the cell after correction for the thermocouple effect is given by:

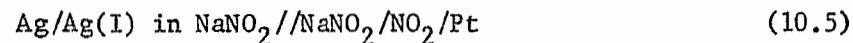
$$E = E' - E_{(\text{Ag-Pt})} \quad (10.3)$$

$$E = E' + 0.0046 \text{ V} \quad (10.4)$$

The values for $E_{(\text{Ag-Pt})}$ in Table 10.2 and equation 10.3 have been used throughout the remainder of chapter 10 to correct all of the gas electrode potentials.

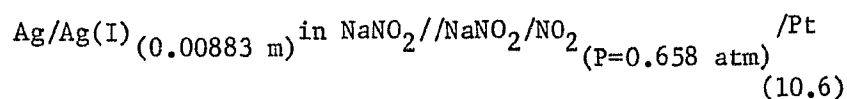
10.2 The $\text{NO}_2^-/\text{NO}_2/\text{Pt}$ Gas Electrode

The gaseous nitrite electrode, $\text{NO}_2^-/\text{NO}_2/\text{Pt}$, was tested at $270 \pm 2^\circ\text{C}$ using the experimental cell:



The 0.00883 molal silver(I)/silver reference electrode was generated coulometrically in a separate fritted compartment to protect the silver from the nitrogen dioxide. The cell emf showed an erratic response to a change in the partial pressure of the nitrogen dioxide. Both the flow rate of the gas mixture ($\text{NO}_2 + \text{N}_2$) and the length of time that the electrode had been in the melt affected the potential of the cell. Reproducible results could not be obtained for any given pressure of nitrogen dioxide. The results from a typical cell at $270 \pm 2^\circ\text{C}$ are compared to the ideal slope predicted by the Nernst equation in Figure 10.2. The results were also plotted in Figure 10.3 in the form of emf versus sequence of measurements. Figures 10.2 and 10.3 show that the behavior of the gaseous nitrite electrode bears no resemblance to that predicted by the Nernst equation and that the emf increases steadily with time except when there is a major change in the partial pressure of the nitrogen dioxide (cf. the P_{NO_2} change from 0.369 to 0.385 atmospheres between the last two points in Figure 10.3).

The observed emf at 270°C for the cell:



was about +0.170 volts or 0.190 volts after correction (to one atmosphere) for the partial pressure of the nitrogen dioxide. In chapter 8.1 (page 178) the emf of the silver nitrite formation cell



was found to be -0.130 volts at 309°C . This cell was combined with

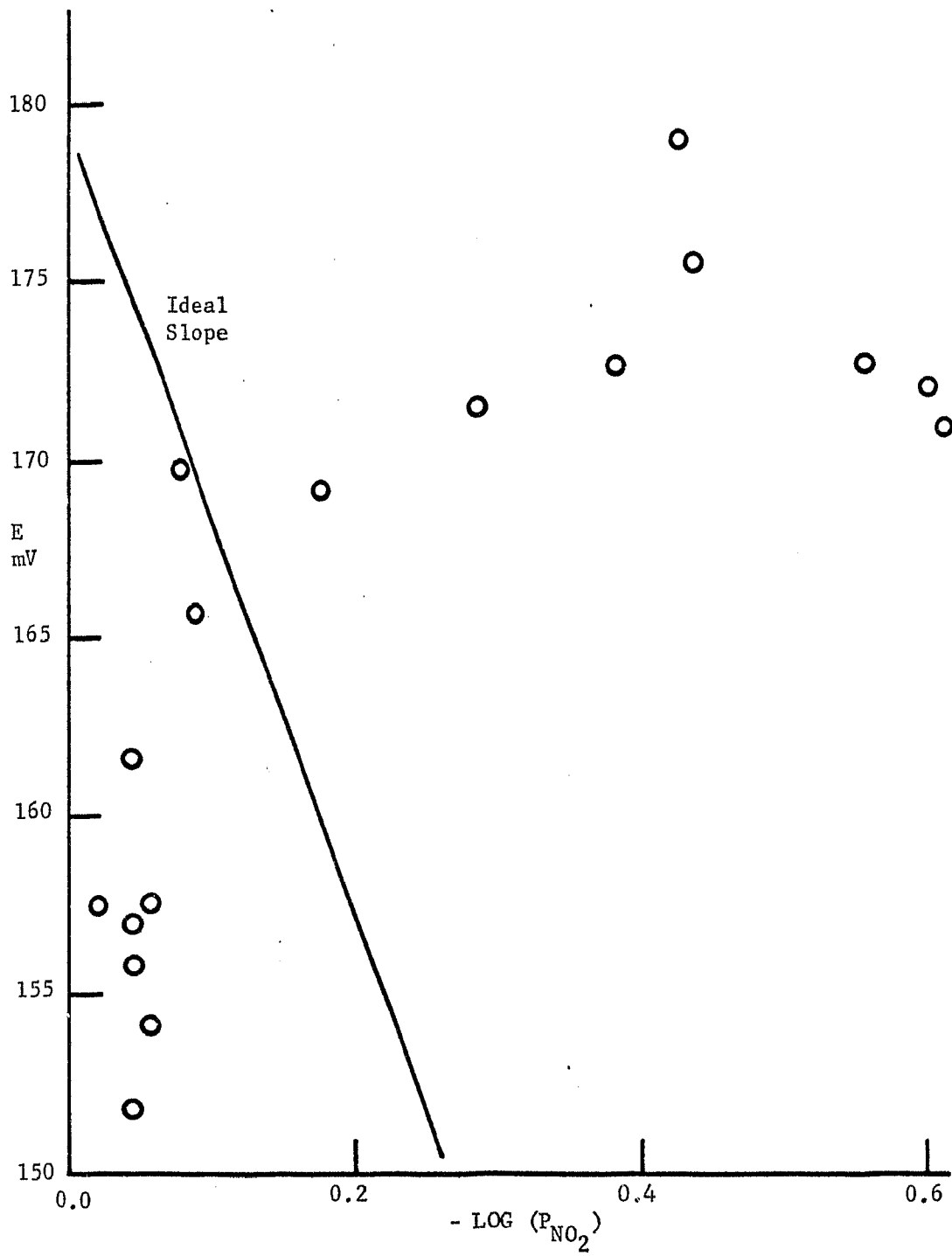


Figure 10.2 EMF of Silver Nitrite Formation Cell at $270 \pm 2^\circ\text{C}$ versus $\log(P_{\text{NO}_2})$

$[\text{AgNO}_3]$ = 0.00883 molal

Solvent = NaNCO_2

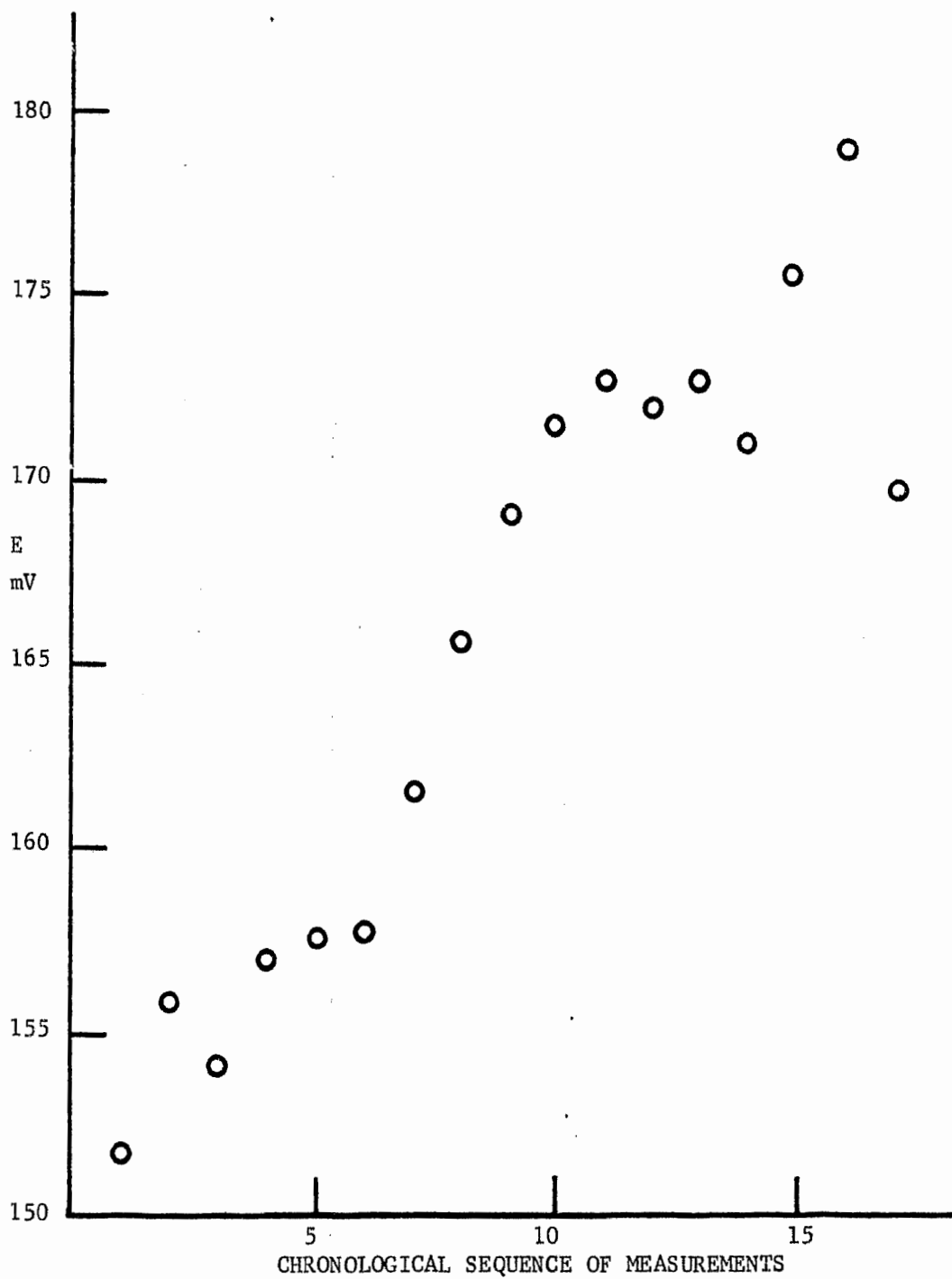


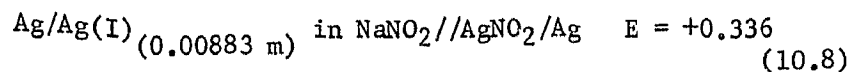
Figure 10.3 EMF of Silver Nitrite Formation Cell at $270 \pm 2^\circ\text{C}$ versus Time

$[\text{AgNO}_2]$ = 0.00883 molal

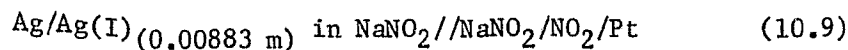
Solvent = NaNO_2

P_{NO_2} varied from 0.95 to 0.25 atm

a silver nitrite concentration cell

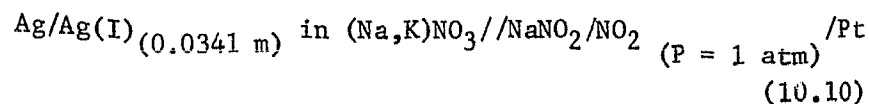


to give a value of +0.206 volts for a cell similar (except for an increase of 39°C) to the experimental cell:

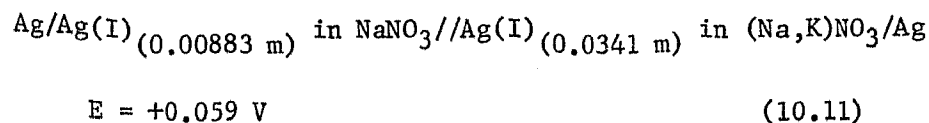


The 16 millivolt difference between the two values for the dilute silver nitrite formation cell is insignificant when compared to the erratic behavior of the emf of the gas electrode.

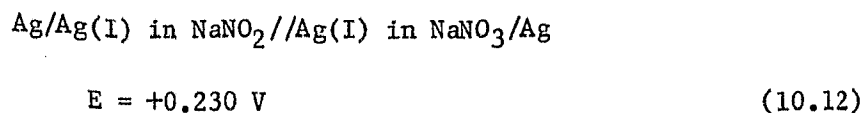
Calandra and Arvia (44) reported a potential of -0.268 volts at 270°C for the cell:



The combination of this cell with a silver concentration cell using the activities from chapter 7.5 (page 142),

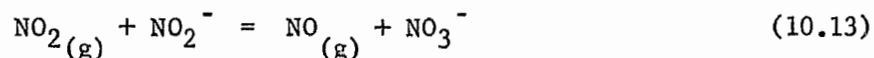


and the solvent junction cell from chapter 8.1, (page 178),



gave a potential of +0.021 volts at 309°C for the experimental silver nitrite formation cell (10.4). The value calculated from Calandra and Arvia's nitrate-nitrite cell differs by as much as 185 mV from the other two determinations and makes the data from their cell suspect.

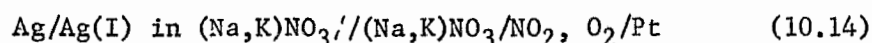
The chemical reaction between the nitrogen dioxide and the nitrite ion



has been verified by several workers (37, 40, 45) and this side reaction may account for the observed time dependancy of the emf of the nitrite gas electrode. It does not appear possible to develop any practical gaseous nitrite electrode and the spurious potentials that are observed have very little if any thermodynamic meaning.

10.3 The $\text{NO}_3^-/\text{NO}_2, \text{O}_2/\text{Pt}$ Gas Electrode

The behavior of the gaseous nitrate electrode was tested by studying the experimental cell



in the temperature range of 250 to 325°C. The silver(I) was generated coulometrically in a separate fritted electrode compartment to protect the silver from the gas electrode and all of the recorded potentials were adjusted to a common 0.030 molal reference electrode by adding the factor

$$\frac{RT}{F} \ln\left(\frac{C}{0.030}\right) \quad (10.15)$$

where C is the molal concentration of the silver nitrate in the compartment.

Gold was used in place of the platinum as the metal in the gas electrode for some of the measurements but there was no substantial difference in the results for the two metals.

The formation potential of the silver nitrate formation cell and the slope of the Nernst plot were found to be a function of the total flow rate of the gases passing through the electrode. The results for several different flow rates after correction for the silver-platinum thermocouple effect (chapter 10.1, page 223) were tabulated in Table 10.3 and plotted in Figure 10.4. The Figure shows that at low flow rates the emf of the cell becomes independent of the flow rate. A total flow rate of 100×10^{-6} moles minute⁻¹ was used in the remainder of the experiments.

TABLE 10.3

POTENTIALS AT $270 \pm 2^\circ\text{C}$ FOR THE CELL:

Ag/Ag(I) (0.030 m) in (Na,K)NO₃//(Na,K)NO₃/NO₂, O₂/Pt

Number of Individual Cells	Total gas flow rate moles minute ⁻¹ x 10 ⁶	Slope of Nernst plot V	E ^o mV
1	300	-0.0903	667 ± 10
1	200	-0.0995	586 ± 5
2	150	-0.1089	558 ± 3
3	100	-0.1102	552 ± 2

The results for the formation cell at $270 \pm 2^\circ\text{C}$ are tabulated in Table 10.4 and presented as a Nernst plot in Figure 10.5 after the silver-platinum thermocouple potential (2.6 mV) correction had been applied to the observed values. The Nernst equation for the experimental nitrate formation cell is:

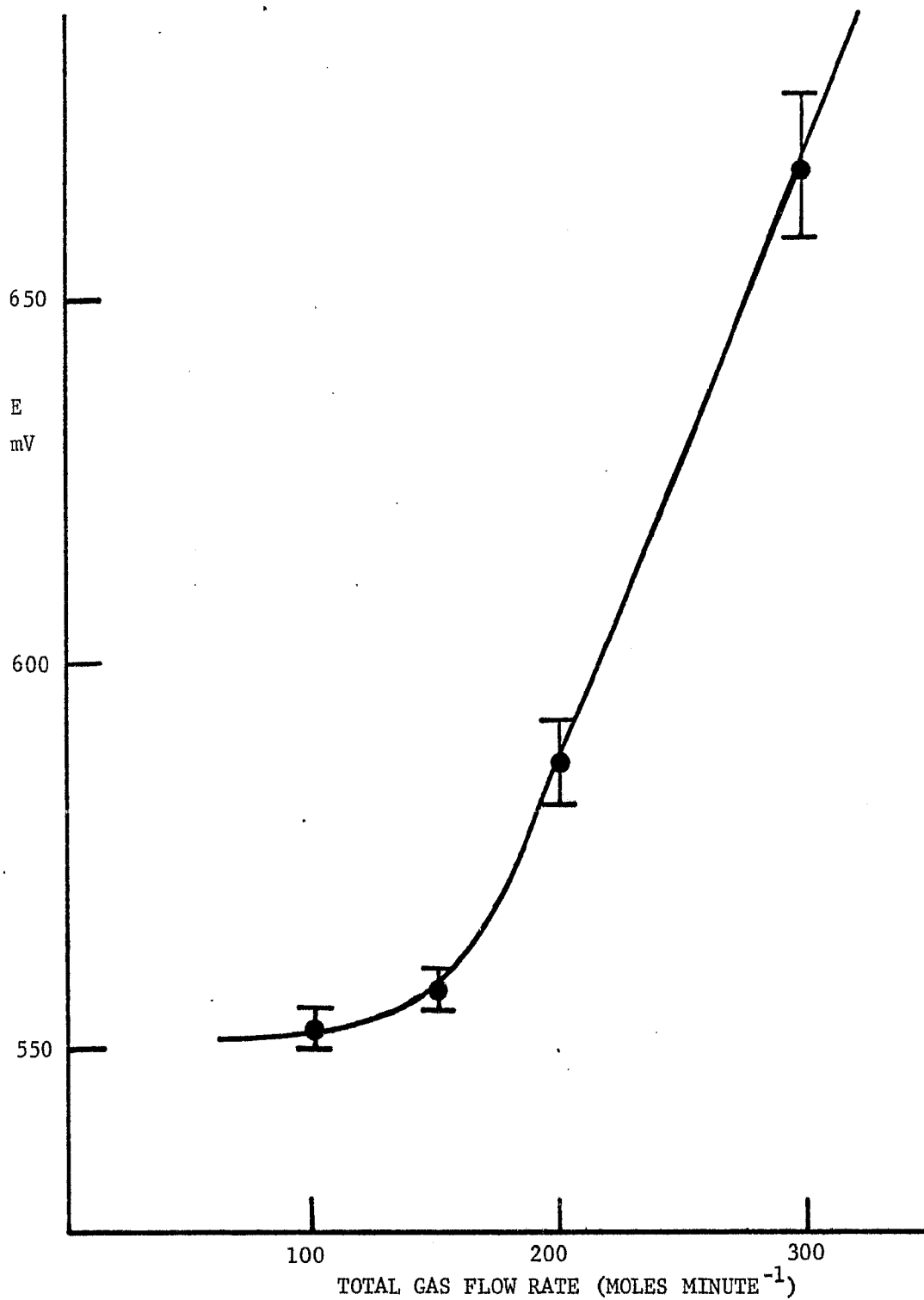


Figure 10.4 Silver Nitrate Formation Cell at $270 \pm 2^\circ\text{C}$ versus Total Flow Rate of $\text{NO}_2 + \text{O}_2$

$[\text{AgNO}_3] = 0.030$

Solvent = $(\text{Na}, \text{K})\text{NO}_3$

TABLE 10.4

CELL POTENTIALS AT 270 ± 2 °C FOR THE CELL:
 Ag/Ag(I) (0.03 m) in (Na,K)NO₃//(Na,K)NO₃/NO₂, O₂/Pt
 (Total gas flow rate = 100×10^{-6} moles minute⁻¹)

P_{N_2} atm	P_{NO_2} atm	P_{O_2} atm	$-\log \left[\frac{P_{NO_2}}{P_{O_2}^{1/2}} \right]$	$-\log [Ag(I)]$ molal	ΔE^* mV	E mV
0.330	0.489	0.119	0.770	-1.4084	12.3	468.8
0.026	0.733	0.179	0.507			498.0
0.129	0.630	0.179	0.573			488.9
0.278	0.481	0.179	0.690			474.4
0.190	0.480	0.268	0.603			488.7
0.103	0.480	0.355	0.542			494.2
0.000	0.484	0.454	0.485			497.3
0.336	0.482	0.120	0.775			468.3
0.117	0.688	0.146	0.580	-1.5732	-5.4	488.9
0.036	0.754	0.161	0.519			497.4
0.184	0.632	0.135	0.634			482.0
0.101	0.740	0.110	0.610			489.1
0.077	0.685	0.189	0.526			497.2

TABLE 10.4--Continued

P_{N_2} atm	P_{NO_2} atm	P_{O_2} atm	$-\log \left[P_{NO_2} P_{O_2}^{1/2} \right]$	$-\log [Ag(I)]$ molal	ΔE^* mV	E mV
0.104	0.608	0.239	0.527			498.1
0.138	0.487	0.326	0.556			490.0
0.118	0.709	0.124	0.603			483.9
0.256	0.363	0.324	0.683	-1.5330	-1.1	474.7
0.099	0.519	0.325	0.527			496.9
0.007	0.616	0.320	0.456			502.9
0.094	0.610	0.239	0.524			492.2
0.000	0.631	0.312	0.451			501.5
0.117	0.623	0.203	0.549			495.0
0.193	0.628	0.122	0.657			484.5

* potential added to cell value to convert to 0.030 molal $AgNO_3$ reference

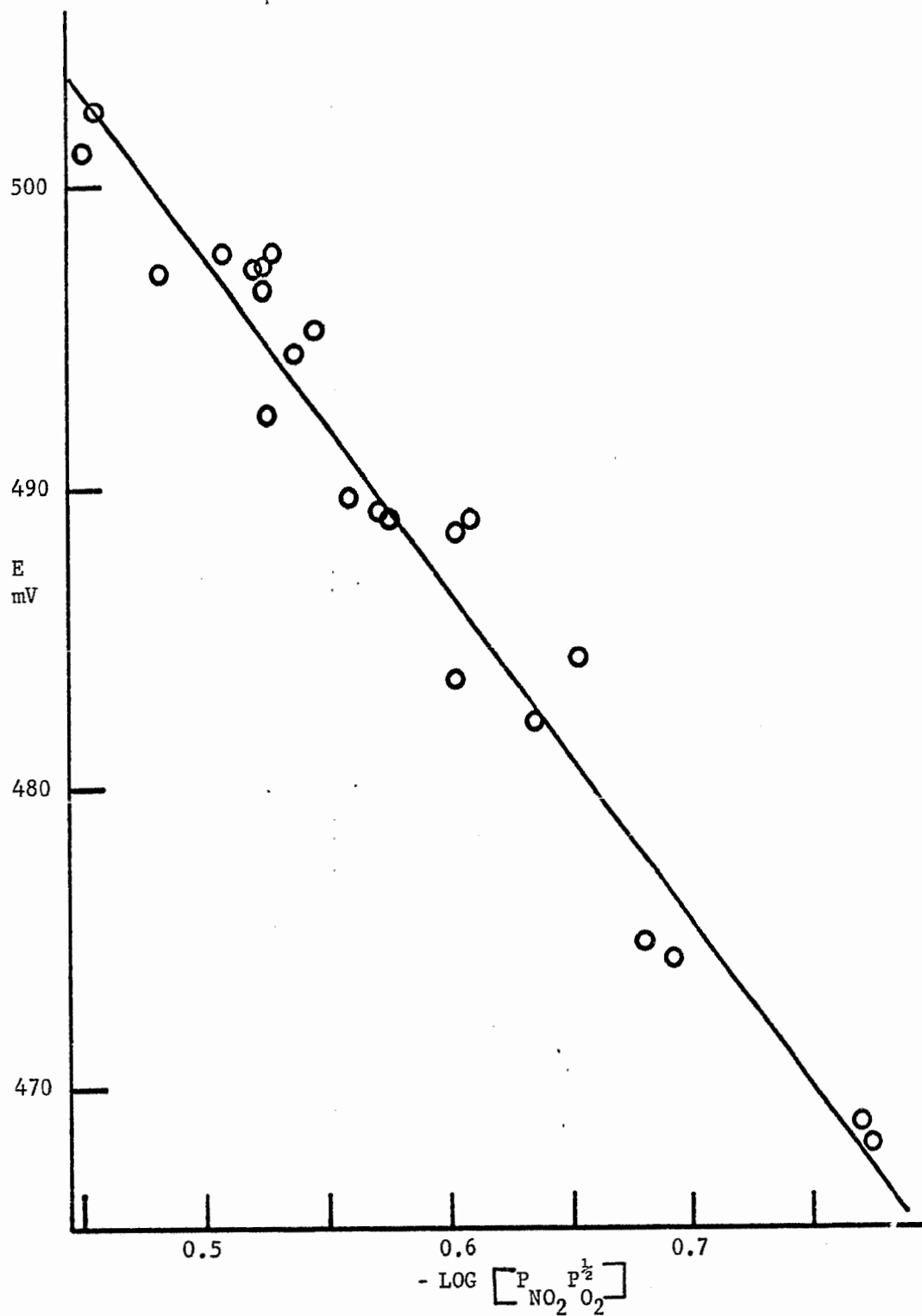


Figure 10.5 EMF of Silver Nitrate Formation Cell at $270 \pm 2^\circ\text{C}$ versus $\log [P_{\text{NO}_2} P_{\text{O}_2}^{1/2}]$

$[\text{AgNO}_3] = 0.030 \text{ molal}$

Solvent = $(\text{Na}, \text{K})\text{NO}_3$

$$E = E_m^{\circ} - \frac{RT}{F} \ln \left[\frac{\gamma_m (0.030)}{P_{\text{NO}_2} P_{\text{O}_2}^{1/2}} \right] \quad (10.16)$$

where γ_m is the silver activity coefficient for a 0.030 molal silver nitrate in the sodium-potassium nitrate eutectic at temperature T. The experimental least squares slope of -0.1103 volts is in agreement with the ideal slope of -0.1077 volts and the standard nitrate electrode potential with respect to the 0.03 molal silver(I) reference electrode at $270 \pm 2^{\circ}\text{C}$ is 0.552 ± 0.002 volts. The experimental cell potential was converted into the three standard formation cell potentials using the activity data in chapter 7.5 (page 142) and equations 7.27 and 7.28. The results are summarized in Table 10.5 along with the results for the cell at several other temperatures (the silver-platinum thermocouple emf has been corrected for).

The calculated E° values in Table 10.5 for the reaction



were derived from published thermodynamic data in the literature (95, 175-177). The experimental E_{N}° and the calculated E° for the chemical reaction 10.17 were in substantial agreement, thus verifying the thermodynamic use of the gaseous nitrate electrode and the $\gamma_{\text{N=O}}$ values determined in chapter 7.5. The plot of E_{N}° versus temperature in Figure 10.6 gave a value of $-0.00203 \text{ V deg}^{-1}$ for dE/dT for the silver nitrate formation cell at 300°C .

The nitrogen dioxide dissociates at elevated temperatures according to the reaction



TABLE 10.5

STANDARD CELL POTENTIALS FOR THE CELL
 Ag/Ag(I) in (Na,K)NO₃//(Na,K)NO₃/NO₂, O₂/Pt
 AS A FUNCTION OF TEMPERATURE (TOTAL GAS
 FLOW RATE OF 100 x 10⁻⁶ moles minute⁻¹)

Number of determinations	Temperature ± 2°C	$\gamma_{N=C}$	E_m^o ± 3 mV	E_M^o ± 3 mV	E_N^o ± 3 mV	$E_{\text{calculated}}^o$ mV
2	250	0.95	443	473	334	332.6
3	270	0.97	403	434	291	291.1
2	300	1.01	344	376	228	229.6
2	350	1.08	252	285	129	128.0
3	400	1.12	159	194	28	28.5

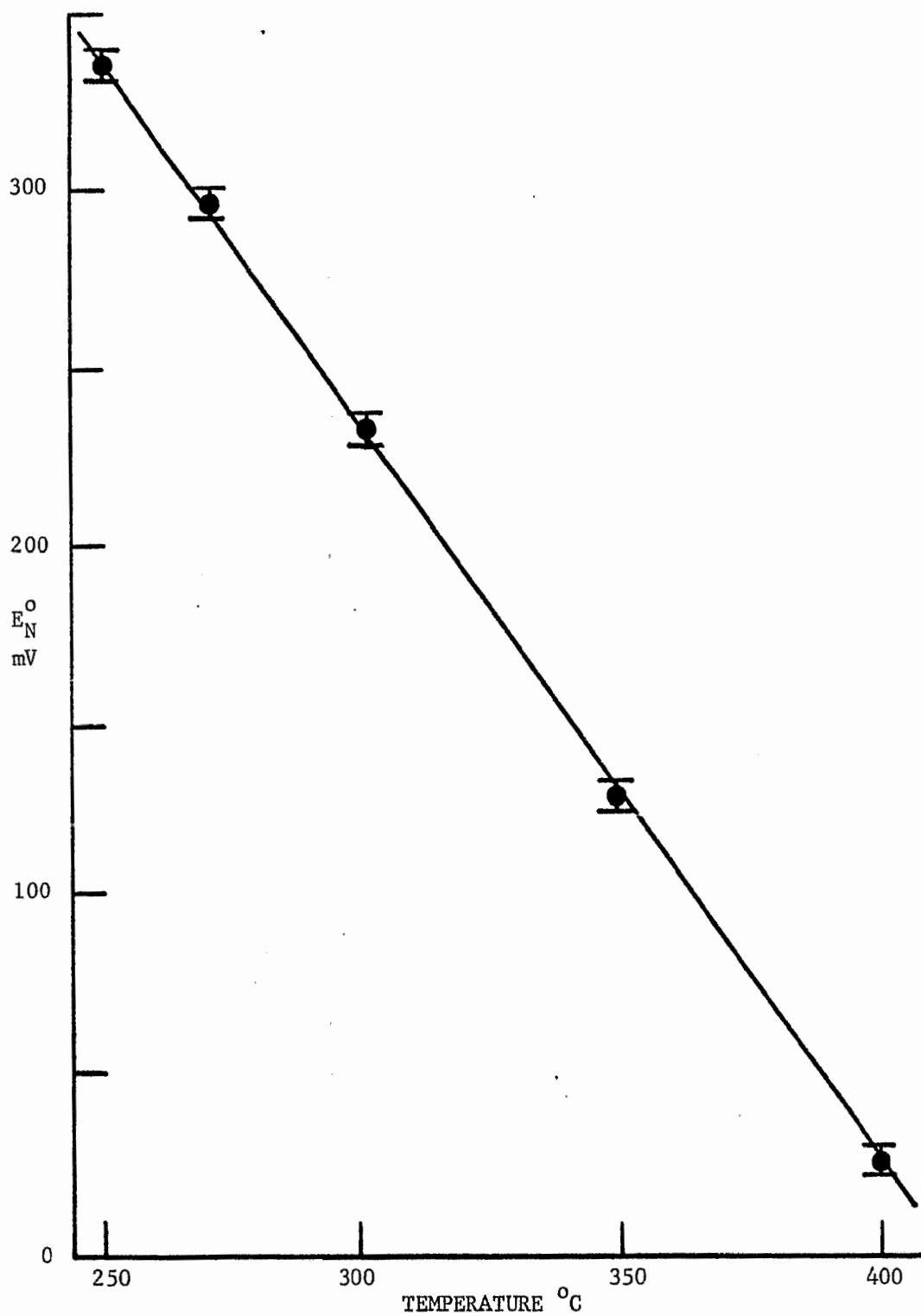


Figure 10.6 Standard Potential of Silver Nitrate Formation Cell Versus Temperature

$$\left[\frac{d E_N^0}{dT} \right]_{300^\circ\text{C}} = -0.00203 \text{ V deg}^{-1}$$

The rate of this relatively slow reaction has been measured by Bodenstein (326) and by Rosser and Wise (181). From their results it can be concluded that the dissociation of nitrogen dioxide under the conditions (e.g., of residence time) prevailing in the experiments can be neglected.

There was close agreement between the results for the nitrate electrode in pure silver nitrate reported by Ketelaar and Dammers-de Klerk (174) and the thermodynamic values; however, there was a considerable difference between their experimental set-up and the flow meters used in this investigation. To obtain the desired mixture of gases they saturated the oxygen stream with nitrogen tetroxide and then partially condensed the nitrogen tetroxide out in a cold trap. The degree of dissociation of nitrogen tetroxide into nitrogen dioxide and the vapor pressure of the two species must be known as a function of the temperature of the cold trap in order to interpret the results of this system. All their measurements were made at a constant gas mixture and the electrode was never tested according to the Nernst equation by varying the partial pressures of the two gases. Their electrode quickly reached its equilibrium emf value and remained constant for long periods of time which is consistent with the results for the electrode in this study. Both of their electrodes and the one in this study were tested for reversibility by subjection to a short pulse of electric current. After the current was switched off, the polarization due to electrolysis vanished completely and the emf of the cell was rapidly restored to its original equilibrium value.

Triaca and Arvia (96) have reported an emf for a nitrate electrode in molten silver nitrate which agreed with the thermodynamic value. Their nitrate electrode was formed by electrolysis of the nitrate melt

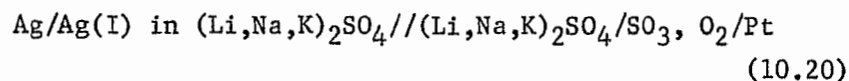


and the emf of the cell was recorded after the current was turned off. As long as the composition of the gas mixture remained constant, so did the emf, but it was destroyed at a faster rate by the bubbling of nitrogen around the anode than by the bubbling of oxygen. In their calculations the total pressure of the 2:1 ratio of nitrogen dioxide and oxygen was assumed to be one atmosphere. As the oxidation of the nitrate ion has been the subject of controversy (chapter 3.2, page 23), their results should first be verified by other independent workers before being accepted.

The advantages inherent in the system used for this study were an ease of construction and a means of independently varying the partial pressures of each gas, including an inert gas. This allows the verification of the ideal Nernst behavior of the electrode and the use of a much more versatile electrode system.

10.4 The $\text{SO}_4^{2-}/\text{SO}_3, \text{O}_2/\text{Pt}$ Gas Electrode

The experimental cell



was used to develop and test the gaseous sulfate electrode in the

ternary eutectic at $550 \pm 2^\circ\text{C}$. A procedure similar to that for the gaseous nitrate electrode (chapter 10.3, page 231) was used in the operation of the gaseous sulfate electrode. The flow rate of the gases through the gas electrode affected the formation potential, E° , of the silver sulfate cell less than it did in the corresponding nitrate cell. Preliminary trials showed the E° value to be independent of the flow rate provided the total flow rate was less than 300×10^{-6} moles minute^{-1} ; therefore, flow rates in the range of 100 to ~~200~~ 100 moles minute^{-1} were used in the remainder of the measurements.

The gas electrode required approximately 15 to 30 minutes to stabilize after each change in the sulfur trioxide-oxygen gas ratio. To test the overall stability of the electrode, a constant gas mixture was passed through the gas electrode for 5 hours during which time the potential remained constant to ± 3 millivolts for the entire period. The gas electrode was shorted out for periods up to 5 seconds using a third counter platinum electrode and within one to two minutes after, the potential of the silver sulfate formation cell would re-establish itself at the original value. These facts established the gaseous sulfate electrode as a stable and reversible reference electrode in sulfate melts.

The results for the silver sulfate cell at $550 \pm 2^\circ\text{C}$ are tabulated in Table 10.6. The potentials have been adjusted to a 1.0 molal silver(I)/silver reference electrode and corrected for the thermocouple emf of 7.4 mV (chapter 10.1, page 223). The least

squares slope of the Nernst plot (Figure 10.7) of the data in Table 10.6 is 0.08357 and the standard deviation of the points is 0.0020 volts from the theoretical slope of 0.08165 volts. Equations 7.27 and 7.28 were used to calculate the formation potentials on the molar and mole fraction concentration scales; however, the lack of data on the activity of silver(I) in the sulfate melts necessitated the assumption of ideal behavior in all the calculations. The results of these calculations are summarized in Table 10.7.

TABLE 10.6

POTENTIALS AT $550 \pm 2^\circ\text{C}$ FOR THE CELL:

Ag/Ag(I) (1.0 m) in $(\text{Li,Na,K})_2\text{SO}_4 // (\text{Li,Na,K})_2\text{SO}_4/\text{SO}_3, \text{O}_2/\text{Pt}$
 (Total gas flow rate = $(100 \text{ to } 200) \times 10^{-6}$ moles minute $^{-1}$)

P_{SO_3} atm	P_{O_2} atm	$-\log \left[P_{\text{SO}_3} P_{\text{O}_2}^{\frac{1}{2}} \right]$	E mV
0.600	0.350	0.4497	737.9
0.572	0.378	0.4538	736.6
0.416	0.534	0.5171	729.6
0.422	0.528	0.5109	729.3
0.428	0.522	0.5097	735.2
0.633	0.317	0.4481	736.2
0.600	0.350	0.4497	736.6
0.552	0.398	0.4581	740.2
0.453	0.497	0.4957	735.0
0.373	0.577	0.5477	735.0
0.390	0.560	0.5348	732.2
0.390	0.267	0.6956	719.0

TABLE 10.6 --Continued

P_{SO_3} atm	P_{O_2} atm	$-\log \left[P_{\text{SO}_3} P_{\text{O}_2}^{\frac{1}{2}} \right]$	E mV
0.606	0.154*	0.6237	720.0
0.842	0.108	0.5580	727.7
0.706	0.022*	0.9800	692.9
0.761	0.036*	0.8423	705.1

* The oxygen was diluted with nitrogen to obtain lower oxygen pressures.

TABLE 10.7

POTENTIALS AT $550 \pm 2^\circ\text{C}$ FOR THE CELL:

Ag/Ag(I) in $(\text{Li,Na,K})_2\text{SO}_4 // (\text{Li,Na,K})_2\text{SO}_4/\text{SO}_3, \text{O}_2/\text{Pt}$

E_m° (measured), V	0.767 ± 0.002
$E_{(\text{Ag-Pt})}$ Thermocouple correction, V	0.0074
E_m° (chemical), V	0.774 ± 0.002
E_M° (chemical), V	0.827 ± 0.002
E_N° (chemical), V	0.575 ± 0.002

Hauffe and Hoeffgen (276) reported an experimental value of 0.555 volts and a calculated value of 0.508 volts for the formation of silver sulfate which compared well with the E_N° value (cf. Table 10.7) of 0.575 volts at 550°C . They assumed the activity coefficient

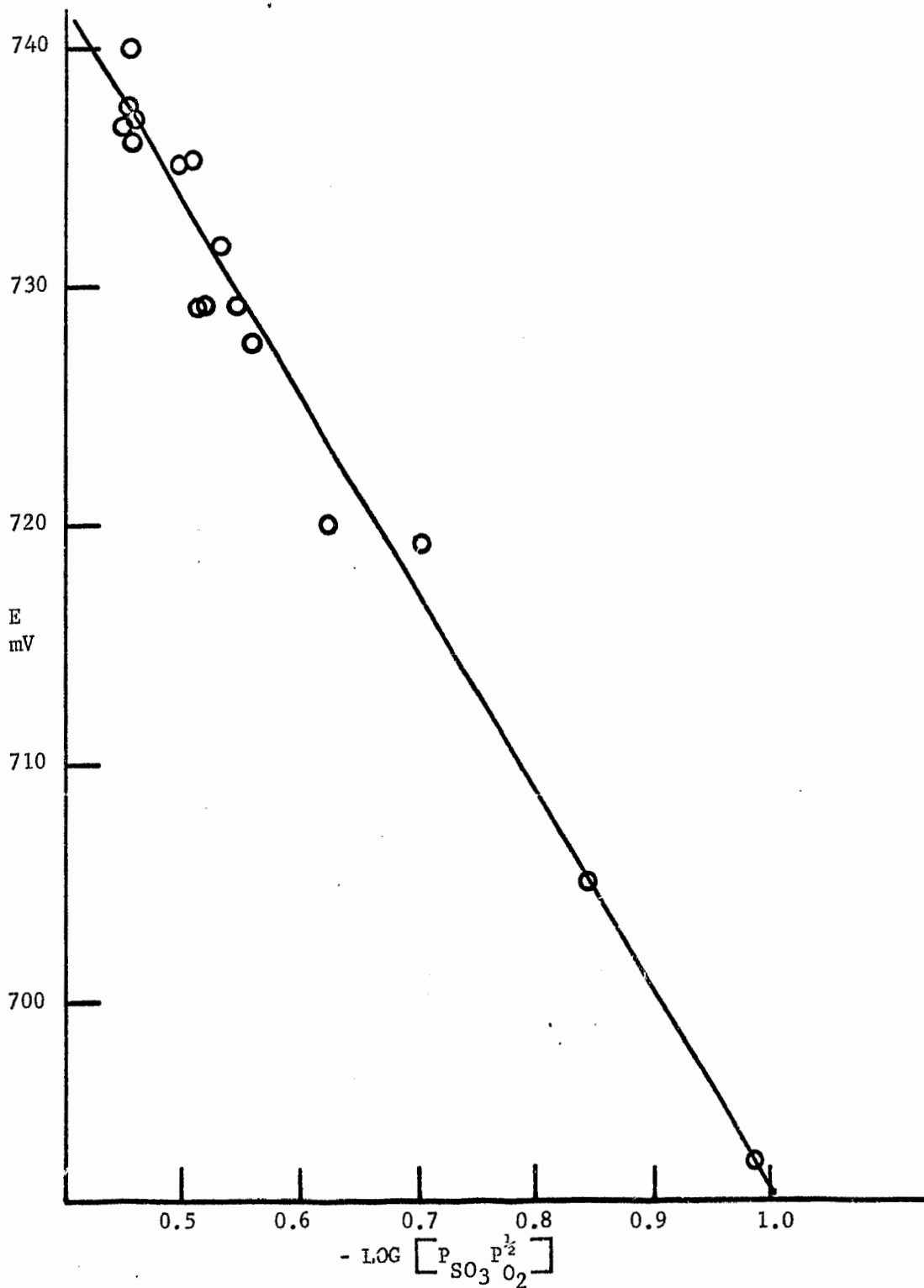


Figure 10.7 EMF of Silver Sulfate Formation Cell at $550 \pm 2^\circ\text{C}$ Versus $\log [\text{P SO}_3 \text{P}^{1/2} \text{O}_2]$

$[\text{Ag(I)}] = 1.0$ molal
 Solvent = $(\text{Li, Na, K})_2\text{SO}_4$

to be unity and operated their cell (containing solid "tempered" pellets of pure silver sulfate) at 600°C; this assumption and the 50 C° difference between their cell and the one used in this study is most probably the source of discrepancy between the two results. From polarographic analysis of the alkali sulfate melts, the oxidation of the sulfate anion has been reported (by Liu (264) using the binary sulfate eutectic at 625°C and by Johnson and Laitinen (261) using the ternary sulfate eutectic at 550°C) to occur between +0.6 and +0.9 volts versus a 1.0 molal silver(I)/silver reference electrode. The E_m^0 value of 0.774 volts (Table 10.7) lies in the middle of the polarographic results and thus supports their validity. Unfortunately, the thermodynamic data necessary to the calculation of the free energy value for the formation of silver sulfate at 550°C was not available in the literature; however, the E_N^0 from Table 10.7 gave a value of

$$\Delta G_{550^\circ\text{C}}^0 = -26.6 \pm 0.1 \text{ kcal mole}^{-1} \quad (10.21)$$

for the reaction



10.5 The H(I)/H₂/Pt Gas Electrode

A Cl⁻/H₂, HCl/Pt gas electrode in the lithium potassium chloride eutectic at 450°C has been developed by Laitinen and Plambeck (196). The electrode consisted of a mixture of hydrogen and hydrogen chloride gas bubbled over a platinum flag immersed in the chloride melt.

The combination of this electrode with a chlorine electrode produces a hydrogen chloride formation cell



The standard cell potentials, regardless of concentration scale, are

$$E_{400}^{\circ} = 1.013 \pm 0.006 \text{ V} \quad (10.24)$$

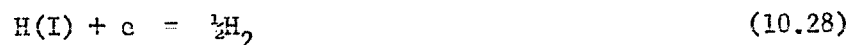
$$E_{450}^{\circ} = 1.016 \pm 0.005 \text{ V} \quad (10.25)$$

$$E_{550}^{\circ} = 1.023 \pm 0.006 \text{ V} \quad (10.26)$$

$$\frac{dE_{450}^{\circ}}{dT} = (0.070 \pm 0.011) \times 10^{-3} \text{ V deg}^{-1} \quad (10.27)$$

and these values compare very well with the thermodynamic values.

Unfortunately, this electrode is a hydrogen chloride/hydrogen gas electrode rather than a hydrogen(I)/hydrogen gas electrode. The experimental electrode reaction consists of two separate reactions:



The concentration of the hydrogen ion produced by equation 10.29 can be calculated from the solubility of hydrogen chloride in the chloride melt provided the dissolved hydrogen chloride is totally ionized in the melt. The rapid ionization of gaseous acids in melts has been verified by the conclusions of Haug and Albright (327) in their study of the kinetics of the reaction between nitric acid vapors and chloride melts to form hydrogen chloride and the corresponding reaction between hydrogen chloride and nitrate melts to form nitric acid. Ukshe and Devijatkin (251, 252) have measured

the solubility of hydrogen chloride in the pure alkali metal chloride melts and a melt containing various proportions of sodium chloride in potassium chloride. By extrapolating their data, the mole fraction concentration of hydrogen chloride in the melt at several temperatures was calculated to be

$$N_{400^{\circ}\text{C}} = 3.0 \times 10^{-5} P_{(\text{atm.})} \quad (10.30)$$

$$N_{450^{\circ}\text{C}} = 6.5 \times 10^{-5} P_{(\text{atm.})} \quad (10.31)$$

$$N_{550^{\circ}\text{C}} = 2.3 \times 10^{-4} P_{(\text{atm.})} \quad (10.32)$$

The hydrogen(I) concentration is given by

$$[\text{H(I)}] = K P_{\text{HCl}} \quad (10.33)$$

and the electrode potential is given by

$$E = E_{\text{N}}^{\circ} - \frac{RT}{F} \ln \frac{[\text{H(I)}]}{(P_{\text{H}_2})^{\frac{1}{2}}} = E_{\text{N}}^{\circ} - \frac{RT}{F} \ln \frac{K P_{\text{HCl}}}{(P_{\text{H}_2})^{\frac{1}{2}}} \quad (10.34)$$

The electrode potential for the hydrogen chloride gas electrode (196) is related to the gas pressures by

$$E = E_{\text{HCl}}^{\circ} - \frac{RT}{F} \ln \frac{P_{\text{HCl}}}{(P_{\text{H}_2})^{\frac{1}{2}}} \quad (10.35)$$

and the difference between the two standard electrode potentials is

$$E_{\text{N}}^{\circ} = E_{\text{HCl}}^{\circ} + \frac{RT}{F} \ln K \quad (10.36)$$

The standard cell potentials for the cell

$$\text{H}_2/\text{H(I)} \text{ in } (\text{Li,K})\text{Cl} // (\text{Li,K})\text{Cl}/\text{Cl}_2/\text{C} \quad (10.37)$$

were calculated from the data for the hydrogen chloride formation

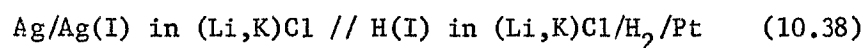
cell using equations 7.27, 7.28 and 10.36 on the assumption that $\gamma_{N=0}$ for the hydrogen ion was unity. The results are summarized in Table 10.8.

TABLE 10.8

STANDARD CELL POTENTIALS FOR THE CELL:
 $H_2/H(I)$ in $(Li,K)Cl // (Li,K)Cl / Cl_2/C$

Temperature ($^{\circ}C$)	E_m° (V)	E_M° (V)	E_N° (V)
400	0.577	0.602	+0.409
450	0.595	0.620	+0.415
550	0.634	0.660	+0.429

The standard cell potentials for the silver chloride formation cell have been reported by Yang and Hudson (207) for the mole fraction scale as a function of temperature. These potentials were converted to corresponding values on the other concentration scales using equations 7.24 and 7.25 and the $\gamma_{N=0}$ values determined from emf data (207). The results are tabulated in Table 10.9 and have been combined with the data from Table 10.8 to give the standard potentials (Table 10.10) for the cell:



The data in Table 10.10 and the silver solvent junction potentials make possible the direct correlation of the hydrogen(I)/hydrogen gas electrode with any emf series in the nitrate and chloride melts

at 400°C, and the sulfate, chloride and carbonate melts at 550°C. The combination of the hydrogen gas electrode with a gas electrode which is reversible to one of the oxyanions provides a direct measure for the formation potential of that oxyacid. This aspect of the project will be discussed more fully in chapter 11 (page 252).

TABLE 10.9

STANDARD CELL POTENTIALS FOR THE CELL:
 Ag/Ag(I) in (Li,K)Cl // (Li,K)Cl/Cl₂/C

Temperature (°C)	$\chi_{N=0}$	E_m° (V)	E_M° (V)	E_N° (V)
400	2.04	1.056	1.081	0.929
450	1.93	1.054	1.079	0.915
550	1.76	1.051	1.077	0.886

TABLE 10.10

STANDARD CELL POTENTIALS FOR THE CELL:
 Ag/Ag(I) in (Li,K)Cl // H(I) in (Li,K)Cl/H₂/Pt

Temperature (°C)	E_m° (V)	E_M° (V)	E_N° (V)
400	0.479	0.479	0.520
450	0.459	0.459	0.500
550	0.417	0.417	0.457

It is interesting to compare the results for the silver chloride cell in lithium potassium chloride at 450°C (Table 10.9) with

those tabulated by Plambeck (20). The comparison (Table 10.11) shows the literature values to be about 1.5% low for the molal and molar scales and 7% low on the mole fraction scale. The difference in the E_N° is due to the different definitions for the standard states of the mole fraction scale. Plambeck's value is based on the definition that $\gamma \rightarrow 1$ as $N \rightarrow 0$, whereas the definition used in this work and by many other workers (36, 133-137, 187) is that $\gamma \rightarrow 1$ as $N \rightarrow 1$ and $\gamma \rightarrow \gamma_{N=0}$ as $N \rightarrow 0$. The difference for the other two scales should be zero. The error may be due to the assumption that the activity of the chloride ion is the same in the silver chloride melt as it is in the lithium potassium chloride eutectic or a small error in the value of $\gamma_{N=0}$ for the silver chloride in the chloride eutectic. The error is equivalent to a change in $\gamma_{N=0}$ from 1.93 to 2.08. The latter is probably the source of the largest portion of error since a change of only 4.7 millivolts will produce a change in $\gamma_{N=0}$ from 1.93 to 2.08 and the normal error in each half cell potential is ± 2 millivolts.

TABLE 10.11

STANDARD CELL POTENTIALS AT 450°C FOR THE CELL:

Ag/Ag(I) in (Li,K)Cl // (Li,K)Cl/Cl₂/C

Source of data	Table 10.9	Plambeck (20)	% Difference
E_m° V	1.054	1.033	2.0
E_M° V	1.079	1.065	1.3
E_N° V	0.915	0.853	7.0

11. CONCLUSIONS AND DISCUSSION

11.1 Summary of Results

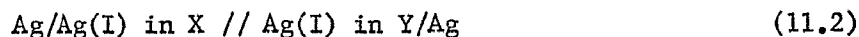
In this study the potentials of the silver(I)/silver electrode and several gaseous electrodes have been determined as a function of the nature of the fused salt solvent and the temperature of the electrochemical cell. In the literature review on the electrochemistry of fused alkali metal salts (chapters 2 through 6) a major portion was devoted to the nitrate melts to complement the published reviews on other fused salt systems. The densities (Table 7.9, page 138) and silver nitrate activity coefficients (Table 7.13, page 168) for the pure and the binary mixtures of the lithium, sodium and potassium nitrate salts were measured in the temperature range of 200 to 400°C. Previously published silver nitrate activity coefficients, γ , for the mole fraction scale are compared with the values from this study along with the calculated values for the molar and molal concentration scales in Figures 7.14 - 7.31 (pages 150 - 167). The silver nitrate exhibited a positive deviation from ideality (i.e., $\gamma > 1$) in the nitrate solvents containing lithium ions, a negative deviation (i.e., $\gamma < 1$) in the potassium nitrate solvent and almost ideal behavior (i.e., $\gamma = 1$) in the sodium-potassium nitrate eutectic. The advantage of the latter is further heightened by the fact

that most of the electrochemistry in nitrate melts has been carried out in the sodium-potassium nitrate eutectic. The results for the thermoelectric measurements in the silver nitrate-sodium-potassium nitrate eutectic system (Figure 9.2, page 218) are about mid-way between the published results which cite either the pure sodium or the pure potassium nitrate as the solvent. The published potentials for the silver nitrate formation cell were substantially close to the experimental values obtained (Table 10.5, page 238) using a new design for the gaseous nitrate electrode,



and a versatile gas control system which allowed the independent variation of the partial pressures of the nitrogen dioxide and oxygen by introducing a known amount of an inert gas (nitrogen) into the gas mixture.

The emf series in two different melts can be correlated by examining a solvent cell of the type:



The nitrite//nitrate solvent cell at 309°C (Table 8.2, page 185), the nitrate//chloride solvent cell at 400°C (Table 8.6, page 199), and the chloride//sulfate solvent cell at 550°C (Table 8.9, page 209) were measured to facilitate the development of a single emf series for all of the electrodes in the various alkali metal salt melts.

The emf series in the ternary sulfate eutectic at 550°C was extended by the development of a reversible gaseous sulfate electrode,

(chapter 10.3, page 231)



to give a potential of 0.575 volts for the pure silver sulfate formation cell (Table 10.7, page 244). In molten sodium nitrite at 270°C, an emf time-dependency (Figure 10.3, page 229) rather than the expected Nernst emf pressure-dependency (Figure 10.2, page 228) was observed for the gaseous nitrite electrode;



The results obtained for a reversible gaseous nitrite electrode are contradictory (chapter 2.3, page 16): however, this study as well as the majority of published results support the existence of a chemical reaction between the nitrogen dioxide and nitrite ion rather than the electro-reduction of the nitrogen dioxide at the electrode. The standard electrode potential for the hydrogen-hydrogen chloride electrode in the lithium-potassium chloride eutectic and the solubility of hydrogen chloride in the eutectic were used to calculate the potential of the hydrogen(I)/hydrogen electrode at 400, 450 and 550°C (Table 10.10, page 250).

11.2 Development of a Unified Emf Series

The electrode potentials in several alkali metal salt melts at temperatures ranging from 300 to 550°C can be related to one common reference electrode, the standard aqueous hydrogen electrode (S.H.E.) at 25°C, by combining solvent cells (chapter 8, page 178) and thermo-electric cells (chapter 9, page 211). Activities rather than

concentrations are used in the calculations involving the nitrate and chloride melts (chapter 7, page 111); however, due to the lack of published data, ideal behavior is assumed for all of the other melts. The mole fraction standard cell potentials, E_N^0 , (tabulated in Table 11.1) are used to correlate the various electrode systems and equations 7.21, 7.24, 7.27 and 7.28 are used to convert the standard potentials from the mole fraction scale to the molar and molal scales. No conversion is required for the gaseous anion electrodes since, for this type of electrode, all three concentration scales use identical units and standard states. The final unified emf series based on the S.H.E. at 25°C is given in Table 11.2. Computational errors were found in the conversion from E_m^0 to E_N^0 in the published emf series for the lithium, sodium carbonate eutectic (287) and the lithium, sodium, potassium sulfate eutectic (261). These errors resulted from using the entire molecular weight of the carbonate and sulfate salts instead of half the molecular weight in the calculations. The activity of an ideal salt is given by the product of the cation and anion ion-fractions raised to their appropriate power; however, in a uni-univalent system containing a single anion, the ion fraction product for a salt is equivalent to its mole fraction (chapter 7.1, page 111). In the sulfate and carbonate melts the anion fractions are equal to unity and since each molecule contains two cations, in the calculations the cation fraction must be used instead of the mole fraction; this is equivalent to using half the solvent's molecular weight. The corrected values are given in Tables 11.3 and 11.4 and have been used throughout chapter 11.

TABLE 11.1

ELECTROCHEMICAL CELLS USED TO DEVELOP UNIFIED EMF SERIES

Left Half Cell		Right Half Cell		Source of data	E_N° (V)
T ^o C	Components	Components	T ^o C		
25	H ₂ /H(I) in H ₂ O	Ag(I) in TlNO ₃ /Ag	86	Eq. 3.170, p. 71	0.856
86	Ag/Ag(I) in TlNO ₃	Ag(I) in NaNO ₃ /Ag	300	Eq. 9.24, p. 220	-0.065
300	Ag/Ag(I) in (Na,K)NO ₃	(Na,K)NO ₃ /NO ₂ , O ₂	300	Table 10.5, p. 238	0.228
300	Ag/Ag(I) in NaNO ₃	Ag(I) in NaNO ₃ /Ag	309	Eq. 9.24, p. 220	-0.003
309	Ag/Ag(I) in NaNO ₃	Ag(I) in NaNO ₂ /Ag	309	Table 8.2, p. 185	-0.219
309	Ag/Ag(I) in (Na,K)NO ₃	(Na,K)NO ₃ /NO ₂ , O ₂	309	Table 10.5, p. 238	0.210
309	Ag/Ag(I) in NaNO ₃	Ag(I) in NaNO ₃ /Ag	350	Eq. 9.24, p. 220	-0.014
350	Ag/Ag(I) in (Na,K)NO ₃	(Na,K)NO ₃ /NO ₂ , O ₂	350	Table 10.5, p. 238	0.129
350	Ag/Ag(I) in NaNO ₃	Ag(I) in NaNO ₃ /Ag	400	Eq. 9.24, p. 220	-0.016
400	Ag/Ag(I) in (Li,K)NO ₃	Ag(I) in (Li,K)Cl/Ag	400	Table 8.6, p. 199	-0.668
400	Ag/Ag(I) in (Na,K)NO ₃	(Na,K)NO ₃ /NO ₂ , O ₂	400	Table 10.5, p. 238	0.028

TABLE 11.1--Continued

Left Half Cell		Right Half Cell		Source of data	E _N ^o (V)
T ^o C	Components	Components	T ^o C		
400	Ag/Ag(I) in (Li,K)Cl	(Li,K)Cl/Cl ₂	400	Table 10.9, p. 250	0.929
400	Cl ₂ /(Li,K)Cl	(Li,K)Cl/HCl, H ₂	400	Ref. 196	-1.013
400	Cl ₂ /(Li,K)Cl	H(I) in (Li,K)Cl/H ₂	400	Table 10.8, p. 249	-0.409
400	Ag/Ag(I) in (Li,K)Cl	Ag(I) in (Li,K)Cl/Ag	450	Eq. 9.37, p. 221	-0.019
450	Ag/Ag(I) in (Li,K)Cl	(Li,K)Cl/Cl ₂	450	Table 10.9, p. 250	0.915
450	Cl ₂ /(Li,K)Cl	(Li,K)Cl/HCl, H ₂	450	Ref. 196	-1.016
450	Cl ₂ /(Li,K)Cl	H(I) in (Li,K)Cl/H ₂	450	Table 10.8, p. 249	-0.415
450	Ag/Ag(I) in (Li,K)Cl	Ag(I) in (Li,K)Cl/Ag	550	Eq. 9.37, p. 221	-0.037
550	Ag/Ag(I) in (Li,K)Cl	(Li,K)Cl/Cl ₂	550	Table 10.9, p. 250	0.886
550	Cl ₂ /(Li,K)Cl	(Li,K)Cl/HCl, H ₂	550	Ref. 196	-1.023
550	Cl ₂ /(Li,K)Cl	H(I) in (Li,K)Cl/H ₂	550	Table 10.8, p. 249	-0.429
550	Ag/Ag(I) in (Li,K)Cl	Ag(I) in (Li,Na,K) ₂ SO ₄ /Ag	550	Table 8.9, p. 209	0.757

TABLE 11.1--Continued

Left Half Cell		Right Half Cell		Source of data	E_N^0 (V)
$T^{\circ}\text{C}$	Components	Components	$T^{\circ}\text{C}$		
550	Ag/Ag(I) in $(\text{Li,Na,K})_2\text{SO}_4$	$(\text{Li,Na,K})_2\text{SO}_4/\text{SO}_3, \text{O}_2$	550	Table 10.7, p. 244	0.575
550	Ag/Ag(I) in $(\text{Li,Na,K})_2\text{SO}_4$	Ag(I) in $(\text{Li,Na})_2\text{CO}_3/\text{Ag}$	550	Ref. 135	0.237
550	Ag/Ag(I) in $(\text{Li,Na})_2\text{CO}_3$	$(\text{Li,Na})_2\text{CO}_3/\text{CO}_2, \text{O}_2$	550	Ref. 135	-0.490

TABLE 11.2

UNIFIED EMF SERIES FOR MOLTEN SALTS

Electrode Couple	Solvent	T°C	E_m° (V)	E_M° (V)	E_N° (V)	
H(I)/H ₂	H ₂ O	25	0.000	0.000	0.000	
Ag(I)/Ag	(Na,K)NO ₃	300	0.675	0.643	0.791	
	NaNO ₃	309	0.687	0.663	0.788	
	NaNO ₂	309	0.457	0.437	0.569	
	(Na,K)NO ₃	309	0.661	0.638	0.788	
		350	0.651	0.618	0.774	
		400	0.627	0.592	0.758	
	(Li,K)NO ₃	400	0.653	0.620	0.758	
	(Li,K)Cl	400	-0.037	-0.062	0.090	
		450	-0.068	-0.093	0.071	
		550	-0.131	-0.157	0.034	
		(Li,Na,K) ₂ SO ₄	550	0.586	0.539	0.791
		(Li,Na) ₂ CO ₃	550	0.334	0.284	0.554
NO ₃ ⁻ /NO ₂ , O ₂	(Na,K)NO ₃	300	1.019	1.019	1.019	
	NaNO ₃	309	0.998	0.998	0.998	
	(Na,K)NO ₃	350	0.903	0.903	0.903	
		400	0.786	0.786	0.786	
Cl ⁻ /Cl ₂	(Li,K)Cl	400	1.019	1.019	1.019	
		450	0.986	0.986	0.986	
		550	0.920	0.920	0.920	
Cl ⁻ /HCl, H ₂	(Li,K)Cl	400	0.006	0.006	0.006	
		450	-0.030	-0.030	-0.030	
		550	-0.103	-0.103	-0.103	
H(I)/H ₂	(Li,K)Cl	400	0.442	0.417	0.610	
		450	0.391	0.366	0.571	
		550	0.286	0.260	0.491	
SO ₄ ²⁻ /SO ₃ , O ₂	(Li,Na,K) ₂ SO ₄	550	1.366	1.366	1.366	
CO ₃ ²⁻ /CO ₂ , O ₂	(Li,Na) ₂ CO ₃	550	0.064	0.064	0.064	

TABLE 11.3

CORRECTED STANDARD ELECTRODE POTENTIALS IN $(\text{Li,Na})_2\text{CO}_3$
FROM REFERENCE (135)

Electrode	Temperature ($^{\circ}\text{C}$)	E°_m (V)	E°_M (V)	E°_N (V)
Co(II)/Co	540	-0.946	-0.921	-1.054
Ni(II)/Ni	570	-0.862	-0.835	-0.973
$\text{CO}_2, \text{O}_2/\text{CO}_3^{2-}$	550	-0.270	-0.220	-0.490
Ag(I)/Ag	540 - 570	0.0	0.0	0.0
Ag(I) in $\text{SO}_4^{2-}/\text{Ag}$	540	0.253	0.250	0.237

TABLE 11.4

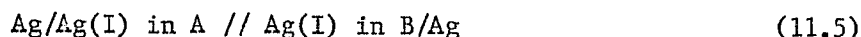
CORRECTED STANDARD ELECTRODE POTENTIALS IN $(\text{Li,Na,K})_2\text{SO}_4$
FROM REFERENCE (136)

Electrode	Temperature ($^{\circ}\text{C}$)	E°_m (V)	E°_M (V)	E°_N (V)
Co(II)/Co	550	-0.689	-0.662	-0.791
Cu(I)/Cu	580	-0.220	-0.220	-0.220
Ag(I)/Ag	545 - 585	0.0	0.0	0.0
Cu(II), Cu(I)	575	0.055	0.110	-0.157
Rh(III)/Rh	575	0.370	0.407	0.229
Pd(II)/Pd	580	0.518	0.546	0.416
* $\text{SO}_3, \text{O}_2/\text{SO}_4^{2-}$	550	0.774	0.827	0.575

* From this study (Table 10.7, page 244)

The measurements of the silver nitrate activity coefficients permit the calculation of the silver(I)/silver electrode potentials in the six different nitrate melts used in this study as a function of temperature. These values were omitted from Table 11.2 for clarity.

In the cell



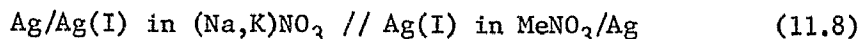
where A and B represent two different alkali nitrate melts, only the mole fraction standard cell potential, E_N^0 , is equal to zero. The standard cell potentials for the other two concentration scales are obtained by rearranging equations 7.21 and 7.24 to give

$$E_m^0 = \frac{RT}{F} \ln \left[\frac{\gamma_{N=0} \text{ (in B)} \frac{\text{Mwt}_B}{\text{Mwt}_A}}{\gamma_{N=0} \text{ (in A)} \frac{\text{Mwt}_B}{\text{Mwt}_A}} \right] \quad (11.6)$$

and

$$E_M^0 = \frac{RT}{F} \ln \left[\frac{\gamma_{N=0} \text{ (in B)} \frac{\text{Mwt}_B D_A}{\text{Mwt}_A D_B}}{\gamma_{N=0} \text{ (in A)} \frac{\text{Mwt}_B D_A}{\text{Mwt}_A D_B}} \right] \quad (11.7)$$

where $\gamma_{N=0}$, Mwt and D represent the activity coefficient of an infinitely dilute solution of silver nitrate, the molecular weight and the density of the solvent in the half cell, respectively. Equations 11.6 and 11.7, in conjunction with silver nitrate activity coefficient (Table 7.13, page 168) and density data (reference (2) and Table 7.10, page 140) are used to calculate the standard cell potentials for the cell



where Me represents one of the first three alkali metal ions or one

of their binary mixtures used in this study. The results of the calculations are summarized in Table 11.5 and the silver(I)/silver electrode potentials versus the S.H.E. are tabulated in Table 11.6.

TABLE 11.5

STANDARD CELL POTENTIALS FOR THE CELL
 $\text{Ag}/\text{Ag(I)}$ in $(\text{Na},\text{K})\text{NO}_3$ // Ag(I) in MeNO_3/Ag

MeNO_3	Temperature ($^{\circ}\text{C}$)	E_m° (V)	E_M° (V)	E_N° (V)
LiNO_3	300	0.024	0.028	0.000
	350	0.020	0.024	0.000
	400	0.018	0.022	0.000
NaNO_3	309	0.026	0.025	0.000
	350	0.023	0.023	0.000
	400	0.021	0.020	0.000
KNO_3	350	-0.028	-0.029	0.000
	400	-0.028	-0.028	0.000
0.46 LiNO_3 0.54 NaNO_3	300	0.023	0.025	0.000
	350	0.019	0.021	0.000
	400	0.016	0.018	0.000
0.59 LiNO_3 0.41 KNO_3	300	0.018	0.019	0.000
	350	0.021	0.022	0.000
	400	0.026	0.028	0.000

TABLE 11.6

STANDARD SILVER(I)/SILVER ELECTRODE POTENTIAL IN NITRATE
MELTS VERSUS A STANDARD AQUEOUS HYDROGEN REFERENCE
ELECTRODE AT 25°C

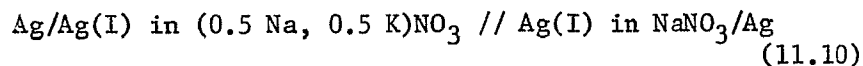
Temperature (°C)	Solvent	E_m° (V)	E_M° (V)	E_N° (V)
300	LiNO ₃	0.699	0.671	0.791
	(Li,Na)NO ₃	0.698	0.668	0.791
	(Li,K)NO ₃	0.693	0.662	0.791
	(Na,K)NO ₃	0.675	0.643	0.791
309	NaNO ₃	0.687	0.663	0.788
	(Na,K)NO ₃	0.661	0.638	0.788
350	LiNO ₃	0.671	0.642	0.774
	NaNO ₃	0.674	0.641	0.774
	KNO ₃	0.623	0.589	0.774
	(Li,Na)NO ₃	0.670	0.639	0.774
	(Li,K)NO ₃	0.672	0.640	0.774
	(Na,K)NO ₃	0.651	0.618	0.774
400	LiNO ₃	0.645	0.614	0.758
	NaNO ₃	0.648	0.612	0.758
	KNO ₃	0.599	0.564	0.758
	(Li,Na)NO ₃	0.643	0.610	0.758
	(Li,K)NO ₃	0.653	0.620	0.758
	(Na,K)NO ₃	0.627	0.592	0.758

The E_m° for the cell

Ag/Ag(I) in (0.45 Na, 0.55 K)NO₃ // Ag(I) in NaNO₃/Ag
(11.9)

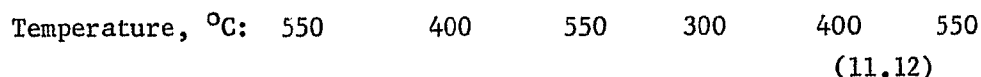
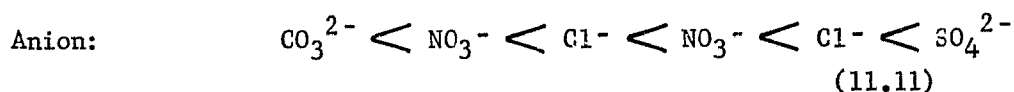
at 309°C is 0.026 volts (Table 11.5) which is slightly less than

the 0.031 volts reported in Table 8.3 (page 186) for the similar cell:

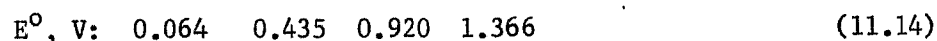
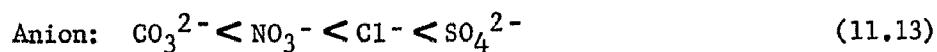


The difference between the direct emf measurement of the nitrite//nitrate solvent cell (Table 8.2, page 185) and the equivalent combination of the cells in Table 8.2 is 0.008 volts; however, if the calculated E_m^0 for cell 11.9 is used instead of the measured emf for the cell 11.10, the difference will be reduced to 0.003 volts with an experimental error of ± 0.003 volts. This result provides additional support for the values in Table 11.5 and for the emf value from the direct measurement of the nitrite//nitrate solvent cell.

The relative stability or resistance to oxidation of the anions in the melts used in this study can be obtained from their respective gaseous anion electrode potentials given in Table 11.2. The order of increasing anion stability at the indicated temperature is as follows:

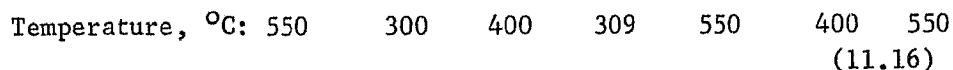
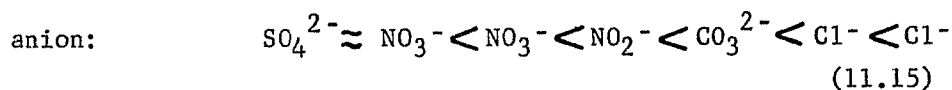


The emf of the gaseous nitrate electrode can be extrapolated to a temperature of 550°C to facilitate the comparison of the various anions. The order of increasing anion stability at 550°C is



where the lower line of figures represent the respective gaseous anion electrode potentials in volts. Carbonate melts are normally used at temperatures in excess of the decomposition temperature of the nitrate melts and for this reason the carbonate ion may appear to be out of sequence; however, at 550°C the carbonate melts require a carbon dioxide atmosphere at all times to prevent decomposition. The other three anions are in the same order as their useful working temperature range and if this trend is extended to the higher melting fluoride, phosphate, borate and silicate salts, an even increasing anion stability should be realized.

The stability of silver(I) in the various melts can be similarly determined by using the data in Table 11.2. The effect the other cations in the melts may have on the stability of the silver(I) ion can be eliminated by using only the mole fraction standard silver electrode potentials to give the following anion series at the indicated temperatures:



The silver electrode potentials in the nitrite and nitrate melts are extrapolated to 550°C to give the series presented in Table 11.7.

The silver(I) stability series at 550°C (Table 11.7) shows that as the number of oxygen atoms in the anion increases, the stability of the silver(I) ion in the corresponding melt decreases. The ΔV values, calculated by dividing the apparent increase in emf due to

the oxygen in the anion by the number of oxygen atoms in the anion, show amazing consistency at around 0.190 volts per oxygen atom. The small discrepancies between the ΔV values may be due to the change in the central atom of the anion. For the nitrate-nitrite mixed solvent, the apparent "n" value of 2/3, from a Nernst type of equation relating the standard solvent cell potential to the composition of the solvent (chapter 8.2, page 190), is identical to the oxygen ratio in the two anions and indicates a possible direct underlying relationship between the silver(I) electrode potential and the number of oxygen atoms in this system as well. These facts are consistent with the decomposition of silver oxide before it melts at about 230°C; however, since definite proof is lacking, the reason for this type of behavior is still a matter of conjecture and all these coincidences may only provide a "handy rule of thumb" for predicting the behavior of the silver(I)/silver electrode in oxyanion melts.

TABLE 11.7

STABILITY OF SILVER(I) IN SEVERAL FUSED ALKALI METAL SALTS
AT 550°C

Anion of the salt	SO ₄ ²⁻	NO ₃ ⁻	CO ₃ ²⁻	NO ₂ ⁻	Cl ⁻
E _N ^o (Ag(I)/Ag), V	0.791	0.708	0.554	0.490	0.034
(E _N ^o - 0.034), V	0.757	0.674	0.520	0.456	0.0
n (number of oxygen atoms per anion)	4	3	3	2	0
ΔV *	0.190	0.225	0.140	0.228	—

* $\Delta V = (E_N^o - 0.034) / n$

The effect that the other cations have on the stability of the silver(I) ion in nitrate melts can be obtained from the E_m^0 data in Table 11.6. The cation and temperature effect on the silver(I)/silver electrode potential is about one order of magnitude less than that observed for a change in anions. A general trend towards an increase in the stability of the silver(I) ion with an increase in either the temperature or the average size of the cations in the solvent is observed and is consistent with the theory of activities in molten salts (chapter 7.6, page 169).

11.3 Practical Application

The unified emf series can be used to predict the reversible emf of a fuel cell which produces one of the oxyanion acids as its end product. The formation potential of nitric acid at 400°C can be calculated by combining the hydrogen electrode and the gaseous nitrate electrode to form the cell



In order to obtain the required cell reaction, viz.,



the solubility of the nitric acid in the nitrate melt must be accounted for in a similar manner as was done for the hydrogen/hydrogen chloride gas electrode (chapter 10.5, page 246). The lack of published data as a result of the instability of nitric acid at 400°C necessitates the assumption that the solubility of nitric acid in the nitrate melt is the same as the solubility of hydrogen chloride

in the chloride melt at a given temperature. The dissolved nitric acid will dissociate to produce the hydrogen(I) ion according to the equations



$$[\text{H(I)}] = K P_{\text{HNO}_3} \quad (11.20)$$

The standard potential for the nitric acid formation cell



is related to the E°_{N} potential by the equation (equation 10.36, page 248):

$$E^\circ_{\text{HNO}_3} = E^\circ_{\text{N}} - \frac{RT}{F} \ln K \quad (11.23)$$

$$E^\circ_{\text{HNO}_3} = E^\circ_{\text{N}} + 0.604 \text{ V (T = 400}^\circ\text{C)} \quad (11.24)$$

Due to the instability of the gaseous forms of carbonic and sulfuric acids at 550°C, a similar approach is used except 2K is used in place of K in equation 11.23 to account for the two hydrogen(I) ions formed when the acids dissociate in the melts. The calculated values for the three oxyacid formation cells are summarized in Table 11.8 along with estimated errors.

A combination of the following equations taken from the literature also gives $\Delta G^\circ_{\text{f}}$ for nitric acid:

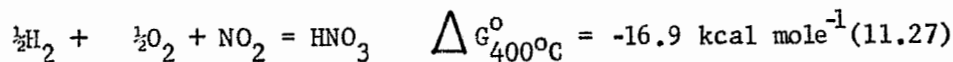
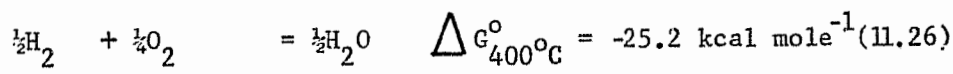
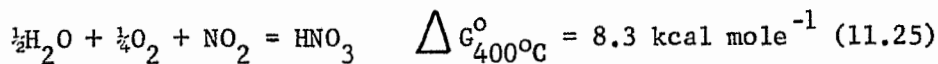
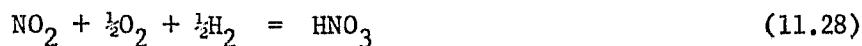


TABLE 11.8

FORMATION POTENTIALS OF OXYACIDS

Cell Reaction	Temperature °C	$E_f^{\circ} \pm 0.010$ V	ΔG_f° (kcal mole ⁻¹)
$\frac{1}{2}\text{H}_2 + \text{NO}_2 + \frac{1}{2}\text{O}_2 = \text{HNO}_3$	400	0.780	-18.0 ± 0.2
$\text{H}_2 + \text{CO}_2 + \frac{1}{2}\text{O}_2 = \text{H}_2\text{CO}_3$	550	0.118	-5.4 ± 0.5
$\text{H}_2 + \text{SO}_3 + \frac{1}{2}\text{O}_2 = \text{H}_2\text{SO}_4$	550	1.420	-65.6 ± 0.5

The accuracy of ΔG° for equation 11.25 is uncertain due to an extrapolation of data from 277 to 400°C (328) whereas the error in ΔG° for equation 11.26 is negligible (329). The agreement between the two ΔG_f° values for nitric acid at 400°C is close considering the number of approximations involved in the calculations. To obtain free energy data for nitric acid Forsythe and Giaque (328) used calorimetric measurements for temperatures up to and slightly above the melting point of pure nitric acid (-42°C) and then spectroscopic measurements up to 277°C. A positive $\Delta G_{400^{\circ}\text{C}}^{\circ}$ value for equation 11.25 shows that at 400°C any attempt to measure the heat of formation of nitric acid by calorimetric methods would result in the following sequence of chemical reactions:



The net thermodynamic values obtained from the calorimetric measurements are only for the formation of water and only when the temperature is below 120°C does the ΔG° for equation 11.25 become negative (328). The reliability of the values for the free energies of formation given in Table 11.8 are superior to most of the previous measurements or estimates reported in the literature for nitric acid. These values also remedy the absence of data on the formation of sulfuric and carbonic acid at 550°C.

The rapid emf response of the gaseous sulfate electrode to changes in gas pressures and the large formation potential suggests that it may be used in a practical fuel cell despite the highly corrosive nature of the sulfur trioxide. The use of higher melting oxyanion salts, such as phosphates or borates, may provide better systems and larger potentials than the sulfate fuel cell as predicted by the observed trends in this study (equations 11.13 and 11.14) and theoretical calculations (330).

12. EXPERIMENTAL

12.1 Preparation and Purification of Melts

12.1.1 Nitrite melts

Because of organic impurities, it was necessary to recrystallize the Analar reagent grade sodium nitrite twice from water. This procedure produced a colorless melt instead of the faintly yellow colored melt which had been produced by the original salt. The purified sodium nitrite was dried at 120°C for 24 hours and then stored over P₂O₅ in a dessicator until needed. Before being used to fill the electrode compartment the salt was melted in a small tube furnace (Figure 12.1) and purged with dried oxygen-free nitrogen for 24 hours; also, between each run (in a given series of trials) the purified nitrogen was used to continuously purge the melt.

12.1.2 Nitrate melts

All of the nitrate salts were reagent grade from Fisher Scientific Company and were refined in the lab by recrystallization (with one exception) followed by a 24 hour drying period. Sodium nitrate and potassium nitrate were recrystallized twice from water, the lithium nitrate only once (due to its low solubility change with temperature) and the silver nitrate not at all. Both the sodium

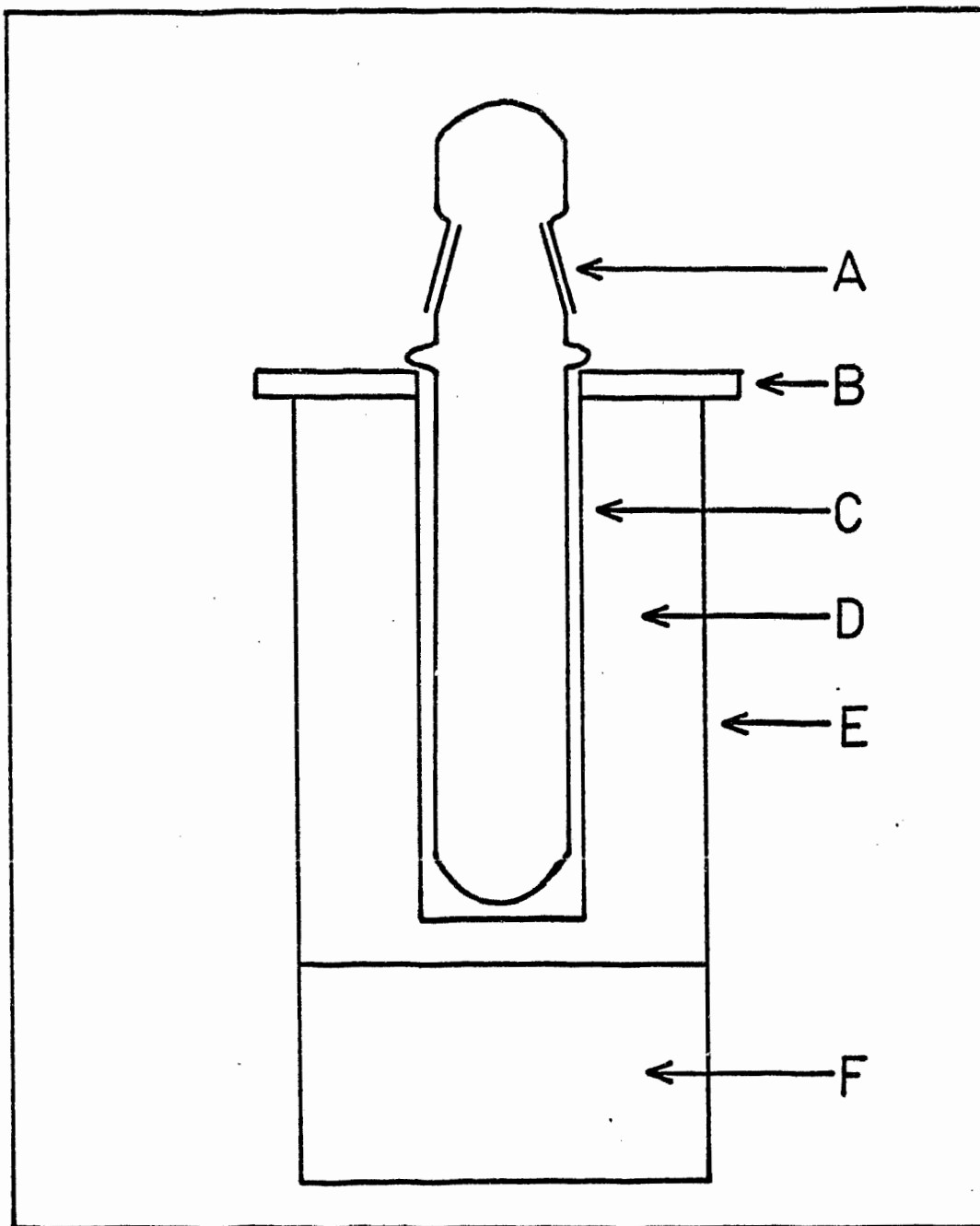


Figure 12.1 Melt Preparation Tube Furnace

A - Pyrex 24/40 ground joint, B - asbestos board, C - 1 inch Vycor tube wound with Chromel A resistance wire, D - Vermiculate insulation, E - metal casing, F - weighted base

and potassium salts were then dried at 120°C and the lithium and silver salts were dried at 100°C under a pressure of less than 2 mm Hg. All of the nitrate salts were stored over P₂O₅ in a dessicator.

Each nitrate mixture was prepared ahead of time in a quantity sufficient to supply all the trials so that a constant composition of the mixture would be maintained throughout. The correct proportions of the salts were weighed out to the nearest 0.1 gram, mixed and fused in a large tube furnace (Figure 12.1). The resulting melt was dried and mixed by purging with the purified nitrogen for two hours and then allowed to solidify in a porcelain evaporating dish in a dessicator. After grinding, the solid mixture was stored over P₂O₅ in a dessicator.

The mixtures contained the following mole percentages of the various alkali nitrate salts.

(Li,Na)NO₃ eutectic m.p. 193°C

54 mole% LiNO₃

46 mole% NaNO₃

(Li,K)NO₃ eutectic m.p. 133.5°C

41 mole% LiNO₃

59 mole% KNO₃

(Li,K)NO₃ mixture

59 mole% LiNO₃

41 mole% KNO₃

(Na,K)NO₃ eutectic m.p. 220°C

45 mole% NaNO₃

55 mole% KNO₃

Before being used in any electrochemical cell the pure nitrate melts and the mixed nitrate melts were prepared by a procedure similar to that described for the sodium nitrite.

12.1.3 Chloride melt

Various methods have been used to purify the lithium-potassium chloride eutectic: Mackenzie (190) has made a critical evaluation of these methods, and the one developed by Marical and Hume (189), with minor modifications, was used in the present work. The lithium chloride, Baker Analyzed Reagent, was dried in a vacuum oven at 120°C and a pressure less than 1 mm Hg for 24 hours and then weighed to make the eutectic mixture containing 59 mole% lithium chloride and 41 mole% potassium chloride. Since potassium chloride is not as hygroscopic as lithium chloride, heating at 120°C for 24 hours in an ordinary oven was sufficient to dry it.

A large quantity of the salt mixture was initially prepared to ensure a uniform composition throughout all the chloride melts. Approximately 125 grams of the salt mixture was first put into the inner tube (A) of the melt purification apparatus (Figure 12.2) and then the entire assembly was placed in the furnace and connected to the vacuum line assembly (Figure 12.3). The advantage of the vacuum line was that the complete purification process could be carried out without exposing the melt to the atmosphere or changing any of the

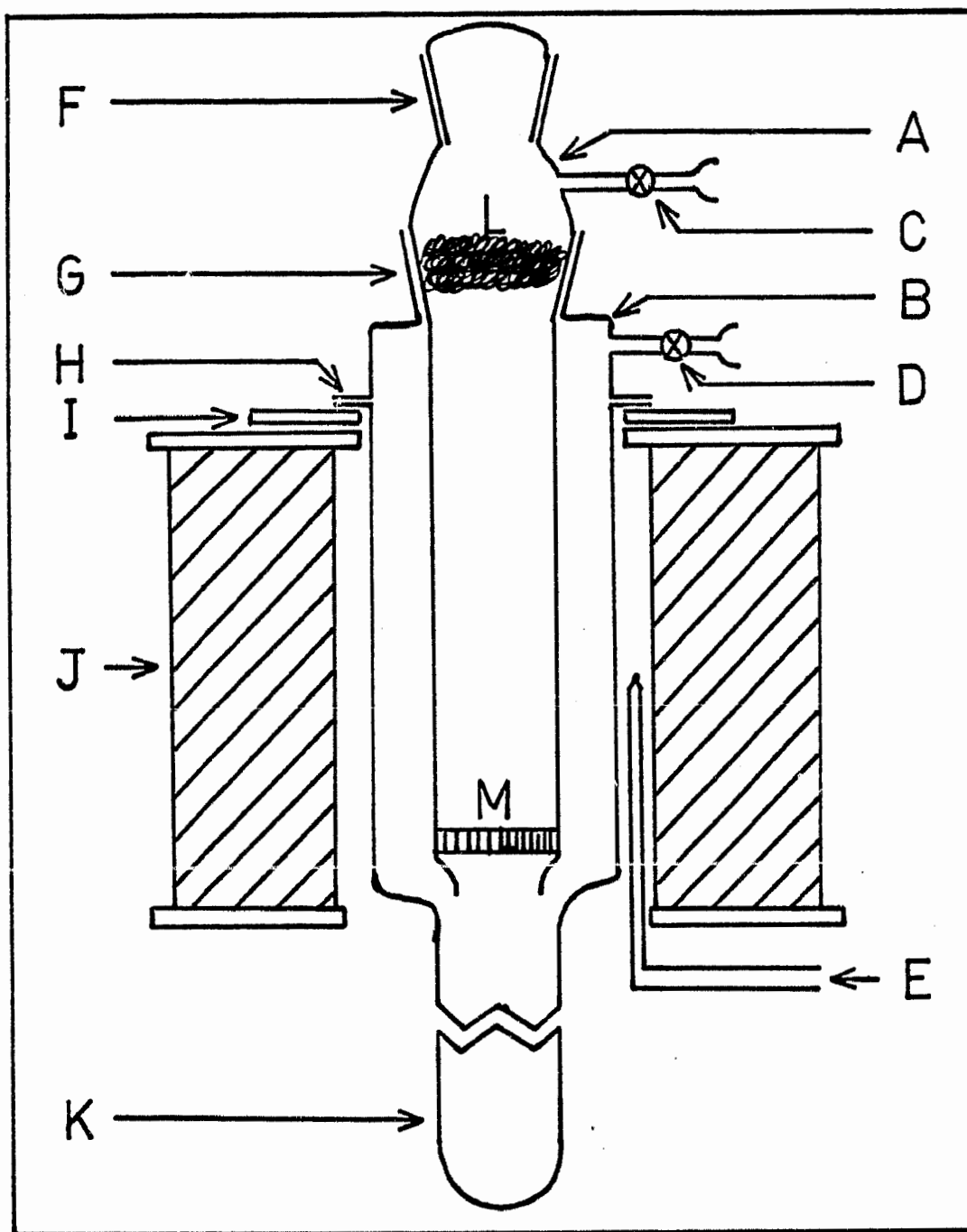


Figure 12.2 Chloride Eutectic Purification Apparatus

A - inner tube, B - top of outer tube, C,D, - vacuum taps,
 E - thermocouple, F - Pyrex 24/40 ground joint, G - Pyrex 35/45
 ground joint, H - 2 inch flange, I - cooling plate, J - 3 inch
 tube furnace, K - sample ampule, L - glass wool, M - 20 mm medium
 fritted disk

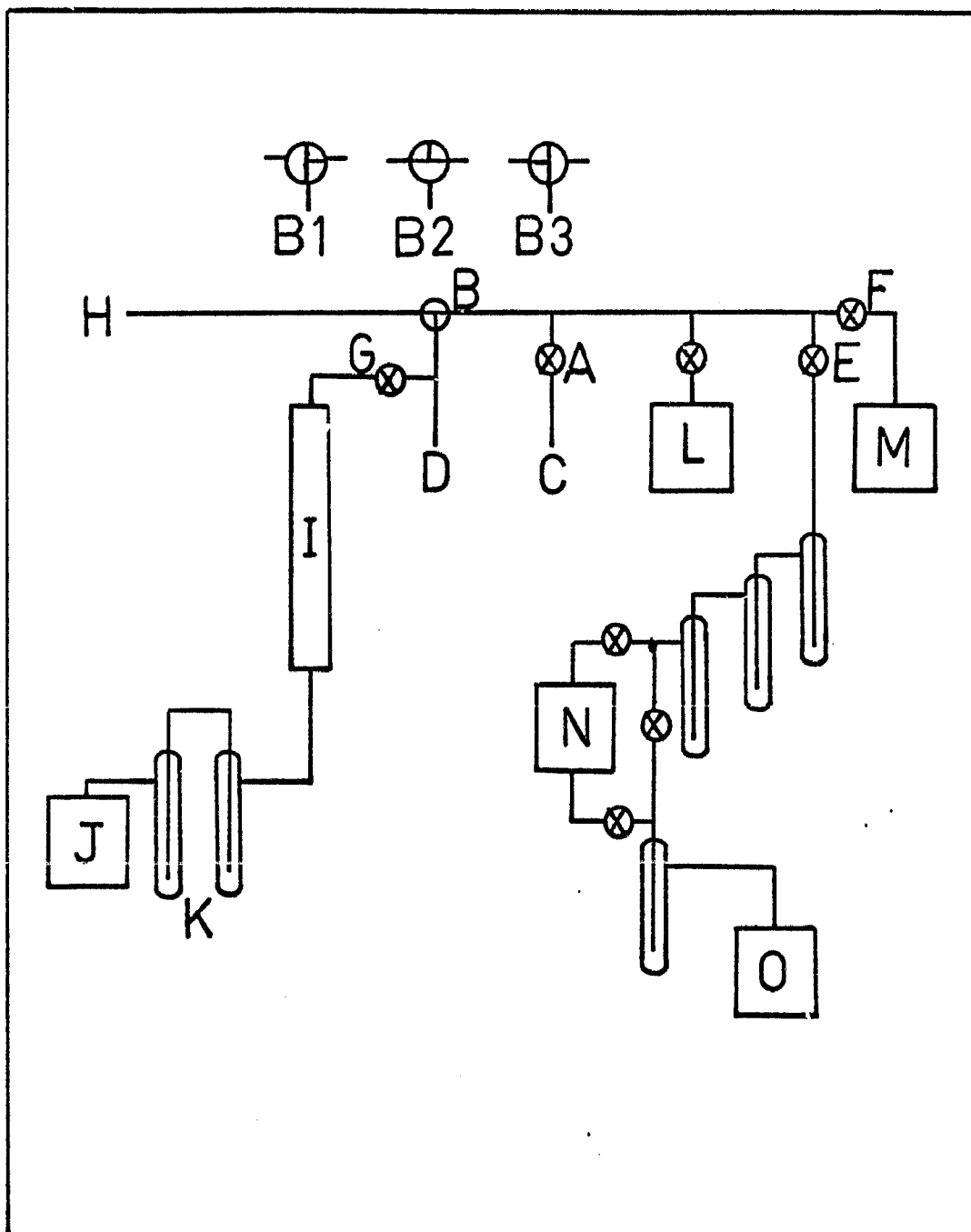


Figure 12.3 Vacuum Line for Chloride Purification

A, E, F, G - vacuum taps, B - T-vacuum tap, C, D - to melt purification apparatus, H - to Cl_2 exhaust, I - drying column, J - regulated Cl_2 source, K - H_2SO_4 gas washers, L - regulated N source, M - vacuum gauge, N - oil diffusion pump, O - 2-stage backing vacuum pump

connections between each step. The temperature of the furnace was controlled to $\pm 10^{\circ}\text{C}$ by the manual adjustment of a Variac power-stat and measured with a chromel-alumel thermocouple and a Cropico P3 potentiometer. The apparatus was evacuated by opening tap "A" first and then turning tap "B" to position "B1"; this sequence prevented the drawing of fine salt particles through the fritted disk with the furnace set at about 100°C . A vacuum of less than 0.01 mm mercury was then maintained overnight after which the temperature was slowly raised to about 300°C and held there for three to four hours. Taps "E" and "F" were turned off and tap "B" was turned to a position between "B1" and "B2". The chlorine pressure was adjusted to about 2 psi and the vacuum in the system was released by slowly opening tap "G". Once the chlorine ceased to flow, tap "B" was turned to position "B2" and the chlorine pressure was adjusted to provide a slow flow of chlorine through the salt mixture. The eutectic mixture was then melted by raising the temperature to about 400°C while maintaining the flow of chlorine through the bottom of the frit and up through the melt. After a period of three to four hours the chlorine flow was stopped by closing stopcock "G" and the pressure was released from below the frit by turning stopcock "B" to position "B3". It was often necessary to apply a slight pressure of nitrogen above the melt by opening stopcock "H" to assist the filtration of the melt through the frit. A hand torch was used to help collect the filtered melt in the bottom of the sample tube projecting out of the bottom of the furnace. Once all the melt was collected and solidified in the bottom of the sample tube, the tube was sealed and cut off just above

the solid, thus providing a sealed sample of chloride eutectic which was still saturated with chlorine. The ampules were then stored in a dry box until needed.

12.1.4 Preparation of the ternary sulfate eutectic

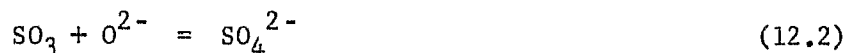
The salts, Baker Analysed Reagent grade, were anhydrous except for the lithium sulfate which was the monohydrate. The salts were dried in a vacuum oven at 120°C for 24 hours before being weighed and mixed to form the eutectic mixture containing the following amounts of the three salts:

78 mole% Li_2SO_4

8.5 mole% Na_2SO_4

13.5 mole% K_2SO_4

The mixture, which has a melting point of 512°C (331), was placed in a Pyrex tube and gradually heated to 550°C in a small tube furnace (Figure 12.1). The sulfate melt was purged with dried oxygen-free nitrogen for several hours to purify the melt and to ensure uniform mixing. At first the melt was slightly cloudy, but it rapidly became clear with the addition of a few milligrams of purified sodium pyrosulfate. The preparation of the pyrosulfate is given in chapter 12.1.5 and the clearing effect is due to the conversion of oxide to sulfate.



The melt was purged with nitrogen after the melt had cleared to remove any excess sulfur trioxide. The frozen melt was ground up in the dry box and stored in a vacuum dessicator until required.

The sulfate melt was prepared in a similar manner to the nitrite melts before use in any electrochemical measurements. A polarogram was run on the melt at 550°C using a Sargent Polarograph Model XVI, a silver(I)/silver reference electrode and a micro platinum electrode (area = 0.128 mm²). The results (given in terms of a one molal silver reference electrode in Figure 12.4) are in agreement with those of Johnson and Laitinen (261) and exhibit no evidence of any substantial amount of impurity in the melt.

12.1.5 Preparation of sodium pyrosulfate

The sodium pyrosulfate was prepared according to a method developed by Hotz (332). The preparation is a tedious operation requiring several days to prepare three to four grams of sodium pyrosulfate. A Vycor (approximately 2 cm diameter) tube which ran through two tube furnaces was sealed off at one end to form the reaction vessel (Figure 12.5). A silica boat one-third full of sodium sulfate was placed in the Vycor tube so that it was centered in the tube furnace next to the closed end of the tube. A silica boat two-thirds full of anhydrous cupric sulfate was then placed in the tube and centered in the other tube furnace. The open end of the Vycor was constricted to form an exhaust tube and to permit the making of a vacuum seal later. Unless the cupric sulfate is next to the exhaust tube, fine cupric

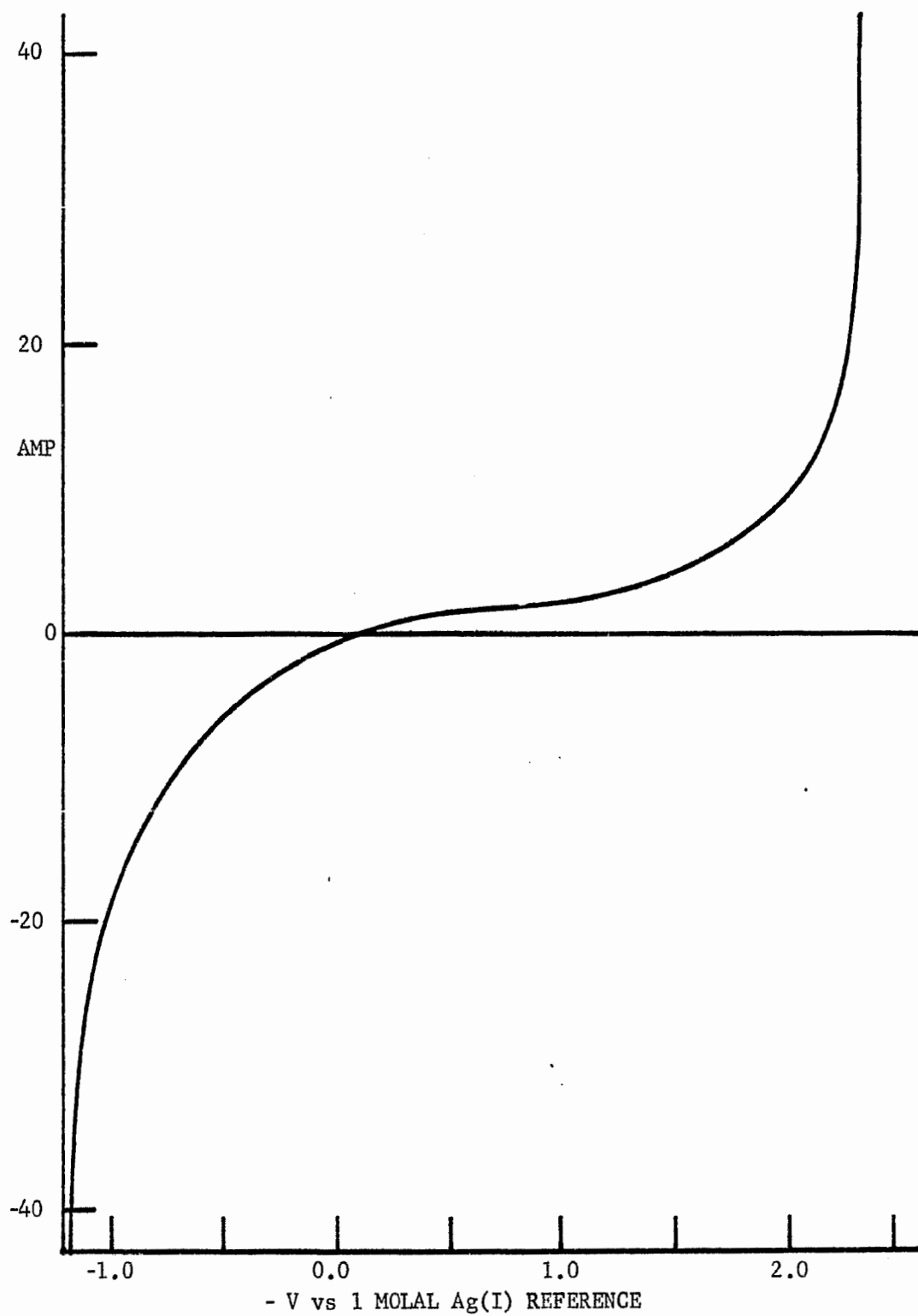


Figure 12.4 Polarogram of $(\text{Li,Na,K})_2\text{SO}_4$ Eutectic Melt at 550°C

Area of micro platinum electrode = 0.128 mm^2

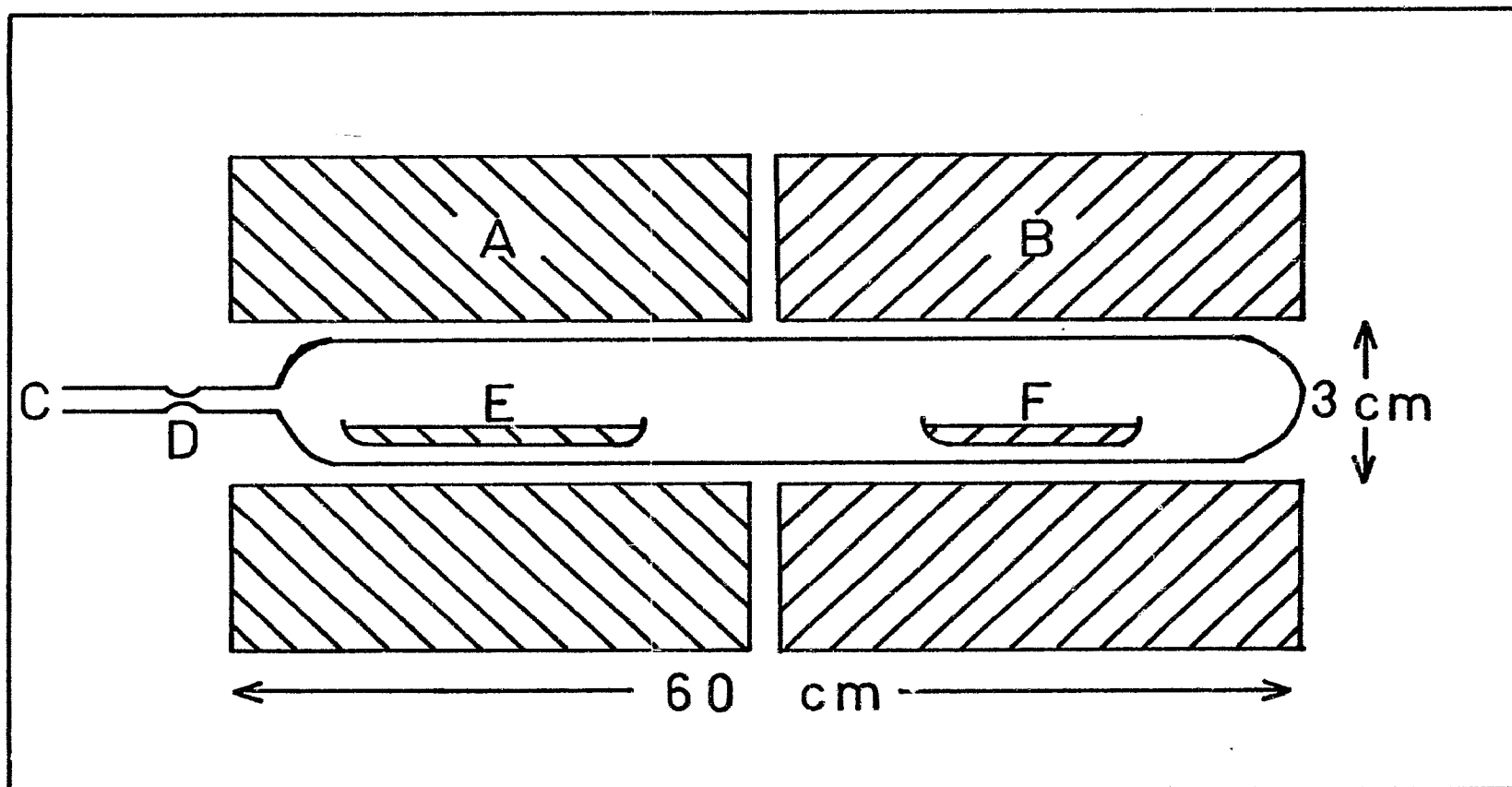


Figure 12.5 Reaction Vessel to Prepare $\text{Na}_2\text{S}_2\text{O}_7$

A - Furnace connected to programmed temperature controller, B - Furnace connected to fixed temperature controller, C - to vacuum system, D - vacuum seal in Vycor reaction vessel, E - CuSO_4 , F - Na_2SO_4

sulfate dust will be drawn across the sodium sulfate. The sodium sulfate furnace was connected to a temperature controller and kept at 700°C to prevent premature formation of pyrosulfate after the tube was evacuated; the cupric sulfate furnace was also connected to a temperature programmed controller which was required later on in the experiment. The cupric sulfate was heated slowly under vacuum to 630 - 650°C (approaching the point of decomposition) to remove all the water, and then the furnace was turned off and opened to prevent extensive decomposition. The exhaust tube was then sealed off. The sodium sulfate furnace was set at 475°C and the cupric sulfate furnace at 900°C. The complete absence of any solid in the sodium sulfate boat, after about 15 hours, indicated the completion of the reaction. The temperature in the sodium sulfate furnace was then lowered to 250°C and the temperature of the cupric sulfate furnace was programmed down from 900°C to 250°C at a rate of about 10°C per hour. The slow rate of cooling removes all the sulfur trioxide from the atmosphere of the tube and prevents the formation of any polysulfate compounds. Once the cooling procedure was completed, both furnaces were opened and allowed to cool to room temperature. The tube was transferred to a dry box and broken open at the sodium pyrosulfate end. The pyrosulfate was crushed in an agate mortar and stored in a screw-capped bottle in a dessicator.

The chemical reactions and results for the preparation are given below:





$$4.9273 \text{ gms } \text{CuSO}_4 \quad (12.5)$$

$$2.4353 \text{ gms } \text{Na}_2\text{SO}_4 \quad (12.6)$$

$$\text{Theoretical yield} = 3.8079 \text{ gms} \quad (12.7)$$

$$\text{Experimental yield} = 3.8020 \text{ gms} \quad (12.8)$$

$$\text{Percent yield (purity)} = 99.8\% \quad (12.9)$$

12.2 Design of Isothermal Cells

The isothermal electrochemical cells consisted of two individual electrode compartments immersed in a bulk melt contained in a thermostated three-neck 250 ml flask (Figure 12.6). One additional inlet to the flask was provided by glass blowing a piece of glass tubing (11 mm) in the top of the flask. The inlet was designed so that when the glass sheathed controller probe was passed through it, the end of the probe was between the two electrode compartments and about 15 mm from the bottom of the flask. Standard tapered inner joints (24/40) were used to extend the length of the three necks on the flask so that the main body of the flask could be covered to a depth of 5 cm with insulation. The entire flask was wrapped with aluminum foil to insure good thermal contact with the heating mantle and then earthed to prevent any a.c. interference from the heaters. The entire assembly was supported on a stand in a large aluminum box and covered with Zonolite insulation with a minimum depth of 5 cm insulation at any point. The furnace was then placed in a fume hood to ventilate the gases from gas electrodes and to protect the furnace

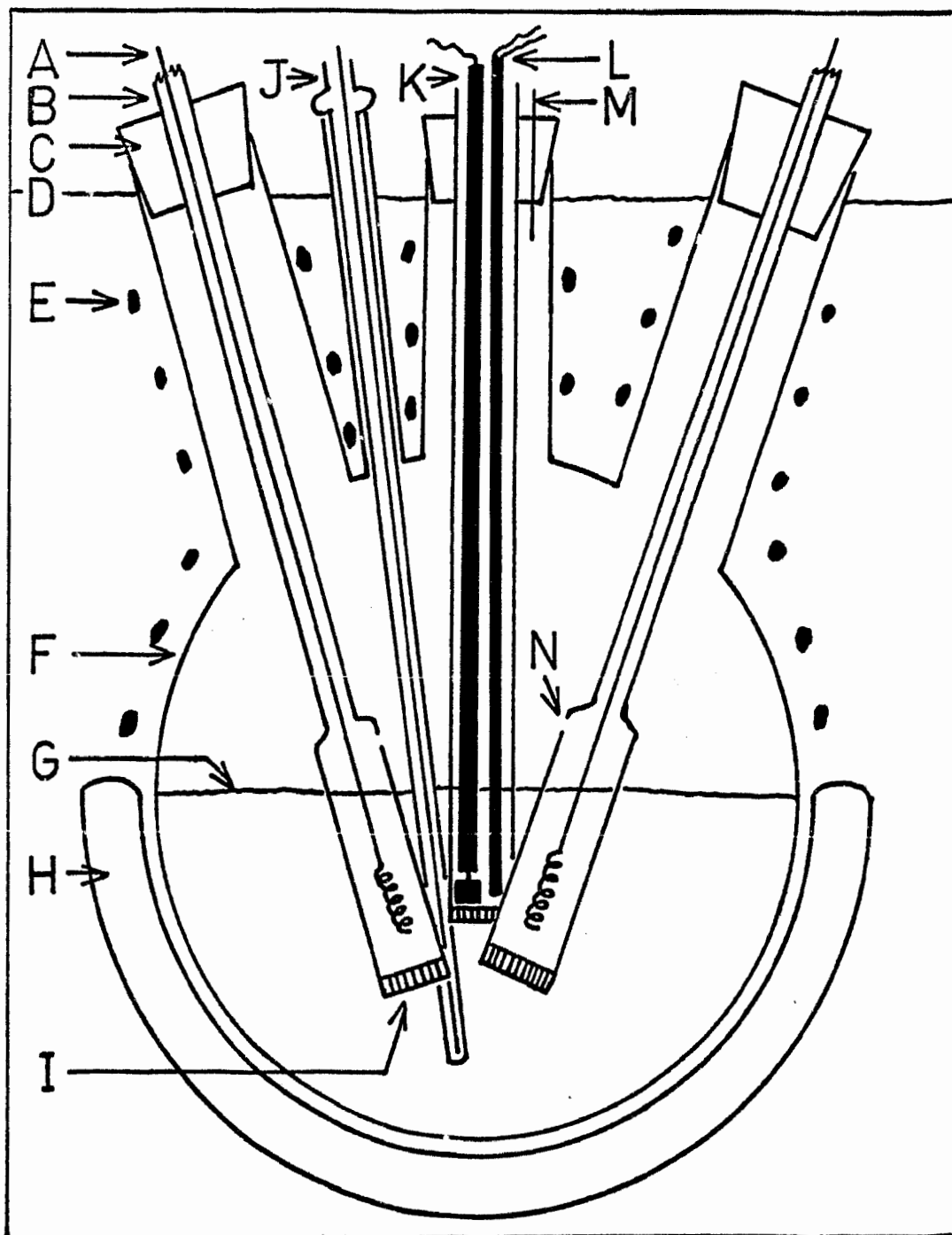


Figure 12.6 Isothermal Electrochemical Cell

A - metal electrode, B - bottom half of electrode compartment, C - foil-wrapped rubber stopper, D - upper level of insulation, E - heating tape wrapped around top of cell, F - foil (earthed) wrapped 250 ml flask, G - melt level, H - heating mantle, I - 10 mm fine fritted disk, J - glass sheathed temperature controller probe, K - Pt counter electrode, L - thermocouple, M - hypodermic needle for N_2 , N - gas inlet in electrode compartment

from drafts.

The power to a heating tape wrapped around the upper portion of the flask was controlled manually by a powerstat so that the temperature, monitored with a chromel-alumel thermocouple, was maintained at 10 to 20°C below that of the bulk melt. The heating tape was necessary to prevent excessive cooling of the melt surface and to prevent thermal conductivity along the metal electrodes from the melt in the electrode compartments. The power to the heating mantle was switched back and forth between two powerstats by a ProportionNull, 1300 Series, controller from the Cole-Parmer Instrument and Equipment Company. One powerstat provided enough power to maintain the furnace 10°C below the desired temperature and the other powerstat 10°C above the required temperature. An auxiliary 20 amp switching relay was required in the electrical heating circuit (Figure 12.7) since the controller could not handle the 8 to 10 amp heating current. The temperature of the melt could be maintained to $\pm 2^\circ\text{C}$.

The flask was half-filled with the required bulk melt and purged with nitrogen for 24 hours, a counter electrode compartment was then inserted into the flask through the central neck to a depth of 20 mm from the bottom of the flask. The compartment consisted of a 10 mm sintered glass frit of fine porosity cut off on one side of the frit and sealed to 14 mm glass tubing so that it could be held in place by means of a tightly fitting aluminum covered rubber stopper in the top of the central neck of the flask. Before the

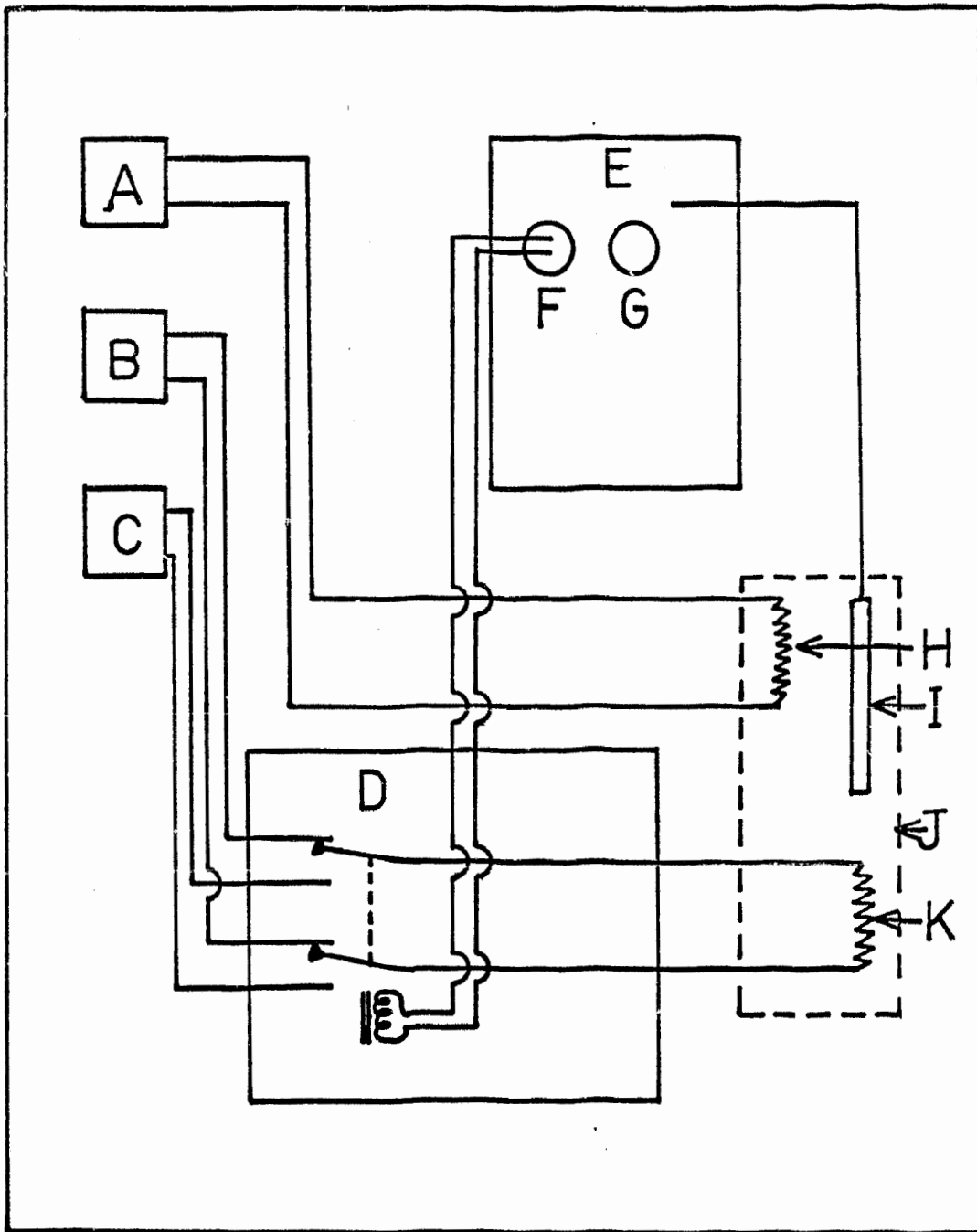


Figure 12.7 Electrical Heating Circuit for Isothermal Furnace

A - powerstat for heating tape, B - low power powerstat for controller, C - high power powerstat for controller, D - a D.P.D.T. relay, E - temperature controller, F - heating output, G - cooling output, H - heating tape, I - probe for temperature controller, J - isothermal furnace, K - heating mantle

compartment was filled by seepage of the bulk melt through the frit, a platinum foil, 1 cm², counter electrode and a glass-sheathed chromel-alumel thermocouple were inserted into it. A hypodermic needle was inserted through the rubber stopper around the counter electrode and then connected to the nitrogen line through a needle valve so that a positive nitrogen atmosphere could be maintained above the melt at all times.

The electrode compartments consisted of a 10 mm fine glass frit cut off next to the frit on one side and sealed to a piece of 8 mm glass tubing 5 cm from the other side of the frit. A 5/20 standard tapered outer glass joint was sealed on the other end of the 8 mm glass tubing to make a unit with a total length of about 28 cm. A number 3 rubber stopper with a 8 mm hole in it and split along one side was fitted around the tubing just below the ground joint and wrapped with aluminum foil after the compartment had been filled with the desired solvent which had been prepared in a separate furnace. A positive nitrogen pressure and an oxygen torch were used to blow a small hole in the wall of the compartment about 10 mm above the melt. The flow of nitrogen through the compartment was maintained until it was placed in the furnace, then the nitrogen over the bulk melt was allowed to flow out through the electrode compartment. The electrode compartment was adjusted so that the level in the compartment was about one to two millimeters above the level required to balance the flow of the melts through the frit. This was accomplished by measuring the distance between the surface of

the bulk melt and the top of the inlet to the cell, the length of the electrode compartment and the depth of the melt in the compartment. The foil wrapped rubber stopper held the compartment in place and provided an air-tight seal at the entrance to the flask. Before making any electrical measurements a minimum period of two hours was allowed for thermal equilibration and cessation of the outward flow of melt from the electrode compartment.

The metal electrode in the electrode compartment was raised and lowered by means of a converted 3 cc syringe which had a glass 5/20 inner joint attached to the bottom of the outer cylinder as shown in Figure 12.8. The modified syringe was attached to the top of the electrode compartment after the electrode wire had been sealed in the top of the plunger with picein wax. A small hole in the side of the plunger at the top permitted a slow flow of nitrogen to escape through the electrode and prevent atmospheric contamination from entering the cell. A high impedance resistance meter connected between the indicator electrode and the metal electrode indicated the sudden drop in resistance when the electrode touched the surface of the melt as the plunger was slowly pushed into the syringe. All of the electrodes were then inserted into the melt a further 15 mm which was equivalent to 1 cc on the syringe. The use of the syringe electrode holder not only provided an accurate method for positioning the electrode but permitted the rotation of the electrode in the electrode compartment to facilitate rapid mixing in the melt. The level of the melt was checked at the end of each

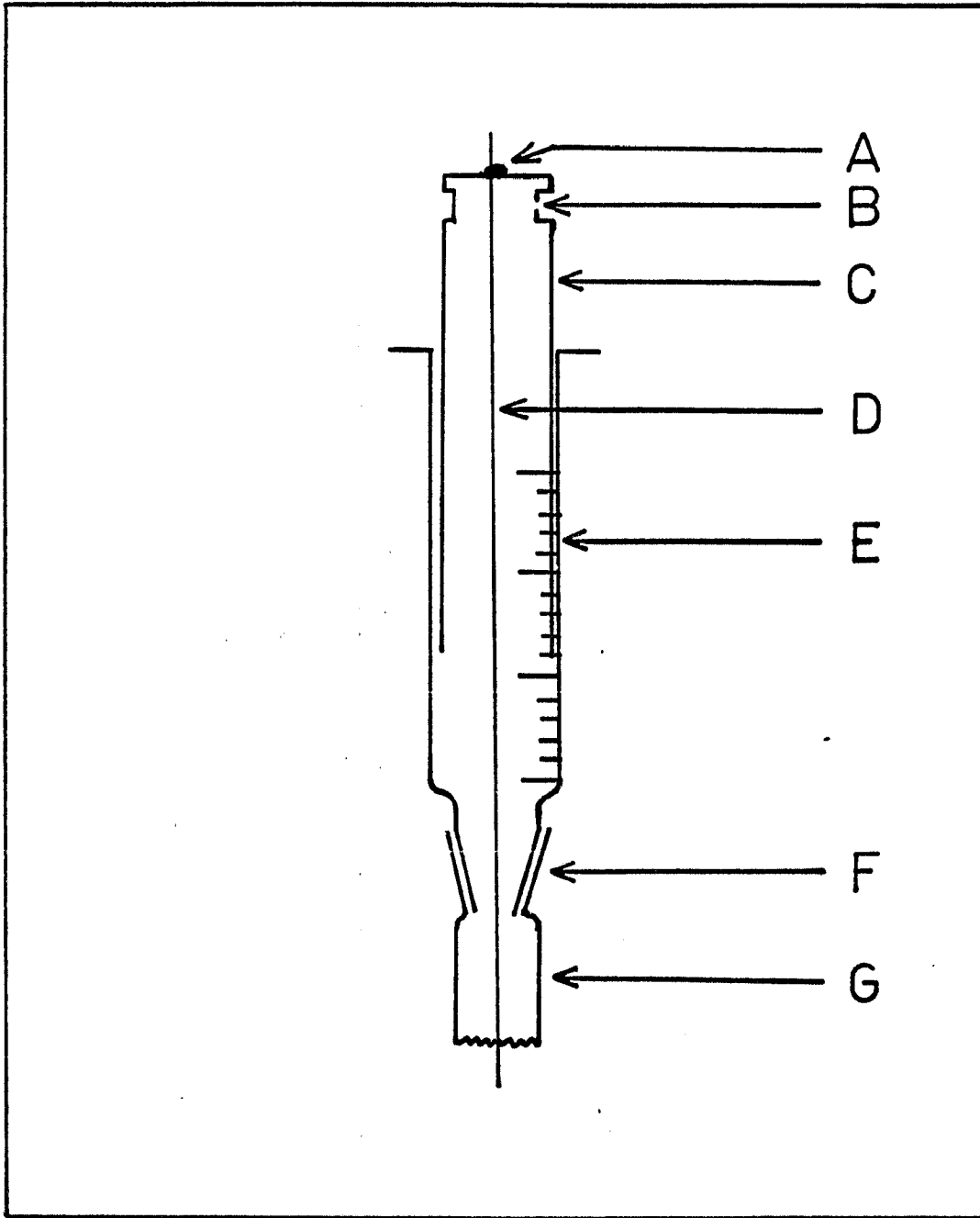


Figure 12.8 Electrode Holder

A - picein wax, B - N_2 outlet, C - plunger, D - metal electrode wire, E - 3 cc syringe, F - 5/20 ground joint, G - top of electrode compartment

experiment with the ohmmeter in a manner similar to that at the beginning. If the levels differed by more than 0.5 mm (about 1.5% of total depth of melt) the results for that trial were automatically rejected. The electrode compartment was removed from the furnace and allowed to cool in a dessicator before its contents were analyzed.

12.3 Electrical Circuits and Measurements

All of the temperature measurements were made using chromel-alumel Pyrex-sheathed thermocouples, ice-water zero point reference and a Cropico Type P3 Potentiometer, to $\pm 0.25^{\circ}\text{C}$. The thermocouples used in the isothermal and nonisothermal furnaces were calibrated against the fixed points used to define the International Temperature Scale of 1948 (333). Thermocouples with an error of more than 1.0°C for any of the calibration points were rejected or used for minor temperature measurements. The calibration points are listed in Table 12.1.

TABLE 12.1
FIXED POINTS FOR CALIBRATION OF THERMOCOUPLES

Fixed Point	Temperature $^{\circ}\text{C}$	Pressure Correction (valid for 680-780 mm Hg)
Ice, melting point	0.00	
Water, boiling point	100.0	$T_P = T_{760} + 0.0367 (P-760) - 2.3 \times 10^{-5} (P-760)^2$
Tin, freezing point	231.9	
Cadmium, freezing point	320.9	
Lead, freezing point	327.3	
Zinc, freezing point	419.5	

All of the electrical measurements were made on a Cropico Type P3 Potentiometer to the nearest 2, 20 and 200 microvolts on the 0.017, 0.17 and 1.7 volt scales, respectively. The potentiometer was checked against a Standard Cadmium Cell (Type 1268, Guildline Instruments Ltd., 1968) and found to have an error of less than 0.02% at 1.01838 volts. The potential of the electrochemical cells was continuously monitored with a Beckman 10 inch, Model 1005, Recorder to observe the behavior of the cell emf during the entire experiment. A Leeds and Northrup Student model millivolt potentiometer was used to back off part of the emf so that the 1 millivolt full scale range could be used on the recorder. The input impedance of the recorder is 10 Kohms at off-balance position and potentiometric at the balanced position. The use of co-axial cable throughout all of the electrical measuring system prevented pick-up of any ac interference. To avoid inconsistent junction potentials resulting from soldered connections, small plastic covered metal connectors with set screws were used to connect the co-axial cable to the silver electrodes. The screw type connectors also made it very easy to make or break connections and greatly decreased the possibility of a poor connection since as the screw was tightened it cut into the silver wire.

Silver(I) was introduced into the melts by the coulometric oxidation of a silver electrode immersed in the melt. This process has been shown to have a current efficiency of 100% in the nitrite (32), nitrate (39, 99, 100), chloride (206) and sulfate (261, 264)

melts. A Sargent Coulometric Current Source, Model IV and a current density of 60 milliamp cm^{-2} was used in all of the experiments except for those in the nitrite melts where the current density was 6 milliamp cm^{-2} . The analysis of the contents of the electrode compartments for silver using Atomic Adsorption (chapter 12.5.7) were in agreement with the value indicated by the coulometer for each of the melts. A switching box enabled the connection of either electrode to the potentiometer or the coulometer as shown in Figure 12.9.

12.4 General Operating Procedure

All of the glassware used for the final preparation of the melts and the electrode compartments were soaked in nitric-dichromate cleaning solution for 24 hours, rinsed with water, boiled in aqua regia for one to two hours, thoroughly washed in deionized water, dried at 120°C for two hours and then baked in a furnace at 550°C for 24 hours. The pieces of glassware were taken from the furnace and used while still hot, where possible, to prevent adsorption of water vapor onto the glass surfaces.

When filling the electrode compartments the same procedure was used for all the melts except the chloride melt where special precautions were required to keep it dry and to remove the dissolved chlorine gas. The other melts were prepared as described in chapter 12.1 and then filtered into the electrode compartment using the vacuum system shown in Figure 12.10. Once the melt filled the electrode compartment to a depth of about 3 cm, the vacuum was shut off and nitrogen

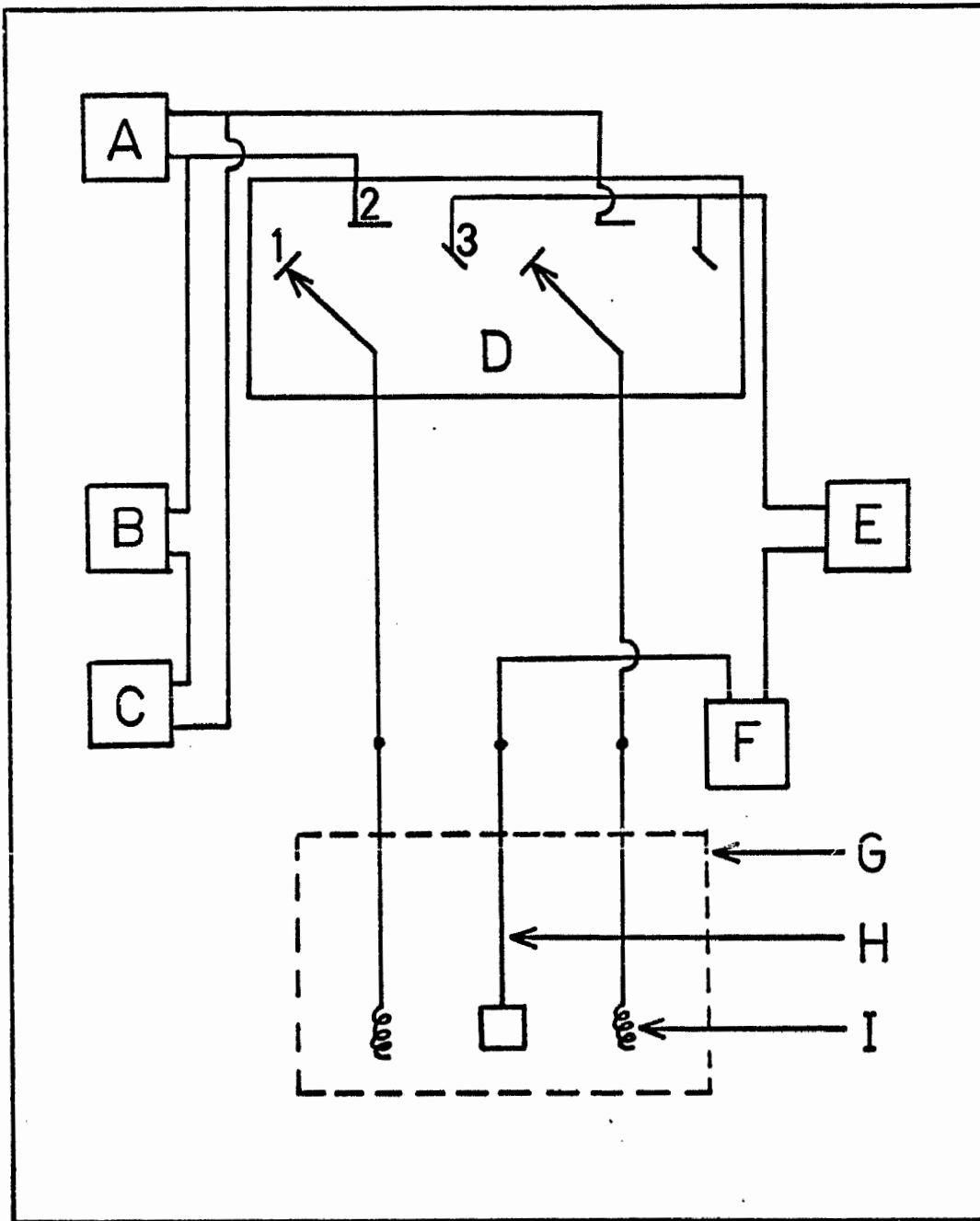


Figure 12.9 Electrical Measuring and Generating Circuit for Isothermal Cell

A - potentiometer, B - backing millivolt source, C - millivolt recorder, D - 2 independent 3-point rotary switches, E - coulometer, F - multi-range ammeter, G - isothermal furnace, H - Pt counter electrode, I - metal electrode
Switch Positions: 1 - open circuit, 2 - measuring circuit
 3 - generating circuit

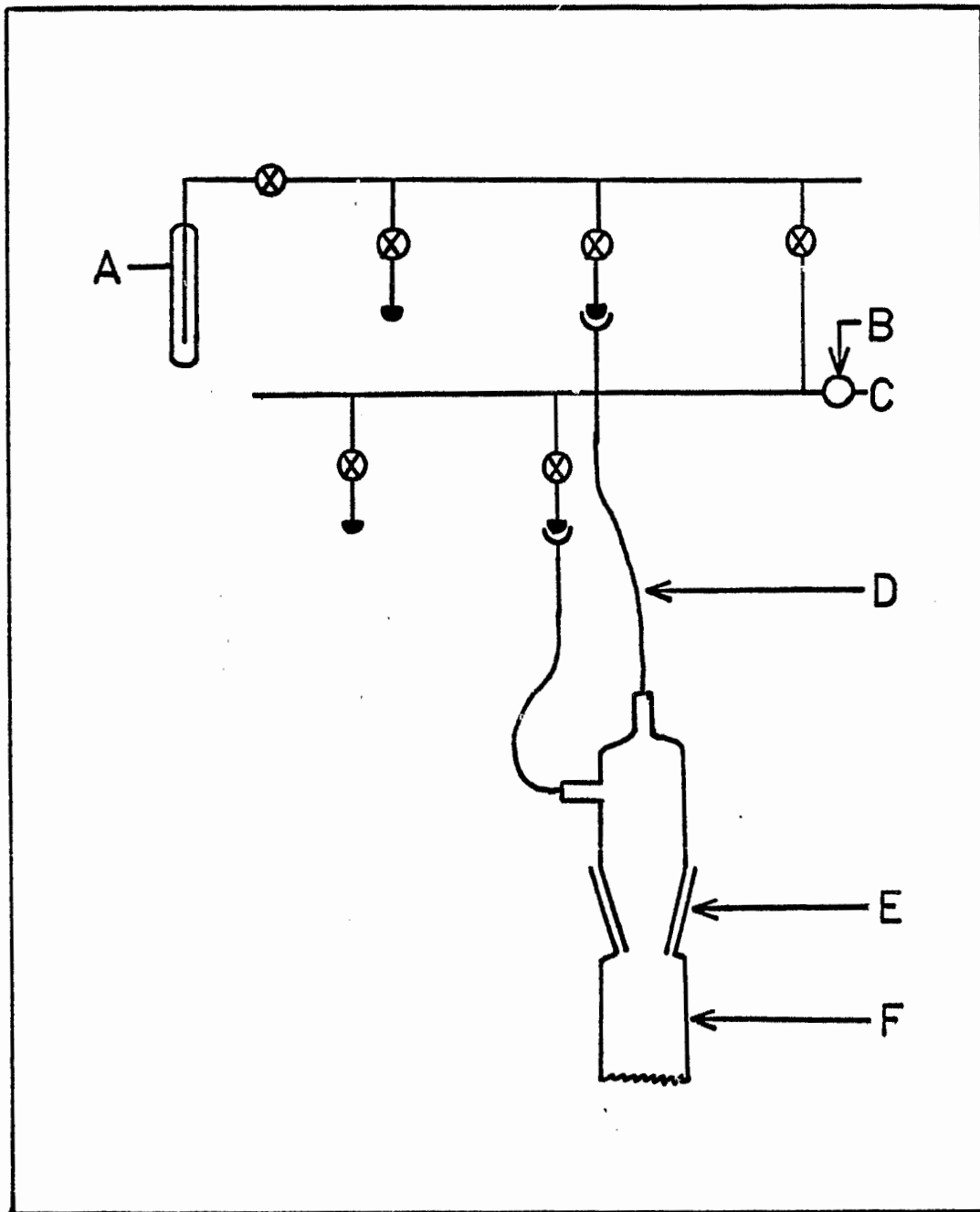


Figure 12.10 System for Filling Electrode Compartments

A - vacuum, B - needle valve, C - source of nitrogen,
 D - connecting Tygon tubing, E - 5/20 ground joint,
 F - top of electrode compartment

was used to release the residual vacuum in the electrode compartment. The blowing of a nitrogen vent in the wall of the compartment and the subsequent transfer and positioning of the electrode compartment in the furnace has been described in chapter 12.2.

Pure, 1 mm diameter, silver wire obtained from Johnson, Matthey and Mallory Ltd. was used for the silver electrodes. About 4 inches of one end of a 16 to 20 inch piece of silver wire was highly polished with fine emery paper to remove all of the surface films. The polished end of the silver wire was then wound into a coil with a diameter small enough to slide through a standard 5/20 inner tapered joint, 2 cm in length. The silver electrode wire was sealed in the top of the syringe electrode holder (see Figure 12.8) with piccin wax so that the lower end of the silver wire was about 1 cm above the melt when the syringe was fully extended and attached to the electrode compartment. Before the mechanical polishing a pretreatment of the wire with hot nitric acid was tried; however, it was discontinued after several trials showed that it had no effect on the performance of the electrode. After a two hour thermal equilibration period the silver electrode was inserted into the melt in the electrode compartment to a depth of 15 mm (see chapter 12.2 for details) and connected to the electrical measuring and generating system (Figure 12.9). There was no need to apply a thermocouple correction (211) to any of the readings since all of the silver to copper lead wire connections were made at the ambient temperature and the entire thermal gradient was over the pure silver wire.

After the required amount of silver(I) had been generated coulometrically in the electrode compartment, the silver electrode was rotated back and forth to facilitate the formation of a homogeneous mixture in the electrode compartment. The final reading for the emf of the cell was recorded only after the emf of the cell showed no signs of any drift in one direction and remained constant to ± 0.1 millivolt for 10 minutes. For most of the melts it would require approximately a 15 to 45 minute time period before the final reading could be taken. The stability of the silver electrode system in each melt was checked by recording the emf of the cell for several hours. After each experimental run had been completed, the two silver electrodes were removed and the electrode compartments were placed in a dessicator to solidify. The analysis of the contents of the electrode compartments and the calculation of the silver(I) concentrations are given in chapter 12.5. The portion of the silver electrode that had been in the melt during the experiment was cut off to prevent any cross contamination between melts and any electrode conditioning that may have occurred during the experiment from affecting the results for the next experiment.

The high viscosity of the sulfate melt caused its stabilization period to be exceedingly long. So, rather than generating the silver(I) in the sulfate reference electrodes, a known mixture of silver sulfate and the ternary sulfate eutectic was used to fill the electrode compartment instead of the pure sulfate eutectic. This procedure produced a reference sulfate electrode which stabilized

rapidly in the furnace and remained stable (± 0.5 mV) for periods in excess of twelve hours.

A special apparatus and procedure was required to remove the chlorine dissolved in the purified chloride eutectic. A glass ampule containing 100 to 125 grams of the chloride eutectic was opened, the solid ground up in a mortar and pestle and then transferred to eight sample bottles with tightly fitting lids in a dry box. The bottles and mortar and pestle had previously been dried in a vacuum oven at 120°C for twelve hours. The filled sample bottles were stored over P_2O_5 in a dessicator until needed and a second ampule was not opened until all of the previous sample had been used. There was enough chloride eutectic in each sample bottle for four complete runs.

The inner melt container (A), a small powder funnel, a nitrogen bubbler and an electrode compartment were cleaned in the normal manner and baked at 550°C for 24 hours before placing them in the chloride preparation apparatus (Figure 12.11). The apparatus was then closed, evacuated and heated to 400°C in the furnace to dry the inner portions of the apparatus. At the end of two hours, the vacuum was released using the purified nitrogen and while maintaining a steady flow of nitrogen through the cell, the top was removed, and the solid chloride eutectic quickly transferred from the sample bottle into the inner melt container with the aid of the small powder funnel. The apparatus was evacuated after the powder funnel had been removed and the top put back on the apparatus. During the fusion of the solid

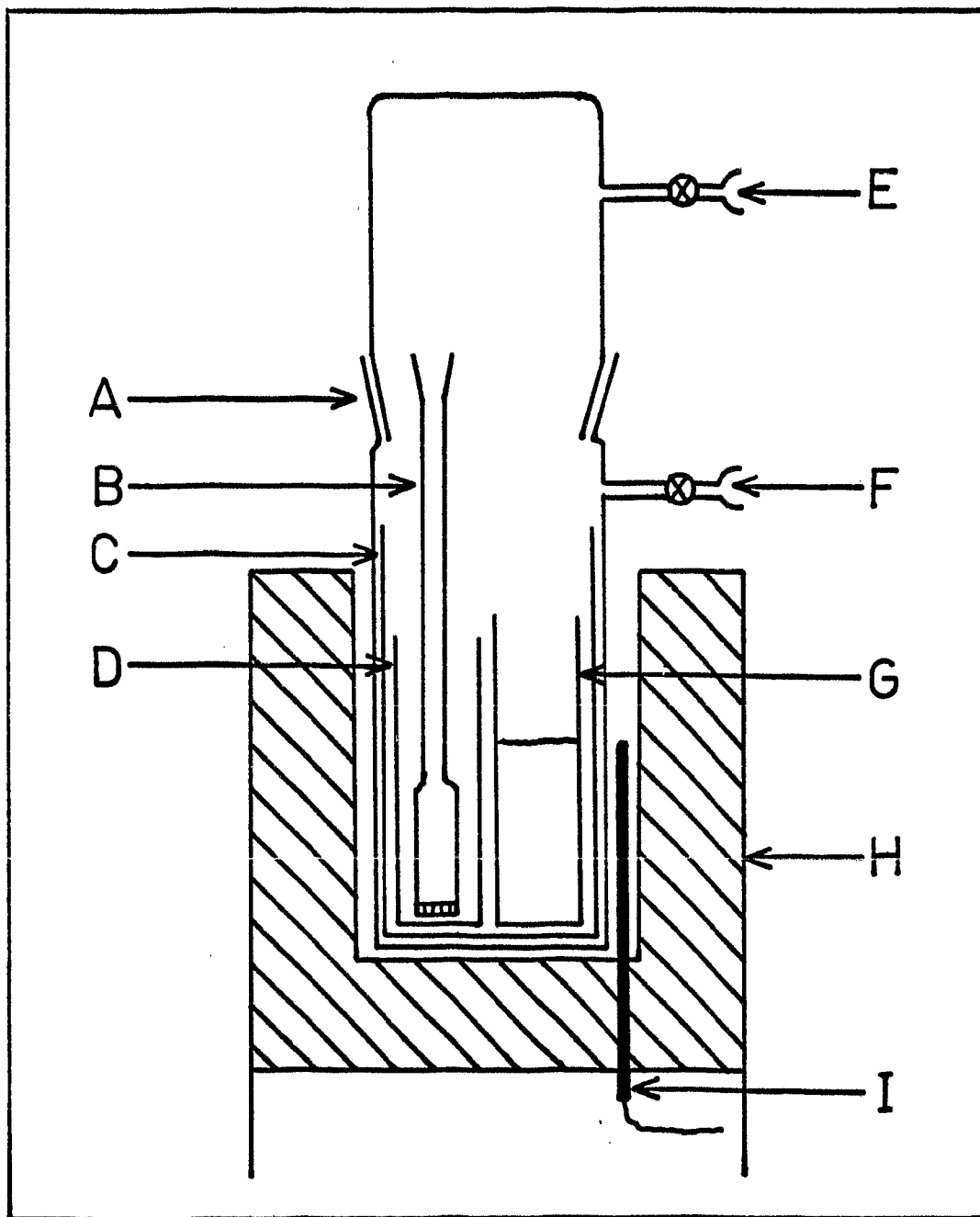


Figure 12.11 Apparatus to Fill Electrode Compartments with Chloride Melt

A - 45/50 ground joint, B - electrode compartment, C - liner to protect outer wall of cell, D - storage container for electrode compartment and nitrogen bubbler, E - vacuum, F - source of nitrogen, G - melt container, H - furnace, I - temperature probe for controller

and for twelve hours afterwards a vacuum was maintained (< 0.1 mm Hg) in the cell to remove the chlorine from the melt. A two hour period of purging with nitrogen followed while a flow of nitrogen was maintained over the melt surface. A strip of magnesium ribbon (Fisher Scientific Reagent Grade) which had been cleaned in hydrochloric acid, washed with water and dried at 120°C in a vacuum oven was added to the melt just before the apparatus was evacuated again. The active magnesium metal displaces any heavy metals in the melt and reacts with any chlorine left in the melt. The standard electrode potential of the magnesium(II)/magnesium couple (-2.58 V) is large enough that it will not interfere with the operation of the silver(I)/silver electrode which has a standard electrode potential of -0.727 volts versus a platinum(II)/platinum reference electrode at 450°C (20).

A minimum six hour magnesium treatment period was used in all of the preparations before filling the electrode compartment with the chloride melt. A flow of nitrogen was maintained over the chloride melt while the electrode compartment was placed in the empty container (B in Figure 12.11) for the next run before the re-evacuation of the apparatus.

In the chloride-nitrate solvent junction measurements, a special double fritted electrode compartment was used to prevent the diffusion of the nitrate melt into the silver(I) in lithium-potassium chloride/silver half cell. A second fine porosity sintered glass frit was attached to the bottom of the normal electrode compartment. The

distance between the two frits was about 1 cm and both the lower and upper compartments were filled with the chloride melt. Filling the compartments under vacuum prevented the formation of any gas bubbles in the lower compartment thus ensuring good electrical contact between the bulk melt and the silver chloride half cell.

A polarogram was run on the purified chloride melt at 450°C using a Sargent Polarograph Model XVI, a silver(I)/silver reference electrode and a micro platinum electrode (area = 0.128 mm²) to check the purity of the melt. The results, presented in terms of a one molal platinum(II)/platinum reference electrode in Figure 12.12 are in substantial agreement with previous reports (188 - 190) and no significant amounts of impurities could be detected by polarography in the chloride melt.

12.5 Analysis of Contents of Electrode Compartments

All of the chemical analyses were done using the standard techniques and primary standards given by Ayres (334). The analytical weighings were made on a Mettler Gram-atic Analytical balance to the nearest 0.1 milligram. The weight of the melt in the electrode compartment was determined by weighing the compartment before and after dissolving the contents in water. The excess melt on the outside of the electrode compartment was removed before the initial weighing by momentarily placing the lower portion of the compartment in hot water, rinsing with deionized water and then drying at 120°C for one hour. To prevent contamination the lower half of the used electrode compartments were never reused in another experiment.

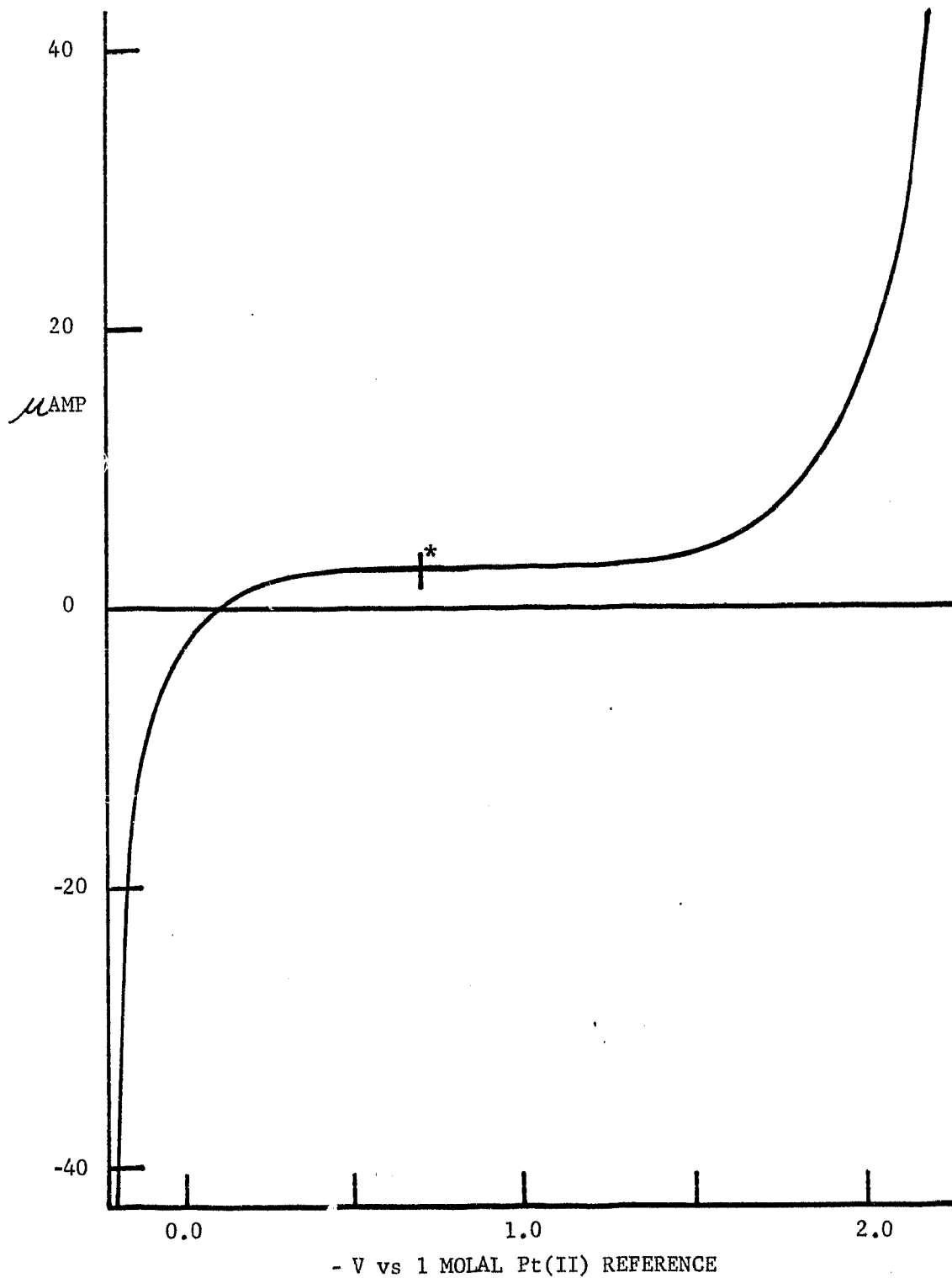


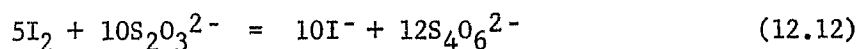
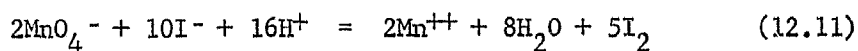
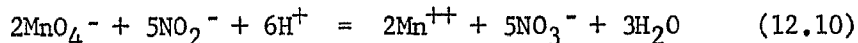
Figure 12.12 Polarogram of (Li,K)Cl Eutectic Melt at 450°C

Area of micro platinum electrode = 0.128 mm²

* potential of the 1.0 molal Ag(I)/Ag reference electrode

12.5.1 Nitrite analysis

The acidic aqueous nitrite solutions were treated with a measured excess of standardized potassium permanganate solution to oxidize the nitrite ion to the nitrate ion. The excess potassium permanganate was then back-titrated with a known sodium thiosulfate solution in the presence of potassium iodide and starch as an indicator. The average purity of $99.6 \pm 0.2\%$ for the purified sodium nitrate salt was determined from three separate trials. The small error may be due to small amounts of the potassium salt.



12.5.2 Chloride analysis

The chloride was determined gravimetrically in the form of silver chloride using silver nitrate as the precipitating agent. The silver chloride was collected in a sintered glass crucible of a fine porosity. Analysis showed that the purified lithium-potassium chloride eutectic contained 63.82 ± 0.05 percent chloride. The theoretical chloride percentage based on a 59 mole percent mixture of lithium chloride is 63.79%.



12.5.3 Sulfate analysis

Barium chloride was used to precipitate the sulfate ion in the form of barium sulfate which was collected and weighed in a fine

porosity sintered glass crucible. The alkali metal sulfate eutectic was found experimentally to contain $79.26 \pm 0.05\%$ sulfate by weight which compares well with the theoretical value of 79.20%.



12.5.4 Lithium analysis

The lithium samples were analyzed using a Perkin-Elmer Atomic Absorption Spectrophotometer, Model 303. A calibration curve (Figure 12.13) was constructed using seven samples in the concentration range of 2 to 16 ppm lithium prepared from a Fisher Scientific lithium reference standard solution (1000 ppm). The results for the lithium analysis of the various solvents are summarized in Table 12.2 and in all cases the results are in agreement with the values calculated from the molecular weights of the salts.

12.5.5 Sodium analysis

A Coleman Flame Photometer, Model 21, with a 21-207 sodium filter was used to analyze for sodium in the aqueous solutions. Standard samples ranging in concentration from 2 to 16 ppm of sodium were made up from a sodium Flame Standard Solution (100 ppm from Fisher Scientific) to construct a calibration curve (Figure 12.14). The analysis of the metals for sodium (Table 12.2) were in agreement with the calculated values.

12.5.6 Potassium analysis

A 21-203 potassium filter was used in the Coleman Flame Photometer in the analysis for potassium. A potassium Flame Standard Solution

TABLE 12.2

ANALYTICAL RESULTS FOR THE ANALYSIS OF VARIOUS MELTS FOR ALKALI METALS

Melt	Lithium		Sodium		Potassium	
	$\pm 0.1\%$ Expt.	% Calc.	$\pm 0.2\%$ Expt.	% Calc.	$\pm 0.2\%$ Expt.	% Calc.
NaNO ₂	0.0	0.00	33.0	33.32	0.1	0.00
LiNO ₃	10.1	10.07	0.0	0.00	0.0	0.00
NaNO ₃	0.0	0.00	27.1	27.05	0.1	0.00
KNO ₃	0.0	0.00	0.0	0.00	38.8	38.67
(Li,Na)NO ₃	4.9	4.91	13.9	13.85	0.0	0.00
(Li,K)NO ₃	5.0	4.99	0.0	0.00	19.5	19.52
(Na,K)NO ₃	0.0	0.00	10.9	11.02	22.9	22.91
(Li,K)Cl	7.4	7.37	0.0	0.00	28.7	28.84
(Li,Na,K) ₂ SO ₄	9.0	8.92	3.0	3.03	8.7	8.70

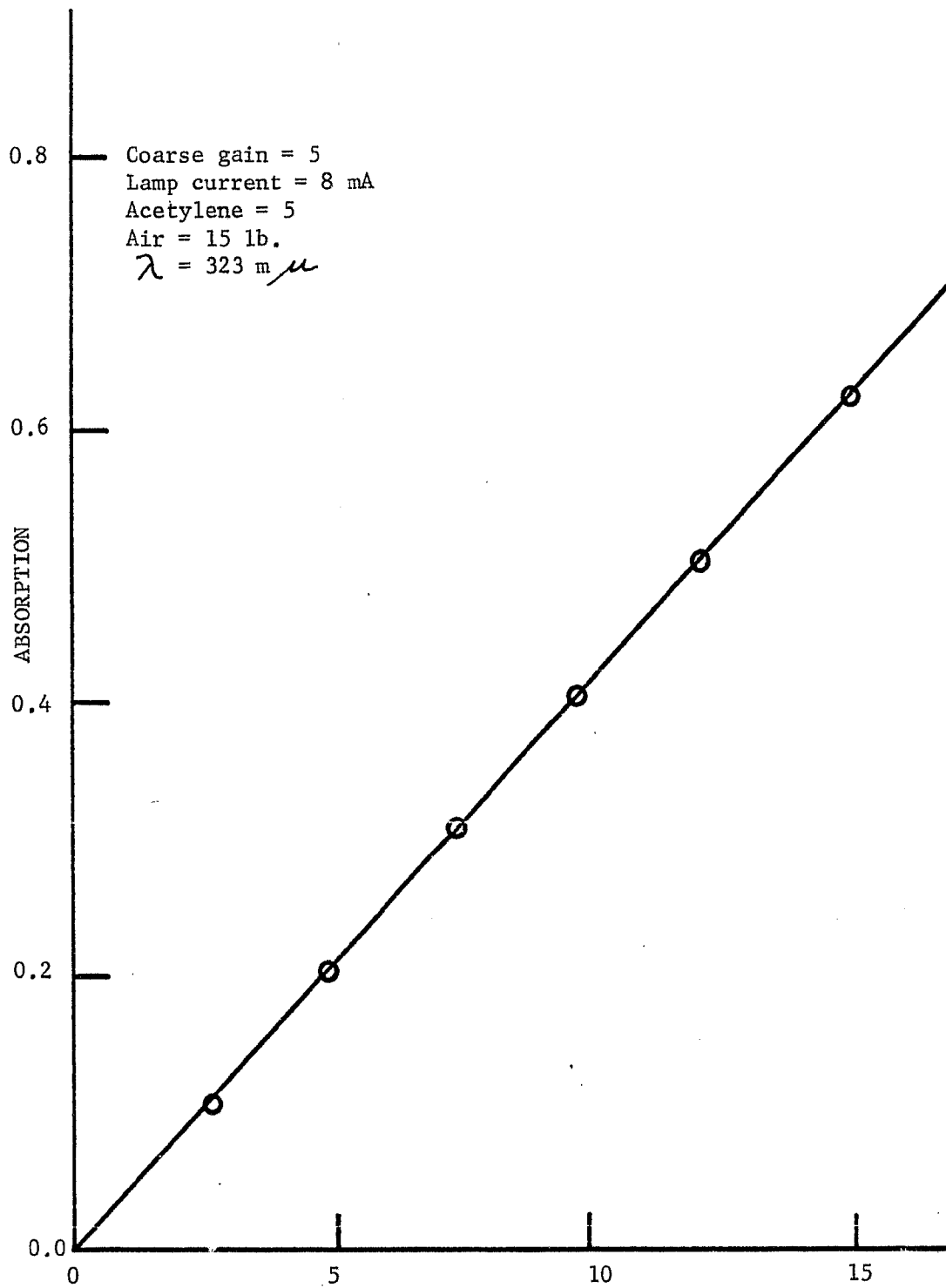


Figure 12.13 Calibration Curve for Lithium Analysis by Atomic Absorption

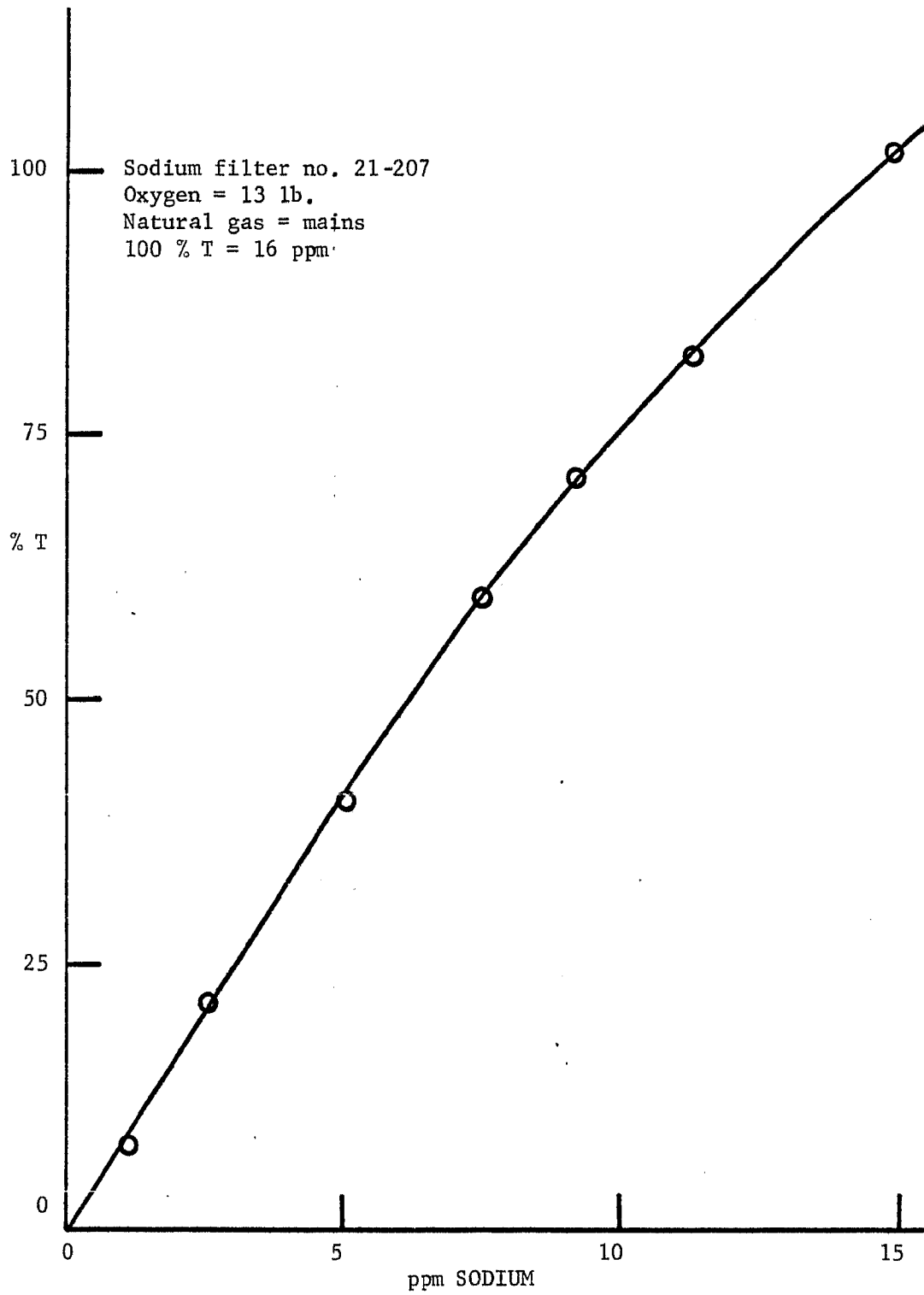


Figure 12.14 Calibration Curve for Sodium Analysis by Flame Photometry

(100 ppm from Fisher Scientific) was diluted down to give several samples ranging from 2 to 16 ppm potassium. The calibration curve from the potassium knowns is given in Figure 12.15 and the results from the analysis of the melts for potassium are given in Table 12.2. The results in Table 12.2 show that potassium salts occur as a slight impurity in some of the sodium salts; however, good agreement with the calculated values is observed throughout the table when the experimental error is taken into consideration.

12.5.7 Silver analysis

The silver was analyzed for by one of two methods depending upon the silver(I) concentration in the melt. The silver was determined gravimetrically if the silver(I) concentration was in excess of 0.2 molal which was equivalent to about 0.1 grams of silver chloride for the average weight of melt in the electrode compartment (3.5 grams). The majority of the silver analyses were done on dilute solutions of silver(I) ($m < 0.01$) using a Techtron Atomic Absorption Spectrophotometer, Model AA-100. Standard silver solutions ranging from 1 to 6 ppm were prepared by diluting a Fisher Scientific Silver Reference Standard Solution containing 1000 ppm silver. The silver atomic absorption calibration curve is given in Figure 12.16.

The silver analysis was used as a check on the amount of silver generated according to the coulometer as well as the amount due to the corrosion of silver wire (chapter 7.5, page 142).

The calculations of the silver(I) on the molal, molar and mole fraction scales were done on an IBM 1130 or IBM 360-50 computer.

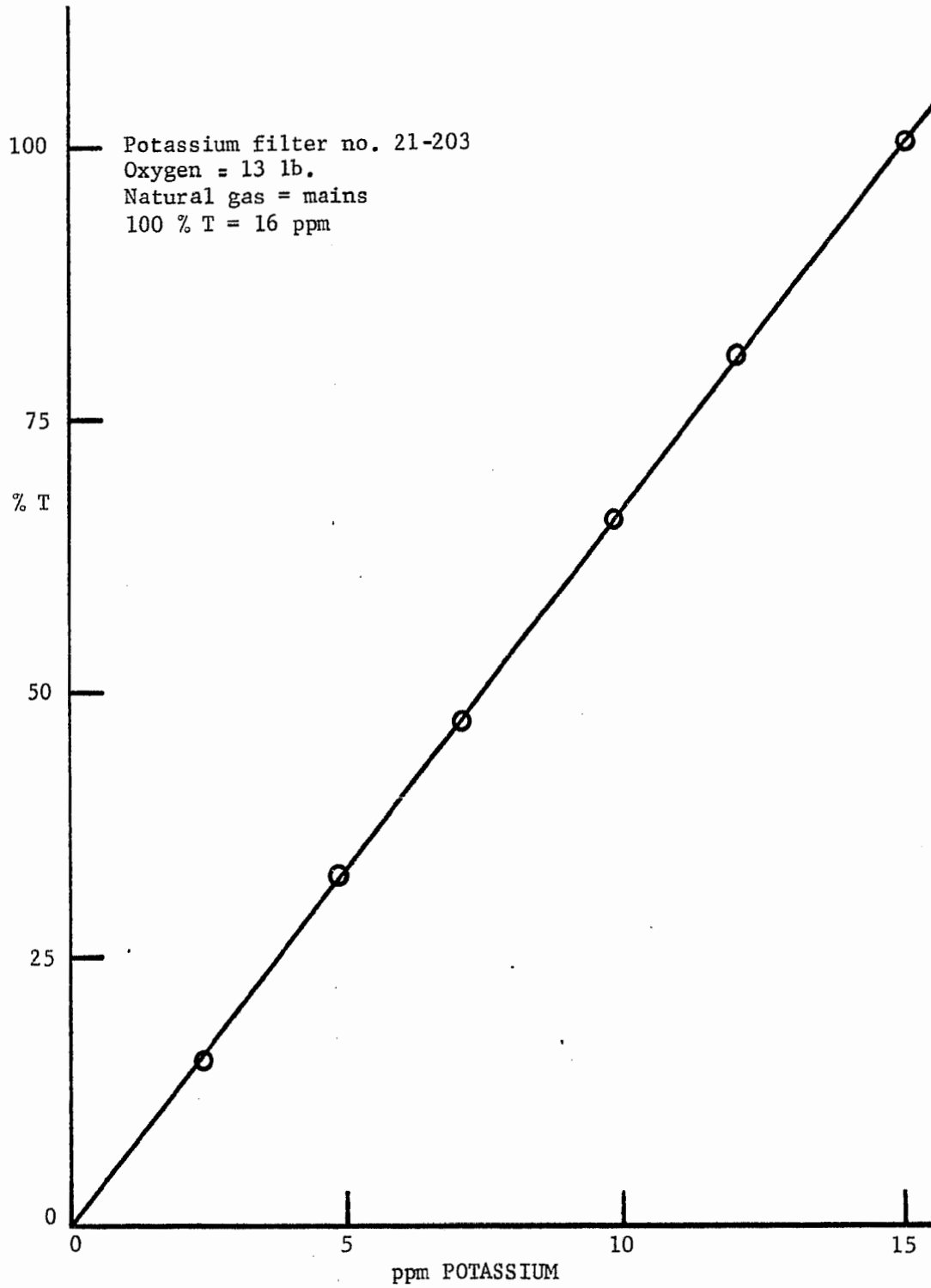


Figure 12.15 Calibration Curve for Potassium Analysis by Flame Photometry

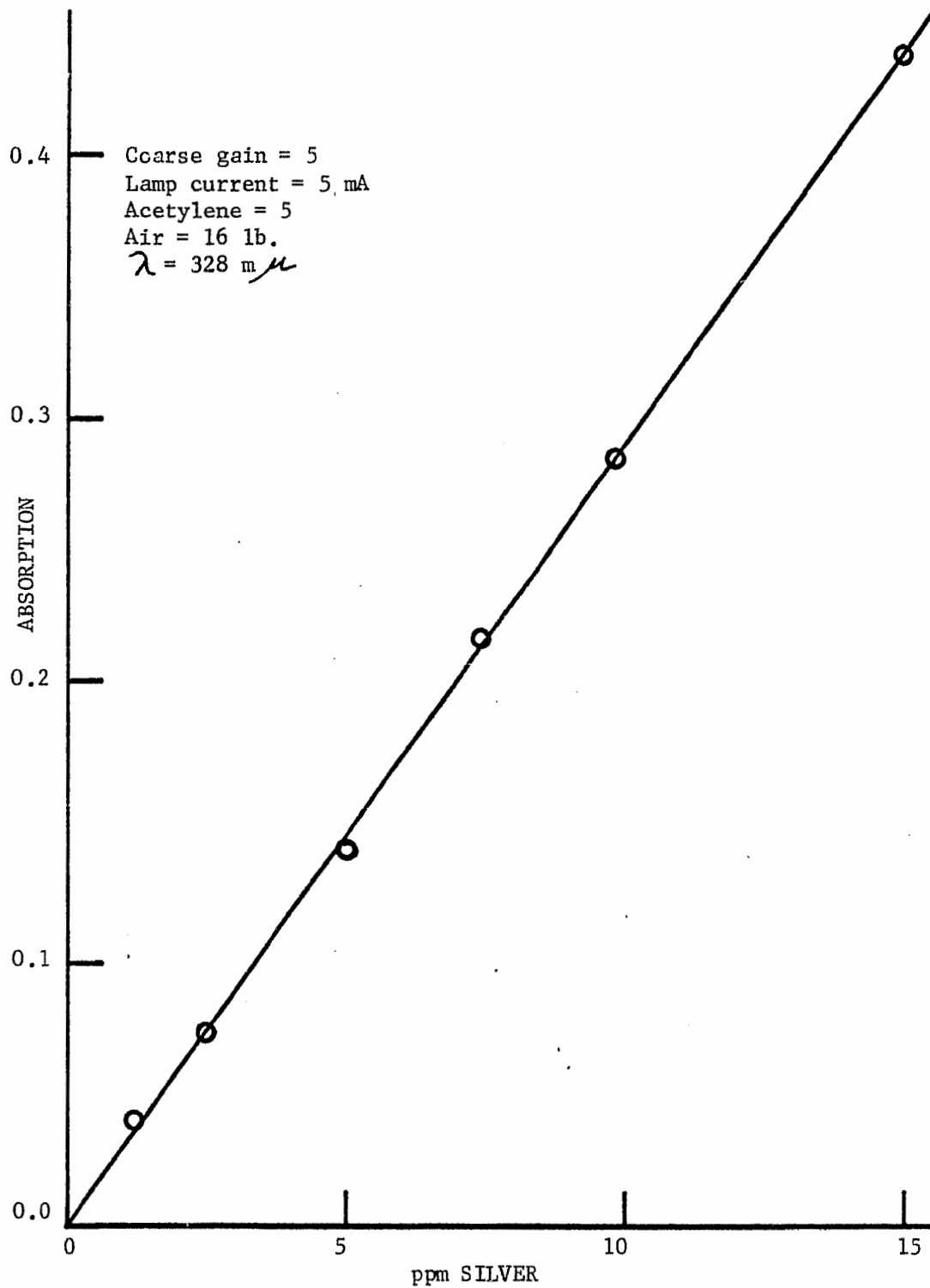


Figure 12.16 Calibration Curve for Silver Analysis by Atomic Absorption

The final weight of melt in the electrode compartment includes the silver salt plus the alkali metal salt, thus it was necessary to calculate backwards to evaluate the actual weight of solute and solvent at each concentration level in the experiment. It was assumed that for every micro-equivalent of silver(I) generated in the electrode compartment one micro-equivalent of alkali ion would leave the compartment through the frit since, as a rule, the smaller cations are more mobile than the bulky anions. The information required for each run was the total number of micro-equivalents of silver(I) generated, the final weight of the melt, the equivalent weight of the solvent, the equivalent weight of the silver salt, the density of the solvent and the total number of micro-equivalents of silver(I) generated at each concentration level. The computer program used to do the calculations is given in Appendix A.2 (page 334).

12.6 Density Measurements

All of the density measurements were made using the bouyancy method and the apparatus is shown in Figure 12.17. A silver bob (about 2 cm diameter and 2 cm length), suspended on a 1 mm diameter silver wire below an analytical balance, was immersed to a depth of 10 ± 1 mm below the surface of the melt in the glass container by raising the container with the screw jack stand. The error of ± 1 mm represents a volume of $\pm 8.0 \times 10^{-4}$ cc which when compared to the total volume of the bob (about 3.8 cc) represents an error of only $\pm 0.02\%$. The temperature of the melt was measured by a chromel-

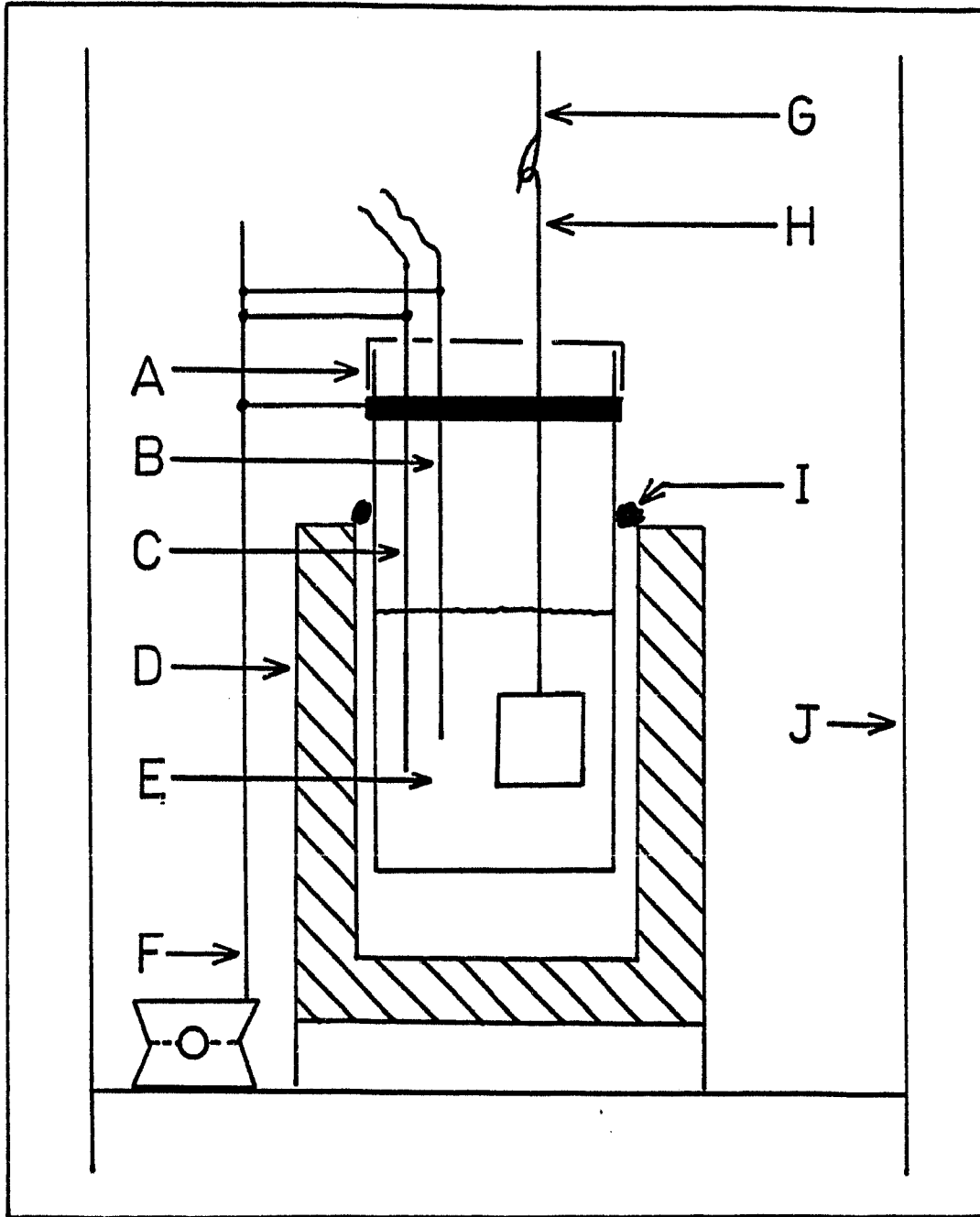


Figure 12.17 Density Apparatus

A - metal cap, B - thermocouple, C - temperature controller probe, D - furnace, E - melt, F - screw jack stand, G - to analytical balance, H - silver wire and bob, I - glass wool, J - enclosed stand to support furnace and balance

alumel thermocouple immersed in the melt along with the probe for the temperature controller (see Figure 12.7 for controller heating circuit). The sides of the stand used to support the apparatus and the top of the melt container were covered with aluminum foil to prevent thermal convection currents.

The melts were prepared in the normal manner and after each change in temperature, the weight and the temperature were not recorded until the two values remained constant to ± 0.0005 grams and $\pm 0.25^\circ\text{C}$, respectively, for 15 minutes. The densities were measured during both a heating and cooling series to average out any nonisothermal conditions that may exist in the system. The volume of the bob was calibrated using pure sodium nitrate and the results for the calibration and density measurements have been discussed in chapter 7.4 (page 128).

12.7 Nonisothermal Furnace

The nonisothermal furnace consisted of a U-shaped piece of glass tubing with each limb wrapped with separately controlled heating tapes (Figure 12.18). Two sintered glass disks were incorporated in the glass tubing to retard the thermal diffusion of the ions in the melt (Soret effect). A central tube was added to the cell to facilitate the filling of the cell with the melt and to provide electrical contact with the melt. The glass cell was protected from any ac interference from the heating tapes by wrapping the cell with aluminum foil before attaching the heating tapes.

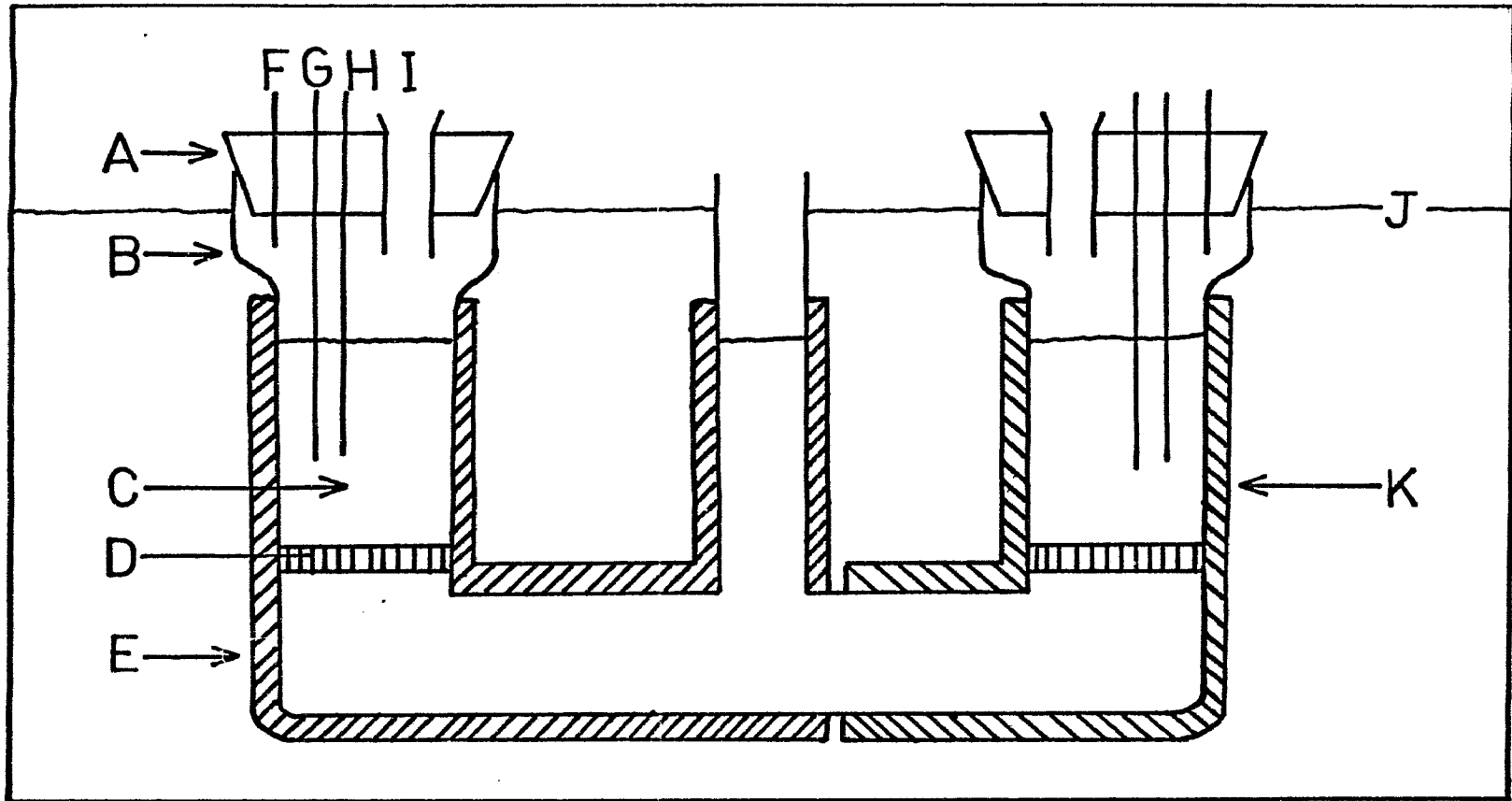


Figure 12.18 Cell for Thermoelectric Studies

A - foil-wrapped rubber stopper, B - foil (earthed) wrapped Pyrex cell, C - melt, D - 20 mm, fine fritted disk, D - heating tape connected to left temperature controller, F - N_2 inlet, G - probe for melt temperature controller, H - thermocouple, I - glass-lined inlet for electrode compartment, J - upper level of insulation, K - heating tape connected to right temperature controller

The procedure for filling and the positioning of the electrode compartments in each limb of the furnace was the same as that used for the isothermal measurements. The temperature of each limb could be varied independently by the use of the two controllers and a maximum temperature gradient of about 100°C could be realized between the two electrodes. After each temperature change the thermal stabilization in each half cell was achieved after 15 to 60 minutes depending upon the magnitude of the increment. The temperature gradient was reversed and the results for the two measurements were combined to eliminate any potentials due to the Soret effect. The results for the various cells examined are given and discussed in chapter 9 (page 211).

12.8 Gas Electrode Design

The final design used for all of the gas electrodes consisted of a piece of 8 mm glass tubing with a roll of platinum or gold gauze sealed in one end. The complete details of the electrode are presented in Figure 12.19.

It was necessary to prepare the roll of platinum gauze in a special manner to provide for the free passage of the gases through the gauze after it has been sealed into the glass tubing. The top one-quarter inch of a piece of 3/4 inch by 3 inch, 50 mesh platinum wire gauze (obtained from Johnson, Matthey and Mallory, Ltd.) was folded over to double the thickness along the top of the gauze. 26 gauge platinum wire was then coiled in a zig-zag fashion across the

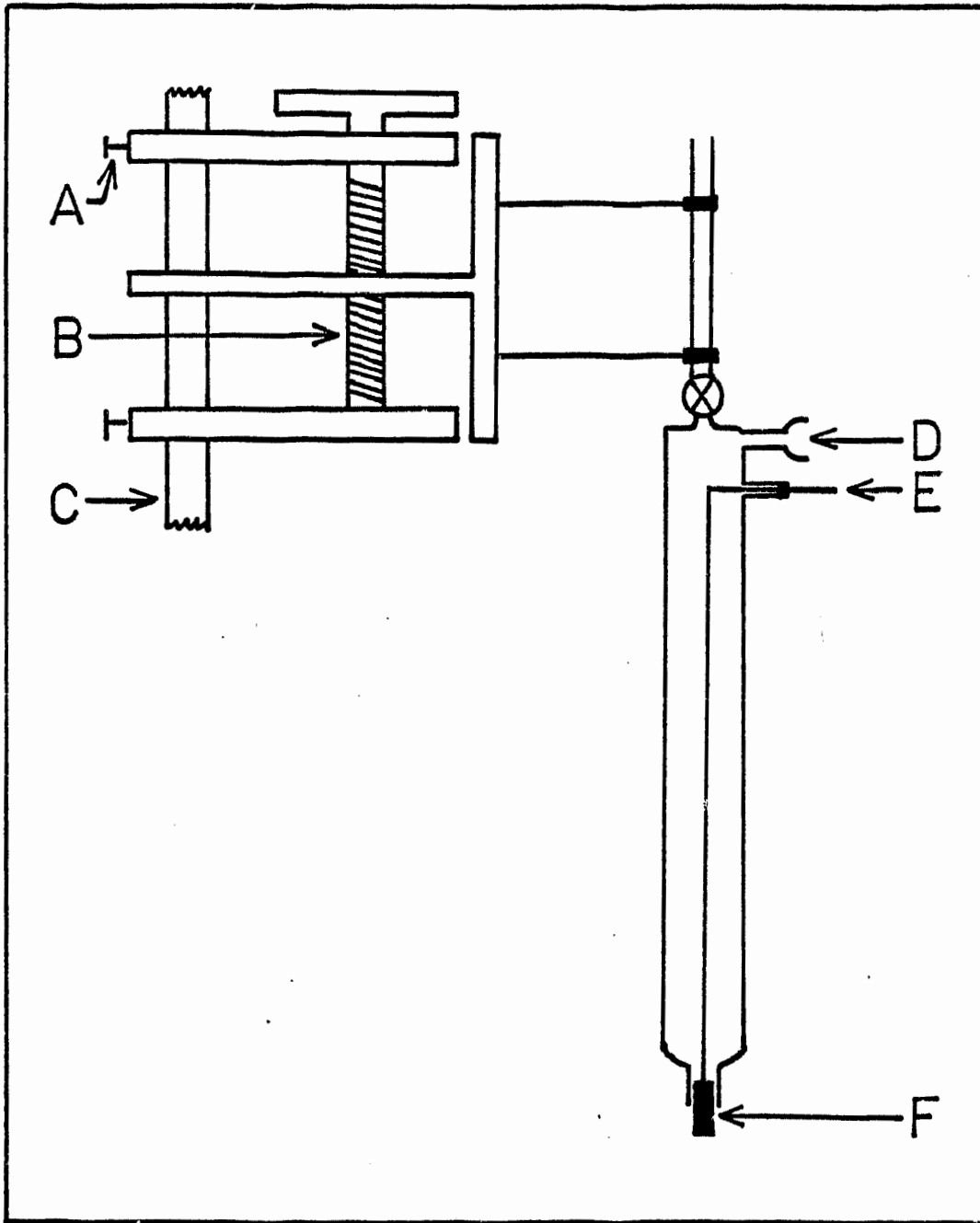


Figure 12.19 Design of Gas Electrode

A - set screws, B - micrometer screw, C - support stand,
 D - gas inlet, E - platinum lead wire, F - platinum
 gauze electrode

upper half of the gauze before the entire assembly was rolled up lengthwise to form the final gauze electrode. Only the upper portion of the gauze containing the platinum lead wire was sealed into the glass leaving approximately one-quarter inch of gauze exposed below the glass. The heavier platinum wire created small channels through the gauze where it was sealed in the glass for the passage of the gases. A special micrometer electrode holder with a travel of 1.5 mm per revolution of the dial was used for the vertical adjustment of the gas electrode in the melt. The gas electrode was used in a fritted electrode compartment inserted through the central inlet to the isothermal furnace. The reference electrode compartment was in one of the side inlets and the thermocouple-counter electrode compartment was in the other inlet. A slow flow of nitrogen through the gas electrode was started before the electrode was adjusted to a depth in the melt just above the point at which bubbling occurred. If there was no flow of gas through the electrode when it was immersed in the melt, the capillary action tended to draw so much melt up into the metal gauze that it was difficult to obtain a proper gas flow through the electrode afterwards. The top of the gas electrode and the delivery tube from the gas control system were wrapped with a heating tape to preheat the gases to the cell temperature to obtain better equilibrium conditions.

The tap on the top of the gas electrode provided an outlet so that the gases in the system could be quickly flushed out with nitrogen. A piece of tubing connected through a dry ice trap to a water

aspirator was used to collect the gases emerging from the top of the gas electrode compartment. The results for the various gas electrode systems have been given and discussed in chapter 10 (page 223).

12.9 Gas Control System and Analysis

12.9.1 Gas purification

The commercial nitrogen was purified by passing it through a 24 inch iron pipe heated to 325°C and filled with copper mesh to remove the oxygen and then through a 3 foot molecular sieve (type 5A) column to dry the gas. Copper tubing was used to carry the purified nitrogen to the various parts of the experimental set up, since oxygen will slowly diffuse through the wall of tygon or rubber tubing. The purity of the nitrogen was checked by bubbling it slowly through a dilute acidic chromous sulfate solution in a gas washing tower. The commercial nitrogen, 99.8% pure, turned the blue chromous solution to the green chromic color in about one minute, whereas after 8 hours of bubbling with the purified nitrogen there was no perceptible change in the blue color. This indicates that the oxygen level had been reduced by a factor greater than 480.

The commercial oxygen was dried in a 2 foot molecular sieve column with no further purification. The nitrogen dioxide was obtained from Matheson of Canada Ltd. in the form of liquid nitrogen tetroxide (minimum purity of 99.5%) and was used without further purification. The E.H. Sargent and Company supplied the sulfur trioxide which was

used without any additional purification.

12.9.2 Gas control system

The flows of the nitrogen, oxygen and nitrogen dioxide were controlled using stainless steel micro-flow valves, Model 151, from Matheson of Canada Ltd. The flows were measured using pressure differential flow meters and n-Butyl Phthalate in the manometers. The nitrogen and oxygen flow meters were similar in design to that for the nitrogen dioxide shown in Figure 12.20 except they were not thermostated. The entire gas control system consisted of the three flow meters connected in series with an open-ended n-butyl phthalate manometer to measure the excess pressure in the system over that of the atmosphere. The nitrogen and oxygen flow meters were calibrated using a bubble meter and the results are plotted in Figures 12.21 and 12.22, respectively (atmospheric pressure = 705.2 mm Hg and the temperature = 24.8°C). The internal pressure of the gas system was varied from 6 to 310 mm n-butyl phthalate in excess of the atmospheric pressure during the calibration of the flow meters with no observable effect on the flow rate. A least squares fit of the two sets of data was used to obtain the equations for the flow rate of the nitrogen gas.

$$\text{Flow (N}_2\text{)} = \Delta P_{(\text{N}_2)} \times 0.4329 \text{ cc minute}^{-1} (\text{mm n-butyl phthalate})^{-1} \quad (12.15)$$

and the oxygen gas

$$\text{Flow (O}_2\text{)} = \Delta P_{(\text{O}_2)} \times 0.1839 \text{ cc minute}^{-1} (\text{mm n-butyl phthalate})^{-1} \quad (12.16)$$

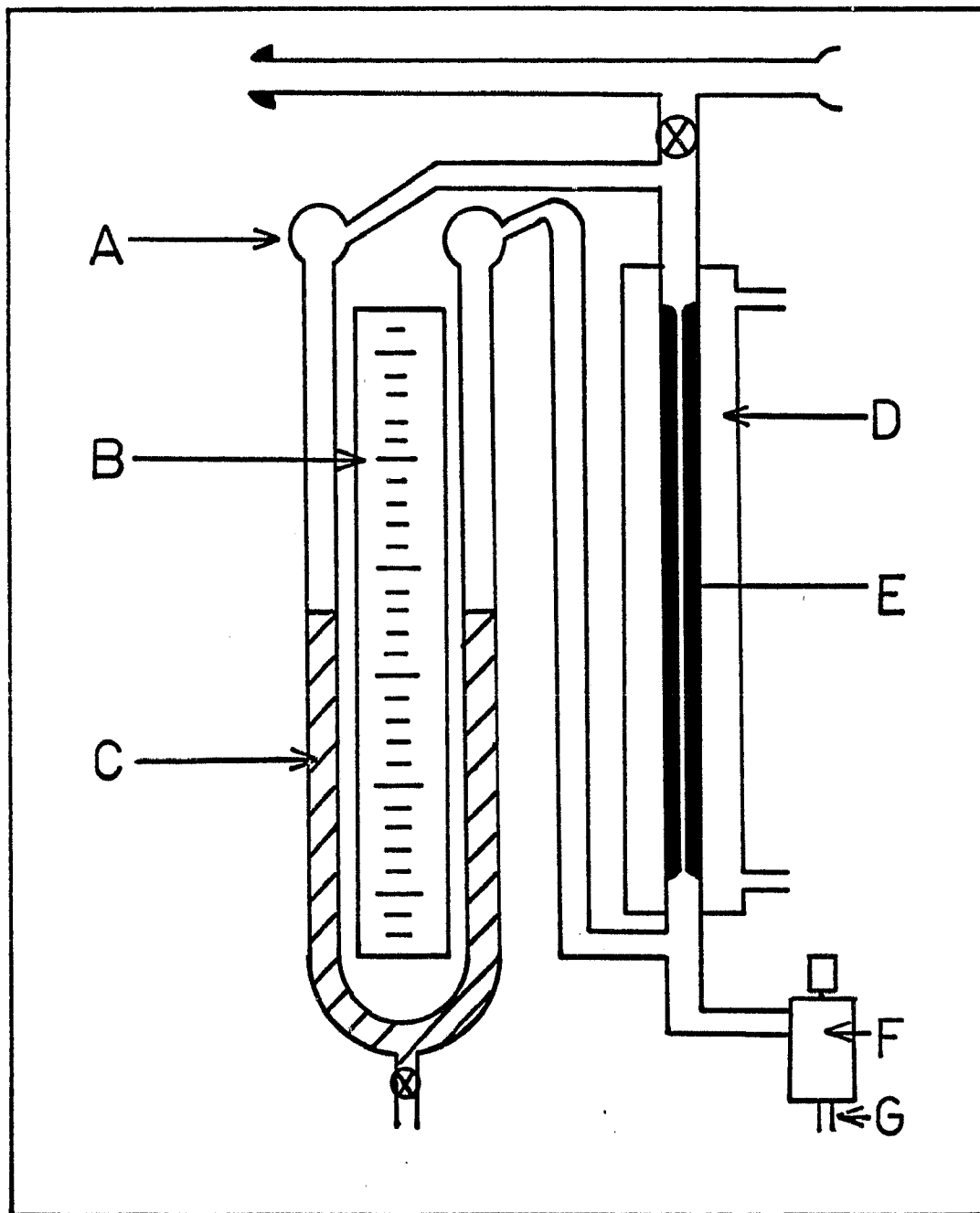


Figure 12.20 Nitrogen Dioxide Flow Meter

A - liquid traps, B - mm scale, C - n-butyl phthalate,
 D - water jacket, E - capillary, F - micro flow valve,
 G - to NO₂ supply

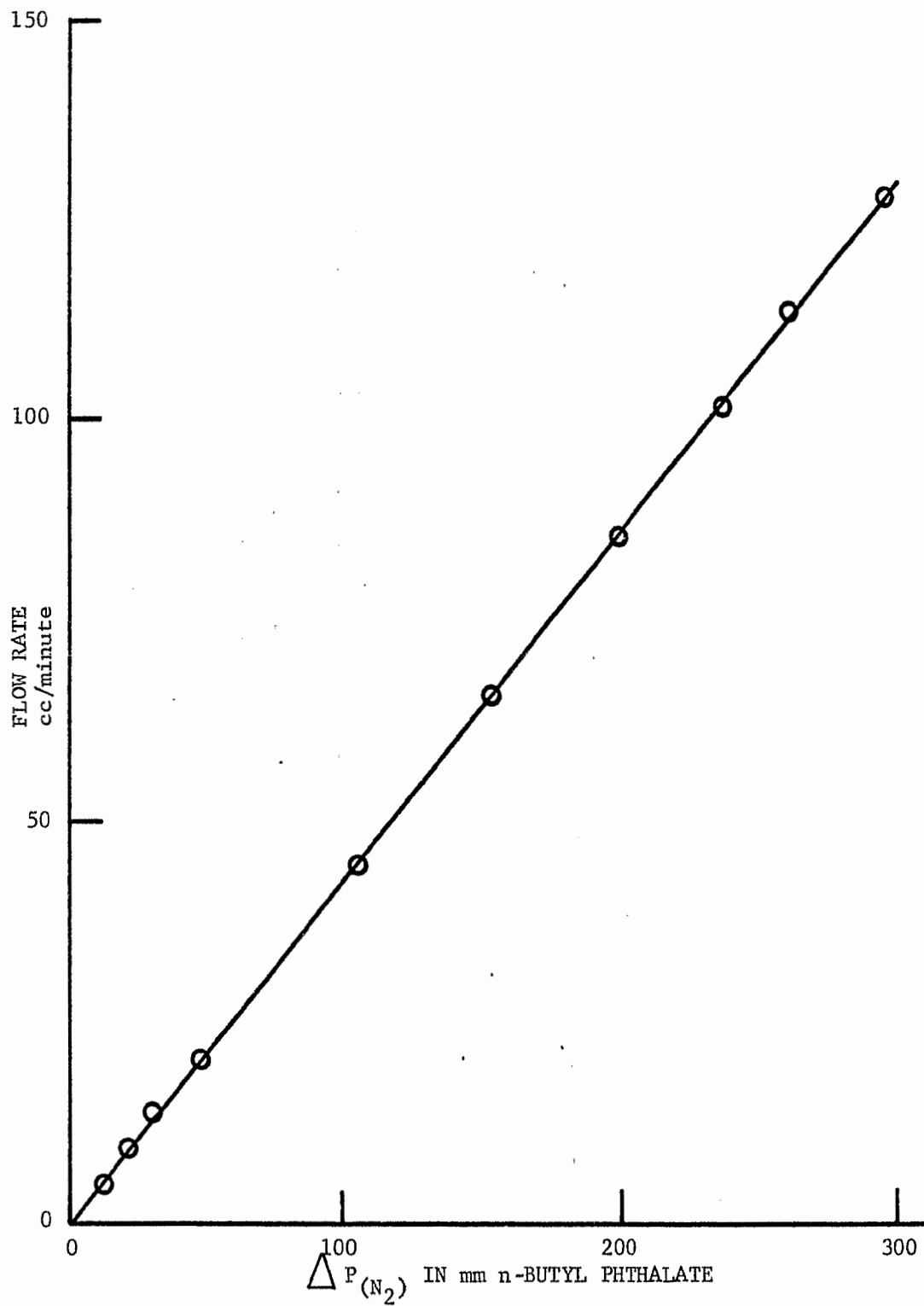


Figure 12.21 Calibration Curve for Nitrogen Flow Meter

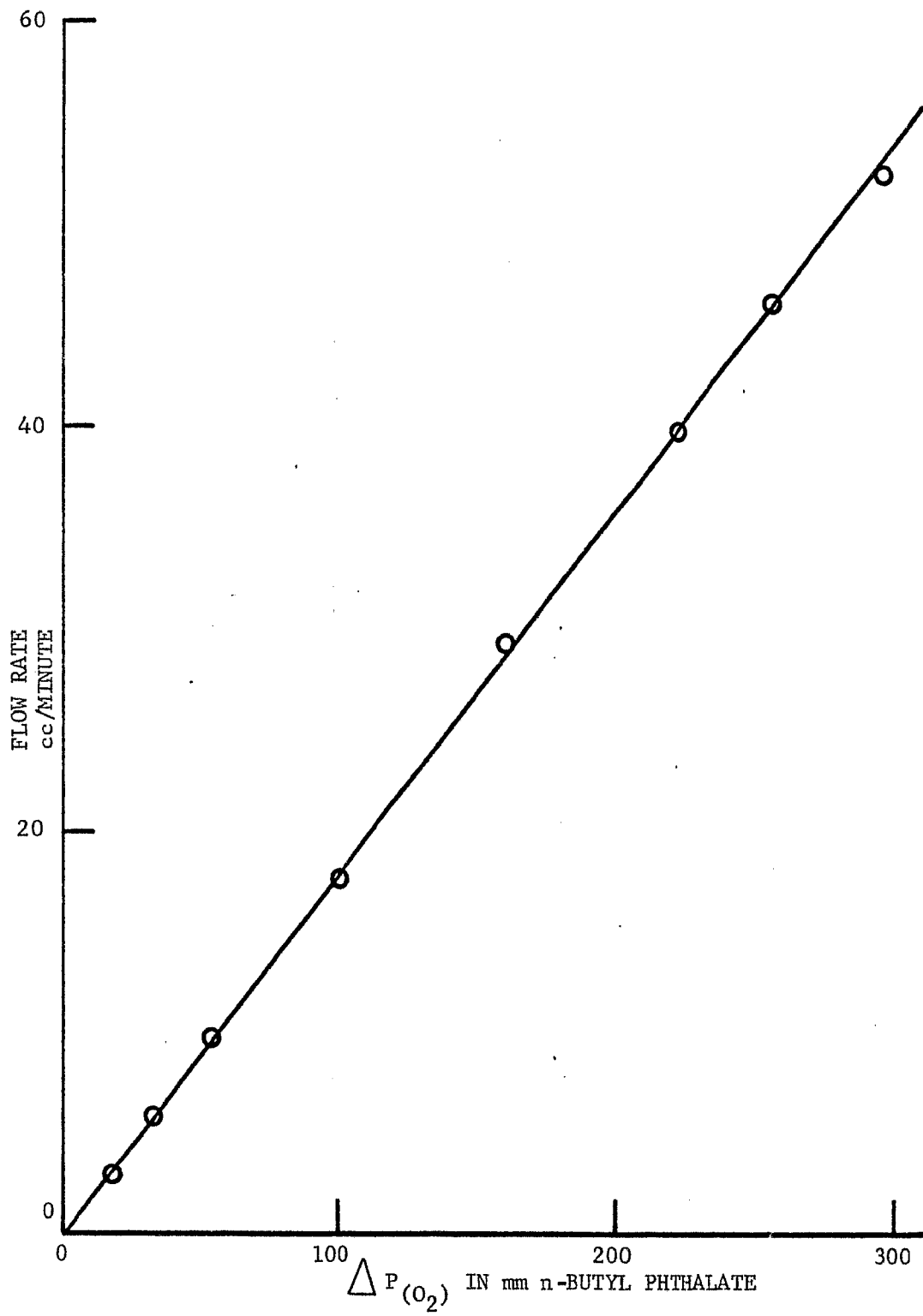


Figure 12.22 Calibration Curve for Oxygen Flow Meter

Using the ideal gas law, equations 12.15 and 12.16 were converted into units of moles minute⁻¹ to give the following equations:

$$\text{Flow (N}_2\text{)} = \Delta P_{(\text{N}_2)} \times 1.643 \times 10^{-5} \text{ moles minute}^{-1} (\text{mm n-butyl phthalate})^{-1} \quad (12.17)$$

$$\text{Flow (O}_2\text{)} = \Delta P_{(\text{O}_2)} \times 0.6979 \times 10^{-5} \text{ moles minute}^{-1} (\text{mm n-butyl phthalate})^{-1} \quad (12.18)$$

The 21.15°C normal boiling point of dinitrogen tetroxide made it necessary to heat the tank of liquid nitrogen tetroxide to obtain a usable pressure of the gas. The flow meter was thermostated at 65°C and the delivery tubes were heated to about the same temperature with a heating tape to prevent the condensation of the dinitrogen tetroxide. The flow meter was calibrated by collecting the nitrogen dioxide in a half saturated potassium hydroxide solution for a given time at a given $\Delta P_{(\text{NO}_2)}$ and then the excess base was back-titrated with hydrochloric acid.



The results for the calibration of the flow meter are plotted in Figure 12.23 in the form of moles of nitrogen dioxide minute⁻¹ versus $\Delta P_{(\text{NO}_2)}$ in mm n-butyl phthalate. A least squares fit of the data relates the flow rate of the nitrogen dioxide to the pressure differential recorded on the flow meters manometer by the equation

$$\text{Flow (NO}_2\text{)} = \Delta P_{(\text{NO}_2)} \times 1.184 \times 10^{-5} \text{ moles minute}^{-1} (\text{mm n-butyl phthalate})^{-1} \quad (12.21)$$

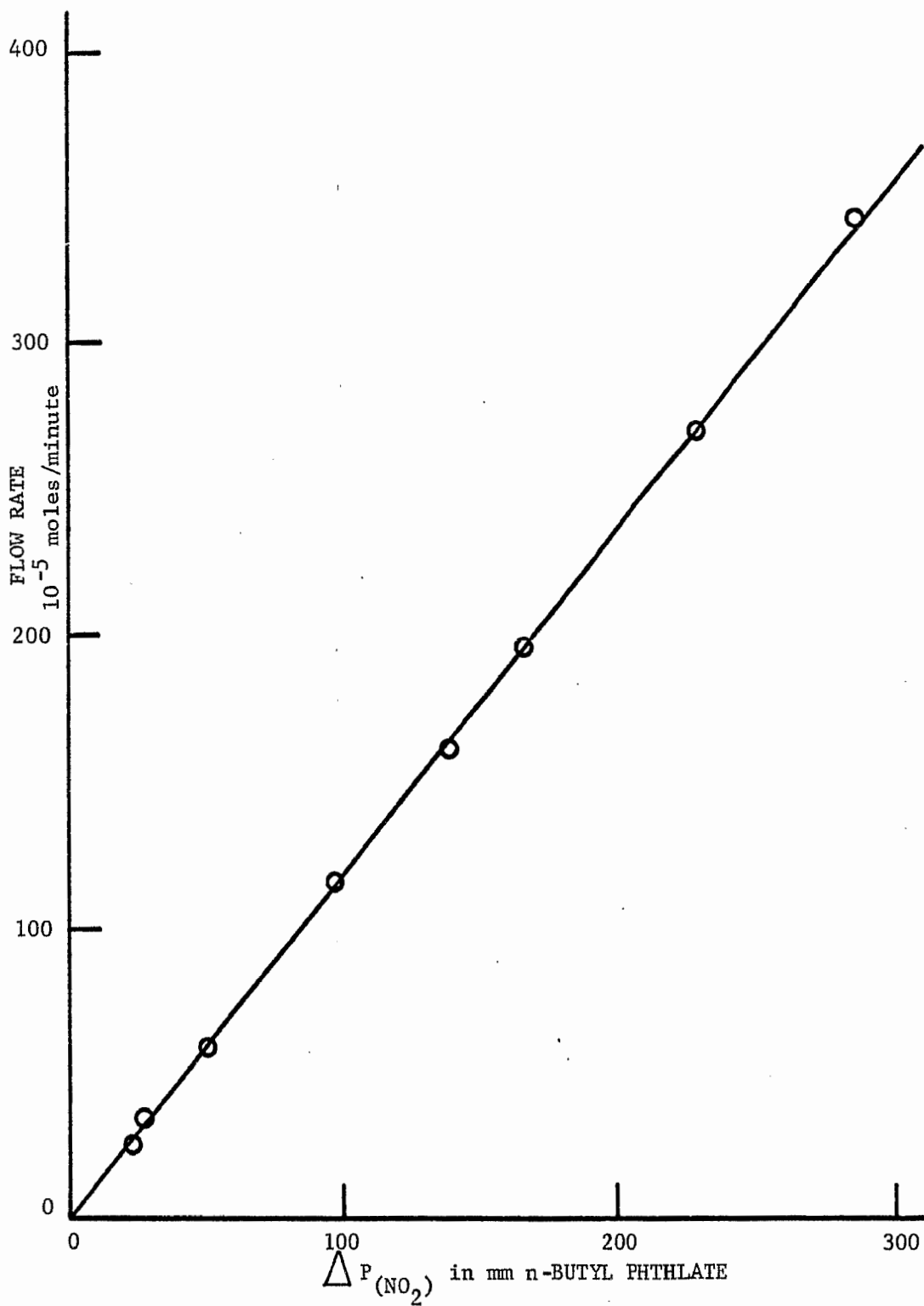


Figure 12.23 Calibration Curve for Nitrogen Dioxide Flow Meter

Temperature of flow meter = 65°C

The partial pressure of each gas in the mixture can be calculated by Dalton's Law of Partial Pressures since the dinitrogen tetroxide dissociates completely into nitrogen dioxide at the cell temperature ($T > 250^{\circ}\text{C}$). The total pressure in the system is given by

$$P = \left[\frac{P_{\text{atm.}} + \frac{P_{\text{exc.}} \times 1.048}{13.59}}{760} \right] \text{ atm.} \quad (12.22)$$

where $P_{\text{atm.}}$ is the atmospheric pressure in mm of mercury and

$P_{\text{exc.}}$ is the excess pressure in the system in mm of n-butyl phthalate.

The computer program given in Appendix A.3 (page 336) was used to calculate all of the partial pressures and logarithms of partial pressures required in the emf calculations. The total number of moles flowing per minute was used as a measure of the over-all flow rate of gases through the gas electrode.

The highly corrosive nature of the sulfur trioxide prevented the use of a flow meter since the gas attacked the n-butyl phthalate and all of the other liquids which are satisfactory to use in a manometer.

It was necessary to use an apparatus similar to the one used by Ketelaar and Dammers-de Klerk (174) in their nitrogen dioxide-oxygen gas electrode experiments. The nitrogen and oxygen flow meters previously described were used to bubble a gas mixture at a known rate and composition through the liquid sulfur trioxide in the

boiling flask (Figure 12.24). The temperature of the boiling flask was maintained at about 10°C above that of the condensing column to ensure a saturation of the gas stream with the sulfur trioxide. By varying the temperature of the condensing column the partial pressure of the sulfur trioxide in the gas mixture could be changed to any desired value. The excess sulfur trioxide was collected in the small bulb at the bottom of the condensing column as the gases passed through the column. All of the connecting glass tubing was 1 mm inside diameter to eliminate as much dead space as possible. The portions of tubing which sulfur trioxide passed through were heated to more than 50°C by either heating tape or infra red heat lamps to prevent the formation of any condensate.

The vapor pressure of the sulfur trioxide is given by

$$\log (760 P_{\text{SO}_3}) = 10.022 - 2269.4/T^{\circ}\text{K} \quad (12.23)$$

where T is the temperature of the condensing column (335). The sum of the partial pressures of the oxygen, P_{O_2} , and the nitrogen, P_{N_2} , is given by

$$P - P_{\text{SO}_3} = P_{\text{N}_2} + P_{\text{O}_2} \quad (12.24)$$

where P is the atmospheric pressure and all of the pressures are expressed in atmospheres. The flow rates of the oxygen, $N_{(\text{O}_2)}$, and nitrogen, $N_{(\text{N}_2)}$, expressed as moles minute⁻¹ are given by equation 12.18 and equation 12.17, respectively. The total flow rate, $N_{(\text{total})}$, in moles minute⁻¹ is given by

$$N_{(\text{total})} = \frac{(N_{(\text{N}_2)} + N_{(\text{O}_2)})P}{P - P_{\text{SO}_3}} \quad (12.25)$$

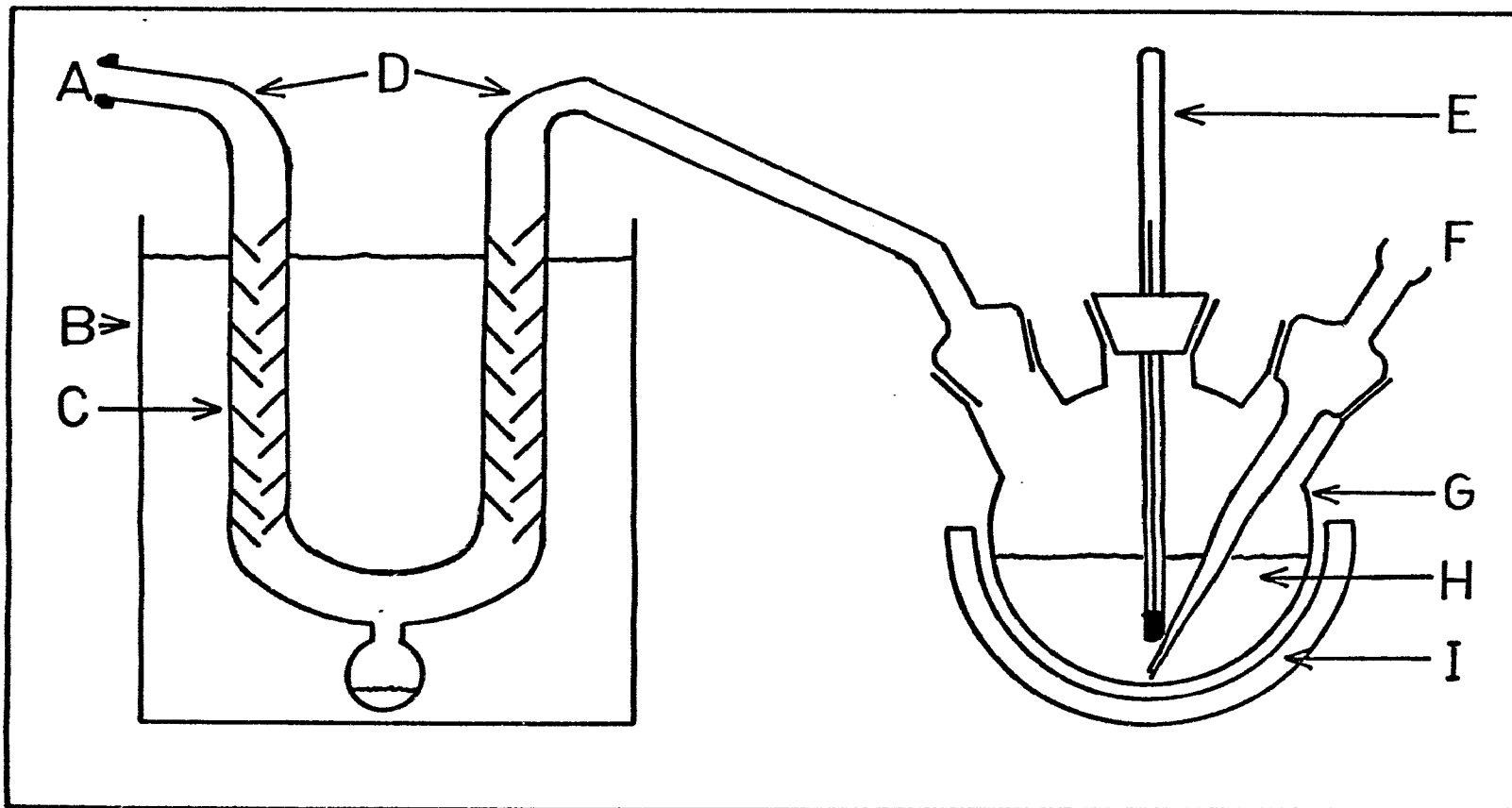


Figure 12.24 Apparatus to Control P_{SO_3}

A - gas outlet to gas electrode, B - thermostated bath, C - condensing column, D - delivery tubes heated by an infrared lamp, E - thermometer, F - O_2 and N_2 gas mixture inlet, G - 250 ml flask, H - liquid SO_3 , I - heating mantle

and the partial pressures of the oxygen and nitrogen are given by

$$P_{O_2} = \frac{P N_{(O_2)}}{N_{(total)}} \quad (12.26)$$

and

$$P_{N_2} = \frac{P N_{(N_2)}}{N_{(total)}} \quad (12.27)$$

respectively. Using the total flow rate it is possible to calculate the flow rate of the sulfur trioxide in moles minute⁻¹ by the equation

$$N_{(SO_3)} = \frac{P_{SO_3} N_{(total)}}{P} \quad (12.28)$$

The sulfur trioxide content of the final gas mixture was checked by collecting it in a cold trap and then weighing it. The results in Table 12.3 show that the calculated quantities of sulfur trioxide are in agreement with the experimental values. The design and the procedure for the operation of the gas electrode has been given previously in chapter 12.8.

TABLE 12.3

ANALYSIS OF GAS MIXTURE FOR SULFUR TRIOXIDE

Temperature Condensing Column °C	ΔP_{O_2} Oxygen Flow Meter (mm)	Time (min.)	Flow Rate of SO ₃ (gms/min)	Calc. Weight of SO ₃ (gms)	Expt. Weight of SO ₃ (gms)	% Difference
35.0	18	60.0	0.01722	1.033	1.012	-2.0
34.2	13	60.0	0.01099	0.659	0.669	+1.5
28.5	15	90.0	0.00653	0.588	0.601	+2.2
41.3	17	30.0	0.07410	2.220	2.205	-0.7

APPENDIX A

Computer Programs

Most of the programs were originally written using Fortran II for an IBM 1130 computer and then converted using Fortran IV for an IBM 360-50. No plotter was available, thus a plotting subroutine, G 402 P, was written to plot the results from the various programs.

Index to Programs

- A.1 - Silver Corrosion in Melts
- A.2 - Silver Concentrations in Melts
- A.3 - Gas Pressures for Nitrate Electrode
- A.4 - Least Squares Straight Line: error in only one variable
- A.5 - Least Squares Straight Line: error in both variables
- A.6 - Data Fitting to n^{th} Order Polynomial
- A.7 - Plotting Subroutine: G 402 P
- A.8 - Determinant Subroutine: G 402 T

A.1 - SILVER CORROSION IN MELTS

PAGE 1

```

C.....A.1 - SILVER CORROSION IN MELTS                                CORR 1
C.....CALCULATE SILVER CORROSION IN NITRATE MELTS                    CORR 2
C*****CORR 3
C.....PROGRAMMER L.BOXALL SEPT. 1969                                  CORR 4
C.....INPUT ON CARDS                                                 CORR 5
C.....COL. 1 = INDICATOR                                             CORR 6
C          = BLANK -DATA CARD                                         CORR 7
C          = 1 -DESCRIPTION CARD                                       CORR 8
C          = 2 -END CF JOB                                             CORR 9
C.....CARD SEQUENCE , 1 DESCRIPTION CARD THEN DATA CARDS FOR EACH RUN , CORR 10
C          AFTER LAST RUN END OF JOB CARD                               CORR 11
C          ARRANGE DATA CARDS IN INCREASING SILVER CONC. SEQ. CORR 12
C          IF A DECREASE IS ENCOUNTERED, THE LOW CONC. CARD CORR 13
C          IS TREATED AS A FIRST CARD OF A NEW SUBSET OF CORR 14
C          DATA UNDER THE TITLE OF THE RUN ON THE PREVIOUS CORR 15
C          DESCRIPTION CARD CORR 16
C.....DESCRIPTION CARD                                               CORR 17
C          COL. 1 = 1 CORR 18
C          COL. 2-10 = TEMPERATURE DEG.C CORR 19
C          COL. 31-70 = TITLE OF RUN CORR 20
C.....DATA CARD                                                       CORR 21
C          COL. 1 = BLANK CORR 22
C          COL. 2-10 = LOG(MOLE FRACTION SILVER GENERATED TODATE) CORR 23
C          COL. 11-20 = OBSERVED VOLTAGE,VOLTS CORR 24
C          COL. 21-30 = LIQUID JUNCTION POTENTIAL,VOLTS CORR 25
C.....END OF JOB CARD                                               CORR 26
C          COL. 1 = 2 CORR 27
C.....OUTPUT ON PRINTER                                              CORR 28
C          TWO LINES PER DATA CARD, ONE BEFORE CORRECTION AND ONE CORR 29
C          AFTER CORRECTION CORR 30
C          RT LN(ACT.COEFF.) = W(1-N)(1-N) CORR 31
C.....INCLUDE DECIMAL POINT IN ALL REAL NUMBER INPUT                CORR 32
C*****CORR 33
C          DIMENSION DES(10) CORR 34
109  FORMAT(' ',E11.4, 6F12.4,26X,F13.4) CORR 35
110  FORMAT(' ',E11.4,6F12.4,E13.4,13X,F13.4) CORR 36
102  FORMAT(' ',E11.4,6F12.4,2E13.4,F13.4) CORR 37
          DIVL=A LOG(10.0) CORR 38
          IFIRST=0 CORR 39
          CORR 40
          CORR 41
          CORR 42
          CORR 43
          CORR 44
          CORR 45

```

A.1 - SILVER CORROSION IN MELTS

PAGE 2

	C1=-1000.0	CORR	46
	ICTN=0	CORR	47
	TEMP=1.	CORR	48
4	READ(8,100)IND,C,V,EJ,DES	CORR	49
100	FORMAT(I1,F9.0,2F10.0,10A4)	CORR	50
	IF(IND)20,20,21	CORR	51
20	IFIRST=1	CORR	52
	IF(C1-C)28,28,29	CORR	53
28	IF(ICTN-2)22,23,23	CORR	54
22	ICTN=ICTN+1	CORR	55
33	V2=V1	CORR	56
	V1=V	CORR	57
	C2=C1	CORR	58
	C1=C	CORR	59
	EJ2=EJ1	CORR	60
	EJ1=EJ	CORR	61
	GO TO 4	CORR	62
21	IF(IFIRST-1)24,25,24	CORR	63
24	IF(IND-1) 2,2,27	CORR	64
27	CALL EXIT	CORR	65
C.....	NEW SET OF DATA , WRITE HEADINGS	CORR	66
2	TEMP=C	CORR	67
	WRITE(5,101)DES,TEMP	CORR	68
101	FORMAT('1CALC. ACTIVITY COEF.',/, '0', 10A4,/, '0TEMP.=', F7.1,/, '0',	CORR	69
	15X, 'X', 11X, 'LOG(X)', 8X, 'V', 10X, 'EJ', 8X, 'V(CHEM)', 4X, 'V(IDEAL)', 6X,	CORR	70
	2 'COEF.', 6X, 'CORR.', 8X, 'DCORR.', 9X, 'W')	CORR	71
	SCOF=0.0	CORR	72
	CCNT=0.0	CORR	73
	C1=-1000.0	CORR	74
	ICTN=0	CORR	75
	GO TO 4	CORR	76
29	INTER = 1	CORR	77
	GO TO 30	CORR	78
25	INTER = 2	CORR	79
C.....	CALCULATION OF LAST 2 DATA POINTS IN THE SET	CORR	80
30	FAC= 0.0542 +TEMP * 0.000198	CORR	81
	X1=10.00 ** C2	CORR	82
	VC1 = V2 - EJ2	CORR	83
	V11 = FAC * C2	CORR	84
	CO1 = 10.00 **((VC1-V11) / FAC)	CORR	85
	W1= 1.9872 *(TEMP +273.2)*ALOG(CO1)/((1.0-X1)*(1.0-X1))	CORR	86
	WRITE(5,109) X1,C2,V2,EJ2,VC1,V11,CO1,W1	CORR	87
	X = 10.00 ** C1	CORR	88
	VC = V1- EJ1	CORR	89
	VI = FAC * C1	CORR	90

331

A.1 - SILVER CORROSION IN MELTS

PAGE 3

	CO = 10.00 **((VC-VI) / FAC)	CORR	91
	Z = 10.00 **((VC-VC1) / FAC)	CORR	92
	CORR = ((X-X1) / (Z-1.0)) - X1	CORR	93
	X1 = X1 + CORR	CORR	94
	IF(X1) 34,34,35	CORR	95
34	WRITE(5,102) X1	CORR	96
	GO TO 36	CORR	97
35	C2 = ALOG(X1) / DIVL	CORR	98
	VI1 = FAC * C2	CORR	99
	CO1 = 10.00 **((VC1-VI1) / FAC)	CORR	100
	W1 = 1.9872 * (TEMP + 273.2) * ALOG(CO1) / ((1.0-X1) * (1.0-X1))	CORR	101
	WRITE(5,110) X1, C2, V2, EJ2, VC1, VI1, CO1, CORR, W1	CORR	102
	SCOF = SCOF + CO1	CORR	103
	CCNT = CCNT + 1.0	CORR	104
	W = 1.9872 * (TEMP + 273.2) * ALOG(CO) / ((1.0-X) * (1.0-X))	CORR	105
36	WRITE(5,109) X, C1, V1, EJ1, VC, VI, CO, W	CORR	106
	X = X + CORR	CORR	107
	IF(X) 37,37,38	CORR	108
37	WRITE(5,102) X	CORR	109
	GO TO 39	CORR	110
38	C1 = ALOG(X) / DIVL	CORR	111
	VI = FAC * C1	CORR	112
	CO = 10.00 **((VC-VI) / FAC)	CORR	113
	W = 1.9872 * (TEMP + 273.2) * ALOG(CO) / ((1.0-X) * (1.0-X))	CORR	114
	WRITE(5,110) X, C1, V1, EJ1, VC, VI, CO, CORR, W	CORR	115
	SCOF = SCOF + CO	CORR	116
	CCNT = CCNT + 1.0	CORR	117
39	SCOF = SCOF / CCNT	CORR	118
	WRITE(6,103) SCOF	CORR	119
103	FORMAT('AVERAGE COEF = ', F8.4)	CORR	120
	SCOF = 0.0	CORR	121
	CCNT = 0.0	CORR	122
	WRITE(5,108)	CORR	123
108	FORMAT('O---', 75X, '-----', /)	CORR	124
	GO TO(31,24), INTER	CORR	125
31	ICTN = 1	CORR	126
	GO TO 33	CORR	127
C.....	CALCULATION USING 3 DATA POINTS	CORR	128
23	FAC = 0.0542 + TEMP * 0.0001984	CORR	129
	X2 = 10.00 ** C2	CORR	130
	X1 = 10.00 ** C1	CORR	131
	X = 10.00 ** C	CORR	132
	VC2 = V2 - EJ2	CORR	133
	VC1 = V1 - EJ1	CORR	134
	VC = V - EJ	CORR	135

A.1 - SILVER CORROSION IN MELTS

PAGE 4

```

VI2 = FAC * C2
CO2 = 10.00 ** ( (VC2-VI2)/FAC )
W2= 1.9872 *(TEMP + 273.2)*ALOG(CO2)/((1.0-X2)*(1.0-X2))
WRITE(5,109) X2,C2,V2,EJ2,VC2,VI2,CO2,W2
Z1 = 10.00 ** ( (VC1-VC2) / FAC )
Z2 = 10.00 ** ( (VC -VC1) / FAC )
CORR1=((X1-X2) / (Z1-1.0)) - X2
CORR= ((X -X1) / (Z -1.0)) - X1
DELC= CORR - CORR1
CORR= ( (X1-X2+DELC) / (Z1-1.0)) - X2
X2 = X2 + CORR
IF(X2) 40,40,41
40 WRITE(5,102) X2
GO TO 33
41 C2 = ALOG(X2)/ DIVL
VI2 = FAC * C2
CO2 = 10.00 ** ( (VC2-VI2) / FAC )
W2= 1.9872 *(TEMP + 273.2)*ALOG(CO2)/((1.0-X2)*(1.0-X2))
WRITE(5,102) X2,C2,V2,EJ2,VC2,VI2,CO2,CORR,DELC,W2
SCOF=SCOF+CO2
CCNT=CCNT+1.0
GO TO 33
END

```

CORR 136
CORR 137
CORR 138
CORR 139
CORR 140
CORR 141
CORR 142
CORR 143
CORR 144
CORR 145
CORR 146
CORR 147
CORR 148
CORR 149
CORR 150
CORR 151
CORR 152
CORR 153
CORR 154
CORR 155
CORR 156
CORR 157
CORR 158

A.2 - SILVER CONCENTRATIONS IN MELTS

PAGE 1

```

C.....A.2 - SILVER CONCENTRATIONS IN MELTS          CONC 1
C.....CALCULATE CONCENTRATIONS IN MOLTEN SALTS      CONC 2
C*****                                              CONC 3
C*****                                              CONC 4
C.....PROGRAMMER L.BOXALL AUGUST ,1968              CONC 5
C.....CARD INPUT SEQUENCE , PARAMETER CARD,DATA CARDS AND THEN A      CONC 6
C      DESCRIPTION CARD FOR EACH RUN , END OF JOB CARD AFTER ALL      CONC 7
C      TRIALS HAVE BEEN RUN                                           CONC 8
C.....PARAMETER CARD                                  CONC 9
C      COL. 1-10 = TOTAL MICROEQUIV. GENERATED IN THE FINAL MELT     CONC 10
C      COL. 12 = BLANK                                                 CONC 11
C      COL. 13-20 = NUMBER OF EQUIV./MOLE OF SPECIES GENERATED       CONC 12
C      COL. 21-30 = FINAL WEIGHT OF CONTENTS IN THE FRIT              CONC 13
C      COL. 31-40 = EQUIV. WEIGHT OF SOLVENT                          CONC 14
C      COL. 41-50 = EQUIV. WEIGHT OF SALT OF ELECTROACTIVE SPECIES   CONC 15
C      COL. 51-60 = DENSITY OF SOLVENT                                CONC 16
C.....DATA CARD                                       CONC 17
C      COL. 1-10 = NUMBER OF MICROEQUIV. GENERATED IN MELT          CONC 18
C      COL. 11-12 = BLANK                                             CONC 19
C.....DESCRIPTION CARD                                CONC 20
C      COL. 12 = 1                                                    CONC 21
C      COL. 31-78 = TITLE OF RUN                                     CONC 22
C.....END OF JOB CARD                                CONC 23
C      COL. 12 = 2                                                    CONC 24
C.....INCLUDE DECIMAL POINT IN ALL REAL NUMBER INPUT  CONC 25
C.....OUTPUT ON PRINTER                                       CONC 26
C*****                                              CONC 27
C      IMPLICIT REAL*8(A-H),REAL*8(O-Z)                               CONC 28
20      IND=0                                                       CONC 29
100     READ(8,100)EQF,IND,F,WTF,WTM,WTE,DEN                       CONC 30
        FORMAT(F10.0,I2,F8.0,4F10.0)                                CONC 31
5       IF(IND-1)5,5,4                                             CONC 32
104     WRITE(5,104)                                               CONC 33
        FORMAT('CALC. MOLALITY, MOLE FRACTION AND MOLARITY IN FUSED SALTS' CONC 34
1       ' )                                                         CONC 35
        WRITE(5,102)EQF,F,WTF,WTM,WTE                             CONC 36
102     FORMAT('TOTAL MICRO EQU.= ',F10.3,/, ' FACTOR = ',F10.3,/, ' FINAL WT' CONC 37
1       ' = ',F10.4,/, ' EQU.WT.MELT = ',F10.3,/, ' EQU.WT.ELECT.= ',F10.3) CONC 38
        WRITE(5,106)DEN                                           CONC 39
106     FORMAT(' DENSITY = ',F10.5,/' MICRO EQU. MOLALITY LOG MOLAL MCONC 40
        CONC 41
        CONC 42
        CONC 43
        CONC 44
        CONC 45

```

334

A.2 - SILVER CONCENTRATIONS IN MELTS

	LOG MOLE F	MOLARITY	LOG MOLAR ²	PAGE	2
	IOLE FRAC.			CONC	46
	F=1.0/F			CONC	47
3	READ(8,101)EQT,IND,D1,D2,D3,D4,D5,D6			CONC	48
101	FORMAT(F10.0,I2,18X,6A8)			CONC	49
	IF(IND-1) 1,2,2			CONC	50
1	AMT=EQT*F*0.001			CONC	51
	D=WTF+(EQF*(WTM-WTE)-EQT*WTM)*0.000001			CONC	52
	AMT=AMT/D			CONC	53
	AL=DLOG(AMT)/2.3026			CONC	54
	X=EQT*F*WTM/(D*1000000.0+EQT*F*WTM)			CONC	55
	BLX=DLOG(X)/2.3026			CONC	56
	BM=EQT*F*0.001*DEN/D			CONC	57
	BLM=DLOG(BM)/2.3026			CONC	58
	WRITE(5,103)EQT,AMT,AL,X,BLX,BM,BLM			CONC	59
103	FORMAT(' ',F10.4,F12.7,F12.6,E12.3,F12.6,F12.7,F12.6)			CONC	60
	GO TO 3			CONC	61
4	CALL EXIT			CONC	62
2	WRITE(5,105)D1,D2,D3,D4,D5,D6			CONC	63
105	FORMAT('0',6A8)			CONC	64
	IF(IND-2) 20,4,4			CONC	65
	END			CONC	66

A.3 - GAS PRESSURES FOR NITRATE ELECTRODE

PAGE 1

```

C.....A.3 - GAS PRESSURES FOR NITRATE ELECTRODE          GAS SP 1
C.....CALCULATE GAS PRESSURES FOR NITRATE ELECTRODE      GAS SP 2
C.....CALCULATE GAS PRESSURES FOR NITRATE ELECTRODE      GAS SP 3
C.....CALCULATE GAS PRESSURES FOR NITRATE ELECTRODE      GAS SP 4
C*****                                                    GAS SP 5
C.....PROGRAMMER L.BOXALL JULY 1968                       GAS SP 6
C.....PROGRAMMER L.BOXALL JULY 1968                       GAS SP 7
C.....INPUT CARD SEQUENCE - DESCRIPTION CARD, DATA CARDS THEN END OF
C      DATA SET OR END OF JOB CARD                       GAS SP 8
C.....DESCRIPTION CARD                                     GAS SP 9
C      COL. 1-48 = TITLE OF RUN                           GAS SP 10
C.....DATA CARD                                           GAS SP 11
C      COL. 5-9 = ATMOSPHERIC PRESSURE , ATM.             GAS SP 12
C      COL. 10-14 = PRESSURE DIFFERENCE FOR OXYGEN        GAS SP 13
C      COL. 15-19 = PRESSURE DIFFERENCE FOR NO2           GAS SP 14
C      COL. 20-24 = PRESSURE DIFFERENCE FOR NITROGEN      GAS SP 15
C      COL. 25-30 = EXCESS PRESSURE DIFFERENCE IN THE SYSTEM GAS SP 16
C.....END OF DATA SET CARD                               GAS SP 17
C      COL. 1 = 1                                         GAS SP 18
C.....END OF JOB CARD                                     GAS SP 19
C      COL. 1 = 2                                         GAS SP 20
C.....INCLUDE DECIMAL POINT IN ALL REAL NUMBER INPUT     GAS SP 21
C*****                                                    GAS SP 22
C*****                                                    GAS SP 23
C*****                                                    GAS SP 24
C*****                                                    GAS SP 25
C*****                                                    GAS SP 26
2      WRITE(5,100)                                       GAS SP 27
100     FORMAT('GAS PRESSURES CALCULATION')              GAS SP 28
      READ(8,101)A1,A2,A3,A4,A5,A6,A7,A8                 GAS SP 29
101     FORMAT(8A6)                                       GAS SP 30
5      WRITE(5,102)A1,A2,A3,A4,A5,A6,A7,A8              GAS SP 31
102     FORMAT('0',8A6,/,',',ATM.',9X,'OXYGEN',17X,'NO2',15X,'NITROGEN',10X,
1'LOG P TOTAL',/,',',MMHG OIL P ATM LOG P OIL P ATM LOG
2P OIL P ATM LOG P NO-O/2 MOLES')
      ICT=1                                              GAS SP 34
4      READ(8,103)IND,ATM,PO,PNO,PN,PB                  GAS SP 35
103     FORMAT(I1,3X,5F5.0)                              GAS SP 36
      IND=IND+1                                          GAS SP 37
      GO TO(1,2,3),IND                                  GAS SP 38
1      TOT=PN*1.643+PO*0.6979+PNO*1.184                 GAS SP 39
      ATC=ATM+PB*1.048/13.6                             GAS SP 40
      ATC=ATC/760.0                                     GAS SP 41
      PCN=ATC*PN*1.643/TOT                              GAS SP 42
      PCO=ATC*PO*0.6979/TOT                            GAS SP 43
      PCNO=ATC*PNO*1.184/TOT                          GAS SP 44
      PCNO=ATC*PNO*1.184/TOT                          GAS SP 45

```

A.3 - GAS PRESSURES FOR NITRATE ELECTRODE

PAGE 2

	EPN=ALOG(PCN)/2.303+0.0005	GASP	46
	EPO=ALOG(PCO)/2.303+0.0005	GASP	47
	EPNO=ALOG(PCNO)/2.303+0.0005	GASP	48
	EPOND=ALOG(PCND*PCO*0.5)/2.303+0.0005	GASP	49
	WRITE(5,104)ATM,PC,PCC,EPO,PNO,PCNO,EPNO,PN,PCN,EPN,EPOND,TOT	GASP	50
104	FORMAT(' ',F4.0,2X,F4.0,2X,F6.3,2X,F6.3,2X,F4.0,2X,F6.3,2X,F6.3,2X)	GASP	51
	1,F4.0,2X,F6.3,2X,F6.3,2X,F6.3,2X,F6.1)	GASP	52
	ICT=ICT+1	GASP	53
	IF(ICT-50)4,4,5	GASP	54
3	CALL EXIT	GASP	55
	END	GASP	56

A.4 - LEAST SQUARES STRAIGHT LINE - ERROR IN ONLY ONE VARIABLE

PAGE 1

C.....	A.4 - LEAST SQUARES STRAIGHT LINE - ERROR IN ONLY ONE VARIABLE	LSQS	1
C.....	LEAST SQUARES STRAIGHT LINE - NO ERROR IN X VALUE ,HORIZONTAL AXIS	LSQS	2
C.....	*****	LSQS	3
C.....	*****	LSQS	4
C.....	PROGRAMMER L.BOXALL JULY 1968	LSQS	5
C.....	*****	LSQS	6
C.....	MAX. 50 POINTS	LSQS	7
C.....	DATA CARDS ,CONTROL CARD -CARD SEQUENCE	LSQS	8
C.....	DATA CARDS	LSQS	9
C.....	COL.1-10 HOR.VALUE X R.J.	LSQS	10
C.....	COL.11-20 VERT VALUE Y R.J.	LSQS	11
C.....	COL.80 BLANK	LSQS	12
C.....	CONTROL CARDS	LSQS	13
C.....	COL.1-30 BLANK	LSQS	14
C.....	COL.21-30 GIVEN SLOPE IF REQUIRED	LSQS	15
C.....	IF SLOPE IS GIVEN,THE DATA IS FITTED TO BEST LINE WITH THE	LSQS	16
C.....	GIVEN SLOPE - OTHERWISE THE PROGRAM CALCULATES ITS OWN	LSQS	17
C.....	SLOPE	LSQS	18
C.....	COL.31-67 COMMENTS ON DATA	LSQS	19
C.....	COL.80 =1 PRINT COMMENTS AND CALCULATE BEST LINE	LSQS	20
C.....	COL.80 =2 END OF JOB NO CALCULATION PREFORMED	LSQS	21
C.....	REJECTS ALL POINTS WITH A DEVIATION GREATER THAN TWICE THE	LSQS	22
C.....	STANDARD DEVIATION FOR THE SET OF POINTS	LSQS	23
C.....	PLOTS POINTS + 2 CALCULATED POINTS USING SUBROUTINE G402P	LSQS	24
C.....	PLOTS ONLY ORIGINAL DATA AND THEN FINAL DATA AFTER REJECTION	LSQS	25
C.....	HAS BEEN COMPLETED	LSQS	26
C.....	INCLUDE DECIMAL POINT IN ALL REAL NUMBER INPUT	LSQS	27
C.....	*****	LSQS	28
C.....	*****	LSQS	29
C.....	*****	LSQS	30
C.....	*****	LSQS	31
C.....	IMPLICIT REAL *8(A-H),INTEGER *2(I-N), REAL *8(O-Z)	LSQS	32
C.....	DIMENSION A(3),D(99),X(99),Y(99)	LSQS	33
C.....	DIMENSION IPT(99),DES(12)	LSQS	34
1	DO 2 K=1,99	LSQS	35
100	READ(5,100)X(K),Y(K),GVSL,DES,IND	LSQS	36
	FORMAT(3F10.0,12A4,12)	LSQS	37
	IND=IND+1	LSQS	38
	GO TO (2,3,20,2),IND	LSQS	39
20	CALL EXIT	LSQS	40
2	CONTINUE	LSQS	41
3	N=K-1	LSQS	42
	IDIR=1	LSQS	43
	IRE J=0	LSQS	44
		LSQS	45

A.4 - LEAST SQUARES STRAIGHT LINE - ERROR IN ONLY ONE VARIABLE

PAGE 2

	NTEST = 1	LSQS	46
30	CONTINUE	LSQS	47
	SX=0.	LSQS	48
	SY=0.	LSQS	49
	SXX=0.	LSQS	50
	SYY=0.	LSQS	51
	SXY=0.	LSQS	52
	SD=0	LSQS	53
	SE=0.	LSQS	54
	DO 4 K=1,N	LSQS	55
	SX=SX+X(K)	LSQS	56
	SY=SY+Y(K)	LSQS	57
	SYY=SYY +Y(K)*Y(K)	LSQS	58
	SXX=SXX + X(K)*X(K)	LSQS	59
4	SXY=SXY + X(K)*Y(K)	LSQS	60
	IF(N-2)5,5,6	LSQS	61
5	WRITE(6,101)	LSQS	62
101	FGN. 'NOT ENOUGH POINTS')	LSQS	63
	GO TO 1	LSQS	64
6	SN=N	LSQS	65
	SL=SXY-SX*SY/SN	LSQS	66
	SL=SL/(SXX-SX*SX/SN)	LSQS	67
	B=(SY-SL*SX)/SN	LSQS	68
	IF(GVSL)31,32,31	LSQS	69
31	SVSL=SL	LSQS	70
	SVB =B	LSQS	71
	SL =GVSL	LSQS	72
	B =(SY-SL*SX)/SN	LSQS	73
32	CONTINUE	LSQS	74
	DO 7 K=1,N	LSQS	75
	D(K)=(SL*X(K)-Y(K)+B)	LSQS	76
	D(K)=-D(K)	LSQS	77
	SD=SD+D(K)	LSQS	78
7	SE=SE+D(K)*D(K)	LSQS	79
	SE=D SQRT(SE/(SN-2))	LSQS	80
	R=(SXY-SX*SY/SN)/((SXX-SX*SX/SN)*(SYY-SY*SY/SN))**.5	LSQS	81
	YC1=SL*X(1)+B	LSQS	82
	YC2=SL*X(N)+B	LSQS	83
	WRITE(6,107)DES	LSQS	84
107	FORMAT('1',12A4)	LSQS	85
	WRITE(6,108)	LSQS	86
108	FORMAT('OBEST FIT ST. LINE LEAST SQUARES')	LSQS	87
	WRITE(6,102)N	LSQS	88
102	FORMAT('ODATA NUMBER OF POINTS =',I4)	LSQS	89
	WRITE(6,104)	LSQS	90

A.4 - LEAST SQUARES STRAIGHT LINE - ERROR IN ONLY ONE VARIABLE

PAGE 3

104	FORMAT('O X',12X,'Y',10X,'DEV.')	LSQS	91
	DO 8 K=1,N	LSQS	92
8	WRITE(6,103) X(K), Y(K), D(K)	LSQS	93
103	FORMAT(' ',F12.5,F12.5,F12.5)	LSQS	94
	WRITE(6,105) SL, B, SE, SD, R	LSQS	95
105	FORMAT('OSLOPE =',F12.5,' INTERCEPT =',F12.5,' ST.ER. =',F12.5,/ 1,' SUM DEV. =',F12.5,' COR.COEF. =',F12.5)	LSQS	96
	WRITE(6,106) X(1), YC1, X(N), YC2	LSQS	97
106	FORMAT('OX(1) =',F12.5,' YC(1) =',F12.5,/, ' X(N) =',F12.5,' YC(N) 1) =',F12.5)	LSQS	98
	IF(GVSL)33,34,33	LSQS	99
33	WRITE(6,35)SVSL,SVB	LSQS	100
35	FORMAT('OSLOPE WAS GIVEN AS A FIXED VALUE',/, ' BEST SLOPE =',F14.7/ 1,/, ' BEST INTERCEPT =',F14.7,/))	LSQS	101
34	CONTINUE	LSQS	102
	GO TO (10,11),NTEST	LSQS	103
C.....	SUPPRESS PLOTS OF INTERMEDIATE CALCULATED FITS	LSQS	104
10	DO 12 K=1,N	LSQS	105
12	IPT(K)=19264	LSQS	106
	NTEST = 2	LSQS	107
	NS=N	LSQS	108
	IF(N-97)13,13,14	LSQS	109
13	N=N+1	LSQS	110
	X(N)=X(1)	LSQS	111
	Y(N)=YC1	LSQS	112
	IPT(N)=23616	LSQS	113
	N=N+1	LSQS	114
	X(N)=X(N-2)	LSQS	115
	Y(N)=YC2	LSQS	116
	IPT(N)=23616	LSQS	117
C.....	PLOT POINTS	LSQS	118
14	CALL G402P(X,Y,IPT,N)	LSQS	119
	N=NS	LSQS	120
	GO TO(11,1),IDIR	LSQS	121
C.....	TEST TO REJECT POINT OF LARGEST DEVIATION	LSQS	122
11	AH=0.	LSQS	123
	DO 17 K=1,N	LSQS	124
	AT= DABS(D(K))	LSQS	125
	IF(AH-AT)16,17,17	LSQS	126
16	NS=K	LSQS	127
	AH=AT	LSQS	128
17	CONTINUE	LSQS	129
	SE=2.0*SE	LSQS	130
	IF(AH-SE)61,18,18	LSQS	131
61	IF(IREJ)1,1,62	LSQS	132
		LSQS	133
		LSQS	134
		LSQS	135

A.4 - LEAST SQUARES STRAIGHT LINE - ERROR IN ONLY ONE VARIABLE

PAGE 4

```
62  IDIR=2  
    GO TO 10  
18  NS=NS+1  
    DO 19 K=NS,N  
19  X(K-1)=X(K)  
    Y(K-1)=Y(K)  
    IREJ=1  
    N=N-1  
    GO TO 30  
    END
```

```
LSQS 136  
LSQS 137  
LSQS 138  
LSQS 139  
LSQS 140  
LSQS 141  
LSQS 142  
LSQS 143  
LSQS 144  
LSQS 145
```

A.5 - LEAST SQUARES STRAIGHT LINE -ERROR IN BOTH VARIABLES

PAGE 1

C.....A.5 - LEAST SQUARES STRAIGHT LINE - ERROR IN BOTH VARIABLES	PERP	1
C.....CALCULATE BEST FIT CURVE PERP. DISTANCE	PERP	2
C*****	PERP	3
C*****	PERP	4
C.....PROGRAMMER L.BOXALL SEPT. 1968	PERP	5
C*****	PERP	6
C.....MAX. 50 POINTS	PERP	7
C.....DATA CARDS ,CONTROL CARD -CARD SEQUENCE	PERP	8
C.....DATA CARDS	PERP	9
C.....COL.1-10 HOR.VALUE X R.J.	PERP	10
C.....COL.11-20 VERT VALUE Y R.J.	PERP	11
C.....COL.80 BLANK	PERP	12
C.....CONTROL CARDS	PERP	13
C.....COL.1-30 BLANK	PERP	14
C.....COL.31-67 COMMENTS ON DATA	PERP	15
C.....COL.80 =1 PRINT CMMMENTS AND CALCULATE BEST LINE	PERP	16
C.....COL.80 =2 END CF JOB NO CALCULATION PREFORMED	PERP	17
C.....REJECTS ALL POINTS WITH A DEVIATION GREATER THAN TWICE THE	PERP	18
C.....STANDARD DEVIATION FOR THE SET OF POINTS	PERP	19
C.....PLOTS POINTS + 2 CALCULATED POINTS USING SUBROUTINE G402P	PERP	20
C.....PLOTS ONLY ORIGINAL DATA AND THEN FINAL DATA AFTER REJECTION	PERP	21
C.....HAS BEEN COMPLETED	PERP	22
C.....INCLUDE DECIMAL POINT IN ALL REAL NUMBER INPUT	PERP	23
C*****	PERP	24
C*****	PERP	25
C.....	PERP	26
C.....	PERP	27
C.....	PERP	28
C.....	PERP	29
C.....	PERP	30
C.....	PERP	31
1 DO 2 K=1,99	PERP	32
100 READ(8,100)X(K),Y(K),DES,IND	PERP	33
FORMAT(2F10.0,10X,12A4,I2)	PERP	34
IND=IND+1	PERP	35
GO TO (2,3,20,2),IND	PERP	36
20 WRITE(5,999)IND	PERP	37
999 FORMAT('1IND =',I6)	PERP	38
CALL EXIT	PERP	39
2 CONTINUE	PERP	40
3 N=K-1	PERP	41
IREJ=0	PERP	42
IDIR=1	PERP	43
NTEST = 1	PERP	44
SX=0.	PERP	45

A.5 - LEAST SQUARES STRAIGHT LINE -ERROR IN BOTH VARIABLES

PAGE 2

```

SY=0.
SXX=0.
SYY=0.
SXY=0.
SD=0.
SE=0.
DO 4 K=1,N
SX=SX+X(K)
SY=SY+Y(K)
SYY=SYY +Y(K)*Y(K)
SXX=SXX + X(K)*X(K)
4 SXY=SXY + X(K)*Y(K)
IF(N-2)5,5,6
5 WRITE(5,101)
101 FORMAT('1NOT ENOUGH PCINTS')
GO TO 1
6 SN=N
SL=SXY-SX*SY/SN
SL=SL/(SXX-SX*SX/SN)
C1= N*SX*SY - N*N*SXY
C2= SY*SY*SY -2.*N*SX*SXY +SY*SX*SX +N*SY*(SXX-SYY)
C3= SY*SY*SXY -SX*SX*SXY +SX*SY*(SXX - SYY)
A1=C2*C2 -4.*C3*C1
R =DSQRT(A1)
A(1)=0
A(2)=- (C2+R)/(2.*C3)
A(3)=- (C2-R)/(2.*C3)
R=10.**30
DO 50 K=1,3
BB=A(K)*SY/(SN+A(K)*SX)
RR = DABS(SL- BB)
IF(RR-R)51,50,50
51 R=RR
AA=A(K)
50 CONTINUE
BB=- (N +AA*SX)/ SY
SL=-AA/BB
B= -1./BB
DO 7 K=1,N
D(K)=(AA*X(K)+BB*Y(K)+1.)/DSQRT(AA*AA + BB*BB)
D(K)=-D(K)
SD=SD+D(K)
7 SE=SE+D(K)*D(K)
SE=DSQRT(SE/(SN-2))
R=(SXY-SX*SY/SN)/((SXX-SX*SX/SN)*(SYY-SY*SY/SN))**.5

```

PERP 46
PERP 47
PERP 48
PERP 49
PERP 50
PERP 51
PERP 52
PERP 53
PERP 54
PERP 55
PERP 56
PERP 57
PERP 58
PERP 59
PERP 60
PERP 61
PERP 62
PERP 63
PERP 64
PERP 65
PERP 66
PERP 67
PERP 68
PERP 69
PERP 70
PERP 71
PERP 72
PERP 73
PERP 74
PERP 75
PERP 76
PERP 77
PERP 78
PERP 79
PERP 80
PERP 81
PERP 82
PERP 83
PERP 84
PERP 85
PERP 86
PERP 87
PERP 88
PERP 89
PERP 90

A.5 - LEAST SQUARES STRAIGHT LINE -ERROR IN BOTH VARIABLES

PAGE 3

	YC1=SL*X(1)+B	PERP 91
	YC2=SL*X(N)+B	PERP 92
	WRITE(5,107)DES	PERP 93
107	FORMAT('1',12A4)	PERP 94
	WRITE(5,108)	PERP 95
108	FORMAT('OBEST FIT ST.LINE LEAST SQUARES PERP.DIST.')	PERP 96
	WRITE(5,102)N	PERP 97
102	FORMAT('ODATA NUMBER OF POINTS =',I4)	PERP 98
	WRITE(5,104)	PERP 99
104	FORMAT('0 X',12X,'Y',10X,'DEV.')	PERP 100
	DO 8 K=1,N	PERP 101
8	WRITE(5,103) X(K),Y(K),D(K)	PERP 102
103	FORMAT(' ',F12.5,F12.5,F12.5)	PERP 103
	WRITE(5,105)SL,B,SE,SD,R	PERP 104
105	FORMAT('OSLOPE =',F12.5,' INTERCEPT =',F12.5,' ST.ER. =',F12.5,/ 1,' SUM DEV. =',F12.5,' COE. COEF. =',F12.5)	PERP 105
	WRITE(5,106)X(1),YC1,X(N),YC2	PERP 106
106	FORMAT('OX(1) =',F12.5,' YC(1) =',F12.5,/, ' X(N) =',F12.5,' YC(N) 1) =',F12.5)	PERP 107
	C..... SUPPRESS PLOTS OF INTERMEDIATE CALCULATED FITS	PERP 108
	GO TO (10,11),NTEST	PERP 109
10	DO 12 K=1,N	PERP 110
12	IPT(K)=19264	PERP 111
	NTEST = 2	PERP 112
	NS=N	PERP 113
	IF(N-97)13,13,14	PERP 114
13	N=N+1	PERP 115
	X(N)=X(1)	PERP 116
	Y(N)=YC1	PERP 117
	IPT(N)=23616	PERP 118
	N=N+1	PERP 119
	X(N)=X(N-2)	PERP 120
	Y(N)=YC2	PERP 121
	IPT(N)=23616	PERP 122
	C..... PLOT POINTS	PERP 123
14	CALL G402P(X,Y,IPT,N)	PERP 124
	N=NS	PERP 125
	C..... TEST TO REJECT POINT OF LARGEST DEVIATION	PERP 126
	GO TO(11,1),IDIR	PERP 127
11	AH=0.	PERP 128
	DO 17 K=1,N	PERP 129
	AT= DABS(D(K))	PERP 130
	IF(AH-AT)16,17,17	PERP 131
16	NS=K	PERP 132
	AH=AT	PERP 133
		PERP 134
		PERP 135

A.5 - LEAST SQUARES STRAIGHT LINE -ERROR IN BOTH VARIABLES

```
17 CONTINUE
   SE=2.0*SE
   IF(AH-SE)61,18,18
61  IF(IREJ)1,1,62
62  IDIR=2
   GO TO 10
18  NS=NS+1
   DO 19 K=NS,N
19  X(K-1)=X(K)
   Y(K-1)=Y(K)
   K=N
   IREJ=1
   GO TO 3
END
```

PAGE 4

```
PERP 136
PERP 137
PERP 138
PERP 139
PERP 140
PERP 141
PERP 142
PERP 143
PERP 144
PERP 145
PERP 146
PERP 147
PERP 148
PERP 149
```


A.6 - FITS DATA TO N TH ORDER POLYNOMIAL

PAGE 2

100	FORMAT(11,F9.0,F10.0,1X,I2,2X,I2,3X,10A4)	POLY	46
	X(K) = X(K)/100.0	POLY	47
	IF(IND-1)1,2,20	POLY	48
20	CALL EXIT	POLY	49
1	CONTINUE	POLY	50
150	READ(8,100)IND,Z,D,N,DES	POLY	51
	IF(IND)150,150,952	POLY	52
952	KS=K-1	POLY	53
	WRITE(5,953)DES	POLY	54
953	FORMAT('1',10A4)	POLY	55
	WRITE(IPR,105)	POLY	56
105	FORMAT('0TOO MANY INPUT POINTS')	POLY	57
	GO TO 954	POLY	58
2	KS=K-1	POLY	59
968	CONTINUE	POLY	60
	WRITE(5,953)DES	POLY	61
954	WRITE(5,103)	POLY	62
103	FORMAT('0VARIABLES FOR POLYNOMIAL',/, '0	POLY	63
	10R',6X,'PERCENT ERROR')	POLY	64
	IF(N)151,151,152	POLY	65
151	N=2	POLY	66
	WRITE(IPR,153)N	POLY	67
153	FORMAT('0ORDER SET TO',I3)	POLY	68
152	IF(N-14)154,154,155	POLY	69
155	N=14	POLY	70
	WRITE(IPR,153)N	POLY	71
154	J=1	POLY	72
	IF(NT-14) 965,965,966	POLY	73
966	NT=14	POLY	74
965	CONTINUE	POLY	75
	N=N+1	POLY	76
	IP=0	POLY	77
	DO 4 K=1,N	POLY	78
	KP=IP	POLY	79
	DO 5 KK=J,N	POLY	80
	Z=0.	POLY	81
	DO 6 K1=1,KS	POLY	82
	IF(KP) 969,969,970	POLY	83
969	Z=Z+1.0	POLY	84
	GO TO 6	POLY	85
970	Z=Z + X(K1)**KP	POLY	86
6	CONTINUE	POLY	87
	C(K, KK)=Z	POLY	88
	C(KK, K)=Z	POLY	89
5	KP=KP+1	POLY	90

A.6 - FITS DATA TO N TH ORDER POLYNOMIAL

PAGE 3

	J=J+1	POLY 91
	IP=IP+2	POLY 92
	Z=0.	POLY 93
	DO 7 K1=1,KS	POLY 94
	IF(K-1) 971,971,972	POLY 95
971	ZZ=1.0	POLY 96
	GO TO 7	POLY 97
972	ZZ=X(K1)**(K-1)	POLY 98
7	Z=Z + Y(K1)*ZZ	POLY 99
4	B(K)=Z	POLY 100
C	SOLVE BY CRAMMERS RULE	POLY 101
	NSIZ=15	POLY 102
	CALL G402T(C,D,N,NSIZ,IC,IV,CT)	POLY 103
	IF(D)8,9,8	POLY 104
9	WRITE(IPR,101)	POLY 105
101	FORMAT('ODETERMINANT = ZERO')	POLY 106
	IF(IND-2)3,20,20	POLY 107
8	DS=D	POLY 108
	DO 10 K2=1,N	POLY 109
	DO 11 K1=1,N	POLY 110
	Z=C(K1,K2)	POLY 111
	C(K1,K2)=B(K1)	POLY 112
11	B(K1)=Z	POLY 113
	CALL G402T(C,D,N,NSIZ,IC,IV,CT)	POLY 114
	DO 55 K1=1,N	POLY 115
	Z=C(K1,K2)	POLY 116
	C(K1,K2)=B(K1)	POLY 117
55	B(K1)=Z	POLY 118
	D=D/DS	POLY 119
	COEF(K2)=D	POLY 120
10	CONTINUE	POLY 121
	SEP=0.	POLY 122
	SER=0.	POLY 123
	DO 51 K=1,KS	POLY 124
	D=0.	POLY 125
	K2=N-1	POLY 126
	DO 50 L=1,K2	POLY 127
	K3=N-L+1	POLY 128
50	D=(D+COEF(K3))*X(K)	POLY 129
	D= D+COEF(1)	POLY 130
	Z=Y(K)-D	POLY 131
	KSS=K+KS	POLY 132
	Y(KSS)=D	POLY 133
	X(KSS) = X(K)	POLY 134
	IPT(KSS)=23616	POLY 135

A.6 - FITS DATA TO N TH ORDER POLYNOMIAL

PAGE 4

	IPT(K)=20032	POLY 136
	IF(Y(K)) 973,974,973	POLY 137
974	D=0.0	POLY 138
	GO TO 975	POLY 139
973	D=100.*Z/Y(K)	POLY 140
975	SEP=SEP + D*D	POLY 141
	SER=SER + Z*Z	POLY 142
51	WRITE(IPR,52)X(K),Y(K),Z,D	POLY 143
52	FORMAT(' ',F11.5,F15.5,F15.6,F15.6)	POLY 144
	SER=DSQRT(SER/(KS-1))	POLY 145
	SEP=DSQRT(SEP/(KS-1))	POLY 146
	WRITE(IPR,53)SER,SEP	POLY 147
53	FORMAT('STANDARD ERRORS IN Y CALCULATED',/, ' ABSOLUTE =' ,E11.4,/,	POLY 148
	1 ' PERCENT =' ,E11.4)	POLY 149
	DO 54 K=1,N	POLY 150
	K2=K-1	POLY 151
54	WRITE(IPR,102)K2,COEF(K)	POLY 152
102	FORMAT('COEF.OF X TO THE',I3,' POWER EQUALS',E11.4)	POLY 153
	KSS=KS+KS	POLY 154
	CALL G402P(X,Y,IPT,KSS)	POLY 155
	IF(N-NT) 968,968,967	POLY 156
967	CONTINUE	POLY 157
	IF(IND-2)3,20,20	POLY 158
	END	POLY 159

A.7 - PLOTTING SUBROUTINE - G402P

PAGE 1

```

C.....A.7 - PLOTTING SUBROUTINE - G402P          PLOT 1
C.....SUBROUTINE G402P - PLOTS POINTS ON A ONLINE PRINTER PLOT 2
C***** PLOT 3
C***** PLOT 4
C.....PROGRAMMER L.BOXALL AUGUST 1967          PLOT 5
C***** PLOT 6
C.....VARIABLES IN CALL STATEMENT              PLOT 7
C      X - NAME OF ARRAY CONTAINING K HORIZONTAL VALUES PLOT 8
C      Y - NAME OF ARRAY CONTAINING K VERTICAL VALUES PLOT 9
C      IZ- NAME OF ARRAY CONTAINING K PLOT CHARACTERS, ONE FOR EACH DATA PLOT 10
C          POINT, IN A1 FORMAT PLOT 11
C      K - NUMBER OF DATA POINTS PLOT 12
C.....PRINTER SET AT 8 LINES/INCH AND SPECIAL PLOT TAPE - ONLY A PLOT 13
C          BEGINING OF PAGE CHANNEL PUNCH AND PAPER SET SO THAT THE PLOT 14
C          FIRST LINE IS 2 PRINT POSITIONS FROM TOP OF PAGE PLOT 15
C.....REQUIRES 11 X 14 INCH PAPER PLOT 16
C.....CALCULATES ITS OWN GRID FOR EACH AXIS PLOT 17
C***** PLOT 18
C          SUBROUTINE G402P(X,Y,IZ,K) PLOT 19
C***** PLOT 20
C          IMPLICIT REAL *8(A-H),INTEGER *2(I-N), REAL *8(O-Z) PLOT 21
C          INTEGER *2 G(101) PLOT 22
C          DIMENSION X(1),Y(1),AX(5),IP(5) PLOT 23
C          DIMENSION IZ(1) PLOT 24
C          YL=10.0 PLOT 25
C          DLN= DLOG(YL) PLOT 26
C          XL=X(1) PLOT 27
C          XS=X(1) PLOT 28
C          YL=Y(1) PLOT 29
C          YS=Y(1) PLOT 30
C          DO 10 J=1,K PLOT 31
C            IF(XL-X(J))3,4,4 PLOT 32
C            XL=X(J) PLOT 33
C            IF(XS-X(J))6,6,5 PLOT 34
C            XS=X(J) PLOT 35
C            IF(YL-Y(J))7,8,8 PLOT 36
C            YL=Y(J) PLOT 37
C            IF(YS-Y(J))10,10,9 PLOT 38
C            YS=Y(J) PLOT 39
C          PLOT 40
C          PLOT 41
C          PLOT 42
C          PLOT 43
C          PLOT 44
C          PLOT 45

```

350

A.7 - PLOTTING SUBROUTINE - G402P

PAGE 2

10	CONTINUE	PLOT 46
	GX=(XL-XS) / 100.0	PLOT 47
	GY=(YL-YS) / 80.0	PLOT 48
	L=1	PLOT 49
	AC=GX	PLOT 50
25	A1= DLOG(AC)/DLN	PLOT 51
	N=A1	PLOT 52
	A2=N	PLOT 53
	A3=A1-A2	PLOT 54
	IF (A1) 21, 22, 23	PLOT 55
23	IF (A3) 22, 22, 27	PLOT 56
21	IF (A3) 24, 22, 22	PLOT 57
24	A2 = A2 - 1.0	PLOT 58
	A3 = A1 - A2	PLOT 59
27	A1 = 10.0 ** (A3 + 1.0)	PLOT 60
	A2 = A2 - 1.0	PLOT 61
	N = A1	PLOT 62
	A3 = N	PLOT 63
	A1 = A1 - A3 - 0.00499999	PLOT 64
	IF (A1) 28, 28, 29	PLOT 65
29	A3 = A3 + 1.0	PLOT 66
28	N = A2	PLOT 67
	AC = A3 * 10.0 ** N	PLOT 68
22	GO TO (124, 26), L	PLOT 69
124	GX=AC	PLOT 70
	AC=GY	PLOT 71
	L=2	PLOT 72
	GO TO 25	PLOT 73
26	GY=AC	PLOT 74
19	WRITE(6,102) GX	PLOT 75
102	FORMAT('OGRID HOR. =',E12.5)	PLOT 76
	WRITE(6,103) GY	PLOT 77
103	FORMAT('OGRID VERT. =',E12.5)	PLOT 78
	ICT=-1	PLOT 79
	DO 112 J=2,5	PLOT 80
112	IP(J)=-14016	PLOT 81
	IP(1)=23616	PLOT 82
	WRITE(6,104)(IP(1), IP(2), IP(3), IP(4), IP(5), J=1,20), IP(1)	PLOT 83
104	FORMAT('1',16X,101A1)	PLOT 84
C.....	PLOT POINTS	PLOT 85
	DO 13 JSP=1,81	PLOT 86
	AC=JSP-1	PLOT 87
	YS=YL-GY*(AC+0.5)	PLOT 88
	XL=YL-GY*(AC-0.5)	PLOT 89
	DO 11 J=1,101	PLOT 90

A.7 - PLOTTING SUBROUTINE - G402P

PAGE 3

11	G(J)=16448	PLOT 91
	DO 30 J=1,K	PLOT 92
	IF(XL-Y(J)) 30,30,32	PLOT 93
32	IF(YS-Y(J)) 31,31,30	PLOT 94
31	JX=(X(J)-XS)/GX +1.5	PLOT 95
	G(JX)=IZ(J)	PLOT 96
30	CONTINUE	PLOT 97
	WRITE(6,105) G	PLOT 98
105	FORMAT(' ',14X'- ',101A1,' -')	PLOT 99
	ICT=ICT+1	PLOT 100
	JCT=(JSP-1) -((JSP/10) * 10)	PLOT 101
	IF(JCT)13,15,13	PLOT 102
15	AY=YL-GY*(JSP-1)	PLOT 103
	AY = AY*1.000001	PLOT 104
	WRITE(6,106) AY	PLOT 105
106	FORMAT(' + ',E12.5,106X,'*')	PLOT 106
13	CONTINUE	PLOT 107
16	WRITE(6,107) (IP(1), IP(2), IP(3), IP(4), IP(5), J=1,20), IP(1)	PLOT 108
107	FORMAT(' ',16X,101A1)	PLOT 109
	DO 17 J=1,5	PLOT 110
17	AX(J)=XS+GX*20.*(J-1)	PLOT 111
	WRITE(6,108)(AX(J), J=1,5)	PLOT 112
108	FORMAT(' ',10X,5(E12.5,8X))	PLOT 113
	RETURN	PLOT 114
	END	PLOT 115

A.8 - DETERMINANT SUBROUTINE - G402T

PAGE 1

```

C.....A.8 - DETERMINANT SUBROUTINE G402T
C.....SUBROUTINE G402T - EVALUATE DETERMINANT
C*****
C.....PROGRAMMER L.BOXALL JULY 1969
C.....VARIABLES IN CALL STATEMENT
C      A - NAME OF TWO DIMENSIONAL MATRIX
C      CO - VALUE OF DETERMINANT RETURNED
C      N - ORDER OF DETERMINANT
C      NSIZ - SIZE OF SQUARE MATRIX A IN DIMENSION STATEMENT OF CALLING
C             PROGRAM
C      IC,IV,CT - NAMES OF TEMPORARY WORKING ARRAYS OF A LENGTH GREATER
C             THAN N
C.....ORIGINAL MATRIX NOT DESTROYED AND SIZE IS UNLIMITED
C*****
C      SUBROUTINE G402T(A,CO,N,NSIZ,IC,IV,CT)
C*****
      IMPLICIT REAL *8(A-H),INTEGER *2(I-N), REAL *8(O-Z)
      DIMENSION A(1),IC(1),IV(1),CT(1)
      IF(N)105,105,106
105    CO=0
      RETURN
106    DO 4 I=1,N
      IC(I)=1
4      CT(I)=0.
      CO=0.
      J=N+1
      DO 7 I=1,J
      IV(I)=1
      OE=0.
      PR=1.
      I=1
      K=IC(I)
      M=K+NSIZ*(I-1)
      PR=PR*A(M)
      J=I+1
12     IF(J-N)13,13,14
13     IF(IC(I)-IC(J))20,31,19
19     OE=OE+1.

```

DET 1
DET 2
DET 3
DET 4
DET 5
DET 6
DET 7
DET 8
DET 9
DET 10
DET 11
DET 12
DET 13
DET 14
DET 15
DET 16
DET 17
DET 18
DET 19
DET 20
DET 21
DET 22
DET 23
DET 24
DET 25
DET 26
DET 27
DET 28
DET 29
DET 30
DET 31
DET 32
DET 33
DET 34
DET 35
DET 36
DET 37
DET 38
DET 39
DET 40
DET 41
DET 42
DET 43
DET 44
DET 45

353

A.8 - DETERMINANT SUBROUTINE - G402T

PAGE 2

```

20  J=J+1
    GO TO 12
14  IF(I-N)21,24,24
21  I=I+1
    GO TO 8
24  M=OE
    MM=(M/2)*2
    IF(MM-M)27,28,27
27  CO=CO-PR
    GO TO 31
28  CO=CO+PR
31  J=N-1
32  IF(CT(J)-N+J)34,33,34
33  CT(J)=0.
    J=J-1
    IF(J)32,36,32
34  CT(J)=CT(J)+1.
    M=J-1
    IF(M)39,39,75
75  DO 35 I=1,M
    DO 37 K=1,N
    IF(IC(I)-IV(K))37,38,37
38  IV(K)=0
    GO TO 35
37  CONTINUE
35  CONTINUE
39  IF(IC(J)-N)41,40,41
40  K=1
    GO TO 42
41  K=IC(J)+1
42  IF(IV(K))44,43,44
43  IF(K-N)45,46,45
46  K=1
    GO TO 42
45  K=K+1
    GO TO 42
44  IC(J)=IV(K)
    IV(K)=0
    IF(J-N)47,6,47
47  J=J+1
    GO TO 39
36  RETURN
    END

```

```

DET 46
DET 47
DET 48
DET 49
DET 50
DET 51
DET 52
DET 53
DET 54
DET 55
DET 56
DET 57
DET 58
DET 59
DET 60
DET 61
DET 62
DET 63
DET 64
DET 65
DET 66
DET 67
DET 68
DET 69
DET 70
DET 71
DET 72
DET 73
DET 74
DET 75
DET 76
DET 77
DET 78
DET 79
DET 80
DET 81
DET 82
DET 83
DET 84
DET 85
DET 86
DET 87
DET 88

```

APPENDIX B

CALCULATION OF LIQUID JUNCTION POTENTIALS (E_J)

The simplest type of electrolytic cell which contains a liquid junction potential is called a "concentration cell with transfer-ence" or "concentration cell with transport." These cells must contain at least two different solutions which make a liquid-liquid contact with each other. In any rigorous thermodynamic treatment of an electrochemical cell it is necessary to take into account the "liquid junction potential, E_J , which makes a contribution to the emf of the system. A cell which contains a liquid junction is never at a true equilibrium due to the irreversible diffusion across the interface of the two solutions which will continue until the composition is uniform throughout the cell. Provided the diffusion is slow enough to prevent any substantial change in the composition of the cell, it can be neglected when considering the reversible flow of electricity through the cell. In order to have such a reversible transfer, the composition must vary continuously from one extreme to the other in the boundary zone between the two solutions. The passage of an infinitesimal amount of current through the boundary zone will not disturb the conditions required for the reversibility.

The current is carried by anions and cations in the opposite directions which will tend to alter the natural potential gradient set-up by the diffusion process. The infinitesimal amount of current is very small with respect to the amounts of ions in the boundary zone, therefore, no change in composition of any consequence will occur even though the calculations are based on changes "per faraday."

The electrical work required to transport an infinitesimal quantity of electricity, dF , across a single element in the boundary zone can be expressed in terms of the increase in Gibbs free energy for the process by

$$-dF \cdot dE_J = dG \quad (B.1)$$

where dE_J is the electrical potential across the element. Each type of ion carries an amount of electricity in proportion to its transport number, t_i , across the single element. Each ion must move through an infinitesimal chemical potential gradient, $d\mu_i$, as it crosses the single element, therefore the dG per faraday for each element is also given by the summation

$$dG = \sum \frac{t_i}{Z_i} d\mu_i \quad (B.2)$$

for each ion, i , with a valency Z_i (sign included) in the element. The activity of the ions, a_i , is introduced by the relationship

$$d\mu_i = RT d \ln a_i \quad (B.3)$$

to give the basic differential equation for the liquid junction potential.

$$-dE_J = \frac{RT}{F} \sum_i \frac{t_i}{Z_i} d \ln a_i \quad (\text{B.4})$$

The total liquid junction potential is determined by integrating from one homogeneous solution, A, on one side of the interface to the other, B, on the other side. The dependence of the transport number, t_i , and activity, a_i , on the composition of the boundary zone must be known or approximated to carry out the integration.

$$E_J = -\frac{RT}{F} \int_A^B \sum_i \left[\frac{t_i}{Z_i} d(\ln a_i) \right] \quad (\text{B.5})$$

The transport number of an ion in molten salts depends strongly on its concentration; therefore, the internal ionic mobility, a less sensitive parameter, is used to replace the transport number. One of the ions, j , is arbitrarily chosen as a point of reference since there is no stationary inactive solvent in the system and the internal mobility, b_{ij} , for the i^{th} ion is defined in terms of its mobility, b_i , and the mobility, b_j , of the reference ion, j , by the equation

$$b_{ij} = b_i - b_j \quad (\text{B.6})$$

The transport number in equation B.5 is replaced by the internal transport number, t_{ij} , which is given by the equation

$$t_{ij} = \frac{F Z_i C_i b_{ij}}{K} \quad (\text{B.7})$$

$$K = \sum_i F Z_i C_i b_{ij} \quad (\text{B.8})$$

where C_i is the concentration of ion i and K is the specific conductance of the system.

The internal mobility, b_{+-} , is calculated from the specific conductance of the pure salt using the equation

$$K = F Z_+ C_+ b_{+-} \quad (\text{B.9})$$

where the units of K require that the concentration C_+ is expressed as the number of gram equivalents per litre. The activity a_i is replaced by C_i by assuming it is an ideal system and the $d(\ln C_i)$ term is eliminated by the relationship

$$d(\ln C_i) = \frac{d C_i}{C_i} \quad (\text{B.10})$$

to give

$$E_J = -\frac{RT}{F} \int_A^B \frac{1}{K} \sum_i (b_{ij} d C_i) \quad (\text{B.11})$$

It has been shown that there is no exact solution to the general equation (B.11) (336); however, if every Z_i has the same value, Z , the general equation can be integrated. The value of Z_j is not considered because

$$b_{jj} = 0 \quad (\text{B.12})$$

for the reference ion and the entire $Z_j b_{jj} C_j$ term is eliminated from the equation. The final equation for the liquid junction potential has the following form:

$$E_J = -\frac{RT}{ZF} \ln \frac{\sum_i b_{ij} C_i^B}{\sum_i b_{ij} C_i^A} \quad (\text{B.13})$$

where C_i^A and C_i^B represent the concentration of the i^{th} component in the solution A and B, respectively, in an electrochemical cell in

which A is taken to be the left hand half of the written form of the cell.

A second type of solution for the general equation can be realized if the system is limited to two cations and one anion or vice versa. The mole fraction scale is used as the concentration scale for two reasons: firstly, the sum of all N_i equals unity and secondly, the contribution of an individual component to the E_J value increases with its concentration and the activity coefficient for the mole fraction scale approaches unity with increasing concentrations. The electrochemical cell considered in the following integration and simplification is:



where the components are numbered as follows:

$$\text{M} = 1 \quad (\text{B.15})$$

$$\text{M}' = 2 \quad (\text{B.16})$$

$$\text{Y} = 3 \quad (\text{B.17})$$

By the use of the relationship:

$$C_1 + C_2 = 1 \quad (\text{B.18})$$

and simplification, the liquid junction potential for the general three component cell B.14 is given by:

$$E_J = -\frac{RT}{F} \left[\frac{b_{13} - b_{23}}{Z_1 b_{13} - Z_2 b_{23}} \right] \ln \left[\frac{Z_2 b_{23} + (Z_1 b_{13} - Z_2 b_{23}) C_1^B}{Z_2 b_{23} + (Z_1 b_{13} + (Z_2 b_{23}) C_1^A)} \right] \quad (\text{B.19})$$

Component number 3 was used as the reference ion and since

$$b_{33} = 0 \quad (\text{B.20})$$

its concentration term does not appear in the final equation. To calculate the liquid junction potential in a multi-cation-single-anion system it is necessary to consider all of the salts which make up the solvent as a single component and to use a single mobility which is applicable to the mixture.

The general equation for the liquid junction potential (B.19) is greatly simplified when the following specific experimental cells are considered.

1. The Silver-Alkali Metal Salt Concentration Cell

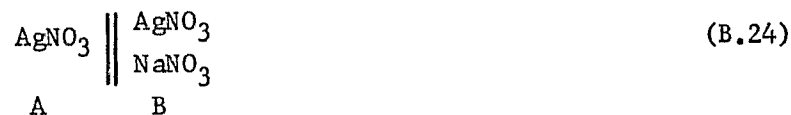
Components:

$$1 = \text{Ag(I)} \quad (\text{B.21})$$

$$2 = \text{single or a mixture of alkali ions (Na(I))} \quad (\text{B.22})$$

$$3 = \text{anion (NO}_3^-)$$

Cell:



$$E_J = -\frac{RT}{F} \ln \left[\frac{b_{23} + b_{12} N_1^B}{b_{13}} \right] \quad (\text{B.25})$$

2. The Silver Cation-Univalent-Univalent Anion Electrochemical Cell

Component:

$$1 = \text{Ag(I)} \quad (\text{B.26})$$

$$3 = \text{NO}_3^- \quad (\text{B.27})$$

$$4 = \text{Cl}^- \quad (\text{B.28})$$

Cell:



$$E_J = \frac{RT}{F} \ln \left[\frac{b_{14}}{b_{13}} \right] \quad (\text{B.30})$$

3. The Silver Cation-Univalent-Divalent Anion Electrochemical Cell

Component:



Cell:



$$E_J = \frac{RT}{F} \left[\frac{b_{14} - b_{15}}{b_{14} - 2b_{15}} \right] \ln \left[\frac{2b_{15}}{b_{14}} \right] \quad (\text{B.35})$$

4. The Silver Cation-Two Divalent Anion Electrochemical Cell

Component:

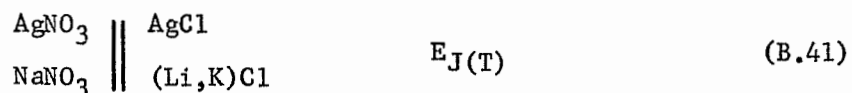


Cell:

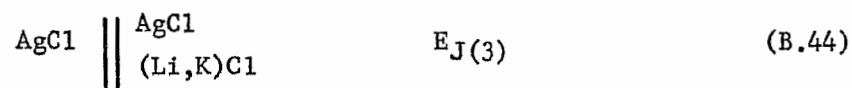
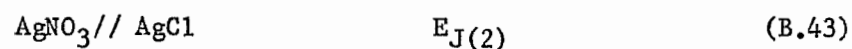
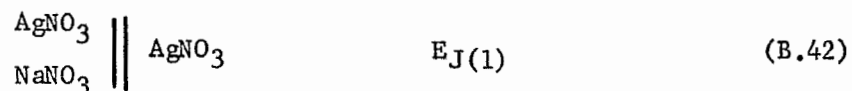


$$E_J = \frac{RT}{2F} \ln \left[\frac{b_{16}}{b_{15}} \right] \quad (\text{B.40})$$

The total liquid junction potential for a more complex cell such as



can be calculated by summing the potentials of a series of simpler cells in which the (Li,K)Cl mixture is considered to be a single salt.



$$E_{\text{J(T)}} = E_{\text{J(1)}} + E_{\text{J(2)}} + E_{\text{J(3)}} \quad (\text{B.45})$$

The internal mobilities of the ions in the electrochemical cell are calculated using the specific conductivity data tabulated by Janz (2) and equation B.9. The composition of the electrochemical cell and the restrictions on the equations derived in this appendix dictates which equation is used to calculate the liquid junction potential for the cell.

APPENDIX C

THE CONVERSION FROM ONE CONCENTRATION SCALE TO ANOTHER FOR UNI-UNIVALENT FUSED SALT SOLUTIONS

Symbols Used

- N - concentration of CA on the mole fraction scale
M - concentration of CA on the molarity scale
m - concentration of CA on the molality scale
W - total weight of sample
Q - number of moles of solute in the sample
Mwt - molecular weight of solute
Mwt' - molecular weight of solvent
D - density of the solution (gms/cc)
D' - density of the pure solvent (gms/cc)

The molality, m, of a solute is defined as:

$$m = \text{number of moles of solute per 1000 grams of solvent} \quad (\text{C.1})$$

or

$$m = \frac{Q (1000)}{W - (Q)(Mwt)} \quad (\text{C.2})$$

Similarly, the molarity, M, is defined as:

$$M = \text{number of moles of solute per 1000 ml of solution} \quad (\text{C.3})$$

or

$$M = \frac{Q (1000) (D)}{W} \quad (\text{C.4})$$

The mole fraction, N, of a solute is given by:

$$N = \frac{\text{number of moles of solute}}{\text{total number of moles of solute and solvent}} \quad (\text{C.5})$$

or

$$N = \frac{Q}{Q + (W - Q \text{ Mwt})/\text{Mwt}'} \quad (\text{C.6})$$

which simplifies to

$$N = \frac{\text{Mwt}'}{\text{Mwt}' - \text{Mwt} + W/Q} \quad (\text{C.7})$$

Solve for W/Q in each equation, equate and simplify each possible pair.

Equations C.2, C.4 and C.7 are solved in terms of W/Q and then each possible pair of equations are equated and simplified to give the following:

$$M = \frac{1000m \cdot D}{1000 + m \cdot \text{Mwt}} = \frac{1000N \cdot D}{\text{Mwt}'(1-N) + N \cdot \text{Mwt}} \quad (\text{C.8})$$

$$m = \frac{1000M}{1000 \cdot D - M \cdot \text{Mwt}} = \frac{1000N}{\text{Mwt}'(1-N)} \quad (\text{C.9})$$

$$N = \frac{m \cdot \text{Mwt}'}{1000 + m \cdot \text{Mwt}'} = \frac{M \cdot \text{Mwt}'}{1000D + M(\text{Mwt}' - \text{Mwt})} \quad (\text{C.10})$$

This set of equations can be further simplified provided the solution is very dilute ($N < 0.01$ for most systems will introduce less than a 1% error) and the density of the solution is approximated by the density of the pure solvent (i.e., $D = D'$)

$$M = m D' = \frac{1000 \cdot N \cdot D'}{\text{Mwt}'} \quad (\text{C.11})$$

$$m = \frac{M}{D'} = \frac{1000 N}{\text{Mwt}'} \quad (\text{C.12})$$

$$N = \frac{m \cdot \text{Mwt}'}{1000} = \frac{M \cdot \text{Mwt}'}{1000 D'} \quad (\text{C.13})$$

REFERENCES

1. M. Blander, ed., "Molten Salt Chemistry," Interscience Publishers, N.Y., 1964.
2. G.J. Janz, ed., "Molten Salts Handbook," Academic Press, N.Y., N.Y., 1967.
3. B.R. Sundheim, ed., "Fused Salts," McGraw-Hill Book Co., N.Y., 1964.
4. J.K. Delimarskii and B.F. Markov, eds., "Electrochemistry of Fused Salts," Sigma Press, Washington D.C., 1961.
5. H.A. Laitinen and R.A. Osteryoung in "Fused Salts," B.R. Sundheim, ed., McGraw-Hill Book Co., N.Y., 1964, p. 255.
6. C.H. Liu, K.E. Johnson and H.A. Laitinen in "Molten Salt Chemistry," M. Blander, ed., Interscience Publishers, N.Y., 1964, p. 681.
7. T.B. Reddy, *Electrochem. Tech.*, 1, 325 (1963).
8. G.J. Janz, *Internat. Symp. High Temp. Chem.*, 169 (1959).
9. G.E. Blomgren, *J. Phys. Chem.*, 66, 1500 (1962).
10. A.F. Alabyshev, M.F. Lantratov and A.G. Morachevskii, eds., "Reference Electrodes for Fused Salts," Sigma Press, Washington, D.C., 1965.
11. C. Dijkhuis, R. Dijkhuis and G.J. Janz, *Chem. Rev.*, 68, 253 (1968).
12. T. Forland in "Fused Salts," B.R. Sundheim, ed., McGraw-Hill Book Co., N.Y., 1964, p. 63.
13. K. Grjotheim and G.M. Rosenblatt, *High Temp. Chem.*, 43 (1966).
14. R.W. Laity in "Reference Electrodes," D.J.G. Ives and G.J. Janz, eds., Academic Press, N.Y., 1961, p. 524.
15. H.C. Gaur and B.B. Bhatia, *J. Scientific and Indust. Research (India)*, 21A, 16 (1962).

16. L.J. Boxall, private translation of P'eng, K'o Hsueh T'ung Pao, 415 (1965), C.A. 64: 6094f.
17. A.D. Graves, G.J. Hills and D. Inman in "Advances in Electrochemistry and Electrochemical Engineering," P. Delahay, ed., Vol. 4, Interscience Publishers, 1955, p. 117.
18. A.G. Morachevskii, J. App. Chem. U.S.S.R., 40, 2017 (1967).
19. E.M. Cohn, Mechanical Engineering, June, 22 (1966).
20. J.A. Plambeck, J. Chem. Engin. Data, 12, 77 (1967).
21. P.I. Protsenko and B.S. Medvedev, Russ. J. Inorg. Chem., 8, 1434 (1963).
22. P.I. Protsenko and R.P. Shisholina, Ibid., 8, 1436 (1963).
23. P.I. Protsenko and R.P. Shisholina, Ibid., 8, 1438 (1963).
24. P.I. Protsenko and G.K. Shurdumov, Ibid., 9, 916 (1964).
25. P.I. Protsenko and N.A. Brykova, Ibid., 10, 659 (1965).
26. P.I. Protsenko, A.V. Protsenko and N.P. Popovskaya, Ibid., 9, 1053 (1964).
27. T.M. Oza and B.R. Walawalkai, J. Indian Chem. Soc., 22, 243 (1945).
28. E.S. Freeman, J. Phys. Chem., 60, 1487 (1956).
29. B.D. Bond and P.W.M. Jacobs, J. Chem. Soc., A, 1265 (1966).
30. P.I. Protsenko and A.V. Protsenko, Zh. Ziz. Khim, 38, 2688 (1964), C.A. 62: 4638 g.
31. F.R. Duke and G. Victor, J. Electrochem. Soc., 110, 91 (1963).
32. H.E. Bartlett and K.E. Johnson, Ibid., 114, 64 (1967).
33. P.I. Protsenko and A.V. Protsenko, Ukr. Khim Zh., 30, 1051 (1964), C.A. 62: 7385 e.
34. A.J. Calandra and A.J. Arvia, Electrochim. Acta, 11, 1173 (1966).
35. A.J. Arvia and A.J. Calandra, Ibid., 12, 1441 (1967).
36. A.J. Calandra and A.J. Arvia, Ibid., 10, 474 (1965).
37. P.G. McCormick and H.S. Swofford, Jr., Anal. Chem., 41, 146 (1969).

38. H.S. Swofford, Jr. and P.G. McCormick, *Ibid.*, 37, 970 (1965).
39. H.S. Swofford, Jr. and H.A. Laitinen, *J. Electrochem. Soc.*, 110, 814 (1963).
40. L.E. Topol, R.A. Osteryoung and J.H. Christie, *J. Phys. Chem.*, 70, 2857 (1960).
41. D. Inman and J. Braunstein, *Chem. Comm.*, 148 (1966).
42. C.D. Hodgman, ed. in chief, "Handbook of Chemistry and Physics," 44th edition, Chemical Rubber Publishing Co., Cleveland, Ohio, 1963.
43. H.E. Bartlett, "Electrochemistry of Oxy-Anion Melts," unpublished doctoral dissertation, London, 1966.
44. A.J. Calandra and A.J. Arvia, *Electrochim. Acta*, 12, 95 (1967).
45. R.N. Kust and R.W. Fletcher, *Inorg. Chem.*, 8, 687 (1969).
46. P.I. Protsenko, N.P. Popovskaya, Z.I. Belova, A.V. Protsenko, O.N. Shokina and R.P. Shisholina, *Tr. Usis. Soveshch. po Fiz. Khim Resplavlen. Solei*, 2nd Kiev, 1963, p. 55 (Pub. 1965), *C.A.* 65: 8080 b.
47. A. Conte, *Electrochim. Acta*, 11, 1579 (1966).
48. D.W. James, *Australian J. Chem.*, 19, 993 (1966).
49. O.J. Kleppa and L.S. Hersh, *Disc. Faraday Soc.*, 32, 99 (1961).
50. O.J. Kleppa and L.S. Hersh, *J. Chem. Phys.*, 34, 351 (1961).
51. S.V. Meschel and O.J. Kleppa, *Ibid.*, 48, 5146 (1968).
52. I.G. Murgulescu and S. Zuca, *Electrochim. Acta*, 14, 519 (1969).
53. R.E. Isbell, E.W. Wilson, Jr., and D.F. Smith, *J. Phys. Chem.*, 70, 2493 (1966).
54. B. Cleaver and B.C.J. Neil, *Trans. Faraday Soc.*, 65, 703 (1969).
55. C.C. Addison and B.J. Hathaway, *Proc. Chem. Soc.*, 19 (1957).
56. M. Peleg, *J. Phys. Chem.*, 71, 4553 (1967).
57. G.P. Smith and G.F. Petersen, *J. Chem. Data*, 6, 493 (1961).

58. D.W. James and C.H. Liu, *Ibid.*, 8, 469 (1963).
59. P.C. Papaioannou and G.W. Harrington, *J. Phys. Chem.*, 68, 2424 (1964).
60. I.G. Murgulescu and C. Volanschi, *Rev. Chim. Acad. Rep. Populaire Roumaine*, 6, 45 (1961).
61. R.F. Bartholomew, *J. Phys. Chem.*, 70, 3442 (1966).
62. H. Bloom and E. Heymann, *Proc. Royal Soc.*, A188, 392 (1947).
63. A. Klemm in "Molten Salt Chemistry," M. Blander, ed., Interscience Publishers, N.Y., 1964, p. 535.
64. B.R. Sundheim, ed., "Fused Salts," McGraw-Hill Book Co., N.Y., 1964, chapter 3.
65. A. Klemm in "Molten Salt Chemistry," M. Blander, ed., Interscience Publishers, N.Y., 1964, p. 564.
66. A. Klemm, NASA Acc. No. N66-14898, Rept. No. EUR-2466. e., p. 31-38 (1965).
67. F.R. Duke, R.W. Laity and B. Owens, *J. Electrochem. Soc.*, 104, 299 (1957).
68. J. Byrne, H. Fleming and F.E.W. Wetmore, *Can. J. Chem.*, 30, 922 (1952).
69. F.R. Duke and B. Owens, *J. Electrochem. Soc.*, 105, 476 (1958).
70. H. Bloom, I.W. Knaggs, J.J. Molloy and D. Welch, *Trans. Faraday Soc.*, 49, 1458 (1953).
71. E.P. Honig and J.A.A. Ketelaar, *Ibid.*, 62, 190 (1966).
72. L.A. King and F.R. Duke, *J. Electrochem. Soc.*, 111, 712 (1964).
73. A.J. Arvia and W.E. Triaca, *Electrochim. Acta*, 11, 975 (1966).
74. H.E. Bartlett and K.E. Johnson, *Can. J. Chem.*, 44, 2119 (1966).
75. A.J. Arvia, A.J. Calandra and W.E. Triaca, *Electrochim. Acta*, 9, 1417 (1964).
76. G.J. Hills and K.E. Johnson, *Proceedings of the 2nd Intern. Congress on Polarography*, Cambridge (1959), Pergamon Press, London, 1961, p. 974.

77. J. Frame and E. Rhodes, *Trans. Faraday Soc.*, 57, 1075 (1961).
78. G.J. Hills and P.D. Power, *J. Polarographic Soc.*, 13, 71 (1967).
79. N. Gupta and B.R. Sundheim, *J. Electrochem. Soc.*, 112, 836 (1965).
80. W.E. Triaca and A.J. Arvia, *Electrochim. Acta*, 9, 1055 (1964).
81. W.E. Triaca and A.J. Arvia, *Ibid.*, 10, 409 (1965).
82. R.N. Kust and F.R. Duke, *J. Am. Chem. Soc.*, 85, 3338 (1963).
83. A.M. Shams El Din, T. Gouda and A.A. El Hosary, *J. Electroanal. Chem.*, 17, 137 (1968).
84. F.R. Duke and S. Yamamota, *J. Am. Chem. Soc.*, 81, 6378 (1959).
85. R.N. Kust, *J. Electrochem. Soc.*, 116, 1137 (1969).
86. R. Littlewood and E.J. Argent, *Electrochim. Acta*, 4, 114 (1961).
87. A.M. Shams El Din, *Ibid.*, 7, 285 (1962).
88. L.E. Topol, R. A. Osteryoung and J.H. Christie, *J. Electrochem. Soc.*, 112, 861 (1965).
89. A. Conte and S. Casadio, *Ric. Sci. Ital.*, 36, 488 (1966).
90. N.S. Wrench and D. Inman, *J. Electroanal. Chem.*, 17, 319 (1968).
91. P.G. Zambonin and J. Jordan, *J. Am. Chem. Soc.*, 89, 6365 (1967).
92. R.N. Kust, *Inorg. Chem.*, 3, 1035 (1964).
93. P.G. Zambonin and J. Jordan, *J. Am. Chem. Soc.*, 91, 2225 (1969).
94. A.M. Shams El Din and A.A. El Hosary, *Electrochim. Acta*, 12, 1665 (1967).
95. National Bureau of Standards Circular 500, Selected Values of Chemical Thermodynamic Properties, Washington, D.C., 1952.
96. W.E. Triaca and A.J. Arvia, *Electrochim. Acta*, 9, 919 (1964).
97. R.W. Laity, *J. Am. Chem. Soc.*, 79, 1849 (1957).
98. A. Conte and M.D. Ingram, *Electrochim. Acta*, 13, 1551 (1968).

99. D.G. Hill, J. Braunstein and M. Blander, *J. Phys. Chem.*, 64, 1038 (1960).
100. M. Blander, F.F. Blankenship and R.F. Newton, *Ibid.*, 63, 1259 (1959).
101. S.N. Flengas and E.K. Rideal, *Proc. Roy. Soc. (London)*, 233A, 443 (1958).
102. C.M. Gordon, *Z. Physik. Chem.*, 28, 302 (1899).
103. F.R. Duke and H.M. Garfinkel, *J. Phys. Chem.*, 65, 461 (1961).
104. M. Bonnemay and R. Pineaux, *Compt. Rendus*, 240, 1774 (1955).
105. D.G. Hill and M. Blander, *J. Phys. Chem.*, 65, 1866 (1961).
106. K.F. Denning, Univ. of Sask. Regina Campus, Sask., personal communication, 1969.
107. D. Inman, *J. Sci. Instrum.*, 39, 391 (1962).
108. J. O'M. Bockris, D.J. Hills, D. Inman and L. Young, *Ibid.*, 33, 438 (1956).
109. D.L. Hill, G.J. Hills, L. Young and J. O'M. Bockris, *J. Electroanal. Chem.*, 1, 79 (1959).
110. D. Inman, J. O'M. Bockris and E. Blomgren, *Ibid.*, 2, 506 (1961).
111. J.E.B. Randles and W. White, *Z. Elektrochem.*, 59, 604 (1955).
112. J. Clavilier and R. Pineaux, *Compt. Rendus*, 260, 891 (1965).
113. G.J. Hills and K.E. Johnson, *J. Electrochem. Soc.*, 108, 1013 (1961).
114. G.J. Hills and P.D. Power, *Trans. Faraday Soc.*, 64, 1629 (1968).
115. V. Sh. Palanker, A.M. Skundin and V.S. Bagotskii, *Elektrokhimiya*, 2, 640 (1966).
116. R. Narayan and D. Inman, *J. Polarographic Soc.*, 11, 27 (1965).
117. A.J. Arvia, A.J. Calandra and M.E. Martins, *Electrochim. Acta*, 11, 963 (1966).
118. J. Braunstein, *J. Chem. Educ.*, 44, 223 (1967).
119. A. Kiszka and K. Gatner, *Electrochim. Acta*, 14, 187 (1969).

120. J.A.A. Ketelaar and Mrs. A. Dammers-de Klerk, Proc. Kon. Ned. Akad. Wetensch. Ser. B, 68, 169 (1955).
121. H. Hildebrand, J. Am. Chem. Soc., 51, 66 (1929).
122. O.J. Kleppa, R.B. Clarke and L.S. Hersch, J. Chem. Phys, 35, 175 (1961).
123. B. Scrosati, H. Flood and T. Forland, Kgl. Norske Videnskabers Selskabs Tronhjem Forhandling, 37, 106, 113 (1964), C.A. 63: 14112 d.
124. M. Temkin, Acta Physicochim, U.R.S.S., 20, 411 (1945), C.A. 40: 5621-1.
125. H. Bloom and B.J. Welch, Disc. Faraday Soc., 32, 115 (1961).
126. J. Brynestad, K. Grjotheim and C. Krohn, Rev. Roum. Chim., 9, 163 (1964).
127. M. Blander and J. Braunstein, Ann. N.Y. Acad. Sci., 79, 838 (1960).
128. K. Grjotheim, C. Krohn and J.M. Toguri, Trans. Faraday Soc., 57, 1949 (1961).
129. G.W. Toop, Trans. A.I.M.E., 233, 850 (1965).
130. R. Baboian and S.N. Flengas, Can. J. Chem., 45, 813 (1967).
131. I.G. Murgulescu and S. Sternberg, Disc. Faraday Soc., 32, 107 (1961).
132. H. Bloom and B.J. Welch, Trans. Faraday Soc., 57, 61 (1961).
133. J. Guion, Compt. Rendus, 262, 169 (1966).
134. M. Bakes and J. Guion, Ibid., 258, 1223 (1964).
135. M. Bakes and Bunsengesell, Phys. Chim, 70, 581 (1966).
136. M. Bakes, J. Guion and J.P. Brenet, Electrochim. Acta, 10, 1001 (1965).
137. J. Guion, J. Chim. Phys., 64, 1635 (1967).
138. I.G. Murgulescu and D.I. Marchidan, Rev. Chim. Acad. Rep. Populaire Roumaine, 5, 17 (1960).
139. C. Sinistri, Ric. Sci. Rendus Sez A, 1, 56 (1961).

140. M. Liguornik and Y. Markus, Rep. Israel Atomic Energy Comiss., 941 (1964), C.A. 62: 13930 d.
141. J. Lumsden, ed., "Thermodynamics of Molten Salt Mixtures," Academic Press, N.Y., 1966.
142. J. Braunstein and M. Blander, J. Phys. Chem., 64, 10 (1960).
143. J. Guion and J. Brenet, Electrochim. Acta, 12, 1383 (1967).
144. J. Braunstein and J.D. Brill, J. Phys. Chem., 70, 1261 (1966).
145. D. Inman, D.G. Lovering and R. Narayan, Trans. Faraday Soc., 64, 2476 (1968).
146. S.V. Meschel, O.J. Kleppa and J.M. Toguri, J. Phys. Chem., 45, 3075 (1966).
147. E.D. Eastman, J. Am. Chem. Soc., 48, 1482 (1926), 50, 283, 292 (1928).
148. C. Wagner, Ann. Physik., 3, 629 (1929).
149. H. Holtan, Jr., Koninkl. Ned. Akad. Wetenschap., Proc., 56B, 498, 510 (1953).
150. P. Mazur, J. Phys. Chem., 58, 700 (1954).
151. H. Holtan, Jr., P. Mazur and S.R. de Groot, Physica, 19, 1109 (1953).
152. C.A. Domenicali, Phys. Rev., 92, 877 (1953).
153. C.A. Domenicali, Rev. Mod. Phys., 26, 237 (1954).
154. A.J. de Bethune, J. Electrochem. Soc., 107, 829 (1960).
155. A.J. de Bethune, T.S. Licht and N. Swendeman, Ibid., 106, 616 (1959).
156. J.N. Agar in "advances in Electrochemistry and Electrochemical Engineering," P. Delahay and C.W. Tobias, eds., Vol. 3, Interscience Publishers, N.Y., 1963, chapter 2.
157. R.H. Detig and D.H. Archer, J. Chem. Phys., 38, 661 (1963).
158. T. Wartanowicz, Bull. Acad. Polon. Sci. Ser. Sci. Tech., 13, 911 (1965).

159. T. Wartanowicz, *Adv. Energy Conversion*, 4, 149 (1964).
160. T. Wartanowicz, *Archiwum Budowy. Maszyn.*, 12, 179 (1965).
161. S. Senderoff and R.I. Bretz, *J. Electrochem. Soc.*, 109, 56 (1962).
162. H. Holtan, Jr., P. Mazur and S. R. de Groot, *Physica*, 19, 1109 (1953).
163. B.R. Sundheim and J. Rosenstreich, *J. Phys. Chem.*, 63, 419 (1959).
164. R. Connan, J. Dupuy and J. Brenet, *Compt. Rendus*, 262 C, 1120 (1966).
165. R. Schneebaum and B.R. Sundheim, *Disc. Faraday Soc.*, 32, 197 (1961).
166. J. Dupuy, *Compt. Rendus*, C262, 8 (1966).
167. J. Dupuy, Y. Nakamura, S. Brillant and J. Brenet, *J. Chim. Phys.*, 63, 886 (1966).
168. C.R. Metz and R.L. Seifert, *J. Electrochem. Soc.*, 117, 49 (1970).
169. K. Wallin and A. Lunden, *Z. Naturforsch.*, a22, 591 (1967).
170. B.R. Sundheim and J.D. Kellner, *J. Phys. Chem.*, 69, 1204 (1965).
171. V. Backlund, J. Dupuy, S. Gustafsson and A. Lunden, *Z. Naturforsch.*, a22, 471 (1967).
172. A.J. Arvia, A.J. Calandra and M.E. Martins, *Electrochim. Acta*, 12, 347 (1967).
173. A. Lunden, *Ibid.*, 14, 1068 (1969).
174. J.A.A. Ketelaar and Mrs. A. Dammers-de Klerk, *Recueil*, 83, 322 (1964).
175. A.P. Altshuller, *J. Phys. Chem.*, 61, 251 (1957).
176. Landolt-Bornstein, eds., "Zahlenwerke und Funktionen," Vol. 2, Part 4, Berlin, 1961.
177. K.K. Kelley, *Contributions to the Data on Theoretical Metallurgy*, Vol. 10, Bureau of Mines, Washington, D.C., 1949.
178. W.F. Giaque and J.D. Kemp, *J. Chem. Phys.*, 6, 40 (1937).

179. C. Frejacques, *Compt. Rendus*, 232, 2206 (1951).
180. C. Frejacques, *Mem. Poudres*, 35, Annexe 7 (1953).
181. W.A. Rosser and H. Wise, *J. Chem. Phys.*, 24, 493 (1956).
182. J.A.A. Ketelaar and J.C.T. Kwak, unpublished results (1965).
183. M. Abraham, *Electrochim. Acta*, 8, 115 (1963).
184. M. Abraham and J.J. Hechler, *Ibid.*, 13, 1681 (1968).
185. M. Abraham and J.J. Hechler, *Ibid.*, 14, 725 (1969).
186. H.A. Laitinen, W.S. Ferguson and R.A. Osteryoung, *J. Electrochem. Soc.*, 104, 516 (1957).
187. S.N. Flengas and T.R. Ingraham, *Ibid.*, 106, 714 (1959).
188. H.A. Laitinen, R.P. Tischer and D.K. Roe, *Ibid.*, 107, 546 (1960).
189. D.L. Maricle and D.N. Hume, *Ibid.*, 107, 354 (1960).
190. J.R. MacKenzie, Ph.D. Thesis, Univ. of London, 1968.
191. G. Delarue, *J. Electroanal. Chem.*, 1, 13 (1959/60).
192. R. Barde, R. Buvet and J. Dubois, *Compt. Rendus*, 254, 1627 (1962).
193. J. Polart, P. Degobert and O. Bloch, *Ibid.*, 255, 515 (1962).
194. J. Polart and P. Degobert, *Ibid.*, 255, 2103 (1962).
195. J. Polart, *Ibid.*, 256, 2159 (1963).
196. H.A. Laitinen and J.A. Plambeck, *J. Am. Chem. Soc.*, 87, 1202 (1965).
197. H.A. Laitinen and B.B. Bhatia, *J. Electrochem. Soc.*, 107, 705 (1960).
198. S. Fukushima, R. Oyamado and H. Hagiwara, *J. Electrochem. Soc. Japan*, 33, 43 (1965).
199. H. Bloom and J.W. Hastie, *J. Phys. Chem.*, 72, 2361 (1968).
200. H.A. Laitinen and R.A. Osteryoung, *J. Electrochem. Soc.*, 102, 598 (1955).

201. H.A. Laitinen and H.C. Gaur, *Ibid.*, 104, 730 (1957).
202. R. Stein, *Compt. Rendus*, 246, 2611 (1958).
203. S. Senderoff and A. Brenner, *J. Electrochem. Soc.*, 101, 31 (1954).
204. K.H. Stern, *J. Phys. Chem.*, 60, 679 (1956).
205. H.A. Laitinen and J.W. Pankey, *J. Am. Chem. Soc.*, 81, 1053 (1959).
206. H.A. Laitinen and C.H. Liu, *Ibid.*, 80, 1015 (1958).
207. L. Yang and R.G. Hudson, *Trans. Metallurgical Soc. A.I.M.E.*, 215, 589 (1959).
208. L. Yang and R.G. Hudson, *J. Electrochem. Soc.*, 106, 986 (1959).
209. W.J. Hamer, M.S. Malmberg and B. Rubin, *Ibid.*, 103, 8 (1956).
210. W.J. Hamer, M.S. Malmberg and B. Rubin, *Ibid.*, 112, 750 (1965).
211. C.R. Metz, Ph.D. Thesis, Indiana Univ., 1966.
212. S.N. Flengas and T.R. Ingraham, *Can. J. Chem.*, 35, 1139 (1957).
213. R. Littlewood, *Electrochim. Acta*, 3, 270 (1961).
214. M. Takashi and Y. Amada, *Denki. Kagaku.*, 32, 140 (1964).
215. A. Haan and H.V. van de Poorten, *Compt. Rendus*, 261, 5462 (1965).
216. S. Asakwra and T. Mukaibo, *Electrochim. Acta*, 13, 881 (1968).
217. M.B. Panish, F.F. Blankenship, W.R. Grimes and R.F. Newton, *J. Phys. Chem.*, 62, 1325 (1958).
218. E.J. Salstrom, *J. Am. Chem. Soc.*, 55, 2426 (1933).
219. S. Senderoff and G.W. Mellors, *Rev. Sci. Instr.*, 29, 151 (1958).
220. L.L. Quill in "Chemistry and Metallurgy of Miscellaneous Materials," Paper No. 6, McGraw-Hill Book Co., N.Y., 1950.
221. J.H. Hildebrand and E.G. Salstrom, *J. Am. Chem. Soc.*, 52, 4650 (1930).
222. J.H. Hildebrand and E.G. Salstrom, *Ibid.*, 54, 4257 (1932).

223. M. Iseki and T. Kirihara, Nagoya Univ., 19, 310 (1967).
224. E.J. Salstrom, T.K. Kew and T.M. Powell, J. Am. Chem. Soc., 58, 1848 (1936).
225. M.B. Danish, R.F. Newton, W.R. Grimes and F.F. Blankenship, J. Phys. Chem., 63, 668 (1959).
226. A.A. Koloty, J. Phys. Chem. U.S.S.R., 30, 508 (1954).
227. K.H. Stern, J. Phys. Chem., 62, 385 (1958).
228. I.G. Murgulescu and S. Sternberg, Rev. Chim. Acad. Rep. Populaire Roumaine, 2, 251 (1957).
229. I.G. Murgulescu and D.I. Marchidan, Acad. Rep. Populaire Romine Studie Cercetariide Chim., 7, 2 (1959).
230. J. Guion, M. Blander, D. Hengstenberg and K. Kagemark, J. Phys. Chem., 72, 2086 (1968).
231. M. Takahashi, J. Electrochem. Soc. Japan, 25, 432 (1957).
232. L.S. Hersh and O.J. Kleppa, J. Chem. Phys., 42, 1309 (1965).
233. J. Lumsden, Disc. Faraday Soc., 32, 138 (1961).
234. B. Chu and J.J. Egan, Ann. N.Y. Acad. Sci., 79, 908 (1960).
235. I.G. Murgulescu and L. Marta, Rev. Chim. Acad. Rep. Populaire Roumaine, 7, 1103 (1962).
236. H. Reinhold, Z. Anorg. Allgem. Chem., 171, 181 (1928).
237. B.F. Markov, Doklad. Akad. Nauk. SSSR, 108, 115 (1956).
238. B.F. Markov and E.B. Kuzyakin, Ukr. Khim Zh., 32, 1180 (1966).
239. W. Fischer, Z. Naturforsch., a21, 281 (1966).
240. J. Dupuy and J. Ruch, Compt. Rendus, 262 C, 1512 (1966).
241. K.S. Pitzer, J. Phys. Chem., 65, 147 (1961).
242. J. Greenberg, J. Electrochem. Soc., 113, 937 (1966).
243. H.P. Meissner, D.C. White and G.D. Uhlrich, Adv. Energy Conversion, 5, 205 (1965).
244. G. Sinistri and E. Pezzati, Z. Naturforsch., a22, 590 (1967).

245. I.G. Murgulescu, S. Sternberg and L. Bejan, *Rev. Roumaine de Chem.*, 11, 447 (1966).
246. W.E. Triaca, C. Solomons and J. O'M. Bockris, *Electrochim. Acta*, 13, 1949 (1968).
247. J.C. Fondanaiche and T. Kikindai, *Bull. Soc. Chim. Fr.*, 1921 (1968).
248. I.G. Murgulescu, S. Sternberg and L. Medintev, *Electrochim. Acta*, 9, 219 (1964).
249. D. Inman in "Electromotive Force Measurements in High-Temperature Systems," C.B. Alcock, ed., *Inst. of Mining and Metallurgy*, London, 1968, pp. 163-81.
250. F.G. Bodewig and J.A. Plambeck, *J. Electrochem. Soc.*, 116, 607 (1969).
251. E.A. Ukshe and V.N. Devyatkin, *Zh. Ziz. Khim*, 39, 3074 (1965), *C.A.* 64: 8980 g.
252. E.A. Ukshe and V.N. Devyatkin, *Ibid.*, 39, 2288 (1965), *C.A.* 64: 4325 b.
253. V.N. Devyatkin and E.A. Ukshe, *Izo. Akad. Nauk. S.S.S.R. Metally*, 79 (1966), *C.A.* 65: 9760 d.
254. S. Yoshizaw, Z. Takehara, Y. Ito and K. Oka, *Denki Kagaku*, 36, 156(1968), *C.A.* 69: 24006 g.
255. B.F. Hitch and C.F. Baes, Jr., *Inorg. Chem.*, 8, 201 (1969).
256. C.E. Johnson, R.R. Heinrich and C.E. Crouthamel, *J. Phys. Chem.*, 70, 242 (1966).
257. J.A. Plambeck, J.P. Elder and H.A. Laitinen, *J. Electrochem. Soc.*, 113, 921 (1966).
258. V.I. Spitsyn and V.I. Shostak, *Zhur. Obschei. Khim*, 19, 1801 (1949).
259. C.H. Liu, *Anal. Chem.*, 33, 1477 (1961).
260. E.K. Akpov and A.G. Bergman, *Russ. J. Inorg. Chem. (Engl. Trans.)*, 4, 520 (1959).
261. K.E. Johnson and H.A. Laitinen, *J. Electrochem. Soc.*, 110, 314 (1963).
262. A. Kvist, *Z. Naturforsch.*, a21, 487, 1221 (1966).

263. K.H. Stern and E.L. Weise, Nat. Stand. Ref. Data Ser., Nat. Bur. Stand. (U.S.) NSRDS-NBS, 7, 38 pp. (1966).
264. C.H. Liu, J. Phys. Chem., 66, 164 (1962).
265. H. Flood and T. Forland, Disc. Faraday Soc., 1, 302 (1947).
266. I.T. Gul'din and A.V. Buzhinskaya, Elektrokimiya, 1, 716 (1965), C.A. 63: 11015 d.
267. D.M. Wrench and D. Inman, Electrochim. Acta, 12, 1601 (1967).
268. E.K. Akopov and A.G. Bergman, Zh. Neorgan. Khim, 5, 1257 (1960), C.A. 56: 14983 h.
269. A. Kvist and A. Randsalu, Z. Naturforsch., a21, 278 (1966).
270. H. Lux, Z. Elektrochem., 45, 303 (1939), 52, 220, 224 (1948), 53, 41, 43, 45 (1949).
271. D.G. Hill, B. Porter and A.S. Gillespie, Jr., J. Electrochem. Soc., 105, 408 (1958).
272. H. Flood, T. Forland and K. Motzfeld, Acta Chem. Scandinav., 6, 257 (1952).
273. H. Flood and N.C. Boye, Z. Elektrochem., 66, 184 (1962).
274. C.L. Bissell and F.R. Duke, Tahanta, 13, 959 (1966).
275. G.E. Walrafen, D.E. Irish and R.F. Young, J. Chem. Phys., 37, 662 (1962).
276. K. Hauffe and D.H. Hoeffgen, Z. Physik. Chem. (Frankfurt), 49, 94 (1966).
277. A.F. Kapustinsky, Acad. Nauk. URSS Compt. Rendus, 53, 719 (1946).
278. D.G. Miller, Ind. Eng. Chem. Fundamentals, 2, 78 (1963).
279. W.H. Evans and D.D. Wagman, J. Research of the National Bureau of Standards, 49, 141 (1952).
280. T.L. Kang, Ph.D. Thesis, The Univ. of Texas, 1960, Diss. Abs. 21: 2649 (1961).
281. R.W. Lovejoy, J.H. Colwell, D.F. Eggers, Jr. and G.D. Halsey, Jr., J. Chem. Phys., 36, 612 (1962).

282. A.W. Coats, D.J.A. Dear and D. Penfold, *J. Inst. Fuel*, 41, 129 (1968).
283. W.T. Thompson and S.N. Flengas, *Can. J. Chem.*, 46, 1611 (1968).
284. A.J. Arvia, F. De Vega and H.A. Videla, *Electrochim. Acta*, 13, 581 (1968).
285. M.C.B. Hotz, R.C. Kerby and T.R. Ingraham, *J. Electrochem. Soc.*, 115, 29 C (1968), Abstract No. 284.
286. G.J. Janz, *J. Chem. Educ.*, 44, 581 (1967).
287. H.E. Bartlett and K.E. Johnson, *J. Electrochem. Soc.*, 114, 457 (1967).
288. A.T. Ward and G.J. Janz, *Electrochim. Acta*, 10, 849 (1965).
289. V.V. Kuz'movich and S.S. Fedorchenko, *Ukr. Khim Zh.*, 32, 846 (1966), C.A. 66: 25648 T.
290. M. Rolin and J.M. Recapet, *Bull. Soc. Chim. France*, 2504 (1964).
291. G.J. Janz, E. Neuenschwander and F.J. Kelley, *Trans. Faraday Soc.*, 59, 841 (1963).
292. M.D. Ingram, B. Baron and G.J. Janz, *Electrochim. Acta*, 11, 1629 (1966).
293. Yu. K. Delimarskii, V.F. Grishchenko and V.A. Vasilenko, *Zh. Prikl. Khim (Leningrad)*, 42, 224 (1969), C.A. 70: 83584 n.
294. G.J. Janz and A. Conte, *Electrochim. Acta*, 9, 1269, 1279 (1964).
295. M. Schenke and G.H.J. Broers, *Power Sources*, 30, 459 (1966).
296. N. Busson, S. Palous, J. Millet and R. Buvet, *Electrochim. Acta*, 12, 1609 (1967).
297. G.J. Janz and M.R. Lorenz, *J. Chem. Eng. Data*, 9, 94 (1964).
298. M.D. Ingram and G.J. Janz, *Electrochim. Acta*, 10, 783 (1965).
299. P. Decobert and O. Bloch, *Bull. Soc. Chim. France*, 1887 (1962).
300. G.J. Janz, F. Colom and F. Saegusa, *J. Electrochem. Soc.*, 107, 581 (1960).
301. A. Borucka and C.M. Sugiyama, *Electrochim. Acta*, 13, 1887 (1968).

302. E. Baur and R. Brunner, *Z. Elektrochem.*, 41, 794 (1935).
303. G.J. Janz and F. Saegusa, *Electrochim. Acta*, 7, 393 (1962).
304. A. Borucka, *Ibid.*, 13, 295 (1968).
305. G.G. Arkhipov and G.K. Stepanov, *Acad. Sci. U.S.S.R., Ural Section, Inst. Electrochem (Eng. Trans.)*, 6, 67 (1965), C.A. 63: 17481 h.
306. Y.L. Sandler, *J. Electrochem. Soc.*, 109, 1115 (1962).
307. N. Busson, S. Palous, R. Buvet and J. Millet, *Compt. Rendus*, 260, 6097 (1965).
308. G. Danner and M. Rey, *Electrochim. Acta*, 4, 274 (1961).
309. I.N. Ozeryanaya, N.A. Krasil'nikova, M.V. Smirnov and V.N. Danilin, *Akad. Nauk. S.S.S.R. Ural. Fil. Proc. Inst. Elektrokhim.*, 7, 85 (1965).
310. R. Baboian, D.L. Hill and R.A. Bailey, *Can. J. Chem.*, 43, 197 (1965).
311. R. Baboian, D.L. Hill and R.A. Baily, *J. Electrochem. Soc.*, 112, 1221 (1965).
312. G.N. Lewis and M. Randal, "Thermodynamics" Revised by K.S. Pitzer and L. Brewer, 2nd edition, McGraw-Hill Book Co., N.Y., 1961, p. 242.
313. M. Blander, ed., "Molten Salt Chemistry," Interscience Publishers, N.Y., 1964, p. 130.
314. T. Forland in "Fused Salts," B.R. Sundheim, ed., McGraw-Hill Book Co., N.Y., 1964, p. 92.
315. J.A. Christiansen and M. Pourbaix, "Conventions Concerning the Signs of Electromotive Forces and Electrode Potentials," *Comptes Rendus of the 17th Conf. of the Int. Union of Pure and Applied Chem.*, held in Stockholm, 1953. *Maison de la Chimie, Paris*, 1954, pp. 82-84.
316. C. Thomas and J. Braunstein, *J. Phys. Chem.*, 68, 957 (1964).
317. J. Braunstein and J.D. Brill, *Ibid.*, 70, 1261 (1966).
318. E.R. Van Artsdalen and I.S. Yaffe, *Ibid.*, 59, 118 (1955).

319. B.F. Powers, J.L. Katz and O.J. Kleppa, *Ibid.*, 66, 103 (1962).
320. J.R. Dickinson, Ph.D. Thesis, University of Saskatchewan, Regina Campus, Regina, 1969.
321. E.S. Woolner, Jr., and D.G. Hill, *J. Phys. Chem.*, 67, 1571 (1963).
322. I.N. Belyaev, *Russ. Chem. Rev.*, 29, 428 (1960).
323. Y. Kaneko and H. Odanaka, *J. Res. Inst. Catalysis, Hokkaido Univ.*, 14, 213 (1966).
324. C. Sinistri, *Z. Naturforsch.*, a21, 753 (1966).
325. H.F. Stimson, J.F. Swindells and R.E. Wilson in "American Institute of Physics Handbook," D.E. Gray, ed., 2nd edition, McGraw-Hill Book Co., N.Y., 1963, pp. 4-8.
326. M. Bodenstein, *Z. Physik. Chem.*, 100, 68 (1922).
327. H. Haug and L.F. Albright, *I. & E.C. Process Design and Development*, 4, 241 (1965).
328. W.R. Forsythe and W.F. Giaouque, *J. Am. Chem. Soc.*, 64, 48 (1942).
329. National Bureau of Standards, Ser. III, Washington, D.C., June, 1948.
330. K.E. Johnson, High Temperature Technology, Proc. Third Intern. Symp., Asilomar, Calif., 1967, pp. 493-501.
331. J.P. Vereshchetina and N.P. Luzhnaya, *J. Appl. Chem. U.S.S.R.*, 24, 165 (1951).
332. M.C.B. Hotz, Department of Energy, Mines and Resources, Ottawa 4, Ontario, personal communication, 1967.
333. International Temperature Scale of 1948, Dept. of Scientific and Industrial Research, H.M. Stationery Office, Great Britain, 1950.
334. G.H. Ayres, "Quantitative Chemical Analysis," Harper and Row Publishers, N.Y., 1958.
335. Intern. Crit. Tables of Numerical Data, Physics, Chemistry and Technology, E.W. Washburn, ed., Vol. III, McGraw-Hill Book Co., N.Y., 1928.
336. Dr. C.L. Wang, Univ. of Sask., Regina Campus, Sask., personal communication, 1969.